Systematic methods to help the identification and evolution of chemical process designs

A Thesis Submitted to the
University of Surrey
for the degree of

Doctor of Philosophy

by

Daniel Montolio-Rodriguez

Under the supervision of
Dr. Patrick Linke and Professor Antonis Kokossis

December 2007

Process and Information Systems Engineering
School of Engineering, University of Surrey
Guildford GU2 7XH, United Kingdom

Dedicated to Claudia

Acknowledgments

After four years at UniS, it is time to thank the people that have work next to me and those that in some manner have helped me reach this point.

For his support and partnership I cannot start with anyone else than my main supervisor Dr. Patrick Linke. Without doubt I have not enough lines to express how satisfying and motivating has been to have worked with him, so I rather keep it brief and thank him for absolutely everything during these years. The next person to thank is my other supervisor Professor Antonis Kokossis as his guidance and support during this time have been invaluable. Thanks to the two of you for sharing with me not only your innovative research ideas but your views in life. It has been a great pleasure to have worked with you. You really are excellent mentors.

I would also like to express gratitude to few people in Germany. First of all, thanks to Dr. David Linke and to all his team for making my visit at ACA so stimulating and useful, and for their constant help and guidance while I was there. I would also like thank Dr. Harvey Arellano and Dr. Pu Li for offering me the possibility to discover the challenging world of research almost six years ago, and for helping me out with my admission at UniS.

Within the Chemical Engineering department, I want to express my gratitude to Dave Arnall, Penny Briggs and Dr. Andy Tate, and to all the guys that have helped me during this experience. I am very grateful to Dr. Sakis Papadopulos and Dr. Vikky Ashley for their friendship and assistance when I started, to Suresh for making my

relationship with computers not that bad, to Dr. Thanos Sotiriadis for his camaraderie and interesting chats over hundreds of cups of coffee, and to (not yet but soon, Dr.) Siyu Yang for being such a good friend during this time.

On a more personal side, I cannot forget the best trio back home, Cunill, Tonetti and Morales, for still calling me when I am back and for keeping alive "el foro sesgai".

My final words are for the most important people in my life. First of all I would like to thank my parents as without their support and efforts I would have never been able to write these words. Thanks guys for helping me always and for having inspired so much in this life. To my two funny sisters, Laura and Marta, thanks for suffering me for such a long time and for always being there when I needed you. Of course I want to show appreciation to my lovely and comic Grandma for bringing so much joy to the family. And finally, I want to say my most special thank you to Claudia, for all her sacrifices and for sharing with me so much. Thanks for being my partner, friend and colleague, for joining me in this adventure and for making my life perfect. Thanks guys for being my great family!

Abstract

This work aims at the development of methods that will allow systematic capitalisation on synergies across the chemical process development cycle. In an initial stage of the research, efforts have been focused towards the development of a conceptual process synthesis tool for the generation of novel design candidates to effectively and reliably screen reactive liquid-liquid extraction as a process synthesis option to compare its potential with that of other options. The primary aim is the identification of design trends as early as possible in the design process, to initialise and guide a posterior optimisation search with rigorous models. Next, the interest of the research is focused on the basic research and development issues required to realise an integrated approach in which key process design issues (the evaluation of catalyst performance, the design of reactors, the design of separation systems) can be addressed in parallel to the investigation of the chemistry from the earliest design stage, to arrive at the most economically viable and sustainable design via the shortest possible route. The developments focus on the conceptual design and evolution of designs for heterogeneously catalysed gas-phase reaction processes on the basis of available kinetic information. Building upon previous efforts in process synthesis, a multi-stage approach that relies on superstructure process representations has been developed. Throughout the multi-stage design cycle, information on the optimal operating envelopes is generated and can be fed back to the kinetics development team to guide additional experiments to ensure that kinetic models match the optimal regions in which the catalyst is to be used. The developments are demonstrated with industrially relevant applications. Novel processing schemes with significantly improved performances as compared to conventional process designs have been identified.

Table of Contents

Nomenclature

Chapter 4

	Basic index sets of superstructure elements for the RLLE approach
sub-index C	refer to carrier or reactive phase
sub-index S	refer to solvent phase

Symbol	**Variables and parameters for RLLE approach**	**Units**
$C^{Carrier}_{rm,sk,cp}$	concentration in the reactive phase of the component cp ∈ CP being extracted in the sub-unit sk ∈ SK_{rm} of rm ∈ RM^A	kg/m^3
$F_{rm,sk}$	mass flow entering the sub-unit sk ∈ SK_{rm} of rm ∈ RM^A	kg/h
$\dot{F}^{Carrier}_{out_{rm,sk}}$	reactive phase outlet volumetric flow from the sub-unit sk ∈ SK_{rm} of rm ∈ RM^A	m^3/s
$K_{D\,cp}$	partition ratio of the component cp ∈ CP being extracted	-
K_i	affinity constant for reaction i	g/l
k_i	rate constant for reaction i	g/g/h
$MTR_{rm,sk,cp}$	mass transfer of the component cp ∈ CP in the sub-unit sk ∈ SK_{rm} of rm ∈ RM^A	kg/s
MW_{cp}	molar weight of the component cp ∈ CP	kg/kgmol
MW	molar weight	kg/kgmol
N_{EtOH}	ethanol mass flow	kg/h
N_{Glu}	glucose mass flow	kg/h
N_S	solvent mass flow	kg/h
r_i	reaction rate of component i	gmol/h
$R_{rm,sk}$	volumetric ratio between extractive and reactive phase in the sub-unit sk ∈ SK_{rm} of rm ∈ RM^A	-
$V_{molar_{rm,sk,cp}}$	molar volume of the component cp ∈ CP being extracted in the sub-unit sk ∈ SK_{rm} of rm ∈ RM^A	m^3/kgmol
$x_{rm,sk,cp}$	molar fraction of the component cp ∈ CP in the sub-unit sk ∈ SK_{rm} of rm ∈ RM^A	-
Greek characters		
$\delta_{rm,sk}$	interfacial layer thickness of the sub-unit sk ∈ SK_{rm} of rm ∈ RM^A	m
$\eta_{rm,sk}$	viscosity in the sub-unit sk ∈ SK_{rm} of rm ∈ RM^A	cP
$\eta_{mixt\ rm,sk}$	viscosity of the mixture in the sub-unit sk ∈ SK_{rm} of rm ∈ RM^A	cP
$\eta_{rm,sk,cp}$	viscosity of the component cp ∈ CP in the sub-unit sk ∈ SK_{rm} of rm ∈ RM^A	cP
γ^{∞}_{cp}	activity coefficient of the component cp ∈ CP at infinite dilution	-

Symbol	**Variables for the kinetics of the Saccharomyces Cerevisiae reaction**	**Units**
$S_{acetald}$	intracellular acetaldehyde concentration	g/l
$S_{acetate}$	intracellular acetate concentration	g/l
S_{EtOH}	intracellular ethanol concentration	g/l
S_{glu}	intracellular glucose concentration	g/l
S_{pyr}	intracellular pyruvate concentration	g/l
X	dry weight biomass concentration	g/l
X_a	percentage of biomass that is active cell material	-
X_{Acdh}	proportion of activity of the protein caused by the enzyme acetaldehyde dehydrogenase	-

Chapter 5, 6 And 7 And Appendixes A2 And A3

Symbol	Variables and parameters	Units
A	pre-exponential factor for the Arrhenius equation	-
A	parameter for distillation expression cost	-
A	heat transfer area	m^2
$A_{HXNETWORK}$	area of the heat exchanger network	m^2
A_T	sectional area the fluid bed reactor	m^2
B	parameter for distillation expression cost	-
Bz	benzene	-
COLD_UTILITY	heat to be removed by the cold utility	kW
$COMPRESSION_{UTILITY}$	cost of the compression utility	M$/yr
$COMPRESOR_{COST}$	compressor fixed cost	M$
$CONDENSER_{COST}$	condenser fixed cost	M$
C	concentration	$kmol/m^3$
CP	component	-
Cp	specific heat	kJ/gmol K
d_b	diameter of the bubble	m
D_G	diffusion coefficient in the mixture	m^2/s
d_p	diameter of the catalyst particle	m
d_p^v	equivalent diameter of the sphere of the catalyst particles	m
d_i	inner diameter of a ring	m
d_t	diameter of the tube	m
D_v	diameter of the vessel	m
$DISTILLATION_{COST}$	distillation column fixed cost	M$
E_a	activation energy	kJ/gmol
Eb	ethylbenzene	-
EP	economic potential	M$/yr
f	friction factor	-
$\dot{F}$	mass flow	kg/h
F	molar flow	gmol/s
F_P	pressure factor	-
F_R	molar flow to be compressed	gmol/s
FBR_{COST}	fixed bed fixed cost	$
$FURNACE_{COST}$	furnace fixed cost	M$
g	gravity constant	m/s^2
k	rate constant for the styrene production process	$kmol/kg/s/bar^n$
k	rate constant for the acetic acid production process	gmol/kg/s/Pa
k_{BE}	mass transfer coefficient	l/s
K1	constant value	-
K2	constant value	-
K3	constant value	-
h	molar enthalpy	J/gmol
h_i	film transfer coefficient for hot stream *i* (including wall and fouling resistances)	$kW/m^2/K$
h_j	film transfer coefficient for cold stream *j* (including wall and fouling resistances)	$kW/m^2/K$
h_p	height of the catalyst particle	m
h_w	wall heat transfer coefficient	$kW/m^2/K$
HOT_UTILITY	heat to be given by the cold utility	kW
HLV	heat limit violation	-
%HV	percentage heat value	-
HX_{COST}	heat exchanger network fixed cost	M$
HX_{UNITS}	minimum heat exchanger units	-

i	interest rate	%
l_p	length of the catalyst particle	m
I	total number of hot streams in enthalpy interval *k*	-
J	total number of cold streams in enthalpy interval *k*	-
K	total number of enthalpy intervals	-
L	inverted mass of utility	1/kg
m	molar flow	mols/s
$m_{utility}$	mass of the utility media	kg/s
M	catalyst mass in the fluidised bed reactors	kg
$mols_r$	mols generated / consumed in fluidised bed reactors	mols
N	aspect ratio	-
ncomp	number of components	-
N_{min}	minimum number of trays	-
no_orifices	number of orifices for the gas distributor	-
no_scstr	number of sub-CSTRs	-
P_{FBLR}	pressure in a fluid bed reactor	bar
P_t	pressure in the tube	bar
P_{max}	maximum pressure inside the reactor	bar
PBP	payback period	yr
q	heat	kW
$q_{attainable}$	attainable heat for a reactor or section of reactor	kW
$q_{i,k}$	stream duty on hot stream *i* in enthalpy interval *k*	kW
$q_{j,k}$	stream duty on hot stream *j* in enthalpy interval *k*	kW
q_{optim}	optimised heat for a reactor or section of reactor	kW
R	constant of ideal gases	Pa m^3 / (gmol K)
R_{min}	ratio of minimum reflux	-
r_i	reaction rate of component i	kmol/kg cat/s
r_t	radius of the tube	m
R_1	parameter for expression in Nagel & Adler (1971)	m
$REBOILER_{COST}$	reboiler fixed cost	M$
S_{ABOVE_PINCH}	number of streams including utilities above the pinch	-
S_{BELOW_PINCH}	number of streams including utilities below the pinch	-
St	styrene	-
t	time	s, hr, yr
t	independent variable in differential equations	-
T	temperature	K
T_{MAX_LIMIT}	maximum temperature limit for reactors	K
T_{MIN_LIMIT}	minimum temperature limit for reactors	K
TLV	temperature limit violation	-
Tol	toluene	-
u	flow mean velocity	m/s
u_b	velocity of the bubble	m/s
u_{mf}	minimum velocity of fluidisation	m/s
u_0	superficial velocity	m/s
U	overall heat transfer coefficient	$W/m^2/K$
V_{BP}	volume for bubble phase	m^3
V_{CP}	volume for cloud phase	m^3
V_{EP}	volume for emulsion phase	m^3
VOLUME	volume	m^3
W	work	kW
y	dependent variable in differential equations	-
z	length of reactor	m
Greek characters		
δ	thickness	m
δ	differential	-
δ_{wall}	wall thickness	m
ΔH_{VAP}	enthalpy of vaporisation	kJ/gmol
ΔT_{LM}	logarithmic mean temperature difference	K
$\Delta T_{LM,k}$	logarithmic mean temperature difference for enthalpy interval k	K

ΔT_{min}	minimum increase of temperature	K
Δ	increase	-
ε	void fraction of the catalyst bed	-
$\bar{\varepsilon}$	mean void fraction of the fluidised or catalyst bed	-
ε_B	hold-up of bubble phase	-
ε_∞	parameter for the equation found in Winterberg & Tsotsas (2000a)	-
γ	ratio of heat capacities	-
η	absolute or dynamic viscosity	Pa·s
κ	ratio of thermal conductivities of the solid and the fluid phase	-
λ	thermal conductivity	kW/m/K
$\lambda_{e,r}$	effective radial thermal conductivity	kW/m/K
λ_f	fluid thermal conductivity	kW/m/K
λ_r	radial thermal conductivity	kW/m/K
λ_r^0	effective thermal conductivity due to conduction in the fluid and the solid phase	kW/m/K
λ_r^f	effective thermal conductivity due to convection	kW/m/K
λ_{wall}	wall conductivity	kW/m/K
ν	cinematic viscosity	m^2/s
θ	normalized surface coverage	-
ρ	density	kg/m^3

Sub- and super-indexes	
B	bubble & cloud phase
B	catalyst bed
Cooling Water	cooling water as cold utility
DISCHARGE	at the discharge point
COMPRESSOR	compressor
CONDESER	condenser
CONDENSATION	condensation
CURRENT	current solution
E	emulsion phase
f	fluid
g	gas
i	index that refers to hot streams
ic	index that refers to each component
ir	index that refers to each reactor
isc	index that refers to each sub-CSTR
j	index that refers to cold streams
k	index that refers to enthalpy intervals
n	index that refers to the cell in the fluid bed model
ncomp	number of components
no_scstr	number of sub-CSTRs
p	particle of catalyst
reactor	reactor
REBOILER	reboiler
STEAM	steam as hot utility
SUCTION	at the suction point
t	tube
utility	utility media
utility_isc	utility media for a specific sub-CSTR isc
W	water
Wall	tube wall

	Dimensionless groups	Formula
Bi	Biot number	$\frac{h_w \cdot r_t}{\lambda_{e,r}}$
Bi_{isc}	Biot number for each sub-CSTR	$\frac{h_{w,isc} \cdot R_t}{\lambda_{e,r,isc}}$
Pe_h^0	Fluid Peclet number for heat transfer	$\frac{u_0 \cdot \rho_f \cdot c_{p,f} \cdot d_p^v}{\lambda_f}$
$Pe_{h,r}$	Peclet number for radial heat conduction	$\frac{u_0 \cdot \rho_f \cdot c_{p,f} \cdot d_p^v}{\lambda_{e,r}}$
Pr	Prandtl number	$\frac{c_p \cdot \mu}{\lambda}$
Re	Reynolds number	$\frac{u \cdot d_t}{\upsilon} = \frac{\rho \cdot u \cdot d_t}{\mu}$

List Of Tables

List Of Figures

CHAPTER 1.

Introduction To The Research Problem

1.1 Introduction

One of the main objectives in process systems engineering is to develop methods that allow the engineer to discover process synthesis options and compare them with many others. During the past few decades the identification of profitable, sustainable and environmentally considerate options has relied on previous experience, and as a result, opportunities for identifying novel alternatives have been missed. In recent years, there has been a growing need for chemical engineers, not only to identify innovative process synthesis options but also to search these options and identify optimal designs. Many advances in process synthesis have been produced so far. The majority of these developments are focussed on the conceptual design around predefined synthesis options (*e.g.* reaction, separation, reactive/separation or heat integration). In contrast, efforts to develop tools for screening process synthesis options are very rare. Likewise, the lack of techniques for evolving the designs proposed by the conceptual design tools is also a fact. The successes of conceptual design tools in process synthesis have been significant only for simple systems. However, most industrially relevant systems are considerably more complex and cannot be addressed with existing technology. The current state of the art in the development and design of a chemical process is largely sequential. Specific design

issues such as the evaluation of catalyst performance, the design of reactors or the design of separation systems are addressed as separate steps one at a time. The overall success of the design activity is hampered by the lack of systematic support tools to assist scientists (*i.e.* experimental model developers) and engineers involved in the design processes to identify innovative solutions reliably and quickly in the context of the overall design goal, *i.e.* to identify the best possible process system that is comprised of these subsystems. Methodological shortcomings are exemplified by the lack of coordination of kinetic model development, reactor design and process synthesis. More often than not, kinetic models are developed for operating regions that do not correspond to the optimal values identified later on in process synthesis, when the experimental studies have long been concluded. The result is either a compromised design dominated by kinetic model reliability issues or a project delay caused by additional experimental investigations. Technological shortcomings are exemplified by the limited capability of current conceptual process synthesis tools to treat complexity (*i.e.* they quickly fail when complexity increases).

The existing lack of these systematic support tools impedes the effective communication between scientists and process engineers and obstructs the coordination of synthesis activities. Such coordination of synthesis activities is not within the scope of this research work. However, before it can be effectively approached, process design engineers must address:

- The effective selection of the best synthesis option for a given system.
- The effective identification of optimal design candidates for the selected synthesis option.

The ultimate benefit of the coordination of synthesis activities would be an experimental model development in the context of the overall process design aim, resulting in the perfect match between chemistry and process design. Therefore, if reliable synthesis strategies are developed for such purpose, step changes in innovation are to be expected.

1.2 Synthesis Strategy

In order to identify the most promising synthesis options and design candidates to arrive to the optimal synergy between chemistry and process design, this research presents a multi-stage process synthesis approach (Figure 1.1), as an alternative to the current obsolete synthesis strategies.

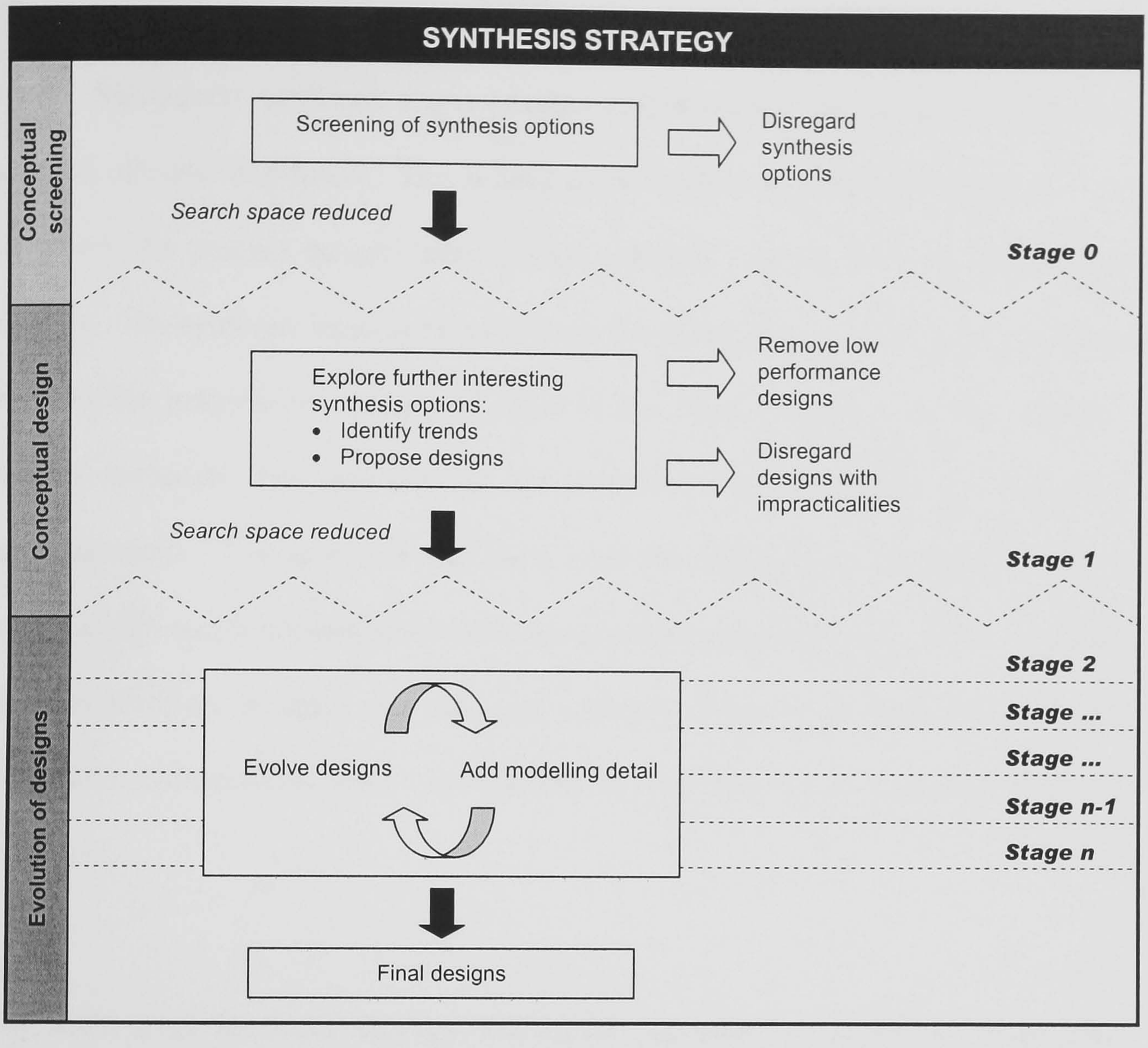

Figure 1.1: Multi-stage process synthesis strategy.

The approach starts at the highest level of abstraction with a **conceptual screening stage**, where the screening of process design options with highly conceptual tools is performed. Once the process design option is selected, a careful balance between the mathematical model complexity and the high-level conceptual designs involved is considered in the **conceptual stage**. At this stage, still highly abstract, the screening of a vast number of processing alternatives is performed and potential design candidates are selected. The further exploration of the design candidates may reveal system trade-offs. As the investigation goes on, the designs that show low performances or impracticalities are disregarded. Consequently, the combinatorial

size of the problem is reduced and the optimisation is focussed on the most promising areas. Subsequent synthesis stages (**design stages**) enrich the process models (*i.e.* addition of modelling detail). This is done to incorporate non-ideal behaviour in order to evolve the process designs into optimal schemes that can be easily reached in practice. The synthesis strategy requires high flexibility in the process representations to allow the progressive addition of detail in the models employed as the synthesis process continues. For such purpose, the presented strategy relies on superstructure representations. The approach also has a need for optimisation tools that can cope with the high non-linearities involved in the experimental models (*e.g.* kinetic models, phase-equilibrium models) and the large amounts of binary decisions to be made. Stochastic optimisation tools have proved in the past to be effective for such problems.

The multi-stage synthesis strategy will allow the effective selection of the best synthesis option and the identification of the optimal design candidates for it. Having reached this point, the integration of the experimental modelling and the process design activities is ready to be approached. The presented strategy can enable at any stage a bidirectional flow of information between synthesis activities. The resulting information on the optimal operating regions from the process design activity can be communicated to the experimental development team. Experimental developers can update the experimental model on the new operating regions, and send it back to the process engineers. Then, process engineers can search again for optimal operating regions and the cycle can continue until the experimental model is validated in the optimal process regions in which it is to be used.

1.3 Research Contributions

The research contributions presented in this work are summarised as follows:

- Within the initial **conceptual screening stage** of the multi-stage synthesis strategy, this research work presents a tool for the conceptual screening of reactive liquid-liquid extraction (RLLE) as a process design option. The tool maps the information of the solvent phase onto the superstructure model of a single-phase reactor network. The mapping involves the overestimation of the transfer rate from the reactive to the solvent phase. The approach can deliver either much better performances than the single reactive system or similar ones to it. If the results of the conceptual screening prove to be promising, the next conceptual design stage can be justified and the results can be employed in the tedious initialisation of more detailed optimisations. Otherwise, the synthesis option is disregarded for not being promising enough and great amounts of time and resources can be spared in the design exercise.

- The core development of this work is a decision support framework (DSF) extended across the **conceptual stage** and the **design stage**. Heterogeneously catalysed gas-phase reaction systems illustrate the developments. The DSF relies on the appropriate balance between the combinatorial complexities of process layouts and the level of detail of the process models employed. At the beginning of the synthesis exercise, the process structure is unknown and the combinatorial complexity is high. Therefore, simple models are employed. Towards the end, the knowledge that has emerged about the process structure is employed to reduce the structural complexity and more complexity in terms of process models can be afforded.

Within the **conceptual design** stage, a superstructure-based optimisation approach has been developed to address the shortcomings of current process synthesis methods when applied to complex systems. Process representations have been customised for heterogeneously catalysed gas-phase reaction systems. The representations include practical constraints that are found in practical applications. In this stage, a multi-level approach aims at the development of design performance targets and the identification of interactions between design performance and design complexity.

Knowledge obtained in the first highly conceptual levels of process design can be used in later concreter stages. This is exploited in a multi-stage design strategy included within the **design stage**. The few designs resulting from the multi-level approach can be carefully explored by employing more detailed and computational demanding reactor models. The extra detail of the models employed allows for the evolution of the designs earlier identified. The evolution is an iterative process carried out in several stages. The solution of each stage becomes the starting point for the optimisation in the next stage.

1.4 Thesis Structure

Chapter 2 identifies the drawbacks of the current process design attitude and reviews the available literature related to previous works in:

i) Reactor networks synthesis approaches.

ii) Reaction-separation integration synthesis approaches.

iii) Reactive / separation integration synthesis approaches.

iv) Reaction-separation and reactive / separation integration synthesis approaches.

The need for new synthesis approaches is also discussed.

Chapter 3 presents the key topics in which the network optimisation is based on:

i) The generic reactor / mass exchanger unit.

ii) The superstructure representation.

iii) The stochastic optimisation method employed to explore the search space in the form of Tabu Search.

Chapter 4 addresses RLLE as an example of the screening of process synthesis options that takes place at the beginning of the design exercise (**conceptual screening stage)**. RLLE is screened making use of aggregated models to avoid unnecessary modelling details while capturing all the major trade-offs at the very initial stages of process design. A new network optimisation-based approach is presented. It allows quickly deciding whether the application of RLLE is a promising option for reactive equilibrium systems or for systems where reactions are inhibited by product formation. The approach is based on a new developed Liquid-Liquid Extraction transfer rate expression that over-predicts mass transfer from the reactive to the solvent phase. Two biochemical examples illustrate the approach. The applications prove that structured search strategies can speed up significantly the process synthesis development and produce improved results if compared with early works found in the

literature.

Chapter 5 and 6 present the DSF developed to address the limitations of current process synthesis approaches so the coordination between the kinetic model development and the process synthesis can be approached in a future phase. The framework relies on a superstructure-based optimisation approach. Chapter 5 details the DSF section related to the **conceptual stage**. The process representations in which the DSF relies on are also described in here. The representations have been tailored for heterogeneously catalysed gas-phase reaction systems and include practical constraints that are found on practical applications. At this stage, the DSF relies on a multi-level synthesis approach. The multi-level synthesis approach aims at the development of design performance targets and the identification of interactions between design performance and design complexity. An application to a styrene production process is presented to illustrate the methodology.

Chapter 6 details the DSF section related to the **design stage**. In this chapter, the multi-stage evolution of designs is outlined. The evolution allows the investigation of the optimal conceptual design candidates identified in the multi-level approach at different stages, where the level of detail of the process models increases from one to another. The aim is to progressively include non-ideal behaviour to evolve the process designs into options that can be easily achieved in practice. The styrene production process also illustrates the methodology.

Chapter 7 presents an application of the DSF in the form of a heterogeneously

catalysed gas-phase selective oxidation of ethane. For this reaction system the experimental kinetic model has already been published. Novel processing schemes with significantly improved performances, if compared to conventional process designs, are identified with the presented approach.

Chapter 8 concludes the research and discusses the advantages and benefits of the novel contributions.

Finally, Chapter 9 recognises the limitations of this work and identifies directions for future developments in process design.

CHAPTER 2.

Literature Review

2.1 Introduction

Much research has been done in process synthesis for the last 50 years (Westerberg, 2004). Most of the existing synthesis techniques are of narrow application and simply focus on the conceptual design stage where predefined process options are explored to search for optimal designs (Figure 2.1). However, the previous conceptual screening of process options and the later evolution of the designs resulting from the conceptual design stage, have not yet received much attention in the process research community.

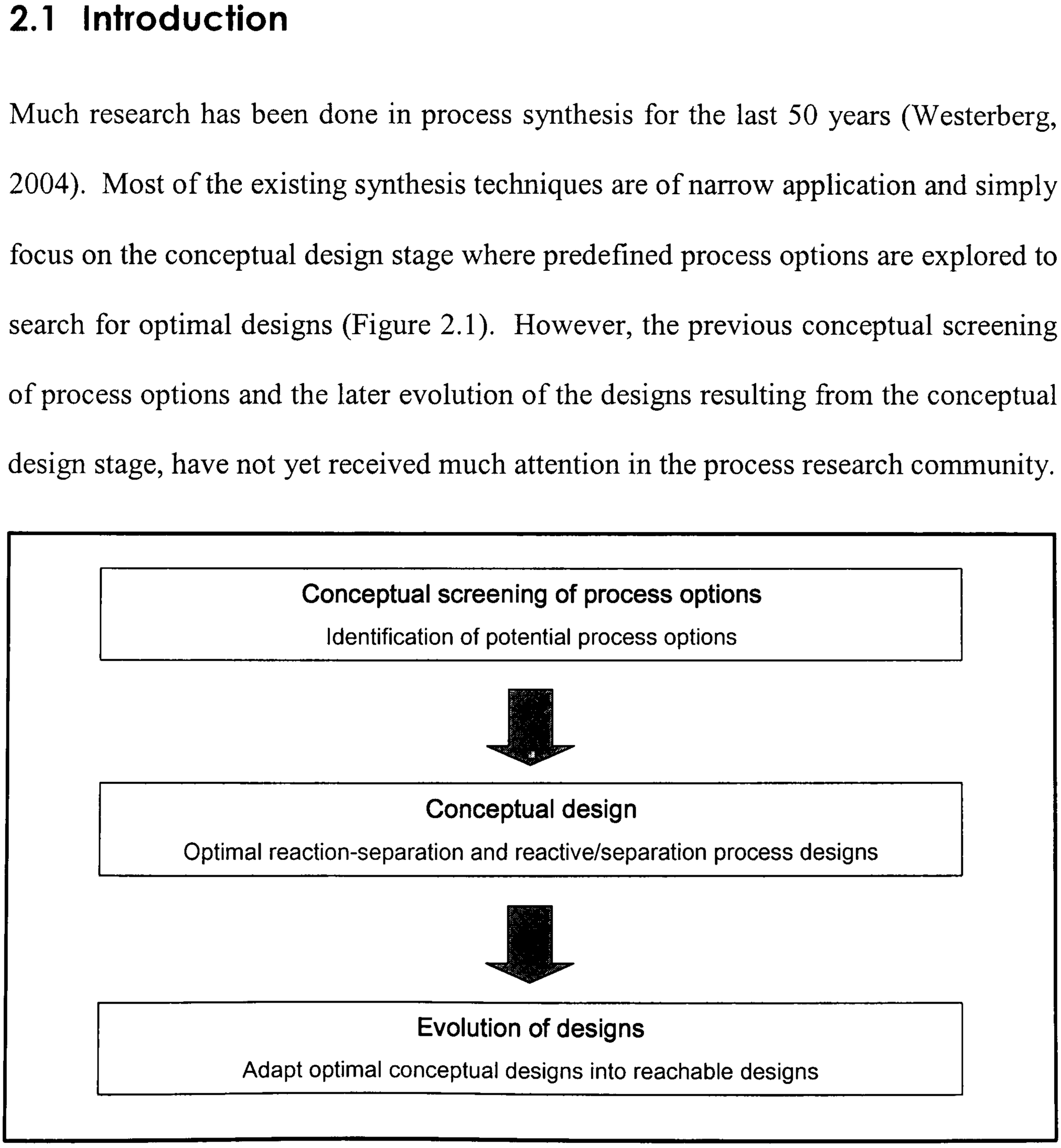

Figure 2.1: Optimal process design strategy.

The conceptual screening of process options has been widely ignored despite being the step in which the most important design decision is considered (*i.e.* the selection of the most suitable processing option for a given system). Two of the few authors that have approached this high level screening stage are Linke & Kokossis (2007), who employ separation task units to search separation systems. The conceptual screening stage aims to introduce simple models that enable the exploration of major trade-offs rapidly and effectively. Rather than suggesting definitive process layouts, the conceptual screening can create insight into optimal mixing patterns, component separation, recycle policies, etc. The conceptual screening has not only the potential to identify possible improvements in process performances delivering potential process options for a system, but also can help the designer to accelerate the design exercise resulting in more profitable projects. Identified layouts can be then explored in the following conceptual design stage.

Techniques that evolve the resulting design candidates from the conceptual design stage have not received much attention either. Therefore, there is a gap between the optimal designs identified in the conceptual design stage during research activities and those designs that are implemented in industry. The trade-offs identified in conceptual design stages may not be realistic and consequently, some extra model non-linearities may be required. Once the combinatorial size of the problem has been reduced by eliminating irrelevant design options in the conceptual design stage, more process modelling detail can be afforded without compromising computational efforts.

The next sections review the past and current developments in reactor network synthesis approaches and integrated approaches for reaction and separation systems. All the developments discussed are within the conceptual design stage of the presented methodology. Finally the need for new synthesis methodologies is highlighted.

2.2 Reactor Network Synthesis

2.2.1 Introduction

Reactor networks are sets of reactors interconnected between them. Their optimisation still constitutes in process synthesis an ongoing process due to their vital importance for process performances. Approaches to optimal reactor network synthesis include the Attainable Region (AR), superstructure-based optimisation methods and combinations of both. The approaches involving superstructure representations use either deterministic or stochastic tools to optimise process designs.

2.2.2 Attainable Region

The AR is a graphical method based on vectors which is defined as the set of all possible outcomes that satisfies the constraints fixed for a given system and that can be reached using fundamental processes operating within the system (*i.e.* mixing, reaction and heat transfer). Initially, the relevant fundamental processes are chosen and the state variables selected and grouped together to form a vector. Next, the geometry of the units is chosen and the necessary conditions determined. A region is

then constructed and the boundaries of this region are interpreted as structures. The optimal solution is an active constraint on the limits of the constructed region.

Early work on AR was conducted by Horn (1964) who was the first to present the AR concept. Glasser *et al.* (1987) applied the AR concept to different isothermal examples with constant density. Hildebrandt *et al.* (1990) applied the AR to adiabatic, non-constant density systems and constrained systems. Hopley *et al.* (1996) presented an application to an adiabatic example with kinetics that incorporated the Arrhenius equation. Their work was later extended by Nicol *et al.* (1997) to integrate optimal cooling strategies. The construction of the AR is performed through graphical methods and consequently it is limited to three-dimensional problems. The application of the AR concept to three-dimensional systems was first presented by Hildebrandt & Glasser (1990). To extend the applicability of the AR method to higher dimensional systems, some efforts on defining theoretically the region have been performed in the last decade. Feinberg & Hildebrandt (1997) established universal properties of the AR, whereas Glasser & Hildebrandt (1997) highlighted prospects of its application to more general systems than those employed up to the date. Later, Rooney *et al.* (2000) employed a new graphical approach to construct ARs with higher dimensions.

Regardless of these developments, AR methods are still limited by modelling flexibility when they are applied to cases of high complexity such as the ones typically found in industry. Besides, they do not succeed in providing methodical comparison of different process design candidates as they only provide a single

solution for a given system.

2.2.3 Superstructure Optimisation

2.2.3.1 Introduction

The term superstructure in process design stands for a mathematical model that embeds all possible combinations and physical connections of processing units. The units are connected through mixers and splitters. Superstructure-based optimisation applications are found in fields such as reactor networks, separation networks, reactive / separation networks, heat exchanger networks, etc. Process designs represented by superstructures can be optimised either by deterministic or stochastic techniques.

2.2.3.2 Deterministic Methods

Deterministic superstructure-based optimisation approaches were initially presented by Jackson (1968), who proposed a network of interconnected plug-flow reactors (PFR) with sinks, sources and side streams. Two decades later, Achenie & Biegler (1986, 1990) applied non-linear programming (NLP) methods to solve the problem. Initially, they formulated an optimal control problem with a constant-dispersion model where a dispersion parameter was used to select a reactor type between the continuously stirred tank reactor (CSTR) and the PFR. Later, they introduced the recycle reactor module (RRM) and made use of the recycle ratio to determine the type of reactor employed: i) when the recycle ratio was approaching to zero a PFR was selected; ii) for recycle ratios close to 100 %, a CSTR was chosen. From a different point of view, they also proposed a synthesis target-based method to convert the

synthesis reactor problem into an optimal control formulation in which the control variables were the residence time density and the micro-mixing functions (Achenie & Biegler, 1988). Meanwhile, Kokossis & Floudas (1990, 1991, 1994) proposed a general superstructure formulated in the form of mixed-integer non-linear programming (MINLP). They applied their developments to isothermal reactor-separator-recycle systems and isothermal and non-isothermal reactor networks. In order to avoid differential equations and handle only algebraic systems, they approximated the PFRs to a series of equal volume sub-CSTRs. Later, Schweiger & Floudas (1999) presented a general framework for the optimisation of reactor networks using an optimisation approach where CSTRs and cross flow reactors (CFRs) were the generic units. The framework was formulated using differential and algebraic equations and the optimisation approach involved the application of a control parameterization method. Then, Esposito & Floudas (2002) proposed a deterministic global optimisation method tailored to the particular structure and characteristics of the isothermal reactor network synthesis problem. They modelled PFRs using differential-algebraic equations. To overcome the multiple local minima exhibited by this formulation, they made use of a branch and bound approach that follows the αBB method presented by Adjiman *et al.* (1998a, b).

Although deterministic superstructure-based optimisation tools are much flexible in the representation of complex systems than AR approaches, they are still limited by mathematical and combinatorial complexities if highly non-linear kinetic and phase-equilibrium models are involved. These approaches present limitations to initialise straightforward the system under consideration and for complex systems, the resulting designs are likely to be out of the globally optimal domain. As in AR methods, they

only produce a single final design candidate and impede the identification of trade-offs for the system. Consequently, they do not provide either confidence in the quality of the solution or understanding of the significant features of the final designs.

2.2.3.3 Stochastic Techniques

The disadvantages of the deterministic optimisation techniques can be overcome with stochastic optimisation tools since they are able to treat problems with any degree of non-linearities and discontinuities. Stochastic studies acquire confidence on the final solution by performing sets of multiple runs that start from several initial points. Multiple final design candidates arise from the optimisation procedure and the identification of systems trade-offs becomes possible. These techniques have been successfully applied to process synthesis problems such as reactor networks, reaction / separation approaches or heat exchanger networks.

Regarding reactor networks, Marcoulaki & Kokossis (1996, 1999) searched single-phase reactor networks using stochastic techniques in the form of Simulated Annealing (SA). They delivered robust objective targets and a set of final design candidates with very similar performances. This approach was later extended to isothermal multi-phase systems (Mehta & Kokossis, 1997, 1998), and non-isothermal multi-phase systems (Mehta & Kokossis, 1998, 2000). These authors developed the shadow compartment concept and included it in a generic unit, which is the basis of their superstructure representation. The shadow compartment includes all possible design options from different combinations of contacting and mixing patterns that exist within and between different phases in the reactive units. The shadow

compartment is divided in sub-units for each phase present in the system. Mass can be transferred across phase boundaries.

Although being an effective alternative to deterministic tools, stochastic methods require very long computational efforts to ensure finding the global optimum based on statistical facts. They also exhibit initialisation problems and convergence difficulties. In an effort to overcome such drawbacks, Ashley & Linke (2004, 2005) introduced the concept of knowledge driven optimisation and employed systems knowledge in order to develop rules to guide and focus the optimisation search. Data mining techniques were used for this purpose. Tabu Search (TS) was the stochastic tool employed.

2.2.4 Combined Methods

The combination of the superstructure representation and the AR methods has been addressed by some authors to overcome the disadvantages of AR techniques. Balakrishna & Biegler (1992a, b) extended the work of Achenie & Biegler (1988) by proposing a multi-compartment mixing model that allowed the simulation of different mixing states ranging from the extremes of plug-flow to well-mix. They also projected a constructive targeting approach where a single isothermal reactor was initially selected and optimised using AR concepts. The superstructure was enriched by adding an extra reactor and then optimised. If a better solution was found the superstructure was further extended, otherwise the optimisation was terminated. In their second paper they energy-integrated non-isothermal reactors. Lakshmanan & Biegler (1996a, 1997) extended this concept by using for each stage, superstructure

units consisting of two different reactor types: CSTRs and differential side stream reactors (DSSRs). They improved the work of Balakrishna & Biegler (1992a, b) by avoiding suboptimal final designs for non-monotonic objective functions. AR properties were included in the mathematical model and the problem was solved with MINLP techniques. Rooney & Biegler (2000) combined MINLP and AR concepts to include model parameter uncertainty in reactor network synthesis. Despite these efforts, such approaches still contain the limitations of the deterministic optimisation methods.

2.3 Reaction-Separation Integration Approaches

Some authors have approached the reaction-separation systems integration. The forementioned Kokossis & Floudas (1991) presented a general MINLP superstructure formulation with two generic reactive units: CSTRs and PFRs. They included sharp-split separators and recycles that connected the separators with the reactive units. In a similar approach, Smith & Pantelides (1995) employed more detailed models in another MINLP formulation. Finally, Fraga (1996) applied dynamic programming techniques to a discretised reactor-separator synthesis problem. These works addressed single phase systems and therefore were not able to treat reactive / separation options. From another viewpoint, Feinberg (2002) identified future potential opportunities and likely limitations of the AR methods for reactor / mixer and reactor / mixer / separation systems.

2.4 Reactive / Separation Integration Approaches

As in reactor networks optimisation, the techniques for approaching reactive / separation processes are graphical and superstructure-based optimisation approaches.

Graphical efforts include the works of Barbosa & Doherty (1988), Okasinski & Doherty (1998) and Hauan *et al.* (2000a) in distillation of reactive mixtures; Samant & Ng (1998) and Hauan *et al.* (2000b) in extractive reaction processes; and Berry & Ng (1997) in reactive crystallisation processes. Regarding the application of the AR to reactive / separation synthesis problems, Nisoli *et al.* (1997) combined the AR approach for reactive systems with geometric methods to account for the feasibility of separations and proved that in the integration of reaction and separation, the composition space is not always attainable. These methods, although useful for illustration purposes and initialising rigorous simulations, fail to compare design candidates systematically. Besides, apart from being limited by dimensionality issues, they approach the integration of reaction and separation in a sequential manner. Initially, they focus on separation feasibility and then designs are build up around it.

Efforts on superstructure reactive / separation representations approached with deterministic tools include the formulation of a reactive distillation synthesis problem as an MINLP by Ciric & Gu (1994). They employed a generalised Benders decomposition method to address it. Stein *et al.* (1999) developed a non-isothermal two-phase model with two types of generic units comprising the superstructure: a reaction-condensation unit and mixers / splitters. Balakrishna & Biegler (1993) formulated a reactive / separation model as a mixed integer optimal control problem

in order to optimise a species-dependent residence time distribution function, which led to a separation profile as a function of the species age. Lakshmanan & Biegler (1996b) integrated their reactor network synthesis algorithm with mass exchange network concepts within a combination of MINLP and AR concepts. As in Balakrishna & Biegler (1993), they provided design targets rather than design alternatives. Finally, on reactive distillation synthesis, Cardoso *et al.* (2000) optimised the same representation as Ciric & Gu (1994) with the stochastic technique SA.

Tools to address reactive / separation synthesis problems share the same advantages and disadvantages as those that address reactor networks applications.

2.5 Reaction-Separation And Reactive / Separation Integration Approaches

Few efforts have addressed the integration of both reaction-separation systems and reactive / separation systems. Regarding deterministic superstructure-based optimisation approaches, Papalexandri & Pistikopoulos (1996) proposed a mass / heat transfer module for modelling a framework formulated as a MINLP problem, to address a prepostulated system (*e.g.* reactive distillation network). Ismail *et al.* (1999, 2001) extended these initial developments into reaction- and reactive / distillation systems. Within the group of stochastic techniques, Linke (2001) and Linke & Kokossis (2003b) introduced a general framework for the selection of process designs

through simultaneous exploitation of reaction and separation options. The superstructure comprised two kinds of generic synthesis units: i) reactor / mass exchangers (RMX units) that follow the concept of the shadow compartment initially developed by Metha & Kokossis (1997, 2000), and; ii) separation task units. In a separate effort, they compared the performance of the stochastic algorithms SA and TS in the context of the synthesis of reaction- and reactive / separation systems (Linke & Kokossis 2003a). They concluded that TS reaches optimal solutions faster than SA when applied to such synthesis problems.

2.6 The Need For New Synthesis Approaches

The systematic identification of optimal chemical process designs is a challenging task. Choosing a process option in the initial stages of process design is a complicated task because of the vast number of possible options, time constraints and the lack of conceptual support tools. Consequently, it is at the moment rather difficult to screen process alternatives rapidly and reliably to evaluate their potential with respect to other options.

Despite the significant successes of conceptual process synthesis methods for simple systems in the past, most industrially relevant systems are considerably more complex and cannot be addressed with existing technology. Current conceptual process synthesis approaches still exhibit multiple limitations:

- Graphical methods are limited by modelling flexibility and dimensionality problems. Although helpful for illustration purposes, they fail to deliver systematic comparison of design candidates and their applications are to systems of reduced complexity.

- Over the past decade, superstructure-based optimisation methods have been proposed to address the systematic identification of designs, by exploiting synergies between the reaction and separation system of a process (Linke & Kokossis, 2003a, b; Ismail *et al.*, 2001; Smith & Pantelides, 1995). Such methods have been highlighted as key technologies to enable improved process efficiencies that would be required for a sustainable development of the chemical process industries (Tsoka *et al.*, 2004). However, applications of these methods to complex systems (*e.g.* gas-phase heterogeneously catalysed reaction systems) are rarely found in industry and academia. The main reasons are the numerical problems associated with the mathematical complexity of the experimental models involved (*e.g.* kinetic and phase-equilibrium) and with the combinatorial complexity of the layouts implicated. Besides, the methods fail to handle practical constraints in practical applications. Deterministic optimisation-based methods are difficult to initialise, converge, and usually do not succeed to identify the global optimum. Moreover, they do not allow the systematic comparison of design candidates either. Stochastic techniques, although more robust and flexible than the previous ones, require long computational times to converge and still struggle to cope with highly non-linear experimental models.

Synthesis tools that attempt to lessen the gap between the optimal designs identified in the conceptual design stage and those that are implemented in industry are very rare. Once the combinatorial size of the problem has been reduced in the conceptual design stage, subsequent design stages offer the opportunity to add modelling detail to the process representations. By adding detail, the description of the selected designs would improve as designs would be evolved into more realistic ones without compromising the computational efforts.

This thesis aims to develop robust and reliable process synthesis methods to address the current limitations of process synthesis and make possible step changes in innovation.

CHAPTER 3.

Network Optimisation

3.1 Introduction

The developments presented in this research are focused on three synthesis problems: i) reaction; ii) reaction-separation; iii) reactive/separation. The starting point to approach such problems is the process representations presented by Linke & Kokossis (2003b). Most of their developments are located in the conceptual design stage of the optimal process synthesis strategy presented in Chapter 1, although few of them relate to the screening of process options. Their representations are based on building blocks that can take the form of pure reactor units, mass exchangers, reactive / mass exchangers or separators in the form of separation tasks. Based on these building blocks, a rich superstructure that includes raw material sources, product sinks and the interconnections between units and compartments of the units can be formulated. Their developments have proven to be robust and systematically highlight relevant structural characteristics that can help the engineer understanding bottlenecks and zones of structural flexibility in the process layout context. However, these representations are very generic and show few drawbacks:

i) They do not support a conceptual screening of all the process options represented.

ii) They do not support the evolution of the final designs proposed in the conceptual design stage.

iii) They do not support specific issues for particular applications. For instance, they show a lack of flexibility to model heat transfer issues for heterogeneously catalysed gas-phase reaction systems.

To overcome the problems emphasized above, this work aims at the development of improved process representations. It also aims at the development of alternative synthesis methods to the current techniques. All the novel developments are presented in the following chapters except for the customisation of the optimisation algorithm, which is presented in this section.

The next sections of this chapter provide a detailed description of the different features of the forementioned building blocks and superstructure network representations. The customisation of the algorithm employed to optimise the networks is described towards the end of the chapter.

3.2 Generic Reactor / Mass Exchanger Unit

3.2.1 Description

The process synthesis representations presented in this work rely on basic synthesis units (Linke & Kokossis, 2003a) called generic reactor / mass exchanger (RMX) units. RMX units are employed for flexible representation of the elemental phenomena in chemical engineering: mixing, reaction, mass exchange and heat

transfer. They allow the compact representation of single-phase units (a reactor or a mass exchanger) or multi-phase units (a reactive / mass exchanger or any combination of the previous). The RMX unit (Figure 3.1) is made of compartments that define each of the phases present in the system. In each phase compartment different reciprocally excluding mixing patterns are included. Flow is fed into each phase compartment and when physically and technically possible, flows can cross phase boundaries. The mass flow across phase-boundaries is a result of phase equilibrium or diffusional transport. The outlet flow of a phase compartment can be recycled to itself, leave the RMX unit or be sent to the inlet of another phase compartment, again, when physically and technically possible. The mixing patterns represented in each compartment are well-mixed and plug flow. The plug flow behaviour typically modelled with differential equations is approximated, at early stages of the optimisation search, as a series of equal volume or equal catalyst load well-mixed units. Such approximation allows transforming the system into one that only contains algebraic equations (Kokossis & Floudas, 1990).

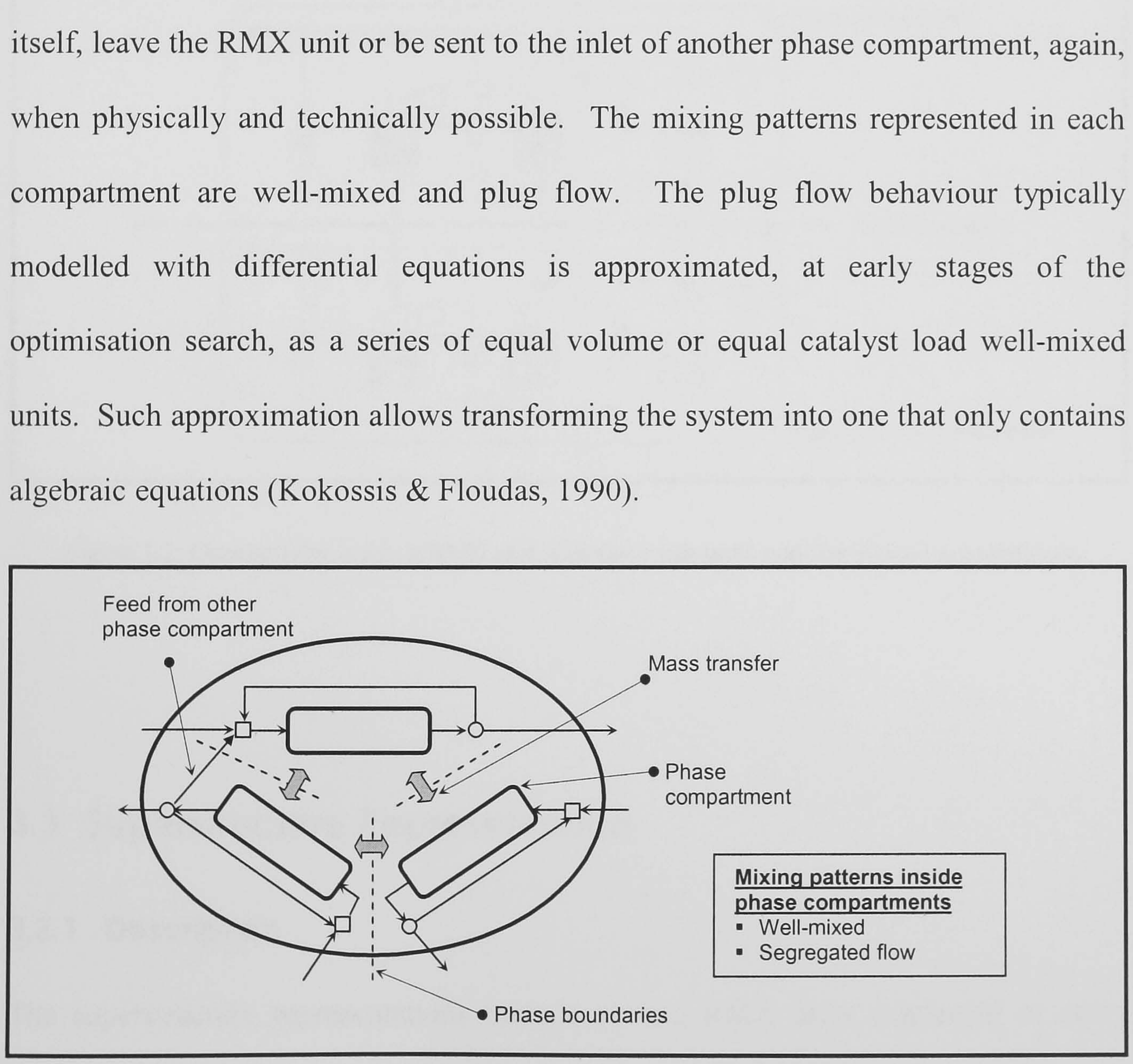

Figure 3.1: RMX unit with three phases.

Each phase compartment consists of sub-units arranged in series / parallel layouts. The interconnection between sub-units is possible through splitters and mixers. For RMX units with multiple phases, each phase compartment has a corresponding shadow phase[1] compartment (Mehta & Kokossis, 1997, 2000), which contains shadow matching sub-units (Figure 3.2). Mass transfer can only occur between matching sub-units. Each sub-unit is fed and the outlet flow can be recycled to itself, recycled to a previous sub-unit, sent to following sub-units or leave the unit.

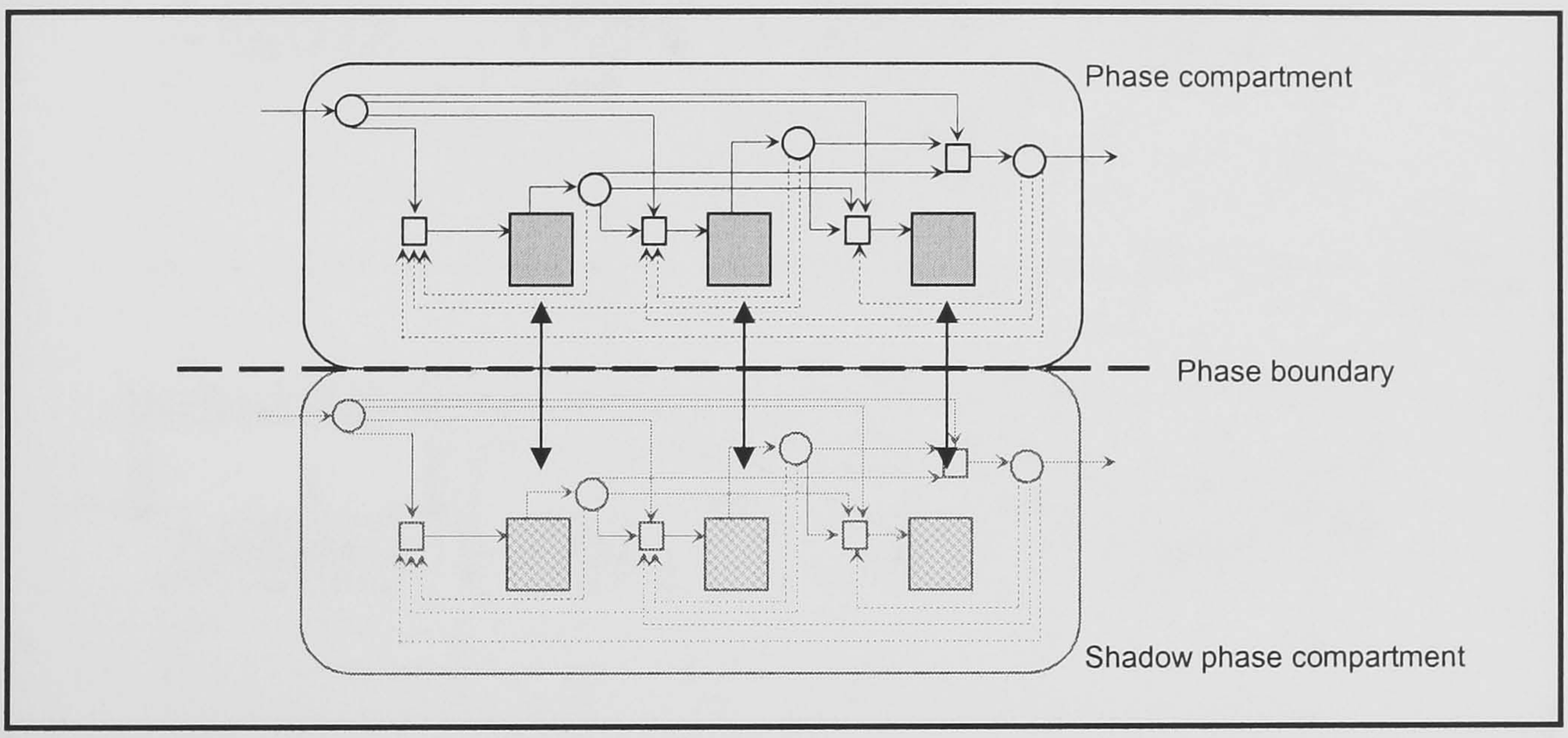

Figure 3.2: Connectivity inside a RMX unit with three sub-units and two phase compartments.

3.3 Superstructure Representation

3.3.1 Description

The superstructure representations include several RMX units connected in every physical possible way through mixers and splitters. Temperature policies, size of the units (volume or catalyst load), number of units and policies of feeding, bypassing

[1] A shadow reactor is the term given to a pair of homogeneous reactors in different phases (Mehta & Kokossis, 1997, 2000).

and recycling in the superstructure are degrees of freedom for the optimisation. Figure 3.3 shows a superstructure network representation with four RMX units including two phases in a co-current arrangement for all the units. The links between the phase boundaries represent exclusively the mass transfer links between matching sub-units of a phase compartment and its corresponding shadow phase compartment.

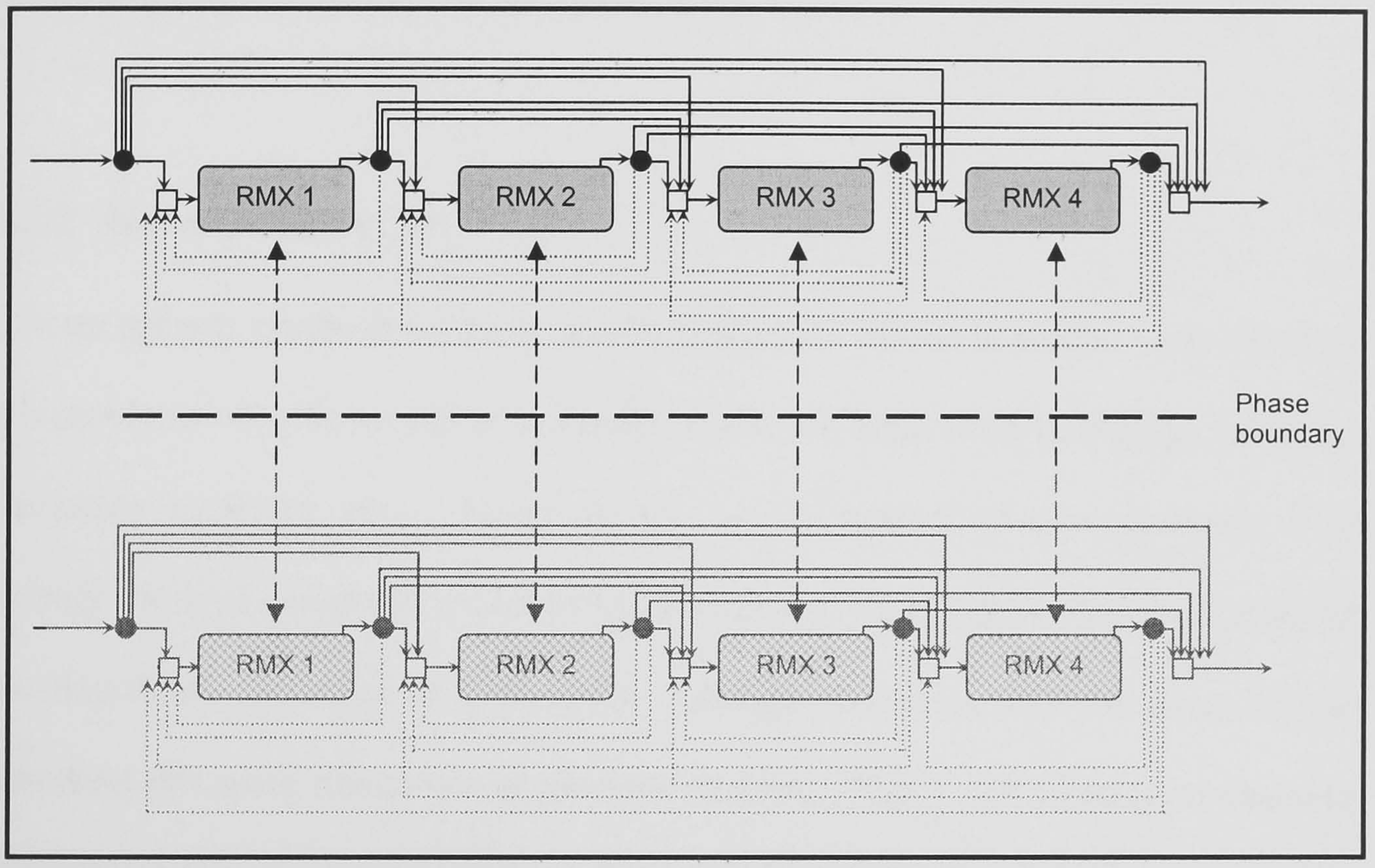

Figure 3.3: Superstructure representation containing four RMX units and two phases arranged in co-current.

The generality of the superstructure framework allows the identification of different structural design options that involve complex feeding and recycle / bypass strategies. In stochastic optimisation (see Section 3.4), the attainable solution space defined by a superstructure depends on its number of structural elements (here reactors, mass exchangers, reactive / mass exchangers). If the superstructure that contains the maximum number of possible structural units does not contain the required minimum number of structural elements required to represent the global optimal solution, the

method will lead to a sub-optimal solution. On the other hand, if too many structural elements are included in the superstructure, the size of the problem to be solved increases unnecessarily. Consequently, high computational efforts are required to obtain solutions, and convergence problems normally appear. The determination of the ideal superstructure size is a question still to be answered in process synthesis design and by no means within the scope of this work.

3.3.2 Network Recycles

Current process synthesis methods usually focus their efforts in single closely defined sub-problems of a flowsheet (*e.g.* reactor networks, separation networks, reactive / separation networks, etc.). However, the overall goal of process synthesis is to identify the best design for a problem that embraces all the areas (sub-problems) of the flowsheet. In order to capture the synergies between different zones of the flowsheet this work makes use of network recycles. Figure 3.4 presents an example of a process flowsheet comprising reaction and separation zones that are connected by a network recycle. The reaction zone is represented by a superstructure consisting of three single phase RMX units. The network recycle connects the outlet flow of the separation zone with the first RMX unit.

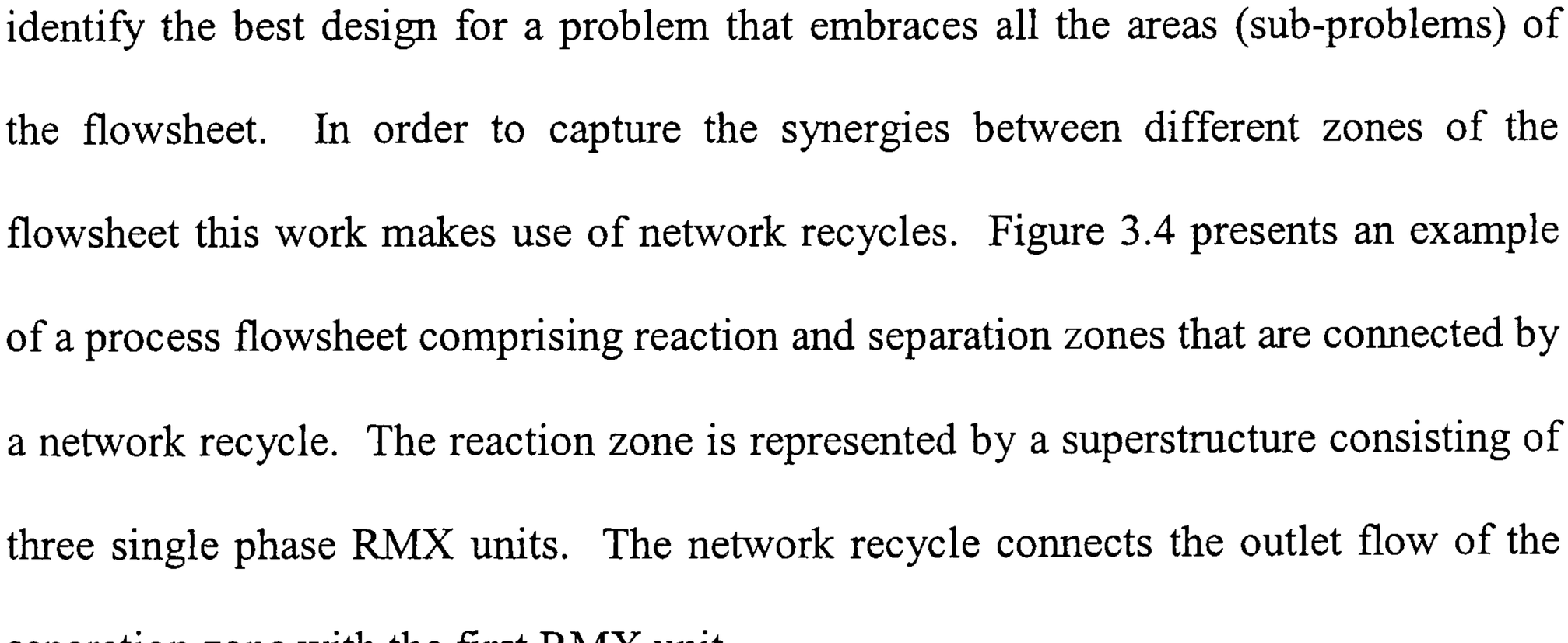

Figure 3.4: Superstructure representation with a network recycle.

3.4 Stochastic Optimisation Algorithm

3.4.1 Introduction

Stochastic optimisation techniques make use of randomness and statistical analysis to approach optimisation problems. A current state moves in a multi-dimensional space with a tendency to move towards directions that improve the objective function. Yet moving in directions against the improvement is also permitted. The transitions continuously occur until a termination criterion is met. The stochastic optimisation methods applied to reactor, reaction-separation and reactive / separation process synthesis are primarily Simulated Annealing (SA) and Tabu Search (TS). TS was firstly applied in the Chemical Engineering domain by Linke & Kokossis (2003a), who compared its performance to SA in the context of reaction-separation and reactive / separation process synthesis. They concluded that TS reaches optimal solutions faster than SA when they are applied to these synthesis problems. Accordingly, the selected stochastic tool to explore the superstructure representations is TS.

3.4.2 Tabu Search

TS (Glover, 1986) is an iterative stochastic search method that incorporates techniques from artificial intelligence. TS applications are found in the synthesis of heat exchanger networks (Lin & Miller, 2004a, b), in batch plant process design (Cavin *et al.*, 2004), and in reaction-separation and reactive / separation systems (Linke & Kokossis, 2003a, b).

At each iteration, a neighbourhood formed by a set of n random moves is explored around the current state (Figure 3.5). A move is an operation that alters the current state to another state. When moves are executed, the resulting states are simulated in order to search for improved performances with respect to the one that the current state has. A short-term memory is included in the form of a Tabu List which includes the latest moves. Reverse moves associated with them are rejected when applying the acceptance criteria. Like this, cycling in certain local optimum states is avoided. The state with the best objective function value in the latest explored neighbourhood becomes the initial state for the next iteration. In such a way, local optimum can be eluded as states with worse objective function values can be accepted and lead to states with more potential. Aspiration criteria are introduced to judge if a move is accepted despite being in the Tabu List. This condition permits taking into account moves in the list that may attain promising previously unvisited states.

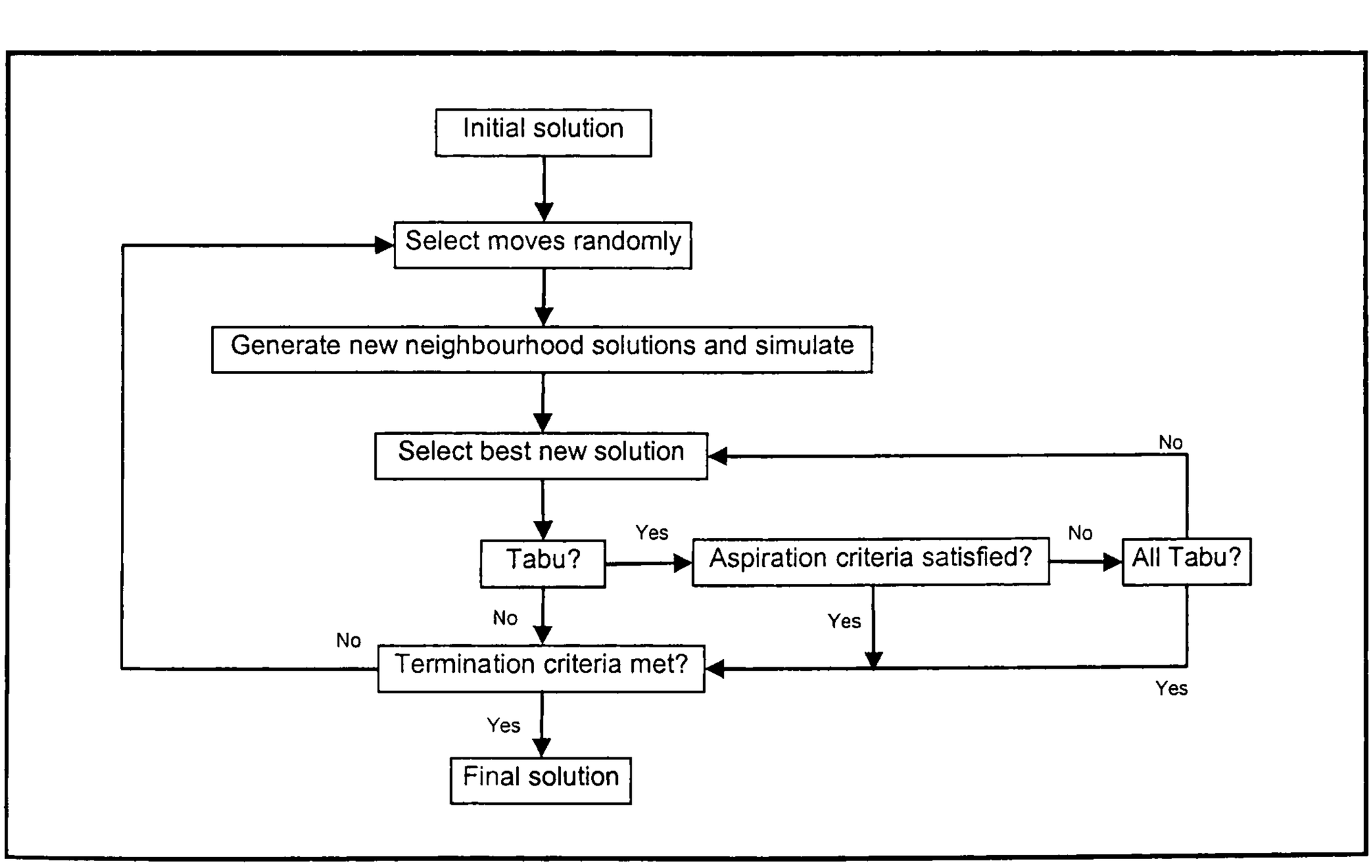

Figure 3.5: Tabu Search algorithm.

Two termination criteria for the TS are adopted in this work:

- A maximum number of iterations without objective improvement is completed.
- A total maximum number of iterations is completed. This criterion is included to avoid excessive elevated CPU times.

3.4.3 Mathematical Problem Formulation

The non-linear constrained optimisation problems treated in this research can be described as:

$$\text{Maximise } f(x) \quad \text{s.t.} \quad \begin{cases} g(x) \leq 0 \\ h(x) = 0 \\ x \in X \end{cases} \qquad \text{(Equation 3.1)}$$

where:

- f(x) is the objective function that can be linked to multiple performance functions (*e.g.* resulting amount of desired product in the reactive system in the form of yield or selectivity, economic potential of the system, etc.).
- g(x) are the inequality constraints that define specifications, bound process variables or constraints for feasible situations.
- h(x) are the equality constraints that describe the performance of the system (mass balances). They can take the form of either algebraic equations or differential equations.
- x are the process variables.

The non-linear system of equations is solved using the NEQLU from Chen & Stadtherr (1981).

3.4.4 Constraint Handling

The constraint handling detailed below only applies to the synthesis exercises presented in Chapter 5 and 6 (except where stated).

Constraints are involved in practically all optimisation problems found in chemical engineering and their presence can lead to multiple local optima. Besides, ratios of feasible regions to search spaces are usually very small and consequently it is vital to have an effective strategy to handle constraints. In this work, such strategy has been tailored depending upon the constraint type:

i) Components fed to the reactive system: Amounts of the components fed to the system depend on the network recycles. Therefore, after the simulation of every structure, solutions presenting violations on the component amount limits are not considered for the optimisation. The same rationale applies for the amount of components split in the separation sections and for the total flow that is recycled by the network recycles.

ii) Longitudinal temperature profile values, catalyst load / volume of generic units, total catalyst load / volume of the network and streams split fractions[2]: When a violation on these limits exists, the value of the violated variable is assigned to be its closest upper or lower limit.

[2] This constraint handling strategy also applies to Chapter 4.

iii) Constraints regarding heat transfer processes: i) radial temperature profile feasibility (see Section 6.3.2); ii) feasibility of the heat exchange strategy (see Section 6.2.2). None of the previous strategies proved to be effective to handle these constraints and another strategy based on constraint violations (CVs) has been developed. CVs are not included as penalties in the objective function but have influence on guiding the optimisation search. The superstructures employed in this work can be formed by several generic units and each generic unit can show CVs. In such a case, for a single type of constraint, the maximum CV among all generic units is selected as the representative value for that kind of constraint. If multiple CV types are present in a superstructure, the overall CV is obtained by adding all the representative CV types. The search is directed towards feasible regions by giving preference to feasible solutions over infeasible solutions according to:

- Any feasible solution (without CVs) has preference over any infeasible solutions (with CVs).
- If two infeasible solutions are compared, the one with lower CV has preference.
- If two feasible solutions are compared, the one with higher objective function value has preference.

3.4.5 Optimisation Degrees Of Freedom

Tabu Search explores the search space of feasible solutions by performing a series of random moves (alterations on the current state). As a result, moves are associated

with the degrees of freedom of the optimisation.

3.4.5.1 Generic Moves For All Superstructure Network Representations

General moves for all the superstructure network representations presented in this work include moves regarding:

- the addition / removal of generic units,
- the change of type of a generic unit,
- the change in size of a generic unit,
- the re-sizing of generic units while keeping the overall network size,
- the addition / removal of streams that interconnect generic units (recycles and bypasses),
- the change of source / sink position of the streams that interconnect generic units,
- the change in the amount of the streams that interconnect generic units,
- changes in temperature profiles for non-isothermal reactors, such as the change of the temperature profile direction (ascending / descending), or the modification of the parameters that define the temperature profile of a generic unit (see Section 5.2.2.4),
- the increase / decrease of the operating temperature for isothermal generic units (if temperature is a variable for optimisation).

3.4.5.2 Specific Moves For Heterogeneously Catalysed Gas-Phase Reaction Systems

For the development of the decision support framework presented in Chapter 5 and 6, superstructure network representations have been tailored for heterogeneously catalysed gas-phase reaction systems. Some new moves have been added and tailored for these systems to explore them more effectively. An important feature in these systems is that the feed can be formed by several streams. For such cases, the feed streams can be split and fed separately to the superstructure. Another significant feature is that combined moves have proved to allow the search to visit new regions when stuck in local optima. The specific moves for heterogeneously gas-phase reaction systems are:

- the general increase / decrease of the temperature of all the generic units that form the network,
- the decrease / increase of the temperature of all units and the increase / decrease of the size of all the generic units,
- the increase / decrease of the size of a generic unit and the decrease / increase of its temperature while increasing / decreasing the temperature of the rest of generic units,
- in the case where the amount of a network feed stream is a variable for optimisation:
    - the change in its amount,
    - the increase / decrease of its amount and the addition / removal of another feed stream bypass,

- the increase / decrease of its amount and the decrease / increase in the temperature of a generic unit,
- the increase / decrease of its amount and the decrease / increase in the temperature of all the generic units.

For heterogeneously catalysed gas-phase reaction systems, generic units represent reactors with catalyst particles inside (see Sections 5.2.2 and 6.4.2). The reactors represented can be continuously stirred tank reactors (CSTRs), fixed bed reactors (FBRs), multi-tubular reactors (MTRs) and fluid bed reactors (FLBRs). Some reactor type dependant moves have also been included:

- For all types of reactor:
  - Moves regarding the size of the catalyst particle (increase / decrease).
- For MTRs:
  - Moves regarding the diameter of tube of the reactor. The nominal sizes of the tubes considered for MTRs are found in Table 3.1. All the tubes have a schedule of 40. The generic units that represent FBRs and FLBRs are considered to be vessels rather than tubes. Their diameters are optimised without considering nominal sizes but finite steps on the sizes.

Table 3.1: Properties and dimensions for steel tubes with a schedule of 40.

Diameter Nominal -DN- (mm)	**Nominal Pipe Size -NPS-** (in)	**Diameter** (mm)	**Thickness** (mm)
10	3/8	12.523	2.311
15	1/2	15.798	2.769
20	3/4	20.929	2.870
25	1	26.645	3.378
32	1 1/4	35.052	3.556
40	1 1/2	40.894	3.683
50	2	52.501	3.912
65	2 1/2	62.713	5.156
80	3	77.928	5.486

  - Moves regarding the number of reactor tubes.

- For FLBRs:

  - Moves regarding the void fraction of the catalyst bed.

CHAPTER 4.

Rapid Screening Of Reactive-Extraction Processes

4.1 Introduction

Choosing a process option in the early stages of process design is challenging because of the large number of possible options, time limitations and a lack of conceptual support tools. Existing process synthesis tools are limited in several aspects:

i) Graphical methods are limited by dimensionality problems and modelling flexibility.

ii) Superstructure-based optimisation methods struggle to cope with highly non-linear kinetic and phase equilibrium models.

As a result, it is presently not possible to screen rapidly and reliably most process alternatives to compare their potential with that of other options.

This chapter presents a conceptual screening design tool to quickly assess the potential of reactive liquid-liquid extraction (RLLE) process options. RLLE is a process option with the potential to improve product yields for systems involving equilibrium reactions or reactions that are inhibited by product formation. The

developments presented by Linke & Kokossis (2003b) and by Pistikopoulos and collaborators (Papalexandri & Pistikopoulos, 1996; Ismail *et al.*, 1999, 2001) would typically consider the presence of two phases in the synthesis units when approaching the exploration of RLLE. As a consequence, even without being certain that the option is attractive from the synthesis point of view (*i.e.* whether it can deliver profitable designs or not), both techniques would require extremely long computational times to explore it. If the option proved to be unattractive at the termination of the conceptual design stage, remarkable amounts of time and resources would have been lost. The conceptual screening tool developed here aims to be located on top of the previous developments, in order to:

- Assist the designer in judging whether the process option has potential to improve process performances and therefore save time and resources if opposite.
- Extract knowledge about the process option (*e.g.* mixing patterns, bypassing and recycling policies, etc.) to use it in the later conceptual design stage (*e.g.* initialising optimisations), once the likely potential of the process option has been proved.

The tool proposes the mapping of the information regarding the solvent phase onto the superstructure model of a single-phase reactor network, in expense of an error when overestimating the transfer rate from the reactive to the solvent phase. The overestimated results can be very helpful if well-interpreted. The approach can deliver either much better performances than the single reactive system or similar ones to it. If the results of the conceptual screening prove to be promising, the next

conceptual design stage can be justified and the results can be employed in the tedious initialisation of more detailed optimisations. Otherwise, the synthesis option is disregarded for not being promising enough and great amounts of time and resources are spared in the design exercise.

4.2 Synthesis Network Optimisation

The mathematical formulation from Linke & Kokossis (2003b), from which the process representations for this application are developed, is found in Appendix 1. The basic elements of the superstructure network are the synthesis units. This section details the synthesis units and the superstructure generated from their combination.

4.2.1 Synthesis Units

The RMX units can represent here a reactor (CSTR or PFR), a reactive / separator or a mass exchanger. The latter two multi-phase options consider only counter-current contacting between the reactive and the mass separating agent (solvent) phases. Conceptual information regarding the design of the process in terms of feeding, bypassing, equipment volumes and mixing patterns for reactive phases is given by the approach. Information regarding the mass separating agent phase is mapped onto the superstructure model of a single-phase reactor network. Therefore, this phase is not physically represented in the RMX unit (Figure 4.1). The mapping is achieved using a transfer rate expression for liquid-liquid extraction (LLE) processes, which over-predicts possible mass transfer from the reactive phase to the solvent phase, based on its composition and solvent properties. Its development is detailed in the next section.

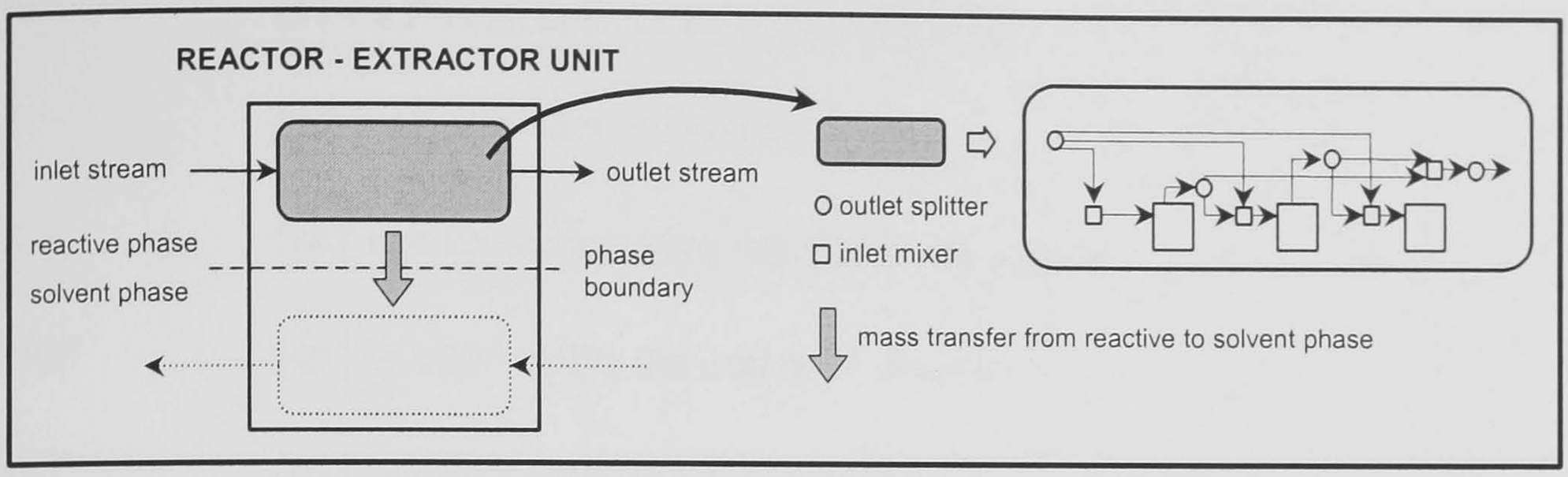

Figure 4.1: Reactive-extractive unit representation.

The mathematical formulation of the RMX units includes the balance equations around the mixers and splitters associated with the sub-units on which they consist. Previous to the formulation, some basic index sets for the superstructure elements are presented:

RM	{rm is a reactor / mass exchanger unit}
F	{f is a raw material source}
P	{p is a product}
SP	{sp is a splitter}
MI	{mi is a mixer}
CP	{cp is a component}
SK_{rm}	{sk is a well-mixed sub-unit in the unit $rm \in RM$ }
RX	{rx is a reaction}

Partitions of the previous basic index sets include the following subsets:

RM^A	$\{rm \mid rm \in RM$ is an active RMX unit$\}$
SP^A	$\{sp \mid sp \in SP$ is an active splitter$\}$
MI^A	$\{mi \mid mi \in MI$ is an active mixer$\}$

F^A {f | f ∈ F is an active raw material source}

P^A {p | p ∈ P is an active product}

RX^A_{rm} {rx | rx ∈ RX is an active reaction in rm ∈ RM^A }

SP^{RM}_{rm} {sp | sp ∈ SP^A splits the outlet of rm ∈ RM^A }

$SP^{IRM}_{rm,sk}$ {sp | sp ∈ SP^A splits the outlet of sk ∈ SK_{rm} of rm ∈ RM^A }

$MI^{RM}_{rm,sk}$ {mi | mi ∈ MI^A is a mixer prior to sk ∈ SK_{rm} of rm ∈ RM^A }

MI^{PRM}_{rm} {mi | mi ∈ MI^A is a final product mixer of rm ∈ RM^A }

Based on the previous sets, the rest of variables are:

$FF_{f,rm,cp}$ {flowrate of component cp in f ∈ F^A through mi ∈ $MI^{RM}_{rm,sk}$ }

$OUTR_{rm,cp}$ {flowrate of component cp through sp ∈ SP^{RM}_{rm} }

$OUTSK_{rm,sk,cp}$ {flowrate of component cp through sp ∈ $SP^{IRM}_{rm,sk}$ }

$INR_{rm,sk,cp}$ {flowrate of component cp through mi ∈ $MI^{RM}_{rm,sk}$ }

$FSF_{f,rm,sk}$ {fraction of the feed flowrates $FF_{f,rm,cp}$ through mi ∈ $MI^{RM}_{rm,sk}$ }

$SKP_{rm,sk}$ {fraction of $OUTSK_{rm,sk,cp}$ entering mi ∈ MI^{PRM}_{rm} }

$SRR_{rm,rm,sk}$ {fraction of $OUTR_{r,cp}$ entering mi ∈ $MI^{RM}_{rm,sk}$ }

$RXR_{rx,rm,sk}$ {specific reaction rate of rx ∈ RX^A_{rm} in sk ∈ SK_{rm} of rm ∈ RM^A }

$\upsilon_{rx,cp}$ {stoichiometric coefficient for component cp ∈ CP in rx ∈ RX^A_{rm} }

V_{rm} {volume of the RMX unit}

$\varepsilon_{rm,sk}$ {hold-up of sk ∈ SK_{rm} }

Next, the equations describing the well-mixed cells sk of the RMX units are presented. Inlet streams to the RMX units are raw material streams and outlet flows

from other units of the superstructure. Initially the balances of each mixer prior to the sub-units are:

$$\sum_{f \in F} FF_{f,rm.cp} \cdot FSF_{f,rm,sk} + PREV_{sk} + OUTR_{rm,cp} \cdot SRR_{rm,rm,sk} - INR_{rm,sk,cp} = 0$$

(Equation 4.2)

$$\forall\ f \in F^A, cp \in CP, sk \in SK_{rm}, rm \in RM^A$$

$$PREV_{sk=1} = 0$$

$$PREV_{sk \in SK_{rm} \setminus \{1\}} = OUTSK_{rm,sk-1,cp} \cdot \left(1 - SKP_{rm,sk-1}\right)$$

The balances of the sub-units are:

$$INR_{rm,sk,cp} + \sum_{rx \in RX_{rm}^A} \nu_{rx,cp} \cdot RXR_{rx,rm,sk} \cdot \frac{\varepsilon_{rm,sk} \cdot V_{rm}}{|SK_{rm}|} - OUTSK_{rm,sk,cp} + MTR_{rm,sk,cp} = 0$$

(Equation 4.3)

$$\forall\ cp \in CP, sk \in SK_{rm} rm \in RM^A, rx \in RX_{rm}^A$$

The balances of the final product mixer are:

$$\sum_{sk \in SK_{rm}} OUTSK_{rm,sk,cp} \cdot SKP_{rm,sk} - OUTR_{rm,cp} = 0$$

(Equation 4.4)

$$\forall\ cp \in CP, sk \in SK_{rm}, rm \in RM^A$$

Finally, the constraints on the split fractions are:

$$SRR_{rm,rm,sk} - 1 < 0$$

$$\forall\ sk \in SK_{rm}, rm \in RM^A$$

(Equation 4.5)

$$\sum_{sk \in SK_{rm}} FSF_{f,rm,sk} - 1 = 0$$

$$\forall\ f \in F, sk \in SK_{rm}, rm \in RM^A$$

4.2.2 Superstructure Generation

The synthesis units are connected in every possible physical combination in the reactive phase through mixers and splitters forming the superstructure representation (Figure 4.2).

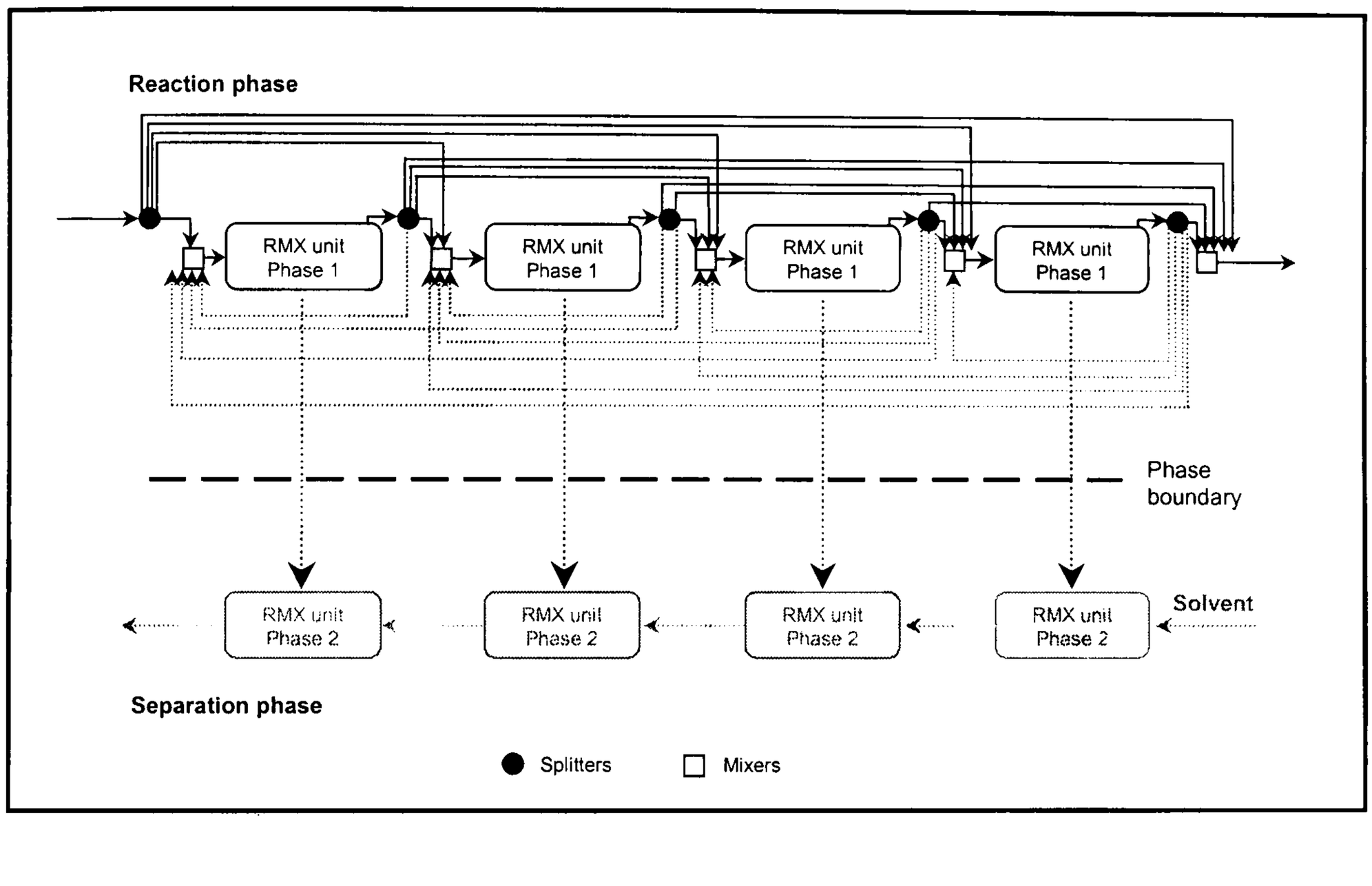

Figure 4.2: Superstructure representation for the RLLE approach.

In order to represent such connectivities, partitions of the previous basic index sets include the next subsets:

SP_f^F $\{sp \mid sp \in SP^A$ splits a raw material stream $f \in F^A\}$

SP_p^P $\{sp \mid sp \in SP^A$ splits a product stream $p \in P^A\}$

MI_p^P $\{mi \mid mi \in MI^A$ is a mixer of product $p \in P^A\}$

CP_p^P $\{cp \mid cp \in CP$ is a component in product $p \in P^A\}$

CP_f^F $\{cp \mid cp \in CP$ is a component in $sp \in SP_f^F\}$

CP_m^{RM} $\{cp \mid cp \in CP$ is a component in the outlet of $sp \in SP_m^{RM}\}$

All the variables employed in the superstructure formulation are defined over the previous index sets and subsets. The following set of variables includes the flow rates of each component through splitters and mixers:

$FD_{f,cp}$ {component flow rate through $sp \in SP_f^F$ }

$INPR_{rm,cp}$ {component flow rate through $mi \in MI_{rm}^{RM}$ }

$INP_{p,cp}$ {component flow rate through $mi \in MI_p^P$ }

$OUTP_{p,cp}$ {component flow rate through $sp \in SP_p^P$ }

The next set of variables includes the split fractions of streams connecting superstructure splitters to mixers:

$SFR_{f,rm,sk}$ {fraction of $FD_{f,cp}$ entering $mi \in MI_{rm,sk}^{RM}$ }

$SFP_{f,p}$ {fraction of $FD_{f,cp}$ entering $mi \in MI_p^P$ }

$SRP_{r,p}$ {fraction of $OUTR_{rm,cp}$ entering $mi \in MI_p^P$ }

$SPR_{p,rm,sk}$ {fraction of $OUTP_{p,cp}$ entering $mi \in MI_{rm,sk}^{RM}$ }

Finally for the transfer rate:

$MTR_{rm,sk,cp}$ {rate of mass transfer from reactive phase to solvent phase of component $cp \in CP$ in $sk \in SK_{rm}$ }

The mathematical formulation for the superstructure is defined as follows; initially, the balance equations around mixers $mi \in MI_{rm,sk}^{RM}$ prior to RMX units are:

$$\sum_{f\in F^A} FD_{f,cp}\cdot SFR_{f,rm,sk}+\sum_{rm\in RM^A} OUTR_{rm,cp}\cdot SRR_{rm,rm,sk}+PREV_{sk}+$$
$$\sum_{p\in P^A} OUTP_{p,cp}\cdot SPR_{p,rm,sk}-INR_{rm,sk,cp}=0$$

(Equation 4.6)

$$\forall f\in F^A, cp\in CP, sk\in SK_{rm}, rm\in RM^A, p\in P^A$$
$$PREV_{sk=1}=0$$
$$PREV_{sk\in SK_{rm}\setminus\{1\}}=OUTSK_{rm,sk-1,cp}\cdot\left(1-SKP_{rm,sk}\right)$$

For outlet mixers of RMX units $mi\in MI_{rm}^{PRM}$:

$$\sum_{sk\in SK_{rm}} OUTSK_{rm,sk,cp}\cdot SKP_{rm,sk}-OUTR_{rm,cp}=0$$

(Equation 4.7)

$$\forall cp\in CP, sk\in SK_{rm}, rm\in RM^A$$

For network product mixers $mi\in MI_{p}^{P}$:

$$\sum_{f\in F^A} FD_{f,cp}\cdot SFP_{f,p}+\sum_{r\in RM^A} OUTR_{rm,cp}\cdot SRP_{rm,p}-OUTP_{p,cp}=0$$

(Equation 4.8)

$$\forall f\in F^A, cp\in CP, rm\in RM^A, p\in P^A$$

4.3 Transfer Rate

The mapping of the information regarding the solvent phase onto the superstructure model of a single-phase reactor network is achieved with the help of a transfer rate expression for LLE processes. The expression allows removing the equations regarding the extractive phase from the system of equations to be solved. Therefore, the highly non-linear equations implied in LLE processes are eliminated. The resulting system of equations consists only of those equations regarding the reactive phase along with the transfer rate equations. Consequently, the size of the problem is

reduced approximately to that of a system where only reaction takes place, and quickly screening is therefore possible.

The transfer rate expression over-predicts possible mass transfer from the reactive phase based on its composition and solvent properties (solvent losses are assumed to be negligible). This transfer rate expression has been developed in the presented research from the work of Zheng *et al.* (1998), where a transfer rate expression for liquid-liquid systems with constant interfacial area cell with laminar flow was presented. The expression for the mass transfer MTR of the extracted component *cp* in the RMX unit *rm* and in the well-mixed cell *sk*, is:

$$MTR_{rm,sk,cp} = \frac{\dot{F}^{Carrier}_{out_{rm,sk}} \cdot K_{D_{cp}} \cdot R_{rm,sk}}{\left(1 + K_{D_{cp}} \cdot R_{rm,sk}\right)} \cdot C^{Carrier}_{rm,sk,cp,out} \cdot \left(1 - \exp\left(Param_{rm,sk,cp} \Big/ \dot{F}^{Carrier}_{out_{rm,sk}} \cdot \delta_{rm,sk}\right)\right)$$

(Equation 4.9)

where F_{out} is the volumetric flow (m^3/s) leaving the cell, K_D is the partition ratio, R is the volumetric ratio between extractive and reactive phase, C is the concentration (kg/m^3), δ is the interfacial layer thickness (m), Carrier refers to the reactive phase and the $Param_{rm,sk,cp}$ is given by:

$$Param_{rm,sk,cp} = -8.83 \cdot 10^{-5} \cdot \left(10\eta_{C\,rm,sk}\right)^{1.40} \cdot \left(10\eta_{S\,rm,sk}\right)^{0.38} \cdot \left(10V_{molar\,rm,sk,cp}\right)^{1.28} \cdot K_{D\,cp}^{1.64} \cdot F_{C\,rm,sk}^{-0.05} \cdot F_{S\,rm,sk}^{1.10} \cdot MW_{cp}^{0.36}$$

(Equation 4.10)

where η is the viscosity of the phase (cP), V_{molar} the molar volume ($m^3/kmol$), F is the mass flow (kg/h) entering the cell, MW the molar weight (kg/kmol), C refers to the reactive phase and S to the solvent phase.

To obtain the $Param_{rm,sk,cp}$ expression, a non-linear least squares regression has been developed in this research as follows. Initially, an extractive column modelled with detailed liquid-liquid equilibrium models is employed to rigorously simulate 24 different cases. All cases are taken from the ternary systems found in Table 4.1. Four different solvent flows for each one of the systems ranging from 20 to 2500 kg/h are employed. Then, with the assumption of an over-prediction of the amount of component transferred between 5 and 100 % in at least 95 % of the sections of the column, the $Param_{rm,sk,cp}$ values for the extracted components in the previous simulations are computed. With the resulting set of $Param_{rm,sk,cp}$ values, the regression is performed.

Table 4.1: Systems used in the estimation of the $Param_{rm,sk,cp}$ expression.

System	Extract	Raffinate	Solvent
1	Acetone	Toluene	Propanediol
2	Toluene	Heptane	Triethylene glycol
3	Ethanol	Water	Butanol
4	Acetic acid	Water	Cyclohexanol
5	Acetic acid	Water	Propylacetate
6	Benzene	Hexane	Ethylene-diamine

In order to known the values of the properties of the system under consideration very few calculations are needed. The interfacial layer thickness calculation follows Bollen (1999), and is related to the viscosity of the mixture (η_{mixt}) by:

$$\delta(\eta)_{rm,sk} = 10^{-2.75} - \eta^{0.75}_{mixt\ rm,sk} \qquad \text{(Equation 4.11)}$$

The viscosity of the mixture is assumed to depend on its molar composition (x):

$$\ln\left(\eta_{mixt\ rm,sk}\right) = \sum_{cp \in CP} x_{rm,sk,cp} \cdot \ln\left(\eta_{rm,sk,cp}\right) \qquad \text{(Equation 4.12)}$$

The partition ratio K_D is calculated as Pretel *et al.* (1994):

$$K_{D_{cp}} = \frac{\gamma^{\infty}_{cp,C}}{\gamma^{\infty}_{cp,S}} \cdot \frac{MW_C}{MW_S} \qquad \text{(Equation 4.13)}$$

where the activity coefficients γ^{∞} are calculated at infinite dilution using the UNIFAC liquid-liquid equilibrium group contribution model.

Six ternary systems (Table 4.2) were used to test the novel expression. Three different solvent flows ranging from 100 to 2500 kg/h were used for each of them. The transfer rates were overpredicted for all the cases.

Table 4.2: Systems used to test the $Param_{rm,sk,cp}$ expression.

System	Extract	Raffinate	Solvent	Transfer rate overprediction (%)[1]
1	Methanol	Water	Butanol	23, 25, 29
2	Propionic acid	Water	Ethyl-acetate	30, 31, 34
3	Toluene	Methyl-cyclo-pentane	Nitrobenzene	86,146, 79
4	Toluene	Heptane	Aniline	94, 97, 48
5	Benzene	Cetane	Aniline	77, 76,77
6	n-Propanol	Water	Benzene	58, 93, 6

[1] The overpredictions are for each one of the solvent flows tested.

4.4 Illustrative Examples

4.4.1 Production Of Ethanol

LLE is commonly used to recover ethanol from reactors where fermentations take place. Fournier (1986) considered improving the ethanol (EtOH) productivity by extracting it as it was being produced through glucose (Glu) by the following biological scheme:

$$Glu \xrightarrow{+Cells} EtOH + Cells \qquad \text{(Equation 4.14)}$$

Linke (2001) optimised reaction-separation and reactive / separation superstructures for the ethanol extractive fermentation using dodecanol as solvent. The objective function for this case was set to:

$$J = \frac{N_{EtOH,S}^2}{N_{Glu,C} \cdot N_S} \cdot 100 \qquad \text{(Equation 4.15)}$$

where N is expressed in kg/h and $N_{Glu,C} = \max(N_{Glu,C}, N_{min})$ with N_{min} =1.0 kg/h. Kinetics (Fournier, 1986) are given by:

$$r_{Cell} = 0.461 \cdot \frac{C_{Gluc} \cdot C_{Cell}}{C_{Gluc} \cdot 0.315} \left(1 - \frac{C_{EtOH}}{87.5}\right)^{0.36} \qquad \text{(Equation 4.16)}$$

$$r_{Gluc} = -9.452 \cdot r_{Cell} \qquad \text{(Equation 4.17)}$$

$$r_{EtOH} = 4.254 \cdot r_{Cell} \qquad \text{(Equation 4.18)}$$

A flow rate of 400 kg/hr of glucose in 1000 kg/hr of water is assumed as fresh feed. According to Fournier (1986), concentrations of ethanol higher than 87.5 kg/m^3

completely inhibit the reaction. Dodecanol is the solvent selected as it does not inhibit cell growth (Fournier, 1986).

Table 4.3 provides a comparison of the results obtained for the optimisation of two reference cases with those achieved by Linke (2001) using detailed equilibrium and mass transfer models. In both cases, the generic unit types were fixed and volumes, recycles and bypasses allowed changing. Volumes are practically identical, whereas CPU times for the novel approach presented are between three and four orders of magnitude smaller. As expected, the objective function values obtained in this work are higher for both cases.

Table 4.3: Comparison of results[1].

	Linke (2001)	**This work**	**Structure** (□Reaction -□Extraction)
Objective	3.66	4.45	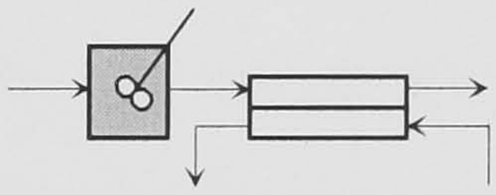
Glu. conversions (%)	60.5	60.5	
CPU (sec)	$1.50 \cdot 10^3$	4.48	
Units volume (m^3)	8.7 (reactor) 1.3 (extractor)	8.5 (reactor) 1.5 (extractor)	Classic design, S=1680 kg/h
Objective	6.46	11.77	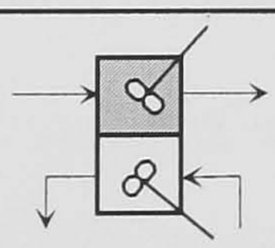
Glu. conversions (%)	84.2	90.9	
CPU (sec)	$1.81 \cdot 10^3$	0.66	
Units volume (m^3)	10.0	10.0	Extractive fermentor, S=1396 kg/h

[1] CPU times correspond to the optimisation of volumes, recycles and bypasses of the system. Number of units, solvent flow and reaction and / or extraction options were preset.

A complex network is optimised next. Up to three synthesis units are allowed in the network. The network volume is limited to ten cubic meters. A set of eleven runs each starting from different initial structures, is searched using TS. Dodecanol is also the selected solvent to perform the study. Results are found in Table 4.4. The

conceptual structures found in this work (screening results) show a clear trend of counter-current contacting with reactive separation dominating at the inlet and separation at the outlet of the reactive phase. Recycles in the first and second reactor are identified in the solutions. The final design candidate is delivered in approximately four minutes of CPU time. These conceptual results can be used to set up posterior detailed time-consuming optimisations. Consequently for demonstration purposes, a detailed optimisation exploration has been carried out using the structures identified in the screening stage as the starting points. The detailed exploration consists of two sets of searches. These optimisations employ the process representations presented by Linke & Kokossis (2003b), which were initially developed by Linke (2001) and that can be found in Appendix 1. In these searches, the option of having in each unit, reaction, extraction or both integrated is explored. The number of generic units with the flow patterns of the initial structures is maintained whilst allowing modifications to the flow rates, volumes of the units, stream connectivity (depending on the case), and direction of the flow. In the first optimisation problem, the stream connectivity is only allowed to change in the reaction phase. The objective reached is 1090 (Table 4.4). In the second search, the stream connectivity is allowed to change in both phases. The optimised structure yields an objective function value of 1230. Both solutions outperform the structure identified by Linke (2001) who allowed the same modifications as in the second case and presents an objective function value of 959. Linke (2001) reported very long CPU times and convergence problems for this case due to the complex models involved. The new approach assisted to identify, quickly, clear design trends at early stages of process design, reducing the search space and delivering final structures that are close to the optimal solutions. For these reasons, the detailed computationally

expensive superstructure optimisations started closer to the final solutions and with reduced search spaces to be explored. As a result, they became focussed and robustly identified better performances.

Table 4.4: Resulting structure for a complex network.

<table>
<tr><th colspan="4">Screening restults</th><th>Optimal structure[1] (□ Reaction - □ Extraction)</th></tr>
<tr><td></td><td>Average</td><td>Max</td><td>Min</td><td rowspan="2"> 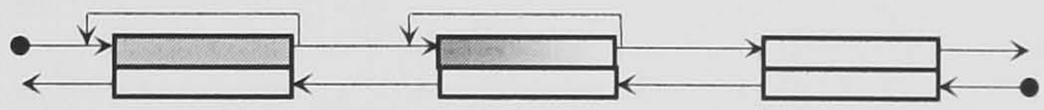
Volume (L) = 3.70 – 4.20 – 1.18
Solvent = 500 kg/h</td></tr>
<tr><td>Objective
CPU (sec)
Conversion</td><td>$6.48 \cdot 10^3$
216.6</td><td>$6.48 \cdot 10^3$
453.6
>99.9%</td><td>$6.48 \cdot 10^3$
69.3</td></tr>
<tr><td colspan="5">Detailed optimisation[1]</td></tr>
<tr><td colspan="5"><u>Recycle - bypass reaction phase</u>
Objective = 1090
Volume (L) = 2.48 - 6.16 - 1.34
Solvent = 2240 kg/h
CPU (h) = 194
Conversion > 99.9%
 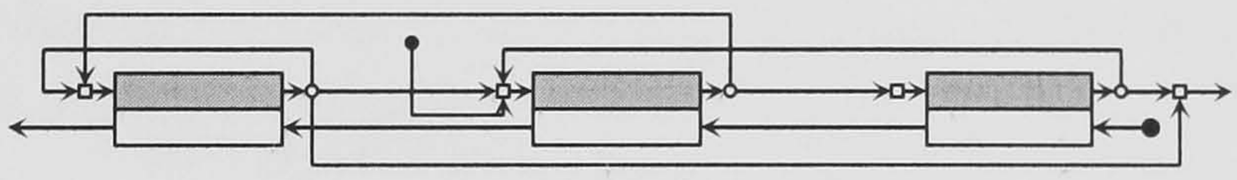 </td></tr>
<tr><td colspan="5"><u>Recycles - bypasses both phases</u>
Objective = 1230
Volume (L) = 4.33 - 5.13 - 0.54
Solvent = 2363 kg/h
CPU (h) = 210
Conversion > 99.9%
 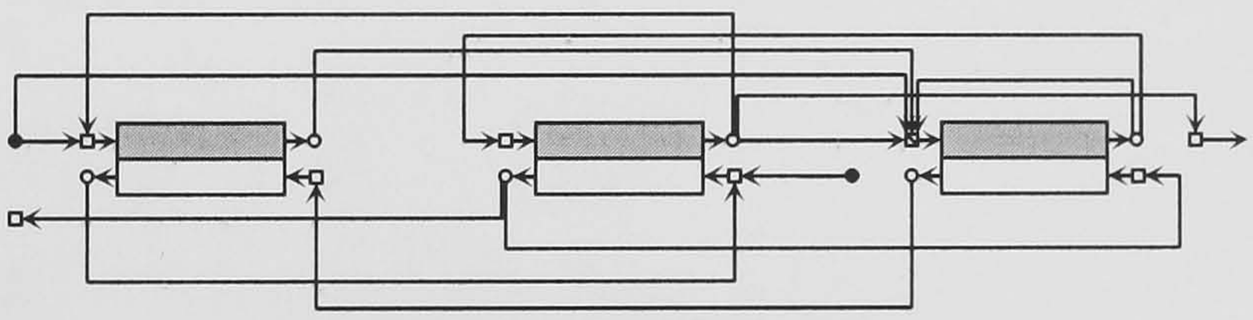 </td></tr>
</table>

[1] Best of 11 runs based on different initial structures.

4.4.2 Growth Of Saccharomyces Cerevisiae

The aim of this case study is to apply the novel approach to a highly complex biochemical system in order to show that within reasonable CPU times, RLLE, as a process design option, can be effectively screened. Lei *et al.* (2001) proposed a kinetic model that describes the growth of yeast on glucose and ethanol. The model consists on twelve reactions with highly non-linear reaction rates that are summarised in Figure 4.3. The reaction equations are in Table 4.5 and the related parameters in Table 4.6.

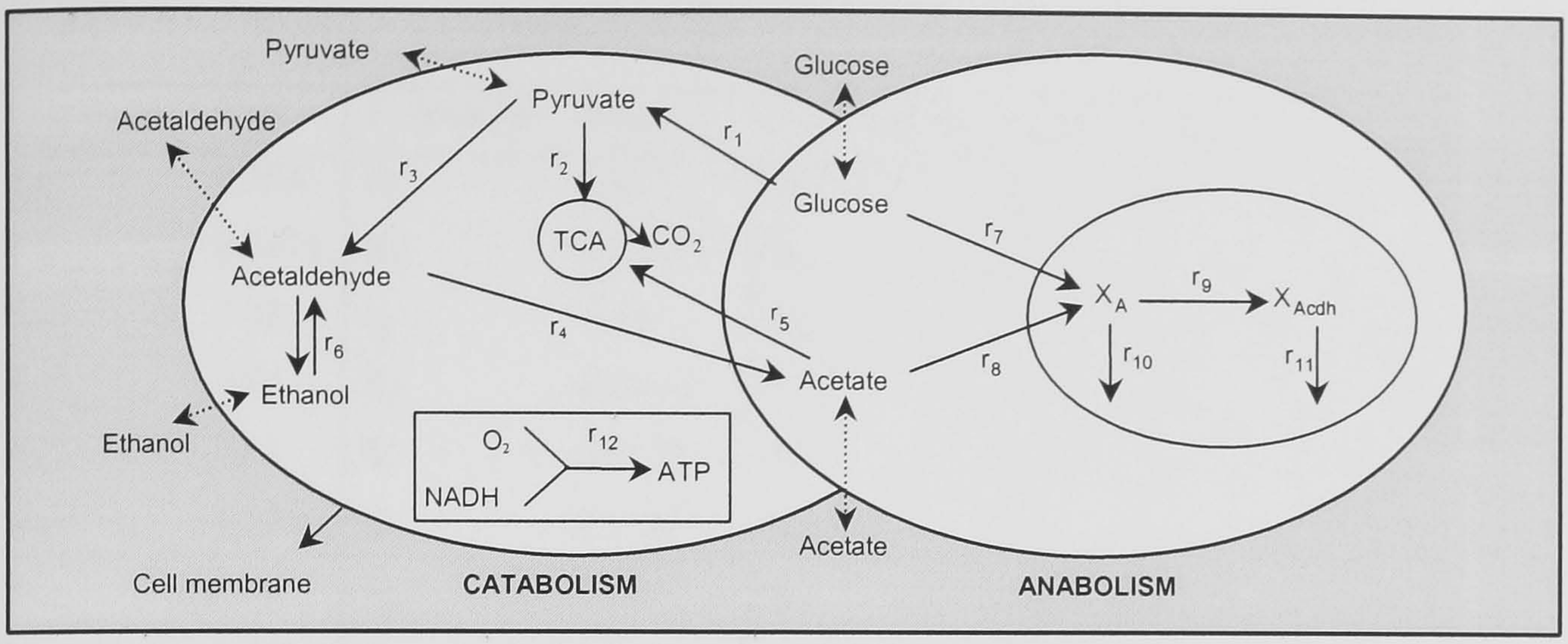

Figure 4.3: Saccharomyces Cerevisiae reaction path (Lei *et al.*, 2001).

Table 4.5: Rate expressions for Saccharomyces Cerevisiae growth reactions (Lei *et al.*, 2001).

Rate expressions	
$r_1 = k_{1l}\frac{s_{glu}}{s_{glu}+K_{1l}}X_a + k_{1h}\frac{s_{glu}}{s_{glu}+K_{1h}}X_a +$	$r_6 = k_6\frac{s_{acetald} - k_{6r}\cdot s_{EtOH}}{s_{acetald}+K_6+K_{6e}\cdot s_{EtOH}}X_a$
$k_{1e}\frac{s_{glu}}{s_{glu}\left(K_{1i}\cdot s_{acetald}+1\right)+K_{1e}}s_{acetald}\cdot X_a$	$r_7 = k_7\frac{s_{glu}}{s_{glu}+K_7}X_a$
$r_2 = k_2\frac{s_{pyr}}{s_{pyr}+K_2}\cdot\frac{1}{K_{2i}\cdot s_{glu}+1}X_a$	$r_8 = k_8\frac{s_{acetate}}{s_{acetate}+K_{5e}}\cdot\frac{1}{1+K_{5i}\cdot s_{glu}}X_a$
$r_3 = k_3\frac{s_{pyr}^4}{s_{pyr}^4+K_3}X_a$	$r_9 = \left(k_9\frac{s_{glu}}{s_{glu}+K_9}+k_{9e}\frac{s_{EtOH}}{s_{EtOH}+K_{9e}}\right)\cdot$
$r_4 = k_4\frac{s_{acetald}}{s_{acetald}+K_4}X_a\cdot X_{Acdh}$	$\frac{1}{1+K_{9i}\cdot s_{glu}}X_a + k_{9c}\frac{s_{glu}}{s_{glu}+K_9}X_a$
$r_5 = k_5\frac{s_{acetate}}{s_{acetate}+K_5}X_a +$	$r_{10} = k_{10}\frac{s_{glu}}{s_{glu}+K_{10}}X_a + k_{10e}\frac{s_{EtOH}}{s_{EtOH}+K_{10e}}X_a$
$k_{5e}\frac{s_{acetate}}{s_{acetate}+K_{5e}}\cdot\frac{1}{1+K_{5i}\cdot s_{glu}}X_a$	$r_{11} = k_{11}X_{Acdh}$

r_{12} is not modelled with a kinetic expression since it is assumed that all NADH produced is converted into ATP instantaneously

Table 4.6: Parameters for the kinetics of Saccharomyces Cerevisiae growth (Lei *et al.*, 2001).

Parameter	Value	Parameter	Value	Parameter	Value	Parameter	Value
k_{1h}	0.584	k_3	5.81	K_6	0.034	K_{9i}	25
K_{1h}	0.0116	K_3	$5.0 \cdot 10^{-7}$	k_{6r}	0.0125	k_{9e}	$3.99 \cdot 10^{-3}$
k_{11}	1.43	k_4	4.80	K_{6e}	0.057	k_{10}	0.392
K_{11}	0.94	K_4	$2.64 \cdot 10^{-4}$	k_7	1.203	K_{10}	$2.30 \cdot 10^{-3}$
k_{1e}	47.1	k_5	0.0104	K_7	0.0101	k_{10e}	$3.39 \cdot 10^{-3}$
K_{1e}	0.12	K_5	0.0102	k_8	0.589	K_{10e}	$1.80 \cdot 10^{-3}$
K_{1i}	14.2	k_{5e}	0.775	k_9	0.008	k_{11}	0.02
k_2	0.501	K_{5e}	0.10	K_9	$1.0 \cdot 10^{-6}$		
K_2	0.002	K_{5i}	440	k_{9e}	0.0751		
K_{2i}	0.101	k_6	2.82	K_{9e}	13		

Single-phase reactor networks were synthesised for this system by Ashley (2004). For comparison purposes, the same representation for the reactive phase used by Ashley (2004) is adopted here. The study starts from ten different initial structures, allowing a maximum number of units of four, a maximum unit volume of 30 litres and a maximum network volume of 50 litres. The Tabu searches are performed with a neighbourhood size of ten. The feed flow rates are the same as for Ashley (2004), which are taken from Lei & Jorgensen (2001): glucose 14 g/s, ethanol 0.13 g/s, biomass X 0.002 g/s, X_a 0.1 g·(g biomass X)$^{-1}$, X_{Acdh} 0.0075 g·(g biomass X)$^{-1}$ in 1 kg/s of aqueous solution. Ethanol is once more the desired product and its total yield the objective. Dodecanol is again the selected solvent to perform the study.

RLLE as a process design option could be screened below 15 hours of average CPU time (Table 4.7). The searches of the RLLE network and of the single-phase reactor network employ very similar CPU times. Therefore, the suitability of the novel method to decide whether RLLE is a potential process design option is clearly proved. In a similar CPU effort, RLLE as a process design option was efficiently screened and

its potential effectively assessed. The search quickly proved that RLLE with dodecanol as solvent is not an attractive process design option for this case. The small improvement obtained in the maximum performance with respect to the single-phase reaction system, suggests that setting up and conducting posterior time-consuming detailed optimisation searches, do not need to be considered as no relevant improvement in performance is expected.

Table 4.7: Results for Saccharomyces Cerevisiae case study.

	Average	Max	Min	Optimal structure[1] (□ Reaction - □ Extraction)
Ashley (2004)				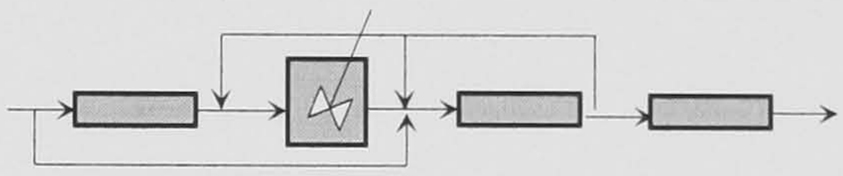
Objective	5.08	5.16	4.91	
CPU (h)	14.79	34.73	3.14	Volume (L) 5.93 0.77 2.76 1.17
This work				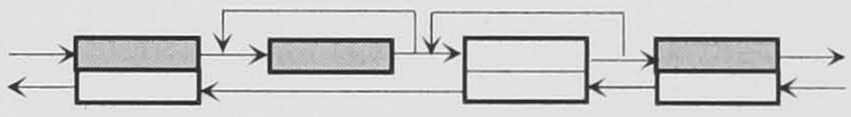
Objective	5.08	5.24	4.84	
CPU (h)	14.39	29.38	3.85	Volume (L) 2.54 4.67 17.3 0.53 Solvent (kg/hr) 300[2]

[1] Best of 10 runs based on different initial structures.
[2] The highest average is obtained with 300 kg/hr of solvent. Sets of 10 runs have been performed with 10, 50, 100, 300, 700 and 1000 kg/hr of solvent. The highest OFV is 5.29, which is obtained with a solvent flow of 700 kg/hr.

4.5 Conclusions

A novel approach to screen quickly and reliably RLLE networks has been presented. The approach is based on mapping the information regarding the mass separating agent (solvent) phase onto the superstructure model of a single-phase reactor network. The novel method has been applied to two biochemical examples of very different complexity. The approach has been proved to be highly computationally efficient as compared with typical reactive separation superstructure-based optimisation approaches that include complex and detailed liquid-liquid equilibrium and mass

transfer models. The accuracies of the approach appear to be adequate for high-level decision-making at early stages of process design.

CHAPTER 5.

A Decision Support Framework For Synthesis Of Heterogeneously Catalysed Gas-Phase Reaction Processes: Systematic Identification Of Conceptual Process Designs

5.1 Introduction

The current sequential nature in the design of chemical processes impedes experimental engineers to have process design information when developing kinetic models. The kinetic modelling team elaborates a model that is given to the process synthesis engineers who identify optimal process designs with it (Figure 5.1). Optimisation results are likely to identify solutions in regions in which the experimental model has not been validated (*i.e.* temperature ranges, concentration of components). There is for that reason, either a design compromised by kinetic reliability or a project delay because some extra experiments must be performed in order to validate the model in the new regions identified, after the kinetic development has long been concluded.

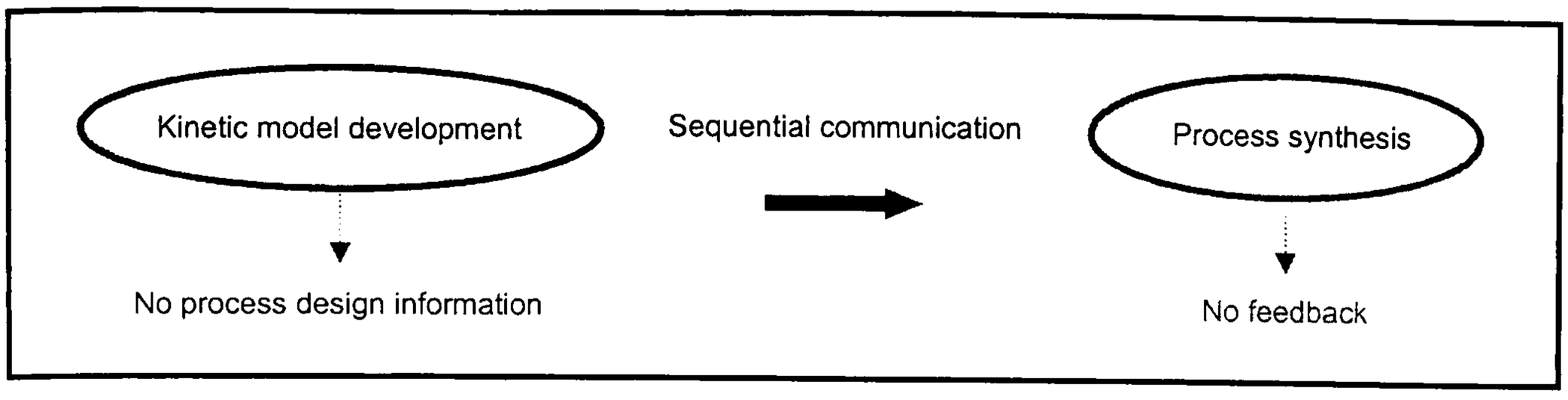

Figure 5.1: Sequential communication between the kinetic model development and the process synthesis.

To break the sequential nature of this practice and allow the existence of a bidirectional flow of information, it would help the kinetic model development to be guided towards the context of the overall design goal (*e.g.* integration of catalyst performance with reactor and separation systems design). The integration of the kinetic model development and the process synthesis activities (Figure 5.2), would seek for the perfect match between the regions identified by the optimisation and the regions for which the model is validated. However, before establishing an effective communication framework that integrates both systems, process synthesis engineers must address the identification of the best process design candidate.

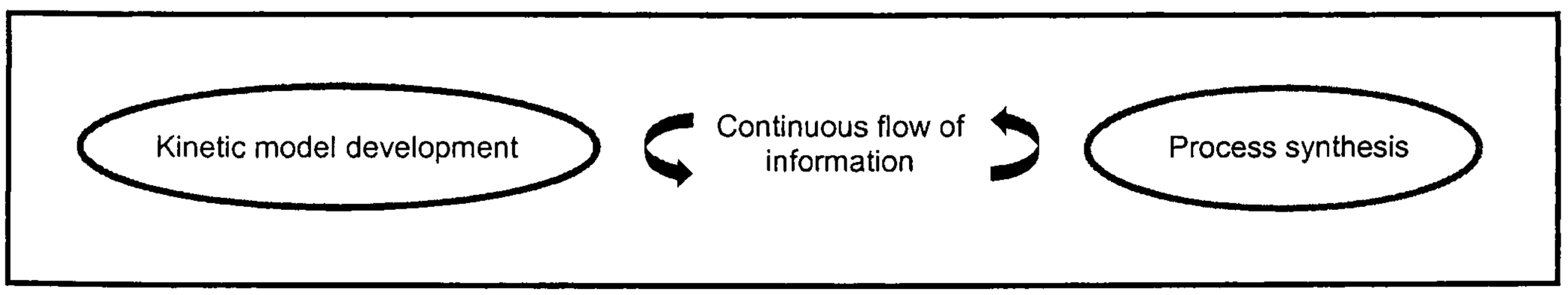

Figure 5.2: Communication framework that integrates the kinetic model development and the process synthesis.

For their technical and economic importance in the process industry, heterogeneously catalysed gas-phase reaction processes have been chosen to illustrate the developments presented in this work. Usually, economic reasons dictate that gas

reaction processes cannot involve systems where separators are placed between reactors (*e.g.* reactor-separator-reactor-separator-reactor). Only membrane separations are excluded from this statement. The reactions involved in gas reaction systems take place at very different conditions from which the separations occur. Reactions occur in the gas-phase at high temperatures whereas separations (except in membrane separation) require liquid phases. An intermediate separation between two reactors would require a gas cooling process and / or a condensing process, previous to the separation in liquid phase. Both processes involve expensive equipments and operations:

i) For a total condensation, particularly expensive equipments would be needed (*e.g.* cryogenic exchangers).

ii) For a partial condensation, the gases would be cooled in a heat exchanger, let-down in a pressure valve and finally flashed in a drum.

Whatever the case, heating utilities and heat exchangers would be necessary after the separation process to evaporate the liquids again into gases, so they could be sent to the next reactor. Even without considering the cost of the actual separations, it is obvious that such systems are not economically viable for gas reaction processes. Only the use of reactor-separator-recycle systems appears to be economically viable for such processes.

Reactor-separator-recycle systems are very complex in terms of possible combinatorial options. Process synthesis knowledge can be used to eliminate numerous impractical connections in this type of systems. However, even with such simplified representations, current process synthesis technologies cannot afford to

treat the full complexity of the kinetic models together with the full complexity of the process models (*i.e.* reactor models, separation models, etc.). On one side, kinetic models enclose key information on how species are formed and consumed inside reactors and their simplification cannot be easily addressed while still capturing all major trade-offs. Such simplification still constitutes an unresolved research problem. On the other hand, process models can be simplified to plain models, which approximate the performances of complex models reasonably well. But even with such simplifications, existing process synthesis methods cannot handle the mathematical complexity inherent in the kinetic models, and cope with the combinatorial complexity of reactor-separator-recycle systems when complex cases are approached. Besides, the process representations in which they rely either embrace too many options that unnecessarily increase the numerical complexity of the system, or do not embrace options that proficiently represent how fundamental processes (*i.e.* heat and mass transfer) occur in these systems. Moreover, the representations are unable to handle practical process constraints found in practical applications (*e.g.* limitations in the maximum amount of heat that the exchange utilities can add/remove to/from the reactive system, limitations in the amount of oxygen concentration at high temperatures which can create explosions, etc.). For all these reasons, the systematic identification of optimal design candidates for heterogeneously catalysed gas-phase reaction systems is nowadays virtually impossible.

In order to approach the synthesis exercise of such reaction systems, this research presents a decision support framework (DSF) that relies on a superstructure-based optimisation approach. The DSF is extended across the **conceptual stage** and the

design stage introduced in Chapter 1. The DSF relies on the appropriate balance along the synthesis exercise between the number of options (*i.e.* combinatorial complexity) and the accuracy of the models employed. Due to the impossibility of reducing the complexity of the kinetic models, the synthesis strategy presented here only applies to process synthesis models. At the beginning of the synthesis exercise, the process structure is unknown and the combinatorial complexity is high. Therefore, simple models are employed. Towards the end, the knowledge that has emerged about the process structure is employed to reduce the structural complexity and the addition of more detail in terms of process models can be afforded.

The current chapter presents the beginning of the synthesis exercise (high combinatorial complexity with simple process models). The synthesis developments presented here form part of the **conceptual design stage.** Compact process representations, in which the DSF (Figure 5.3) counts on, have been customised for heterogeneously catalysed gas-phase reaction systems and have been adapted to include practical constraints that are found in practical applications. The DSF also relies on a multi-level approach that aims at the development of design performance targets and the identification of interactions between design performance and design complexity.

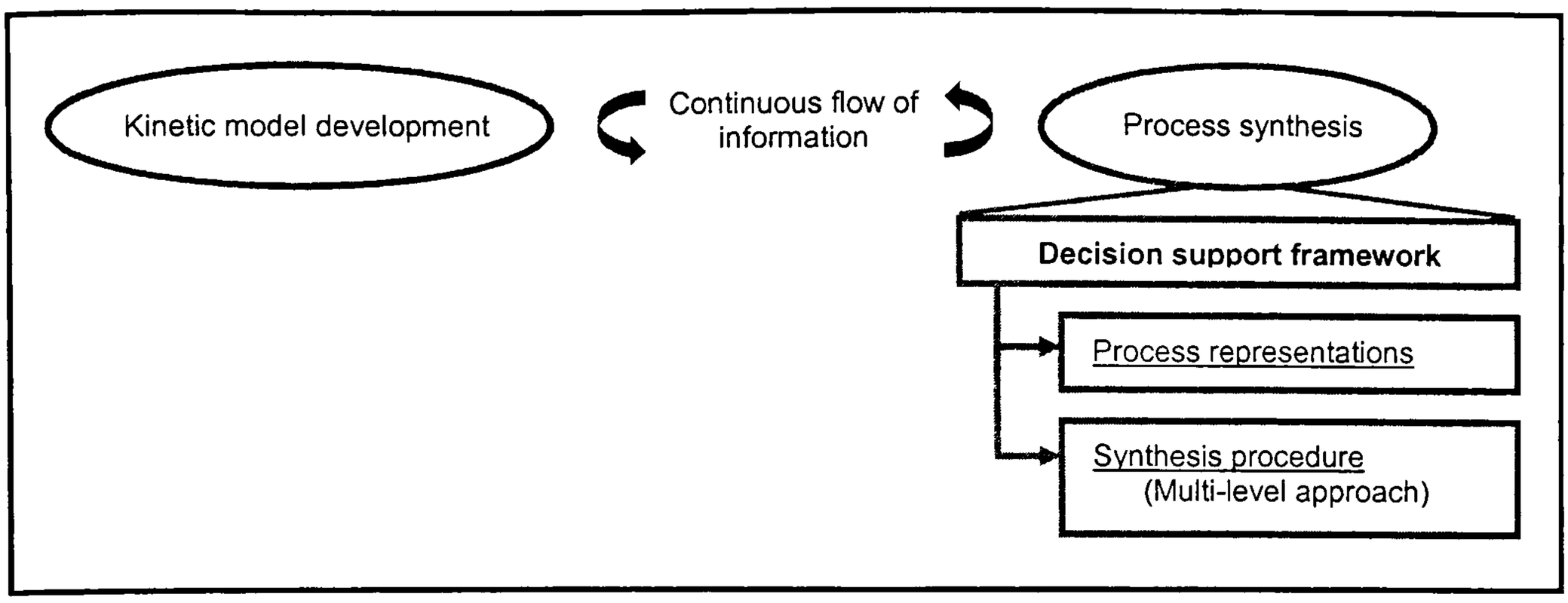

Figure 5.3: Decision support framework within the communication framework that integrates the kinetic model development and the process synthesis (1).

The knowledge obtained from the conceptual design stage can be used in later concreter stages. This is exploited in Chapter 6 where the balance of the numerical and combinatorial complexities along the synthesis process is at the other end: low combinatorial complexity with high model accuracy. The multi-stage synthesis strategy presented in Chapter 6 is extended across the **design stages** introduced in Chapter 1 (Figure 1.1). In the multi-stage strategy, the few designs resulting from the multi-level approach are carefully explored by employing more detailed and computational demanding reactor models.

The following sections detail the process representations, the performance evaluation, the network optimisation and the multi-level approach employed for the DSF. Finally, a case study used to illustrate the developments is presented.

5.2 Process Representations

5.2.1 Introduction

The superstructure process representations employed by the DSF have been tailored for heterogeneously catalysed gas-phase reaction systems. To allow the screening of a large number of design options, conceptual process synthesis representations must be used to cope with:

i) the large combinatorial size of the search space involved in reactor-separator-recycle systems;

ii) the elevated mathematical complexity of the process models (*i.e.* reactor models, separator models);

iii) the non-linearites of experimental kinetic models.

The main design decisions that need to be made for heterogeneously catalysed gas-phase reaction systems include reactor design and operation, interactions via recycles between reaction and separation systems, and separation system design and operation. The reaction representations include combinations of generic units that embed options relating to mixing (plug flow or well-mixed), temperature policies, mass of catalyst and constraints regarding heat management and component concentrations. The energy management constraints are derived from physical limits that are present in different heterogeneously catalysed reaction system designs. Concentration limits are incorporated as design constraints and are set with respect to different components. Separation options can be represented in aggregated form to decompose the design problem. Energy and area targets are used to assess the performance of the heat exchanger network.

In the next section, a detailed explanation of the process representations is given. The representations are structured in reactor representations, separation representations and energy integration.

5.2.2 Reactor Representation

5.2.2.1 Reactor Modelling

The models employed for the representation of catalytic reactors are:

- Continuously stirred tank reactor (CSTR).
- Approximation of the pseudo-homogeneous one dimensional plug-flow reactor (PFR) model without radial temperature profile approximation. The PFR approximation relies on assuming the plug-flow behaviour as the behaviour that a series of isothermal equal catalyst load sub-CSTRs (Kokossis & Floudas, 1990) would have. Fixed-bed reactors (FBRs) or multi-tubular reactors (MTRs) can be represented by this approximation.

Theoretically, if catalyst pellets are considered, internal mass transfer limitations inside the pellets must be expected. However, as happens in all the cases considered in this work, internal diffusion processes are either neglected or have been lumped into the kinetic expressions (Sections A2.2 and A3.3). If internal diffusion cannot be neglected for the specific case study or is not lumped in the kinetic expressions, instead of a pseudo-homogeneous PFR model, a more detailed heterogeneous model that takes into account the diffusion in the catalyst pellet should be employed. Such situation has not been explored in this research.

5.2.2.2 Pressure Losses Inside Reactors

The pressure losses inside the reactors vary depending on the type of reactor. The pressure losses for CSTRs are assumed to be a typical value of 0.5 bars. On the other hand, the pressure losses for the approximation of the pseudo-homogeneous one-dimensional PFR model without radial temperature profile approximation are considered to follow Ergun (1952). The Ergun expression models the pressure losses (P_t) along the length of the reactor (z) as:

$$-\frac{\delta P_t}{\delta z} = f \cdot \frac{\rho_g \cdot u_0^2}{d_p} \qquad \text{(Equation 5.1)}$$

where f is the friction factor, ρ_g is the gas density, u_0 is the superficial velocity and d_p is the diameter of the catalyst particle. If the reactor is discretised in segments, the pressure losses can be represented as:

$$\frac{\Delta P_t}{\Delta z} = f \cdot \frac{\rho_g \cdot u_0^2}{d_p} \qquad \text{(Equation 5.2)}$$

Ergun proposed the following expression for the friction factor:

$$f = \frac{1-\varepsilon}{\varepsilon} \cdot \left[a + \frac{b \cdot (1-\varepsilon)}{Re} \right]$$
$$a = 1.75$$
$$b = 150 \qquad \text{(Equations 5.3)}$$

where ε is the void fraction of the catalyst bed and Re is the Reynolds number.

5.2.2.3 Reactor Constraints

Certain constraints are particular to the heterogeneously catalysed gas-phase reaction systems. They can be divided in:

- Concentration constraints: Limits on the amounts of specific components have been incorporated to avoid situations where excessive amounts of them can lead to dangerous scenarios (*e.g.* high concentrations of oxygen at elevated temperatures), produce fouling, etc. Concentration limits can be directly incorporated as constraints in the problem formulation.

- Temperature and heat transfer constraints: Heterogeneously catalysed gas-phase reactions normally occur at high temperature. Problems arise when heat needs to be removed from the system as fast as it is produced or when it needs to be supplied as fast as it is required. Temperature and heat management issues are addressed in more detail in Sections 5.2.2.4 and 5.2.2.5. For the appropriate management of heats and temperatures, the heat transfer phenomena occurring inside the catalytic reactors need to be addressed in depth. Detailed heat transfer representations for catalyst beds are the focus of Section 5.2.2.6.

5.2.2.4 Reactor Temperature Profiles

For each solution that the optimisation algorithm searches, temperature profiles are imposed to the reactors and then mass balances are converged (simulation step). CSTRs are considered to be isothermal whereas for those reactors with plug-flow behaviour, the longitudinal temperature profiles considered are: flat (isothermal), linear (increasing or decreasing), exponential, logarithmic and peaked (Figure 5.4).

The implementation of the longitudinal temperature profiles follows the work by Metha & Kokossis (2000).

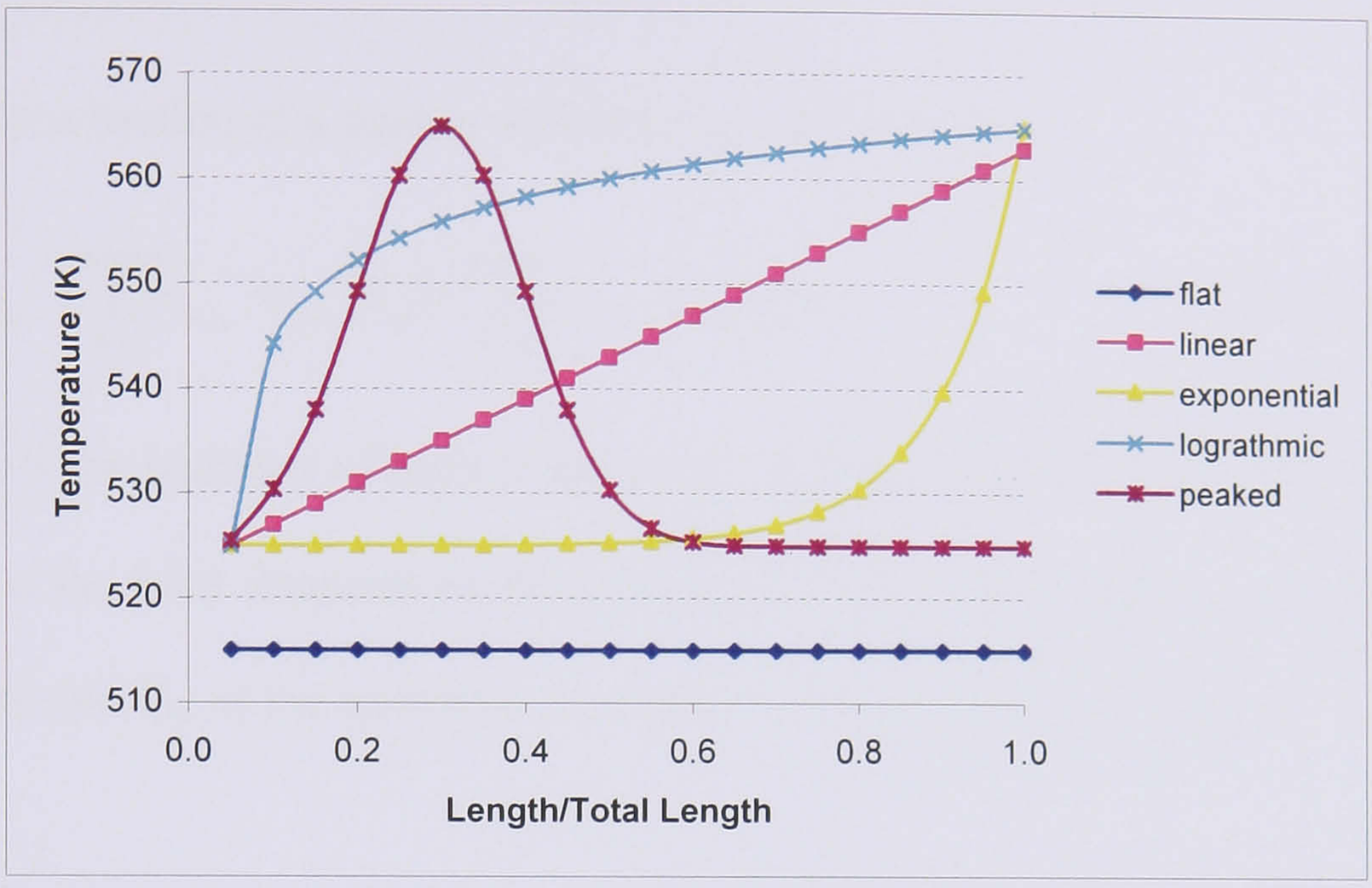

Figure 5.4: Temperature profiles (Mehta & Kokossis, 2000).

5.2.2.5 Reactor Heat Transfer Modelling - Heat Transfer Limits

Practical constraints for heat transfer, developed from physical limits of catalytic reactors, are included in the reactor representations. In order to maintain the imposed temperature profile (see Section 5.2.2.4), the amount of heat to be exchanged between every reactor ($q_{reactor}$) / section of reactor (q_{isc}) and its utility media has to be physically reachable. To ensure that, once the simulation step is finished two heat balances are performed. First of all, a heat balance is carried out within the streams leaving and being fed to each reactor / section of reactor:

- For a reactor:

$$q_{reactor} = \sum_{ic=1}^{ncomp} m_{ic,reactor} \cdot h_{ic,reactor}\left(T_{reactor}\right) - \sum_{ic=1}^{ncomp} m_{ic,in\_reactor} \cdot h_{ic,in\_reactor}\left(T_{in\_reactor}\right)$$

(Equation 5.4)

- For the first section of a reactor:

$$q_{isc=1} = \sum_{ic=1}^{ncomp} m_{ic,isc=1} \cdot h_{ic,isc=1}\left(T_{isc=1}\right) - \sum_{ic=1}^{ncomp} m_{ic.in\_reactor} \cdot h_{ic.in\_reactor}\left(T_{in\_reactor}\right) \qquad \text{(Equation 5.5)}$$

- For a section of a reactor different than the first one:

$$q_{isc} = \sum_{ic=1}^{ncomp} m_{ic.isc} \cdot h_{ic.isc}\left(T_{isc}\right) - \sum_{ic=1}^{ncomp} m_{ic.isc-1} \cdot h_{ic.isc-1}\left(T_{isc-1}\right) \qquad \text{(Equation 5.6)}$$

where h_{ic} is the enthalpy of each component, m_{ic} is the molar flow of each component, $T_{in\_reactor}$ is the inlet temperature of the reactor, $T_{reactor}$ is the operating temperature of the reactor and T_{isc} is the operating temperature of each section of reactor.

Next, another heat balance is performed between each reactor / section of reactor and its corresponding utility media:

- For a reactor: $q_{reactor} = U \cdot A \cdot \left(T_{reactor} - T_{utility}\right)$ (Equation 5.7)
- For a section of reactor: $q_{isc} = U \cdot A \cdot \left(T_{isc} - T_{utility\_isc}\right)$ (Equation 5.8)

where U is the overall heat transfer coefficient, A is the heat exchange area, $T_{utility}$ is the temperature of the utility media for a reactor and $T_{utility\_isc}$ is the temperature of the utility media for each section of reactor.

After few manipulations, the utility temperature can be expressed as:

- For a reactor: $T_{utility} = T_{reactor} - \frac{q_{reactor}}{U \cdot A}$ (Equation 5.9)
- For a section of a reactor: $T_{utility\_isc} = T_{isc} - \frac{q_{isc}}{U \cdot A}$ (Equation 5.10)

from where its value can be calculated, as the rest of variables in the equations are known: the temperature of the reactor / section of reactor is imposed; the heat exchanged per reactor / section of reactor is estimated in the first heat balance; the

heat exchange area can be calculated from the shape of the reactors; the overall heat transfer coefficient can be calculated as explained in the next section.

If the temperature of the utility media for every reactor / section of reactor does not go beyond some defined limits (Figure 5.5), which are directly linked to the reactor types and features, the amount of heat exchanged is considered to be reachable. Therefore, the structure is feasible and included for the optimisation search. Otherwise, the structure is rejected and not taken into account for the optimisation.

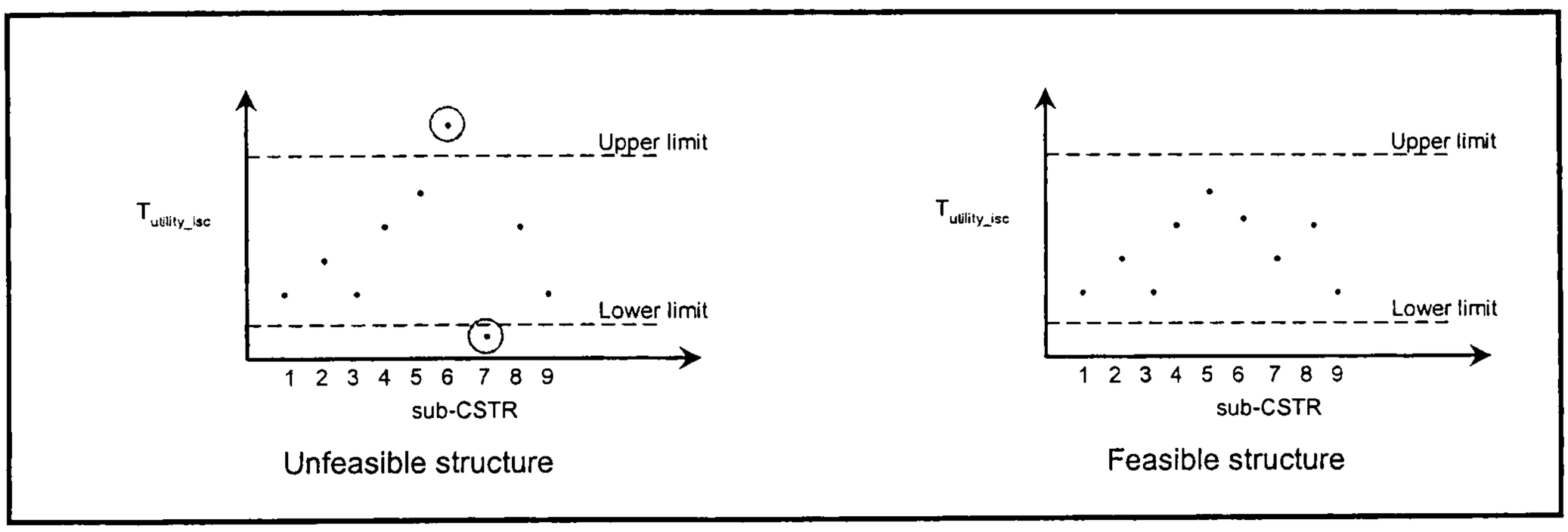

Figure 5.5: Heat exchange media temperature profiles for a PFR formed by 9 sub-CSTRs that exchanges heat with 9 heat exchangers.

For the approximation of a pseudo-homogeneous one dimensional PFR model without radial temperature profile approximation, the temperature imposition method (Section 5.2.2.4) assumes that the reactor exchanges heat with as many heat exchangers as sub-CSTRs employed for the PFR approximation (Figure 5.6). Such a scenario leads to a temperature profile of the utility media that does not follow a progression along the reactor, which can be physically achieved with a single heat exchanger (see in Figure 5.5 the scattered points of $T_{utility\_isc}$ vs. sub-CSTR). Although this situation can be considered as an ideal case due to its lack of practicality from an industrial point of view (n heat exchangers are required to exchange heat with a single reactor), it allows

reducing the optimisation search area and focussing the efforts on promising regions disregarding the options that even in these ideal circumstances, still require impossible heat exchange scenarios. Other impossible scenarios identified are those in which a reactor exchanges simultaneously heat with a cooling and with a heating utility.

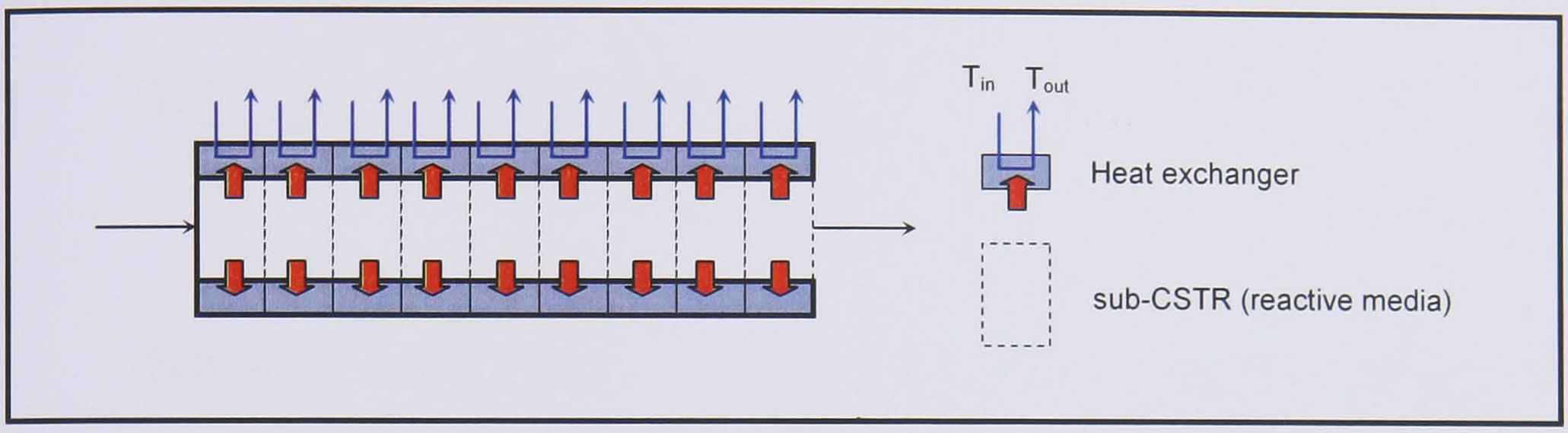

Figure 5.6: Cooled PFR formed by 9 sub-CSTRs that exchanges heat with 9 heat exchangers.

5.2.2.6 Reactor Heat Transfer Modelling - Heat Transfer Coefficient

To calculate the overall heat transfer coefficient (U), the following expression is employed:

$$\frac{1}{U} = \frac{1}{U_{reactive\_media}} + \frac{\delta_{wall}}{\lambda_{wall}} + \frac{1}{U_{utility\_media}} \qquad \text{(Equation 5.11)}$$

where δ_{wall} is the thickness of the wall of the reactor tubes and λ_{wall} its conductivity. The overall heat transfer coefficient for the utility media ($U_{utility\_media}$) is set to a typical value for its kind. The calculation of the overall heat transfer coefficient for the reactive media ($U_{reactive\_media}$) depends on the mixing pattern (CSTR or PFR):

- CSTRs are assumed to have a conical section shape and their overall heat transfer coefficient for the reactive media is assumed to be 600 W/m²/K. A FLBR is a type of reactor that can be represented by a CSTR and has the best heat transfer properties. Since what it is intended to do is to set a maximum

limit on the heat exchanged, the heat transfer coefficient for the reactive media has been chosen to be 75 % of the highest value for a FLBR found in the literature (Kelkar & Ng (2000) suggest values between 50 and 800 W/m²/K).

- For PFRs (FBRs or MTRs), the overall heat transfer coefficient for the reactive media is calculated from Dixon (1996):

$$\frac{1}{U_{reactive\_media}} = \frac{1}{h_w} + \frac{r_t}{3 \cdot \lambda_{e,r}} \cdot \frac{Bi + 3}{Bi + 4} \qquad \text{(Equation 5.12)}$$

Following Konig (2002), the wall heat transfer coefficient (h_w) can be correlated to the effective radial thermal conductivity ($\lambda_{e,r}$) of the bed using the Biot number (Bi) and the radius of the tube (r_t):

$$Bi = \frac{h_w \cdot r_t}{\lambda_{e,r}} = 1.5 \cdot N \cdot Re^{-0.25} \qquad \text{(Equation 5.13)}$$

where the aspect ratio (N) is:

$$N = \frac{d_t}{d_p} \qquad \text{(Equation 5.14)}$$

and d_t is the diameter of the tube and d_p is the diameter of the catalyst particle.

For the cases where the catalyst particles are cylinders, the diameter of the sphere of the catalyst particles is substituted by the equivalent diameter of the sphere of the catalyst particles (d_p^v):

$$d_p^v = d_p \cdot \left(\frac{3}{2} \cdot \frac{h_p}{d_p} \right)^{1/3} \qquad \text{(Equation 5.15)}$$

where h_p is the height of the catalyst particle.

Then, the effective radial thermal conductivity can be expressed as the sum of two terms:

$$\lambda_{e,r} = \lambda_r^0 + \lambda_r^f \qquad \text{(Equation 5.16)}$$

where $\lambda_r{}^0$ is the effective thermal conductivity due to conduction in the fluid and the solid phase and $\lambda_r{}^f$ is the effective thermal conductivity due to convection. With the help of the fluid conductivity (λ_f), the previous equation can be written in dimensionless form as:

$$\frac{\lambda_{e,r}}{\lambda_f} = \frac{\lambda_r^0}{\lambda_f} + \frac{Pe_h^0}{Pe_{h,r}^\infty} \qquad \text{(Equation 5.17)}$$

where $Pe_{h,r}$ is the Peclet number for radial heat conduction (∞ indicates at sufficient high velocity) and $Pe_h{}^0$ is the fluid Peclet number for heat transfer, which can be expressed as:

$$Pe_h^0 = \frac{u_0 \cdot \rho_f \cdot Cp_f \cdot d_p^v}{\lambda_f} = Re \cdot Pr \qquad \text{(Equation 5.18)}$$

where u_0 is the superficial velocity, ρ_f is the density of the fluid, Cp_f is the fluid specific heat and Pr is the Prandtl number.

Bauer & Schlünder (1978a) proposed the following expression for the Peclet number for radial heat conduction:

$$Pe_{h,r}^\infty = 8 \cdot \left[2 - \left(1 - \frac{2}{N} \right)^2 \right] \qquad \text{(Equation 5.19)}$$

After omitting radiation and direct particle-to-particle heat transfer contributions and the system pressure influence, Bauer & Schlünder (1978b) found the following expression for the ratio λ_r^0/λ_f :

$$\frac{\lambda_r^0}{\lambda_f} = \left(1-\sqrt{1-\varepsilon}\right)+\frac{2\cdot\sqrt{1-\varepsilon}}{1-B\cdot\kappa^{-1}}\cdot\left[\frac{B\cdot\left(1-\kappa^{-1}\right)}{\left(1-B\cdot\kappa^{-1}\right)^2}\cdot\ln\left(\frac{\kappa}{B}\right)-\frac{B-1}{1-B\cdot\kappa^{-1}}-\frac{B+1}{2}\right]$$

$$B = C_f\cdot\left(\frac{1-\varepsilon}{\varepsilon}\right)^{1.11} \qquad C_f = 2.5\cdot\left(1+\left(\frac{d_i}{d_p}\right)\right)(\text{for rings}) \qquad \text{(Equations 5.20)}$$

$$C_f = 2.5\ (\text{for cylinders}) \qquad C_f = 1.25\,(\text{for spheres})$$

where d_i is the inner ring diameter and the ratio of thermal conductivities of the solid and the fluid phase (κ) can be considered to be 10 (Smirnov *et al.*, 2004). The void fraction (ε) for randomly filled beds can be measured following Winterberg & Tsotsas (2000a) who proposed its calculation as:

$$\varepsilon(r) = \varepsilon_\infty\cdot\left(1+A\cdot\exp\left[-B\cdot\frac{r_t-r}{d_p}\right]\right)$$

$$A = \frac{0.65}{\varepsilon_\infty}-1 \qquad \text{(Equations 5.21)}$$

$$B = 0.6$$

where r accounts for the radial position inside the tube. For dense beds of cylinders with height of particle similar to length of particle, ε_∞ takes values between 0.25 and 0.35 (Winterberg & Tsotsas, 2000a). The value selected in this work is $\varepsilon_\infty = 0.3$. ∞ accounts here for an infinite expanded bed.

By integration, the average bed porosity is derived:

$$\bar{\varepsilon} = \frac{2}{r_t}\int_0^{r_t}\varepsilon(r)r\,dr \qquad \text{(Equation 5.22)}$$

5.2.3 Separation Representation

If a detailed reactor network formulation is coupled with a detailed separation network formulation, the resulting combinatorial complexity of the system is enormous. In addition, the kinetic models involved in the reactor formulations enclose considerable non-linearities. Subsequently, if a full process synthesis model including the full combinatorial complexity and the full numerical complexity is formulated, the resulting problem is too complex to be solved with any of the existing optimisation approaches. This is exactly the case of the reactor-separator-recycle systems approached in this work. In these systems, both reactor and separator representations must be included in the model formulation as both impacts are essential on the process performance. Reactor systems have a very strong impact on the performance and consequently the ability to represent the reactions in the model should not be sacrificed. Separation systems are also important because they determine the trade-offs between separation costs, recycling costs, reactor cost and raw material conversion efficiency. Opportunely, information about optimal solutions for separation systems can be obtained much quicker in comparison to the ability to solve the reactor problems. As a result, one can benefit from the fact that separation synthesis problems are simpler to solve, and solve them multiple times in order to include the resulting information in aggregated form into the process synthesis model. This exercise can take place in a separate effort before the beginning of the synthesis exercise.

The following methodology is a suggestion of how the separation synthesis calculations can be decoupled, but by not means, is the focus of this work (it is worthwhile to mention that the process representations for all the systems considered

from now onwards include both reaction and separation representations). The separation section could be represented as a sequence of separators in the form of simple input-output models (Linke & Kokossis, 2003b). In such models, the input to each separator fixes its output based on pre-set split fractions. By repeatedly solving the separation-sequencing problem for different feeds, a separation sequence cost could be developed as a function of the feed flow and feed composition. Optimal costs functions could be obtained if the separation sequence cost was to be developed by using separation synthesis methods. Since the components sent from the reaction section to the separation section are known for each problem, their flows and compositions could be estimated to narrow the ranges to be used in developing the cost function.

5.2.4 Energy Integration

The process heat exchanger network performance is assessed in different steps that allow measuring the performance of the complete network design, without having to carry out the actual design:

1) Initially, the *Problem Table algorithm* is solved for each specific superstructure simulated. The algorithm presented by Linhoff & Flower (1978) identifies, within all the streams included for the heat integration (heating / cooling reactor utilities are excluded), sources of heat (hot streams) and sinks of heat (cold streams). The algorithm maximises the heat recovery in the heat exchange network and allows calculating the heating and cooling duties, not provided by heat recovery, which must be serviced by external utilities (energy targets).

2) The external utilities are selected according to the temperature at which they are required and their flows are estimated through heat balances.

3) Next, the heat exchange area targets (Townsend & Linhoff, 1984) are predicted. The hot and cold composite curves, including the utilities, are divided into enthalpy intervals. The hot composite curve is one stream equivalent to all the individual hot streams in terms of temperature and enthalpy. Similarly, the cold composite curve is equivalent to all the individual cold streams in terms of temperature and enthalpy. The heat exchange area ($A_{HXNETWORK}$) is targeted with:

$$A_{HXNETWORK} = \sum_{k}^{INTERVALS\_K} \frac{1}{\Delta T_{LM,k}} \cdot \left[\sum_{i}^{HOT\_STREAMS\_I} \frac{q_{i,k}}{h_i} + \sum_{j}^{COLD\_STREAMS\_J} \frac{q_{j,k}}{h_j} \right]$$

(Equation 5.23)

where $\Delta T_{LM,k}$ is the logarithmic mean temperature difference for the enthalpy interval k, $q_{i,k}$ is the stream duty on hot stream i in enthalpy interval k, $q_{j,k}$ is the stream duty on cold stream j in enthalpy interval k, and h_i and h_j are the film transfer coefficients for hot stream i and cold stream j.

4) Finally the minimum number of heat exchange units (HX_{UNITS}) is calculated according to:

$$HX_{UNITS} = \left(S_{ABOVE\_PINCH} - 1\right) + \left(S_{BELOW\_PINCH} - 1\right) \quad \text{(Equation 5.24)}$$

where S refers to the number of streams and PINCH to the heat recovery pinch (Linhoff *et al.*, 1979). The heat recovery pinch value and position correspond to an economic minimum temperature difference between the energy and the capital costs of the heat exchanger network.

The outputs of the energy integration are the heat exchange area, the number of units that form the network and the external utilities required.

5.3 Performance Evaluation

The optimisation objective function for process designs screening can be a function of any of the variables of the system. It can consider waste production minimisation, yield maximisation, conversion maximisation, etc. An alternative approach would be the development of indexes to assess the safety, controllability or environmental friendliness of a process. This work considers for the current application an objective function linked to the maximisation of the Economic Potential (EP). The EP considered here is a modified EP where just the capital and operational costs of the key equipments are included. When screening process design candidates, many operational units are not significantly different from one design to another (*e.g.* vessels of the flashes, distillation columns, absorbers, etc.). For that reason, all these units are not considered in the EP function and only the equipments identified to be different among the designs are included in it. Besides, for those equipments that are not operational units and may vary in number (controllers, valves, pipes, etc.), the difference of their impact on the EP function is assumed to be negligible. The key equipments identified may vary on the case study but usually they are: compressors, reactors, reboilers and condensers of distillation columns and the heat exchanger network.

The EP can be calculated as:

$$EP = \text{Product value} - \text{Operating cost} - \text{Capital cost} \cdot \text{Annualization factor} \qquad \text{(Equation 5.25)}$$

where:

$$\text{Annualization factor} = i \cdot \frac{(1+i)^{PBP}}{\left((1+i)^{PBP} - 1\right)} \qquad \text{(Equation 5.26)}$$

in which i is the interest rate and PBP the payback period.

In order to estimate the cost of the equipments at the same reference time (December 2004), the Chemical Engineering Plant Cost Index (CECI) has been employed (Table 5.1).

Table 5.1: CECI (http://www.eng-tips.com).

Year	CECI
2000	394.1
2001	394.3
2002	395.6
2003	402.0
2004 - December	464.4

5.4 Network Optimisation

The network optimisation is performed according to the implementation of the stochastic tool Tabu Search, first introduced in Chapter 3. The solution obtained after each simulation is considered for the optimisation only when the component concentrations and the heat transfer flows from / to the reactors are within bounds (Figure 5.7).

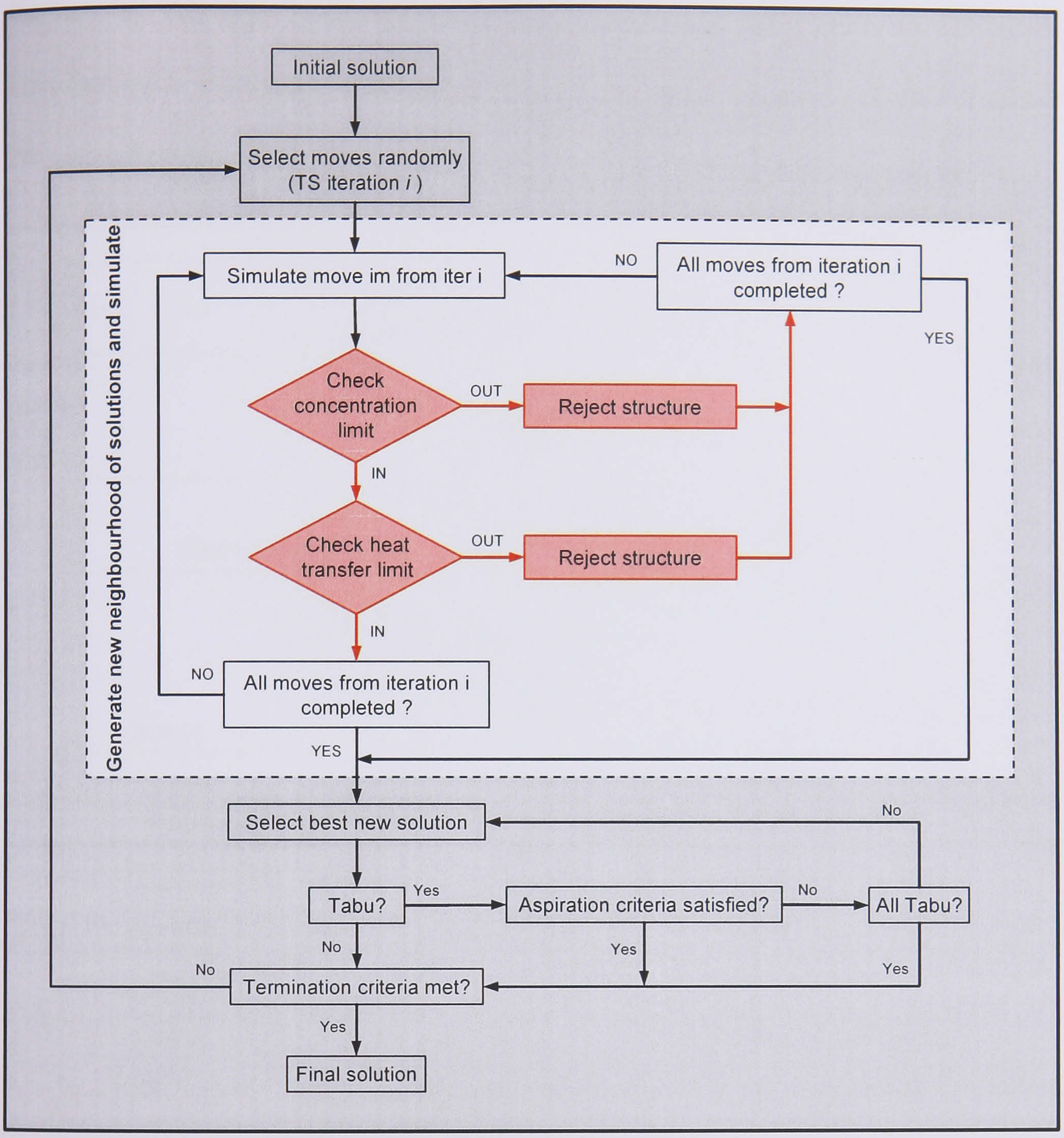

Figure 5.7: Tabu Search algorithm for the multi-level approach.

5.4.1 Synthesis Procedure

The current applications of superstructure-based optimisation approaches only consider optimisations on the entire superstructure. The **multi-level approach** (Figure 5.8) developed here, carries out the optimal searches in structured steps to facilitate the understanding of the complexity of the system by the engineer and enable the reliable identification of potential improvements in process performance along with the process complexities associated. The approach includes two separate

levels. In the first level, the optimal performance of conventional **base case structures** is assessed. The second level is formed by two stages: i) the **Performance targeting** stage; ii) the **Increase search space** stage.

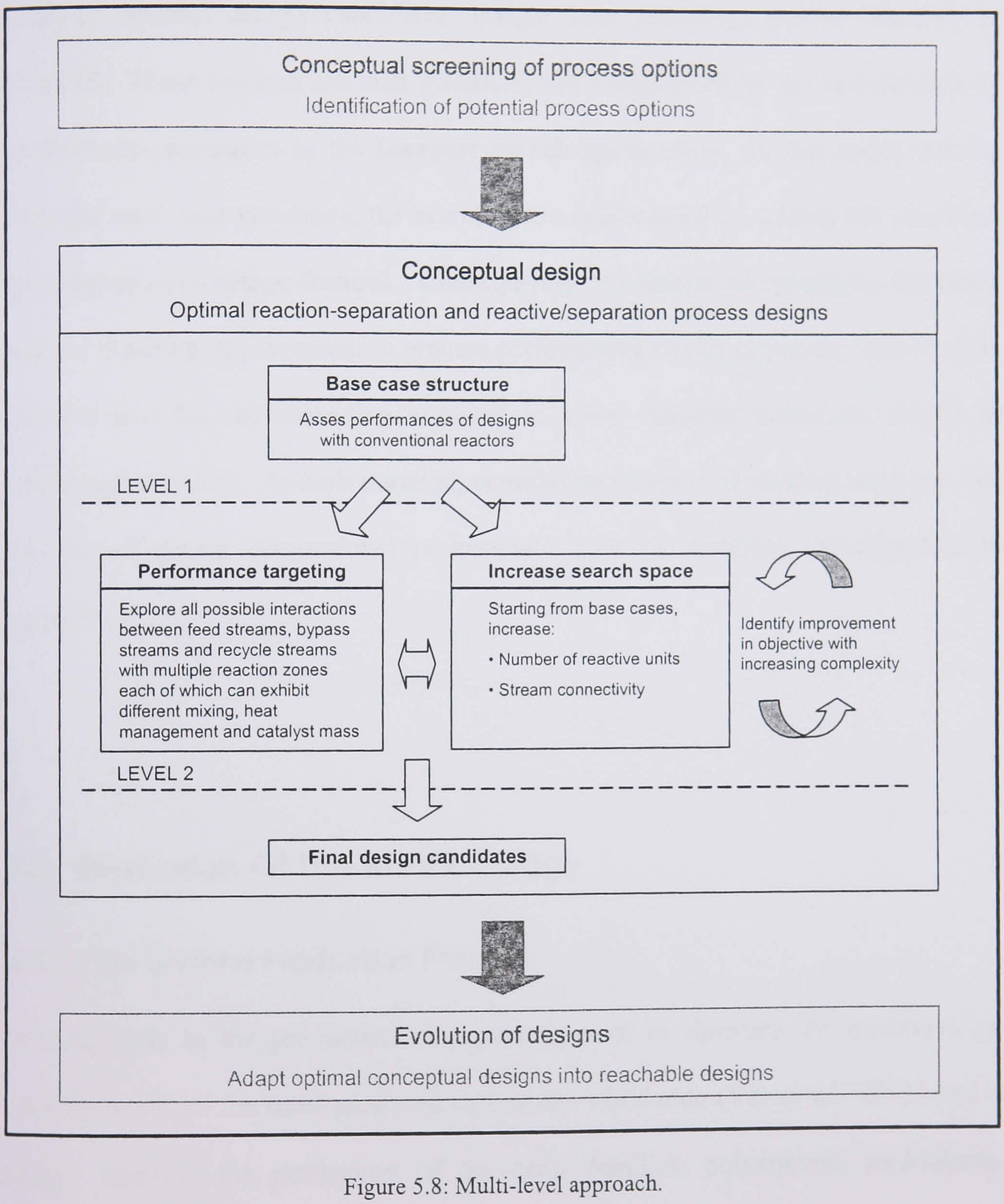

Figure 5.8: Multi-level approach.

In the **Performance targeting** stage (Level 2,), all possible interactions between feed, bypass and recycle streams with multiple reaction zones are allowed. The full superstructure optimisation identifies the targeting performance limit. From the resulting optimal design candidates, insight into promising process features is obtained. These features are then systematically investigated by the optimisation of reduced superstructures in the **Increase search space** stage. In this stage, starting from the base case structures, the search space is increased by adding the identified potential process design features. Consequently, the design complexity is increased and the resulting improvement in process performance can be assessed. This stage is iterative and the understanding acquired in every iteration drives the search in subsequent searches. In each iteration, complexity (number of reactive units and / or number of stream connections) is increased and the resulting superstructure is optimised.

5.5 Illustration Of The Methodology

5.5.1 The Styrene Production Process

A case study in the production of styrene is used to illustrate the methodology. Styrene is one of the most produced monomers worldwide (Yee *et al.*, 2003) and is mainly used in the production of six resin families: polystyrene, acrilonitrile-butadiene styrene, styrene-acrilonitrile, styrene-butadiene rubber, styrene-butadiene latex and unsaturated polyester resins. Styrene can be produced commercially by dehydrogenation of ethylbenzene or via ethylbenzenehydroperoxide. In this work, the gas-phase heterogeneously catalysed dehydrogenation of ethylbenzene (Elnashaie *et*

al., 2001) is the selected production process. The feed in gaseous state (ethylbenzene with impurities along with steam) is heated before being fed to the reaction units (Figure 5.9). Classic approaches for designing chemical processes assume a fixed production rate of the desired product (here styrene). However, in this work the process is optimised given a fixed feed rate of ethylbenzene with impurities of 32 kilotons/yr (Sheel & Crowe, 1969). The amount of the second feed (steam) will be determined by the optimisation search. Unreacted and produced components (ethylbenzene, styrene, toluene, benzene, ethylene, methane, steam, carbon monoxide, carbon dioxide and hydrogen) are cooled before entering the condenser. The condenser separates the condensable components (ethylbenzene, styrene, toluene and benzene) from the rest, which are purged. Condensable components are separated in a distillation sequence and benzene, toluene and styrene are the products of the process, whereas unreacted ethylbenzene is recycled to the first reactor. The objective of this application is to identify trends and key features of the system of reactors that enhance the overall process performance in terms of economic profit. Appendix 2, presents the data for the process, the kinetic model employed, the relevant process design features of the system and the capital and operational cost expressions along with the cost of the raw materials and products.

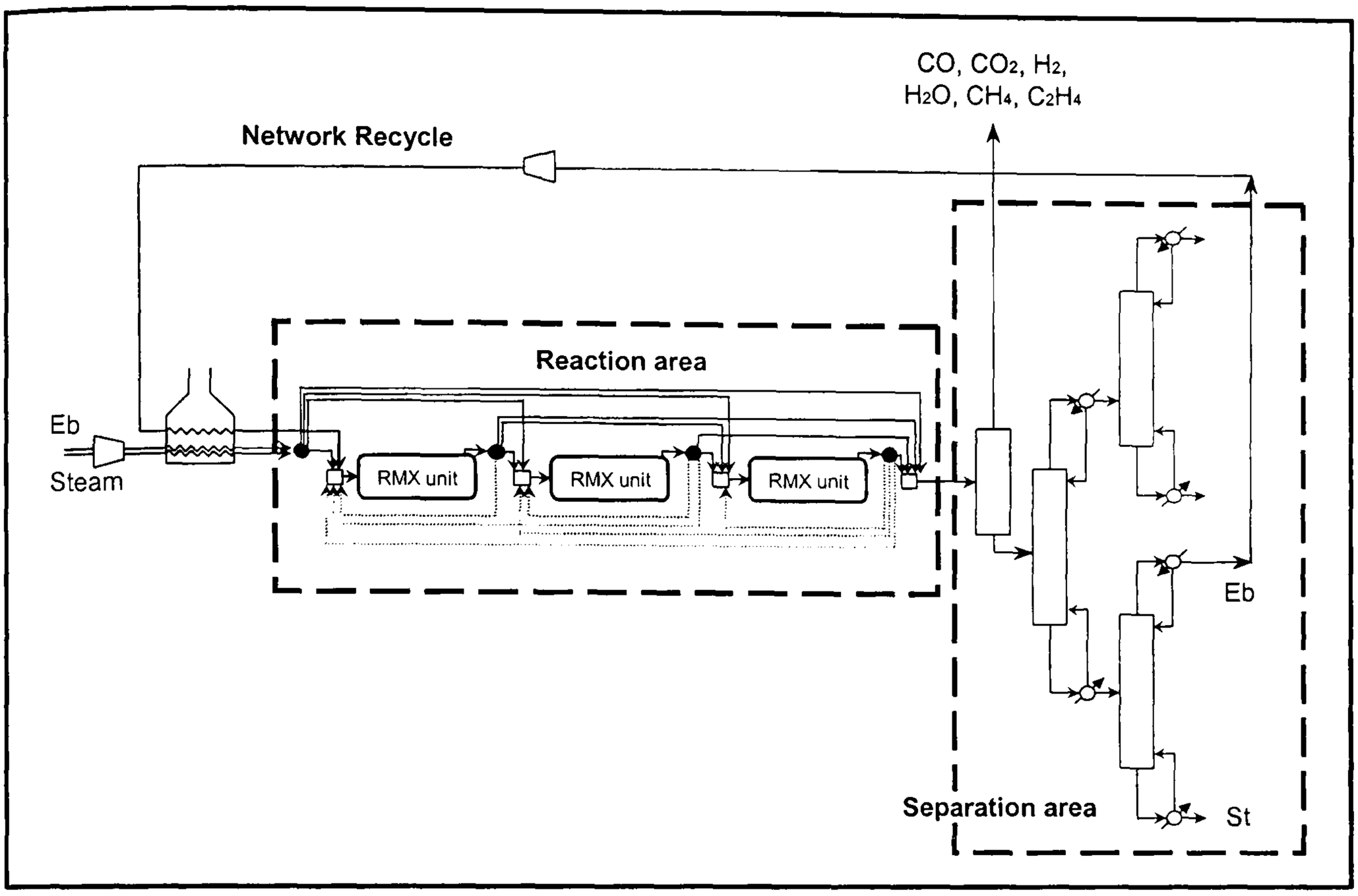

Figure 5.9: Superstructure representation for the styrene production process.

5.5.2 Synthesis Procedure: Level 1 (Base Case Structures)

The reactor used in industry for the production of styrene by dehydrogenation of ethylbenzene is typically the adiabatic reactor (Elnashaie *et al.*, 2001). The process representations for such reactor have not been integrated in this work. However, in order to have an objective function value (OFV) of the typical industrial case, a reactor operating adiabatically has been optimised in terms of volume and inlet temperature. The optimal volume identified for this case is the maximum allowable and the optimal inlet temperature is 929 K. The design and operating conditions for the adiabatic reactor are presented in Table 5.2.

Table 5.2: Design and operating conditions for the adiabatic reactor (Sheel & Crowe, 1969) for the styrene production process.

Design or operating conditions	Value
Reactor diameter	1.95 m
Catalyst bulk density	2146 kg/m^3
Catalyst particle diameter	4.7 mm
Bed void fraction	0.445
Inlet pressure	2.4 bar
Inlet temperature	To be optimised

Apart from the adiabatic reactor, the base cases optimised in this stage are a CSTR and a MTR. The option of exchanging heat with either a heating or cooling media is explored in both cases. The OFVs for these two cases and the adiabatic reactor are presented in Table 5.3. Heating is the utility media identified for both CSTR and MTR.

Table 5.3: OFV for the structures optimised in the base case structure step[1] for the styrene production process.

Structure	OFV (M$/yr)	CPU (hr)
Adiabatic reactor	9.66	6.65
PFR (MTR)	10.73	0.93
CSTR	8.05	0.15

[1] OFVs are taken from the best cases out of ten converged optimisation runs. CPUs are average values.

The MTR improves by 11 % the performance of the adiabatic industrial reactor whereas the CSTR worsens it by 17 %.

5.5.3 Synthesis Procedure: Level 2 (Performance Targeting)

In the Performance targeting step, 30 optimisation experiments are performed. All the experiments start from different initial feasible points, in which the superstructure is optimised without imposing structural constraints (*i.e.* reactor units can be added / deleted in the superstructure, bypasses and recycles between reactors can be identified, feeds can be distributed to any reactor zone present in the superstructure).

PFRs (FBRs and MTRs) and CSTRs are considered for the optimisation. The maximum OFV obtained is 11.37 M$/yr (Figure 5.10), which represents an 18 % improvement with respect to the adiabatic reactor.

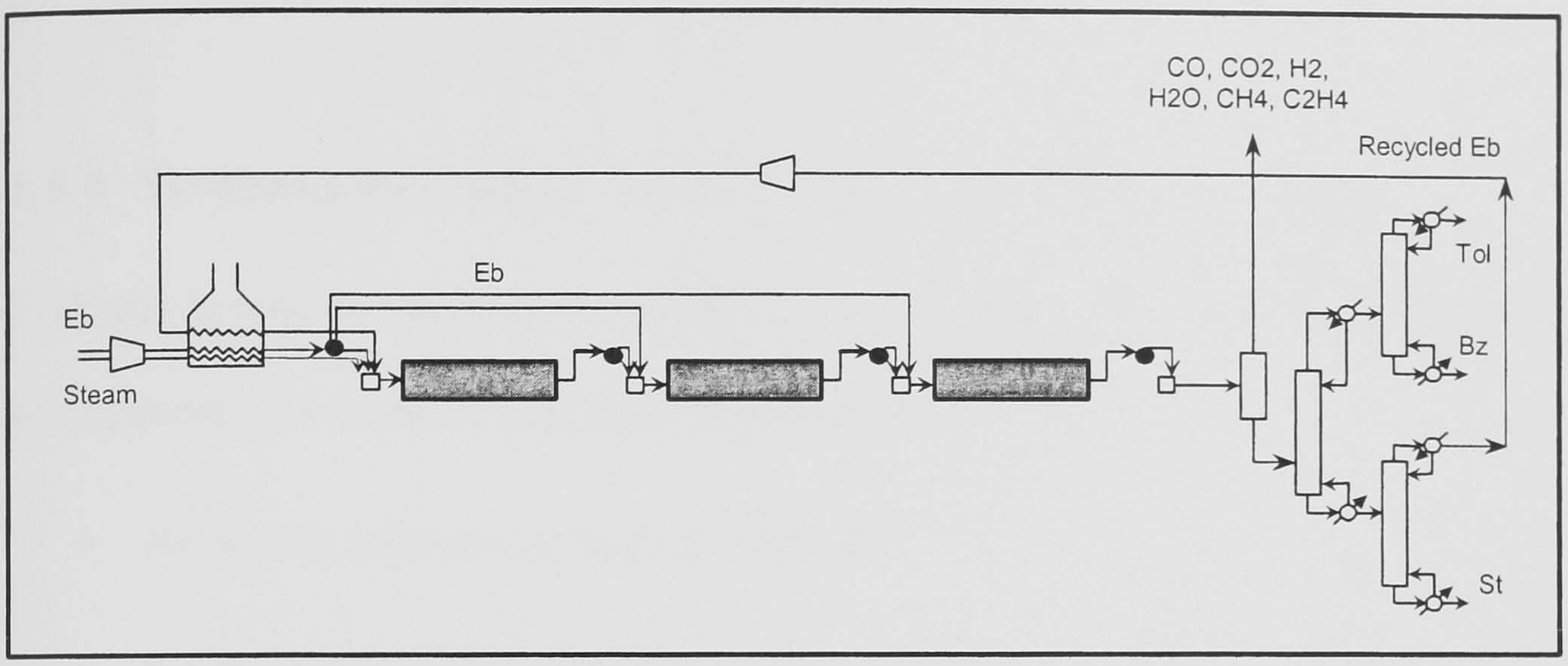

Figure 5.10: Resulting superstructure representation for the performance targeting step in the styrene production process.

The analysis of all the experiments shows that:

- Multiple reactors are present in all the solutions. All the reactors for the cases with higher OFVs are PFRs (MTRs) except for approximately 10 % of them, where the superstructure consists of a PFR (MTR) followed by a CSTR.
- Ethylbenzene side stream feeding is present in many of the final process design candidates. Superheated steam side stream feeding is not present in any of the final process design candidates.
- Internal recycles between reactors are present in a third of the final process design candidates. The OFVs for most of these structures are far from the maximum identified, and for the few ones that are close to the maximum OFV, the recycled fractions are very close to its lower limit (5 %). From experience,

it is concluded that this fact is due to the limitations of the search algorithm to treat discrete variables when solutions are close to constraints.

- Bypasses are present in almost none of the final process design candidates.

5.5.4 Synthesis Procedure: Level 2 (Increase Of Search Space)

Targeted structures based on the analysis of results from the previous structures are investigated. Two structural limitations are imposed:

- No reactor units can be added or deleted.
- No bypasses and recycles between reactors are allowed. However, feed bypasses to the reactors are possible.

The case studies explored are:

- PFR + CSTR.
- PFR + PFR.
- PFR + PFR + PFR.

The analysis of these designs shows that for the structure formed by a PFR and a CSTR, the volume of the CSTR becomes only 6 % of the total network volume. Therefore, its influence on the OFV is small. The main reason for the improvement in the OFV if compared with the single PFR (Table 5.3) resides in the fact that 0.5 M$/yr is saved in superheated steam due to the ethylbenzene side stream feeding identified. The two structures that consist of series of PFRs, in which there is also ethylbenzene side stream feeding, produce very similar results. For two PFRs in

series, the OFV improves with respect to the single PFR by 5.9 % whereas for the three PFRs in series, it is improved by 6.0 % (Table 5.4) and reaches the maximum objective identified in the targeting stage.

Table 5.4: OFV for the structures optimised in the increase search space step[1] for the styrene production process.

Structure	OFV (M$/yr)	CPU (hr)
PFR + CSTR	11.13	2.87
PFR + PFR (MTRs)	11.36	7.05
PFR + PFR + PFR (MTRs)	11.37	12.47

[1] OFVs are taken from the best cases out of ten converged optimisation runs. CPUs are average values.

In order to understand where the difference in performances between the one and the three PFRs structures are, the results for both cases are compared next. The benefit / detriment in Tables 5.5, 5.6 and 5.7 is of the three PFRs structure with respect to the one PFR structure. For both cases, the results of the solutions with the best OFVs are presented.

Table 5.5: Fixed costs for one and three PFRs in series for the styrene production process.

Structure	External Compressor	Feed compressor	Reactor	Heat exchange network
One PFR (MTR) structure (M$)	0.30	1.04	0.22	1.75
Three PFRs (MTRs) structure (M$)	0.25	0.75	0.32	1.65
Benefit (+) / Detriment (-) (M$)	+0.05	+0.29	-0.10	+0.10
Annualized Benefit / Detriment (M$/yr)	**+0.018**	**+0.108**	**-0.038**	**+0.037**

Table 5.6: Product value, operational costs and heat absorbed per reactor section for one and three PFRs in series for the styrene production process.

Structure	Product profit (M$/yr)	Raw material (M$/yr)	External Compression (M$/yr)	Feed compression (M$/yr)
One PFR (MTR) structure	29.17	16.11	0.11	0.47
Three PFRs (MTRs) structure	28.77	15.42	0.08	0.32
Benefit (+) / Detriment (-) (M$/yr)	**-0.40**	**+0.70**	**+0.02**	**+0.16**
Structure	**Hot utility** (M$/yr)	**Cold utility** (M$/yr)	**Reactor heating utility** (M$/yr)	**Heat absorbed per reactors** (W)
One PFR (MTR) structure	0.00	0.01	0.52	2.99E+06
Three PFRs (MTRs) structure	0.00	0.01	0.47	2.72E+06
Benefit (+) / Detriment (-) (M$/yr)	**0.00**	**0.00**	**+0.05**	-

Table 5.7: Selectivities, ethylbenzene conversion and SOR[1] for one and three PFRs in series for the styrene production process.

Structure	Styrene selectivity (%)	Benzene selectivity (%)	Toluene selectivity (%)	Ethylbenzene conversion (%)	SOR inlet reactors (%)	SOR outlet reactors (%)
One PFR (MTR) structure	92.56	2.77	4.35	98.97	7.0	11.0
Three PFRs (MTRs) structure	90.28	3.10	6.30	99.17	7.0, 7.1 and 7.0	8.9, 8.3 and 8.8

[1] SOR is the molar ratio of steam over reactant (see Appendix 2).

The analysis of results shows that:

- The ethylbenzene side feeding identified for the three PFRs structure results in a lower steam profile inside the reactors (SOR at the inlet of the three PFRs in series is at its lower bound), which increases the ethylbenzene conversion, the toluene and the benzene selectivity and reduces the styrene selectivity (Table 5.7).

- The side feeding also results in less steam feed required for the three PFRs in series with respect to the single PFR (from 194 to 126 mol/s) saving 0.70$M/yr in buying steam, 0.16 M$/yr in its compression and requiring a smaller feed compressor (annualised value of 0.11 M$/yr).

- The lower product profit for the three PFRs in series (-0.40 M$/yr, Table 5.6) is explained as follows. If the ethylbenzene conversion is multiplied by the selectivity of each component, the amount of component generated per mol of ethylbenzene fed to the process is obtained. For the three PFRs structure, 89.6 % (90.28 x 0.9917) of all the ethylbenzene fed to the system is converted into styrene, whereas for the single PFR structure this value is 91.6 % (92.56 x 0.9897). Due to the high price of the ton of styrene (988.94 $/ton), a decrease in this percentage of 2.0 reduces the styrene selling profit by 0.61 M$/yr. The

increase in the amount of ethylbenzene transformed into benzene and toluene improves their selling profit by 0.03 M$/yr and by 0.192 M$/yr respectively.

- The higher conversion of ethylbenzene for three PFRs in series implies a lower amount of ethylbenzene recycled from the distillation section to the first reactor (from 17.5 to 14.1 mol/s) resulting in a smaller external compressor (annualised cost of 0.018 M$/yr) and in operational savings (0.02 M$/yr).

- The fewer heat absorbed in the reaction section (Table 5.6) for the three PFRs in series implies 0.05 M$/yr less costs on heating the reactors. The temperature profile for both structures is presented in Figure 5.11 and since the profiles cross each other, it cannot be concluded why there is less heat exchanged for the three PFRs in series.

- Due to the cost expression employed, three reactors are more expensive than just one with the same overall catalyst load (see in Figure 5.11 the x-axis).

- The inlet temperature to the reactive section is three degrees lower for the three PFRs structure. The outlet temperature of the third PFR in series is 22 degrees higher than the outlet of the single PFR (Figure 5.11). These differences have positive effects on the heat exchange network as a smaller heat sink is required and a larger heat source is available. Therefore, a cheaper heat exchanger network is expected.

- The cheaper heat exchanger network required for the three PFRs structure can be mainly explained as a combination of two factors: i) there is less recycle from the distillation section to the inlet of the reactor to be heated; ii) there is 36 % less water to be fed and therefore to be heated. The overall effect is a 24 % reduction of the heat exchange area. Besides, the three PFRs structure

requires four more heat exchangers than the single PFR structure. The combination of both facts results in a cheaper heat exchanger network (annualised benefit of 0.037 M$/yr).

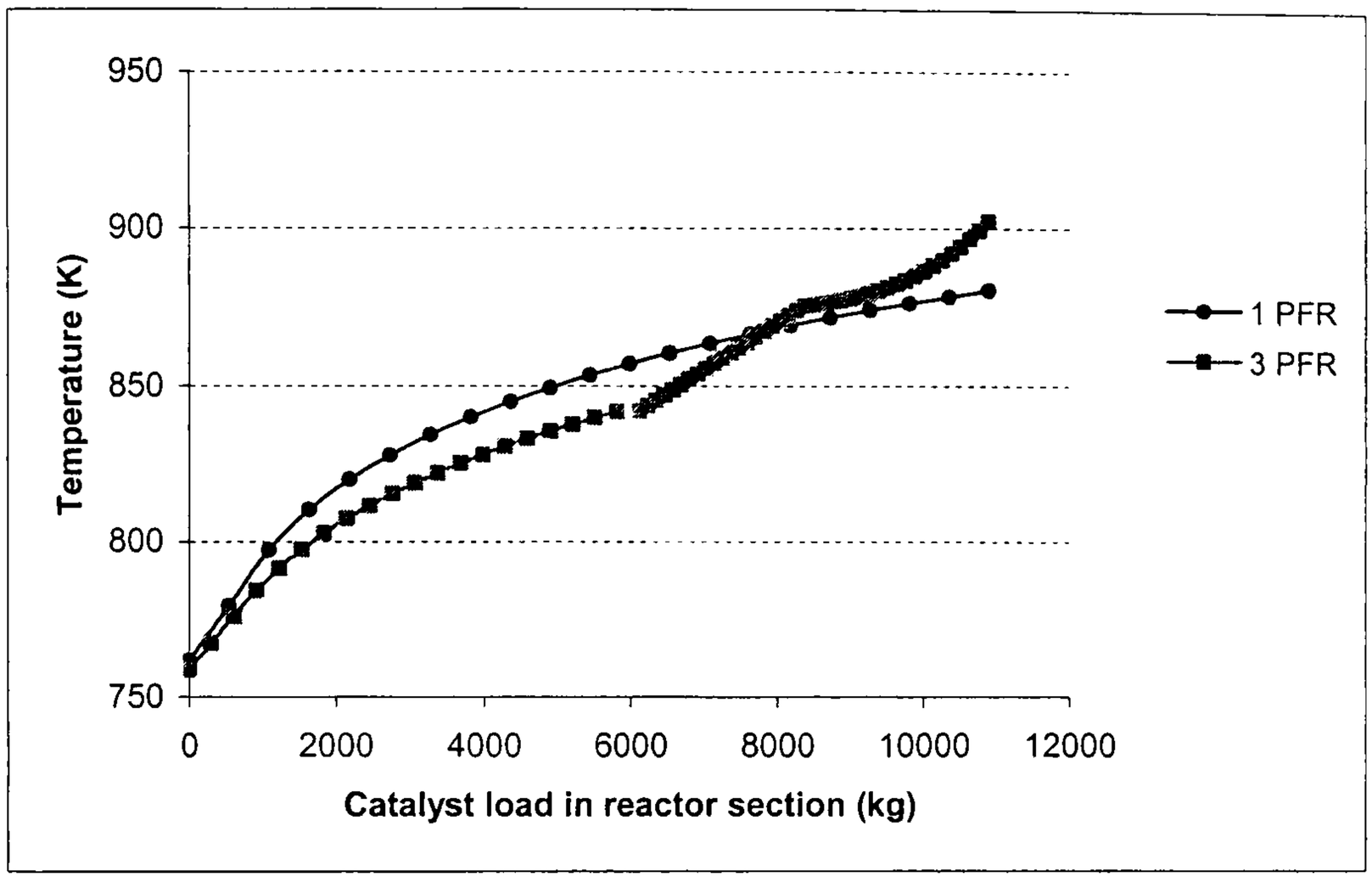

Figure 5.11: Temperature profiles for one and three PFRs in series for the styrene production process.

5.5.5 Optimal Conceptual Process Design Identified

As a result of the conclusions extracted in the multi-level approach, the proposed optimal conceptual process design candidate is the structure formed by three PFRs in series with ethylbenzene feed distribution (Figure 5.12).

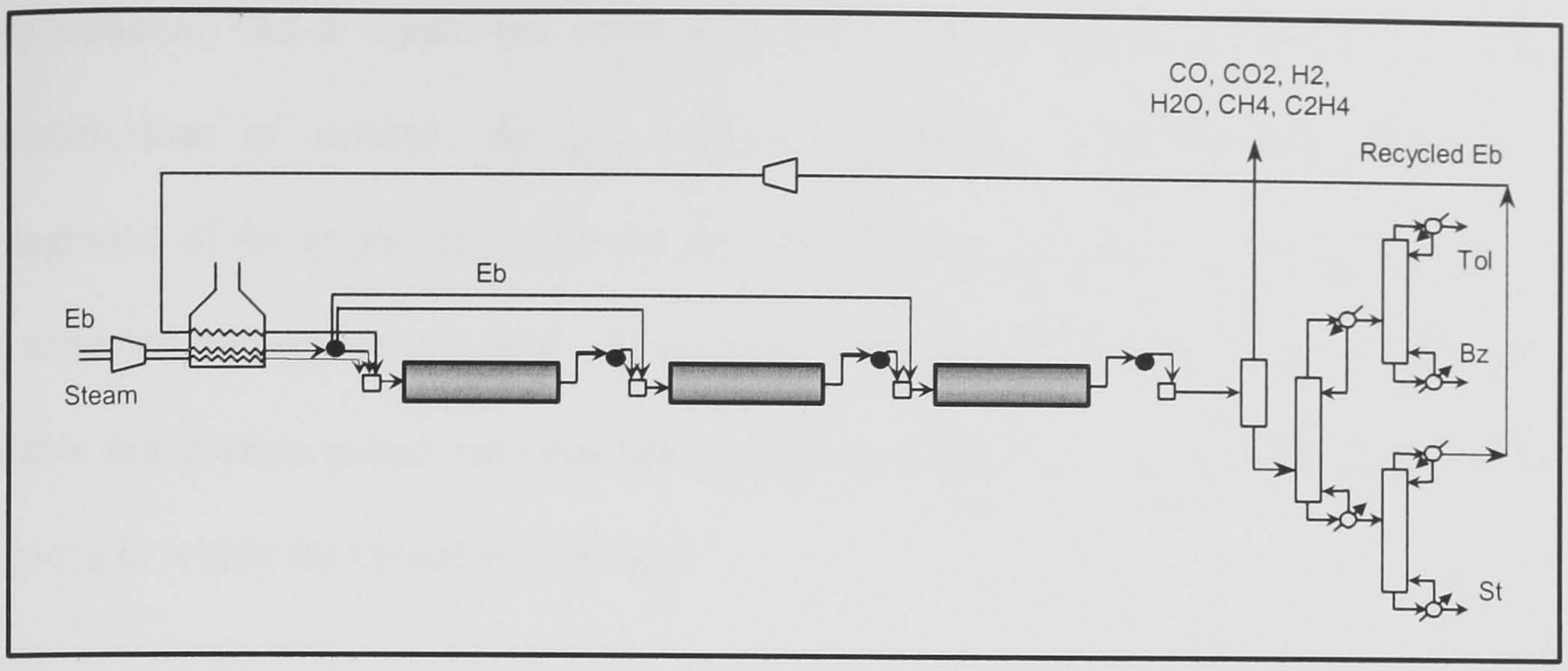

Figure 5.12: Optimal conceptual design candidate proposed as a result of the multi-level approach for the styrene production process.

5.6 Conclusions

A process design framework for heterogeneously catalysed gas-phase reaction systems has been outlined. The framework is based on process superstructure optimisation schemes and enables the identification of the performance limits of the system as well as the evaluation of the relationship between design complexity and performance. The framework leads to a number of potential design candidates that provide the design engineers with insight into the performance gains that can be expected by increasing design complexity. Once they have this information, the design engineers are able to decide on the level of complexity, and thus performance, they are prepared to afford.

The design framework allows handling efficiently the mathematical complexity of the kinetic models involved in experimental modelling at early stages of process design. It also provides a solution to managing practical process constraints found in practical

applications. As a result, the screening of process candidates is enabled and the identification of optimal designs becomes possible. Reached this point, the integration of the experimental model development and the process synthesis systems is expected to become a reality. The communication between the two systems will enable the perfect match between the regions identified by the optimisation and the regions in which the model is validated.

The application of the design framework to a case study in the styrene production process has been presented. The approach systematically identifies optimal process candidates for the kinetically complex system investigated and highlights the improvement that can be delivered by such an approach. Improvements up to 18 % in the OFV have been identified with respect to the standard industrial reactor layout. The structure consisting of three PFRs in series with ethylbenzene feed distribution, is the resulting optimal conceptual design identified by the multi-level approach.

The developments regarding temperature profiles employed here, first introduced by Metha & Kokossis (2000) have proved in many applications to be effective for the screening of multiple design candidates. In this work, their developments are complemented with an upper design layer that accounts for reactor physical limits to produce more realistic designs. The approach proves to handle reliably operating temperature issues in combination with the complex kinetics involved in experimental modelling for the heterogeneously catalysed gas-phase reaction systems. However, having the temperature profiles fully controlled, as it is done in this approach, is not the case of practical implementations. The idea of having multiple heat exchangers

within a single reactor seems rather unpractical and uneconomical. Besides, heat issues appear to play a very important role in the designs for such systems, and radial heat transfer effects involved in catalytic fixed beds have not been taken into account. In order to assess the practical heating / cooling for PFRs, temperature and heat management issues need to be addressed. That is the main purpose of the next chapter, in which the multi-stage evolution of designs is presented. Once very few design candidates are proposed by the multi-level approach and the complexity of the superstructure has dramatically been reduced, the designs can be enriched by adding more detail into the models employed. With the re-assessment of the designs, practical cooling / heating strategies, which are attainable with common co-current schemes found in industry, are proposed. Radial heat transfer effects inside the catalyst beds are also accounted for. The new information on the designs will increase the confidence in the results, to better assist kinetic investigations once they are integrated with process design activities.

CHAPTER 6.

A Decision Support Framework For Synthesis Of Heterogeneously Catalysed Gas-Phase Reaction Processes: Multi-Stage Evolution Of Reactor Designs

6.1 Introduction

The Decision Support Framework (DSF) introduced in Chapter 5 relies on a synthesis strategy to effectively approach the process design of heterogeneously catalysed gas-phase reaction systems. The strategy is based on effectively balancing the numerical and combinatorial complexities along the synthesis exercise. At the beginning of the exercise, the process structure is unknown and the combinatorial complexity is high. Therefore, simple models are employed. This early stage of the synthesis exercise is addressed in Chapter 5 with the multi-level approach. As the exercise progresses, the knowledge that has emerged about the process structure is employed to reduce the structural complexity, and more complexity in terms of the process models can be afforded. This is the core of the multi-stage strategy presented in this chapter. By employing more detailed and computational demanding reactor models in later design stages, the few optimal conceptual designs resulting from the multi-level approach can be explored thoroughly. The addition of modelling detail accounts for the extra

non-linearities that enable evolving the optimal conceptual designs into more realistic options. The evolution takes the form of an iterative process performed in multiple stages. The solution of each stage becomes the starting point of the next one. Even though the number of stages is not limited and the evolution could progress in as many stages as desired, results at the end of this chapter suggest that for these kind of reaction systems four stages are sufficient. For consistency reasons, the multi-level approach presented in Chapter 5 is referred from now on as Stage 1. The multi-stage evolution of process designs, in which the DSF relies on, is schematically shown in Figure 6.1.

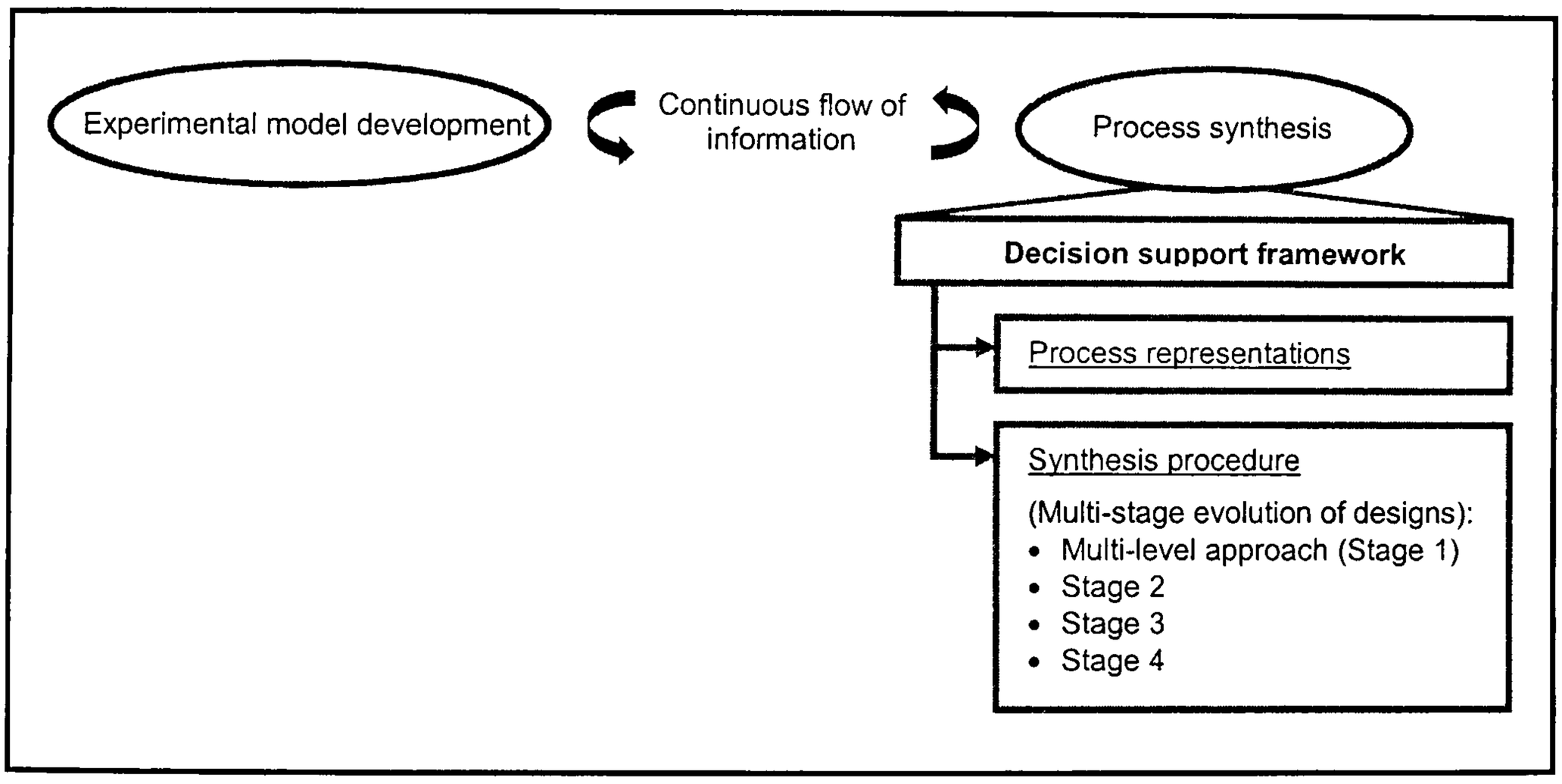

Figure 6.1: Decision support framework within the communication framework that integrates the kinetic model development and the process synthesis (2).

Figure 6.2 (introduced in Chapter 1) shows the location, within the proposed synthesis strategy, of each one of the stages in which the multi-stage evolution is based on.

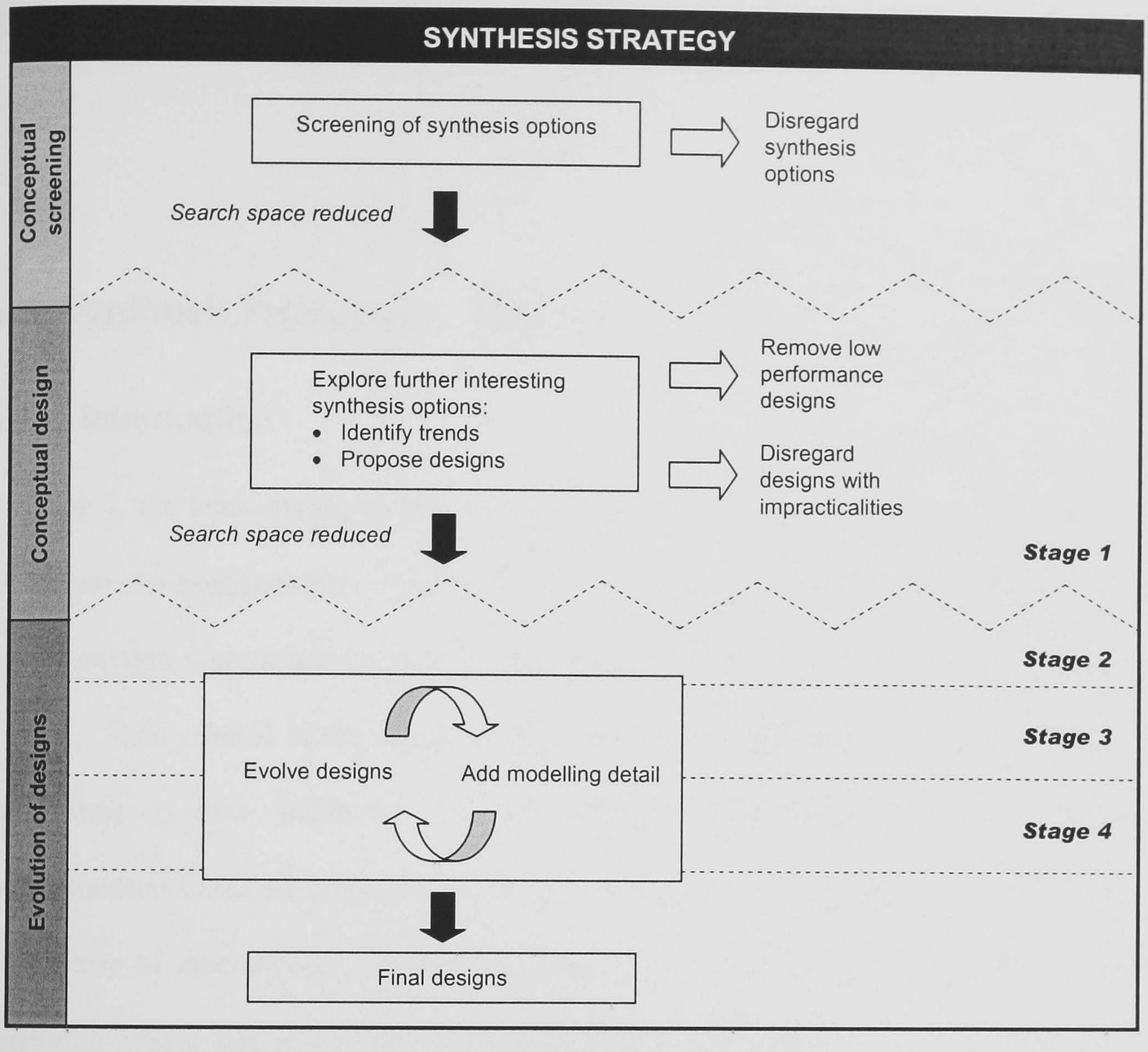

Figure 6.2: Location of the stages involved in the multi-stage evolution of designs within the synthesis strategy.

This research focuses the efforts exclusively on the evolution of the reaction representation. However, a similar approach could be applied for the separation representations. Improved aggregated models could be developed to include more precise information about the separation systems as the synthesis exercise progresses.

In the next sections, the synthesis methodology followed in each stage is detailed. The explanation includes descriptions of the process representations and the network optimisation for each of the stages. The styrene production process is employed for

illustration purposes.

6.2 Synthesis Procedure: Stage 2

6.2.1 Introduction

In Stage 1, the temperature profiles for the reactors modelled with the approximation of the pseudo-homogeneous one dimensional PFR model without radial temperature approximation were assumed to be fully controlled with several heat exchangers per reactor. Such control of the temperature profiles avoids solving heat balances at the same time as mass balances. By omitting this combination of efforts, fewer computational times are required and higher percentages of conversions are obtained in expense of inaccuracies. Such an approach is in agreement with the purpose of screening stages but is not the case of practical implementations. Generally, the temperature profiles proposed in Stage 1 cannot be reproduced with typical heat exchanging strategies found in industry. In order to suggest practical solutions to the heat exchange between the reactors and their utility media, a methodology that aims at producing temperature profiles for PFRs that can be attained with common co-current cooling / heating strategies is presented in Stage 2.

6.2.2 Variations In Process Representations: Reactor Heat Transfer Modelling - Heat Transfer Limits

The approach employed in Stage 1 rarely assigns temperature profiles that close heat balances for PFRs (this is not the case for CSTRs, as the management of heat transfer

limits already closes these balances). In order to obtain closed (or nearly closed) heat balances, a non-linear minimisation problem is solved after the simulation of each TS move. Its purpose is to indicate the magnitude of the gap between the current solution and a corresponding solution in which the heat balance would be closed. The formulation of the problem assumes co-current heat exchange strategies with single utilities for each reactor. Olbert & Corr (2007) present the advantages of co-current strategies over counter-current policies, which are summarized as higher throughputs, lower catalyst hotspot temperatures, desired increase in the heat exchange medium in the direction of the final reaction inside the catalyst fix beds and good temperature uniformity of the heat exchange medium over the reactor cross section. These features allow good horizontal temperature stratification and clearly defined operating states over the length of the catalyst tube space due to the lack of feedback by the heat exchange utility.

The problem has the following objective:

$$OBJ = \min \frac{1}{2} \cdot \left[\sum_{isc=1}^{no\_scstr} \left(q_{optim\_isc} - q_{attainable\_isc} \right)^2 \right] \qquad \text{(Equation 6.1)}$$

where isc refers to the index of the sub-CSTRs and $q_{attainable}$ and q_{optim} are defined as:

1. **Attainable heat values** ($q_{attainable\_isc}$): heats obtained for every sub-CSTR in Stage 2 following the methodology presented in Section 5.2.2.4:

For the first section of reactor:

$$q_{attainable\_isc=1} = q_{isc=1} = \sum_{ic=1}^{ncomp} m_{ic,isc=1} \cdot h_{ic,isc=1}\left(T_{isc=1}\right) - \sum_{ic=1}^{ncomp} m_{ic,in\_reactor} \cdot h_{ic,in\_reactor}\left(T_{in\_reactor}\right)$$

(Equation 6.2)

For a section of reactor different than the first one:

$$q_{attainable\_isc} = q_{isc} = \sum_{ic=1}^{ncomp} m_{ic,isc} \cdot h_{ic,isc}\left(T_{isc}\right) - \sum_{ic=1}^{ncomp} m_{ic,isc-1} \cdot h_{ic,isc-1}\left(T_{isc-1}\right) \qquad \text{(Equation 6.3)}$$

where m is the molar flow, h is the molar enthalpy, T is the operating temperature of the reactor and ic refers to the components in the system.

2. **Optimised heat values** (q_{optim_isc}): heats obtained for every sub-CSTR in Stage 2 as a result of the non-linear optimisation problem.

First of all, the attainable heat values for each sub-CSTR are equalled to:

$$q_{attainable\_isc} = \Delta T_{utility\_isc} \cdot m_{utility} \cdot Cp_{utility} \qquad \text{(Equation 6.4)}$$

where $T_{utility\_isc}$ is the utility temperature for a sub-CSTR, $m_{utility}$ is the flow of the utility media and $Cp_{utility}$ is its specific heat.

The expression can be modified as follows:

$$\Delta T_{utility\_isc} = \frac{q_{attainable\_isc}}{m_{utility} \cdot Cp_{utility}} \qquad \text{(Equation 6.5)}$$

When it is combined with the next equation:

$$T_{utility\_isc} = T_{utility\_isc-1} + \Delta T_{utility\_isc} \qquad \text{(Equation 6.6)}$$

the result is:

$$T_{utility\_isc} = T_{utility\_isc-1} + \frac{q_{attainable\_isc}}{m_{utility} \cdot Cp_{utility}} \qquad \text{(Equation 6.7)}$$

At this point, if the mass of the utility media is inverted:

$$L = \frac{1}{m_{utility}} \qquad \text{(Equation 6.8)}$$

the final expression becomes linear as the specific heat is a parameter:

$$\boxed{T_{utility\_isc} = T_{utility\_isc-1} + \frac{q_{attainable\_isc}}{Cp_{utility}} \cdot L} \qquad \text{(Equation 6.9)}$$

Next, the optimised heat values for each sub-CSTR, which are found as a result of the minimisation problem, are defined as:

$$q_{optim\_isc} = U \cdot A_{isc} \cdot \left(T_{isc} - T_{utility\_isc}\right) \qquad \text{(Equation 6.10)}$$

where U is the overall heat transfer coefficient and A_{isc} is the heat exchange area per sub-CSTR. This expression can be manipulated as follows:

$$\boxed{T_{isc} - T_{utility\_isc} = \frac{q_{optim\_isc}}{U \cdot A_{isc}}} \qquad \text{(Equation 6.11)}$$

Finally, a constraint is imposed to guarantee a minimum temperature gradient between the reactor and its utility media (ΔT_{min}):

$$\boxed{\begin{array}{l}\text{For cooling utility : } T_{isc} - T_{utility\_isc} \geq \Delta T_{min} \\ \text{For heating utiliy : } T_{utility\_isc} - T_{isc} \geq \Delta T_{min}\end{array}} \qquad \text{(Equations 6.12)}$$

The selection of ΔT_{min} depends on the phases exchanging heat and on the type of heat exchangers employed.

The sets of equations represented by Equations 6.9, 6.11 and 6.12 along with the

objective function (Equation 6.1), define the linear optimisation problem that is solved with a sequential quadratic programming (SQP) method integrated in the E04UNF NAG Fortran Library Routine Mark 19. The outcome of the minimisation problem is the temperature profile and the mass of the utility media and the value of the objective function.

Once the minimisation problem is solved for each move of the TS algorithm, a percentage heat value (%HV) is calculated. %HV gives a measure of how far away are the "current" temperature profiles that characterise the solution, from the temperature profiles that are "achievable" with a co-current heat exchange strategy. In other words, %HV is an indicator of the difference between the heat that is required to be exchanged for a given temperature profile and the feasible heat that can be exchanged with a co-current heating strategy. %HV is defined as:

$$\%HV = \frac{\sqrt{\min \frac{1}{2} \cdot \left[\sum_{i=1}^{no\_scstr} \left(q_{optim\_isc} - q_{attainable\_isc} \right)^2 \right] \cdot 2 \cdot no\_scstr}}{\sum_{i=1}^{nscstr} \left(abs\left(q_{optim\_isc} \right) \right)} \times 100 \qquad \text{(Equation 6.13)}$$

where no_scstr is the number of sub-CSTRs.

%HV values for CSTRs are always zero as their energy balances have already been closed in the previous stage. For PFRs, if the %HV is over a maximum limit, the structure will have a heat limit violation constraint (HLV) defined as:

$$HLV = \%HV_{current} - \%HV_{maximum\_limit} \qquad \text{(Equation 6.14)}$$

On the other hand, if the current %HV is below the maximum limit, HLV will be zero. The maximum limit for %HV is a parameter that needs to be specified for every case study. For superstructures consisting of more than one reactor, the overall %HV for the superstructure is the highest %HV among all. The approach of the stochastic algorithm regarding constraints management has been presented in Chapter 3.

6.2.3 Variations In Network Optimisation

The TS algorithm employed in Stage 2 is shown in Figure 6.3. The same algorithm as in Stage 1, with the addition of the calculations for the linear minimisation problem and for the HLV, applies in this stage.

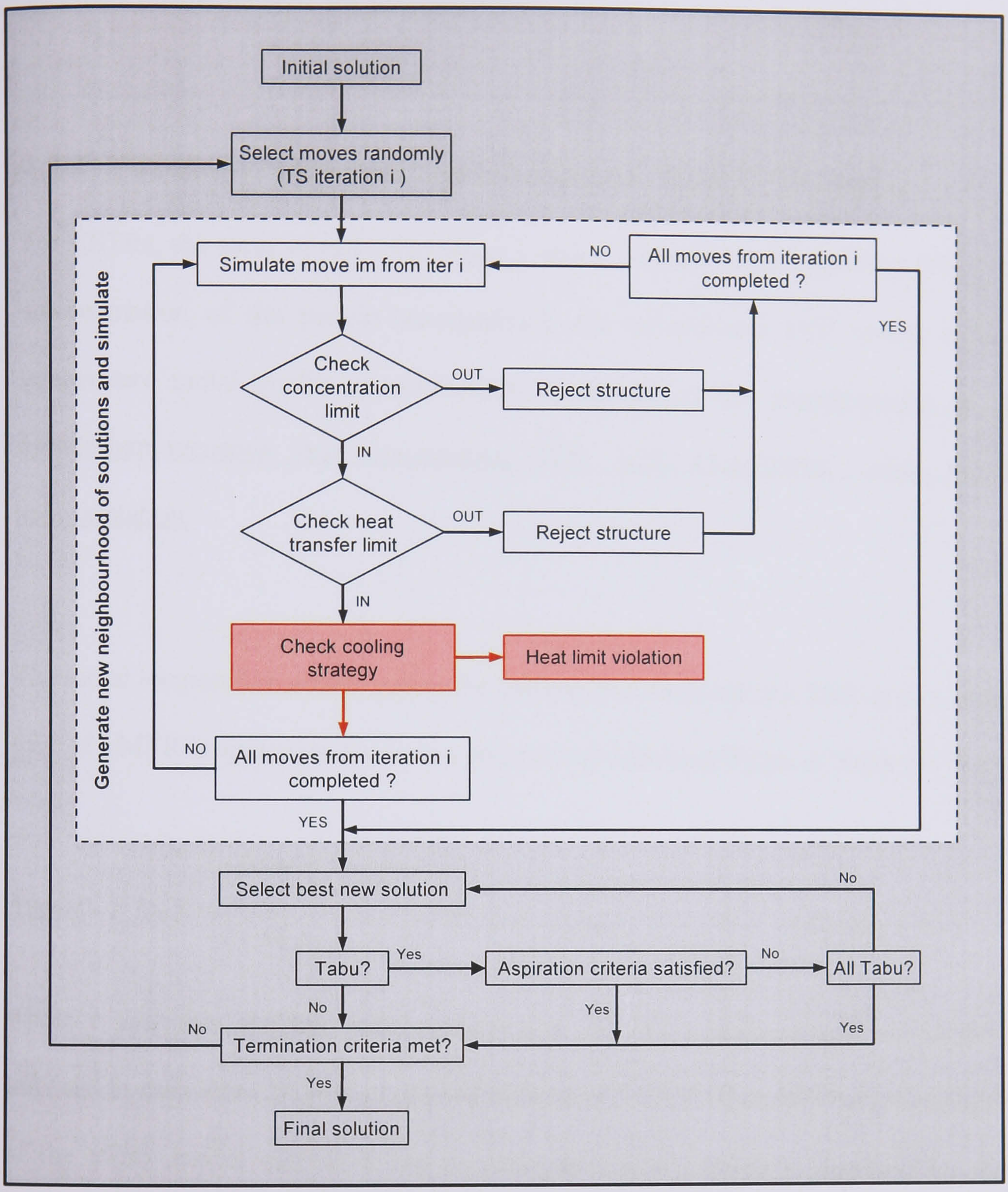

Figure 6.3: Tabu Search algorithm for Stage 2.

6.3 Synthesis Procedure: Stage 3

6.3.1 Introduction

Stage 3 presents a tool to improve the approach towards handling temperature and heat transfer issues inside fixed catalytic beds. With this tool, radial temperature

gradients inside the beds are accounted for.

6.3.2 Variations In Process Representations: Reactor Modelling

For CSTRs, the same model as in Stage 1 and 2 is employed. Regarding PFRs, the approximation of the pseudo-homogeneous one dimensional PFR model without temperature radial profile approximation, is updated to the approximation of the pseudo-homogeneous one dimensional PFR with temperature radial profile approximation.

The radial temperature profile inside the catalyst bed enclosed in a FBR or in a single tube of a MTR is approximated with a polynomial following Nagel & Adler (1971):

$$T(r,isc) = T_K(isc) + \frac{2 + Bi(isc)\cdot\left(1-\left(\frac{r}{R_1}\right)^2\right)}{2 + Bi(isc)\cdot(1-R_1{}^2)}\cdot\left(T_1(isc) - T_K(isc)\right) \qquad \text{(Equation 6.15)}$$

where r accounts for the radial coordinates, $T_1(isc)$ represents the temperature imposed in each sub-CSTR as explained in Section 5.2.2.4, $T_K(isc)$ is the temperature of the utility media corresponding to each sub-CSTR, which is obtained by the minimisation problem described in Stage 2, and Bi is the Biot number. The value proposed by Nagel & Adler (1971) for R_1 is 0.707. This means that the imposed temperature value for each sub-CSTR is equivalent to the temperature found at 0.5 times the radius of the reactor from its centre.

If the reactor is being cooled, Equation 6.15 indicates that the highest temperature inside the bed for each sub-CSTR is at its centre:

$$T(0,isc) = T_{CENTER}(isc) = T_{MAX}(isc) = T_K(isc) + \frac{2 + Bi(isc)}{2 + Bi(isc) \cdot \left(1 - R_1^{\,2}\right)} \cdot \left(T_1(isc) - T_K(isc)\right)$$

(Equation 6.16)

If this temperature is higher than the maximum temperature limit (T_{MAX_LIMIT}), the temperature limit violation constraint (TLV) for that sub-CSTR is defined as:

$$TLV(isc) = T(0,isc) - T_{MAX\_LIMIT}$$ (Equation 6.17)

When the temperature at the centre of the catalyst bed is lower than or equal to the maximum temperature limit, the TLV for that sub-CSTR is zero. If several sub-CSTR show TLV, the highest value among them is selected as the representative value for that reactor. Similarly, if several reactors show TLV, the highest value among them is selected as the value to represent the superstructure.

The same rationale applies for the reactors being heated with the minimum temperature limit. The temperature at the centre of the bed will be the lowest if the reactor is being heated:

$$T(0,isc) = T_{CENTER}(isc) = T_{MIN}(isc) = T_K(isc) + \frac{2 + Bi(isc)}{2 + Bi(isc) \cdot \left(1 - R_1^{\,2}\right)} \cdot \left(T_1(isc) - T_K(isc)\right)$$

(Equation 6.18)

If this temperature is lower than the minimum temperature limit (T_{MIN_LIMIT}), the temperature limit violation constraint (TLV) for the sub-CSTR is defined as:

$$TLV(isc) = T_{MIN\_LIMIT} - T(0, isc) \qquad \text{(Equation 6.19)}$$

T_{MAX_LIMIT} and T_{MIN_LIMIT} are parameters that need to be specified depending on the case study. The TLVs for CSTRs are always zero as no temperature gradients are assumed in their catalytic beds.

6.3.3 Variations In Network Optimisation

The TS algorithm for this stage is presented in Figure 6.4. In order to account for the possibility that radial temperature profiles in catalytic fixed beds go beyond their limits, calculations regarding these profiles and TLVs computations are added with respect to the previous stage.

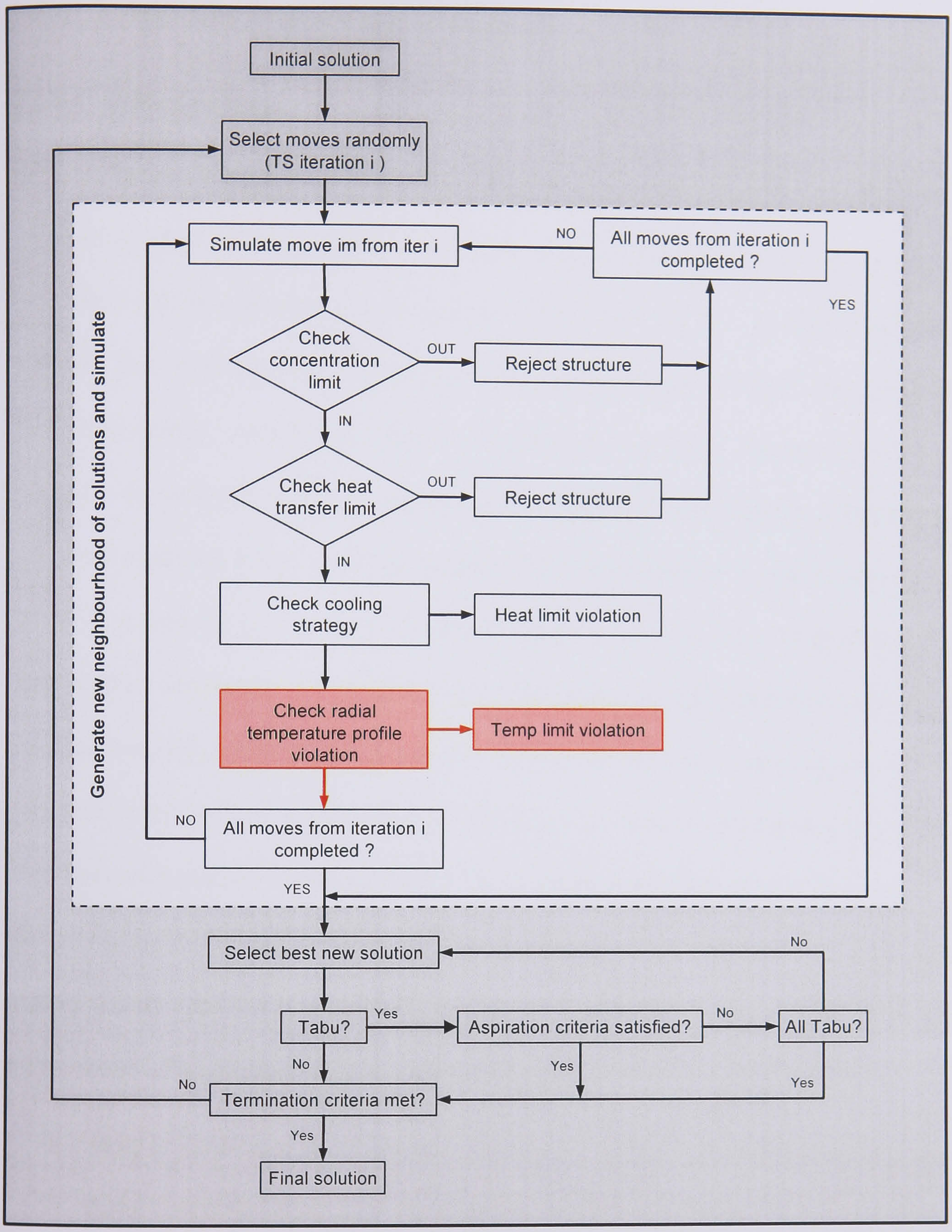

Figure 6.4: Tabu Search algorithm for Stage 3.

6.4 Synthesis Procedure: Stage 4

6.4.1 Introduction

The flowsheet simulation can be approached either with modular or equation-based methods (Seider, 1999). In this research, an equation-based method has been used so far. As it will be explained in later sections, Stage 4 involves a combination of reactor models that include both differential algebraic equations (DAEs) and algebraic equations (AEs). As a result, systems of differential algebraic equations need to be solved. In order to continue relying on an equation-based method, a differential algebraic equation solver would be required. The implementation of such solvers can result in a genuine contribution of a Ph.D. thesis as they are not straightforward to implement. For being out of the scope of this work, an approach that combines a modular method, containing input-output models for the RMX units, along with an equation-based method is adopted here. Usually, in modular approaches, the input-output models remain unchanged while the simulation is being solved. However, in this work, in between the iterations performed by the NLE solver, the input-output models for the reactors are constantly updated by solving the DAEs / AEs that model each reactor. The adopted multipliers approach (Figure 6.5) is outlined below:

- **Step 1**: given an input feed molar flow ($F_{in,ir,ic}$) for each component (ic) and RMX unit (ir) of the reaction superstructure from previous stages, calculate the related output molar flow ($F_{out,ir,ic}$) solving the DAE / AE systems.

- **Step 2**: calculate a set of two multipliers that represent the input-output relationship for each component and RMX unit comprising the reaction superstructure:

$$\text{if}\left(F_{out,ir,ic} \geq 1.0\right)$$

$$\text{multiplier}(ir,ic,1) = \frac{F_{out,ir,ic}}{F_{in,ir,ic}}$$

$$\text{multiplier}(ir,ic,2) = 0$$

$$\text{elseif}\left(F_{out,ir,ic} \leq 1.0\right) \qquad \text{(Equation 6.20)}$$

$$\text{multiplier}(ir,ic,1) = 0$$

$$\text{multiplier}(ir,ic,2) = F_{out,ir,ic}$$

$$\text{endif}$$

Two sets of multipliers are created to avoid values of a similar order of magnitude to that of the accuracy of the solver, as they would difficult the convergence of the system.

- **Step 3**: Solve the system of equations that includes the global mass balance (defined by network connections) and the mass balances around RMX units (defined by the multipliers input-output models) with the NLE solver. The solution of the system of equations produces a new OFV and a new feed molar flow for each component and RMX unit of the reaction superstructure.

- **Go to Step 1**: The procedure is repeated iteratively until the OFV of two consecutive iterations does not change and the system is considered to be converged.

With this approach, the problem can be solved for superstructures with any number of network connections and any detailed time-consuming reactor model types.

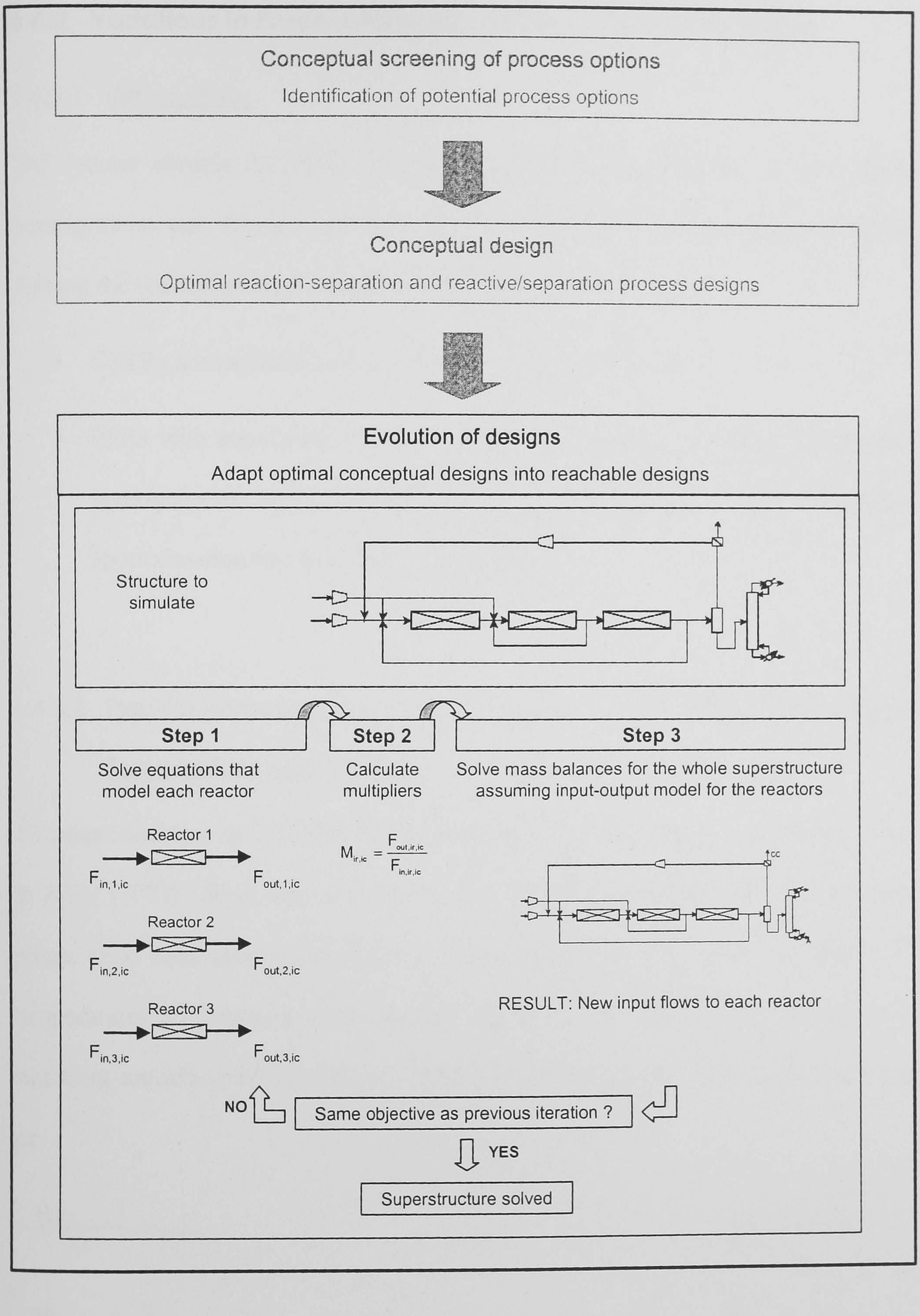

Figure 6.5: Multipliers approach.

6.4.2 Variations In Process Representations - Reactor Modelling

6.4.2.1 Introduction

The reactor models for PFRs involved in Stage 4 are upgraded to the pseudo-homogeneous one dimensional PFR model with radial temperature approximation. Among the reactors that presented back-mixing in previous stages:

- CSTRs are modelled in this stage with a FLBR cell model.
- PFRs with significant internal recycles are modelled with both the pseudo-homogeneous one dimensional PFR model with radial temperature approximation and with the FLBR cell model.

6.4.2.2 Pseudo-Homogeneous One Dimensional PFR Model With Radial Temperature Approximation

The approximation of the radial temperature profile is also calculated following Nagel & Adler (1971). Such approximation is calculated along the reactor in n discretised points (n is equivalent to the number of sub-CSTRs used in previous stages). If temperatures are imposed to the reactor, as detailed in Section 5.2.2.4, the set of equations modelling the pseudo-homogeneous one dimensional PFR can be expressed as:

$$-\frac{\delta(u_0 \cdot C_{ic})}{\delta z} = r_{ic} \cdot \rho_B \qquad \text{(Equation 6.21)}$$

$$-\frac{\delta P_t}{\delta z} = f \cdot \frac{\rho_g \cdot u_0^2}{d_p} \qquad \text{(Equation 6.22)}$$

where u_0 is the superficial velocity, r is the reaction rate, C is the concentration, ic refers to each component, ρ_B is the catalyst bed density, P_t is the pressure loss inside

the reactor, d_p is the diameter of the catalyst particle, ρ_g is the gas density, f is the friction factor (see Section 5.2.2.2) and z refers to the length of the reactor.

The resulting DAE system is solved with the D02NMF NAG Fortran Library Routine Mark 19, which is a general-purpose routine for integrating the initial value problem for a stiff system of explicit ordinary differential equations:

$$\frac{\delta y}{\delta t} = g(t, y) \qquad \text{(Equation 6.23)}$$

where y are the dependent variables that are functions of the independent variable t.

6.4.2.3 Fluidised Bed Reactor Model

The FLBRs employed in this stage are modelled with a cell model (Figure 6.6) based on the "Bubble Assemblage Model" (BAM) presented by Kato & Wen (1969).

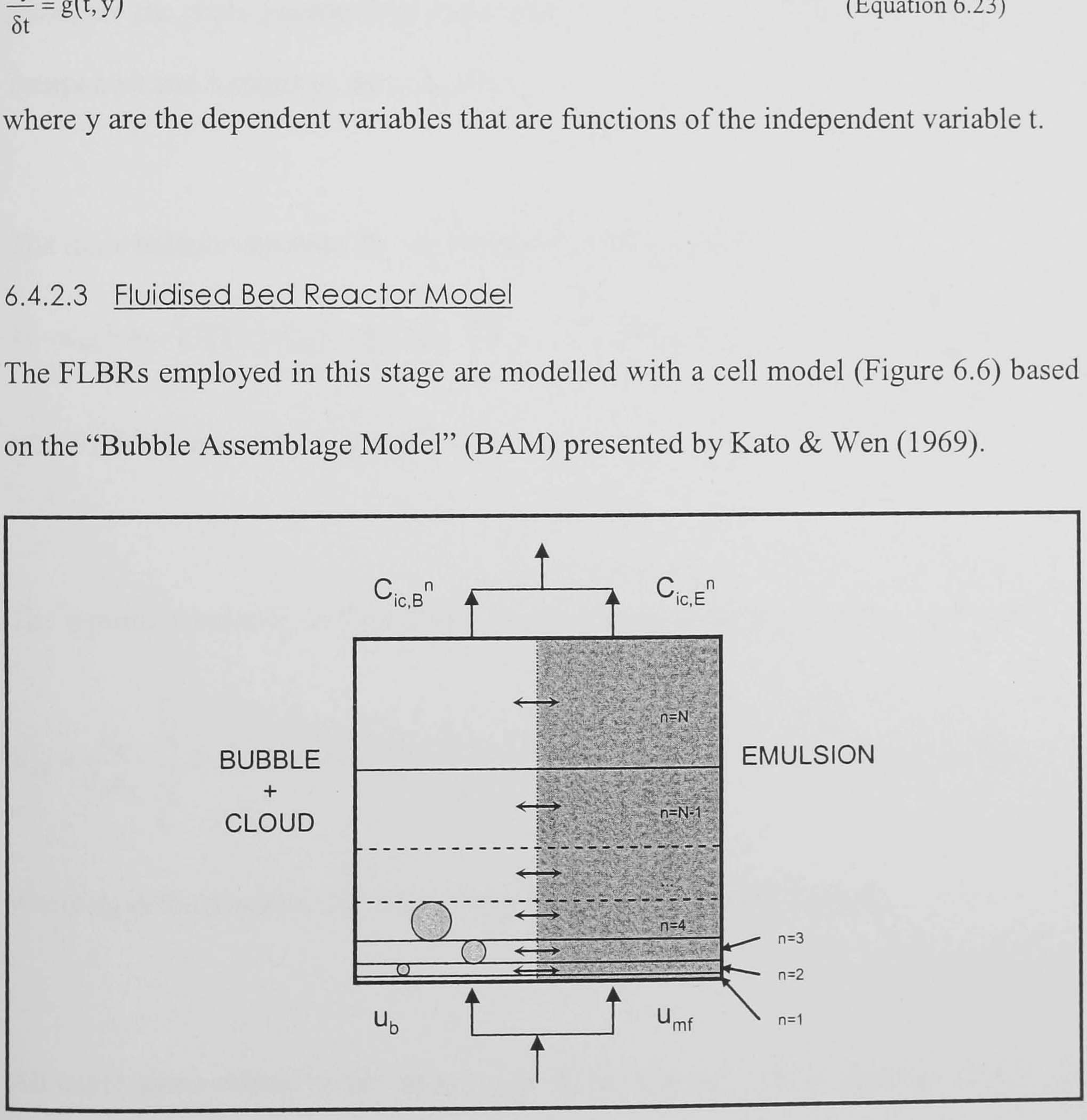

Figure 6.6: Cell model for FLBRs.

The model assumes an isothermal reactor and describes the fluidised bed as a two-phase system: a bubble & cloud phase (B) and an emulsion phase (E). The mass balance equation for the emulsion phase is:

$$u_{mf} \cdot A_T \cdot \left(C_{ic,E}^{n-1} - C_{ic,E}^{n}\right) + k_{BE}^{n} \cdot V_{BP}^{n} \cdot \left(C_{ic,B}^{n} - C_{ic,E}^{n}\right) + \sum_{j} mols_{r,ic,E}^{n} = 0 \qquad \text{(Equation 6.24)}$$

where u_{mf} is the minimum velocity of fluidisation, k_{BE} is the mass transfer coefficient, A_T is the cross sectional area of the reactor, V_{BP} is the volume for the bubble phase, $mols_r$ are the mols generated or consumed, C is the concentration, ic refers to each component and n refers to the cell index.

The mass balance equation for the bubble & cloud phase is:

$$\left(u - u_{mf}\right) \cdot A_T \cdot \left(C_{ic,B}^{n-1} - C_{ic,B}^{n}\right) - k_{BE}^{n} \cdot V_{BP}^{n} \cdot \left(C_{ic,B}^{n} - C_{ic,E}^{n}\right) + \sum_{j} mols_{r,ic,B}^{n} = 0 \qquad \text{(Equation 6.25)}$$

where u is the mean flow velocity.

The minimum velocity of fluidisation is calculated according to Wen & Yu (1966):

$$u_{mf} = \frac{\eta_g}{d_p \rho_g} \cdot \left[\left(29.5^2 + 0.0408 \frac{d_p^3 \cdot \rho_g \cdot \left(\rho_p - \rho_g\right) \cdot g}{\eta_g^2} \right)^{\frac{1}{2}} - 29.5 \right] \qquad \text{(Equation 6.26)}$$

where η_g is the dynamic viscosity of the gas and g the gravity constant.

All expressions related to the diameter of the bubble (d_b) follow Werther (1992). Its specific expressions are:

$$d_{b(n=1)} = 1.3 \cdot \left(\frac{v_0}{g} \right)^{0.2} \quad \text{with} \quad v_0 = \frac{u}{no\_orifices}$$

$$d_{b(n\neq1)} = \left(\frac{2 \cdot \varepsilon_{B(n-1)}}{9 \cdot \pi} \right)^{\frac{1}{3}} - \frac{d_{b(n-1)}}{3 \cdot \lambda \cdot u_{b(n-1)}} \quad \text{with} \quad \lambda = 280 \cdot \frac{u_{mf}}{g}$$

(Equations 6.27)

where no_orifices is the number of orifices per square meter of the gas distributor. u_b is the velocity of the bubble based on fixed axis and ε_B is the hold-up of the bubble phase, which follows Murray (1965):

$$\varepsilon_{B(n)} = \frac{0.8 \cdot (u - u_{mf})}{u_{b(n)}}$$

(Equation 6.28)

The equations relating to the velocity of the bubble are (Werther, 1992):

$$u_{b(n)} = 0.8 \cdot (u - u_{mf}) + 0.71 \cdot \phi \cdot (g \cdot d_{b(n)})^{0.5}$$

$$\phi = 3.2 \cdot d_t^{\,0.33}$$

(Equations 6.29)

where d_t is the diameter of the reactor tube.

The volumes for the different phases (V_{BP}, V_{CP}, V_{EP}) also follow Murray (1965):

- For the bubble phase:

$$V_{BP(n)} = \varepsilon_{B(n)} \cdot d_{b(n)} \cdot A_T$$

(Equation 6.30)

- For the cloud phase:

$$V_{CP(n)} = \frac{V_{BP(n)}}{0.71 \cdot \phi \cdot (g \cdot d_{b(n)})^{0.5} \cdot \frac{\bar{\varepsilon}}{u_{mf}} - 1}$$

(Equation 6.31)

where $\bar{\varepsilon}$ is the void fraction of the fluidised bed.

- For the emulsion phase:

$$V_{EP(n)} = d_{b(n)} \cdot A_T - V_{BP(n)} - V_{CP(n)} \qquad \text{(Equation 6.32)}$$

The bubble and cloud phase volumes are calculated separately in order to obtain the V_{EP} by difference.

The mass transfer coefficient follows Sit & Grace (1981):

$$k_{BE(n,ic)} = \left(\frac{u_{mf}}{3} + \left(\frac{4 \cdot D_{G(ic)} \cdot \bar{\varepsilon} \cdot u_{b(n)}}{\pi \cdot d_{b(n)}} \right)^{\frac{1}{2}} \right) \cdot \frac{6}{d_{b(n)}} \qquad \text{(Equation 6.33)}$$

The diffusion coefficient ($D_{G(ic)}$) is calculated as Hirschfelder *et al.* (1954).

The void fraction for the bed can take values between 0.15 and 0.6 (Kelkar & Ng, 1998). According to Levenspiel (1998) the fraction u / u_{mf} should be between 5 and 30. This range has been widened in this work from 3 to 35 to widen the FLBR model applicability.

6.4.3 Variations In Process Representations: Reactor Temperature Profiles

FLBRs are operated at isothermal conditions, as heat transfer coefficients and effective thermal diffusivities are very large (Kato & Wen, 1969).

6.4.4 Variations In Process Representations: Reactor Heat Transfer Modelling - Heat Transfer Coefficient

The overall heat transfer coefficient for the reactive media in a FLBR is assumed to be 600 W/m²/K as introduced in Section 5.2.2.6.

6.4.5 Variations In Process Representations: Pressure Losses Inside Reactors

As already shown in Section 6.4.2.2, the differential form of the Ergun expression for reactors showing plug-flow behaviour is solved as:

$$\frac{\delta P_t}{\delta z} = f \cdot \frac{\rho_g \quad u_0^2}{d_p} \qquad \text{(Equation 6.34)}$$

The loss of pressure for the FLBRs is calculated according to Wolf (2004):

$$\Delta P_{FLBR} = 1.2 \cdot \frac{M \cdot g}{A_T} \qquad \text{(Equation 6.35)}$$

where M is the catalyst load of the FLBR.

6.4.6 Variations In Network Optimisation

The TS algorithm in Stage 4 is kept as in Stage 3 when PFRs are considered (Figure 6.7). However, after each TS move simulation, if there is no violation of the heat and the temperature limits, the performance of the structure is re-assessed taking into consideration the radial temperature profile inside the reactors. When FLBRs are considered, the TS algorithm is kept as it was in Stage 1 (Figure 5.7).

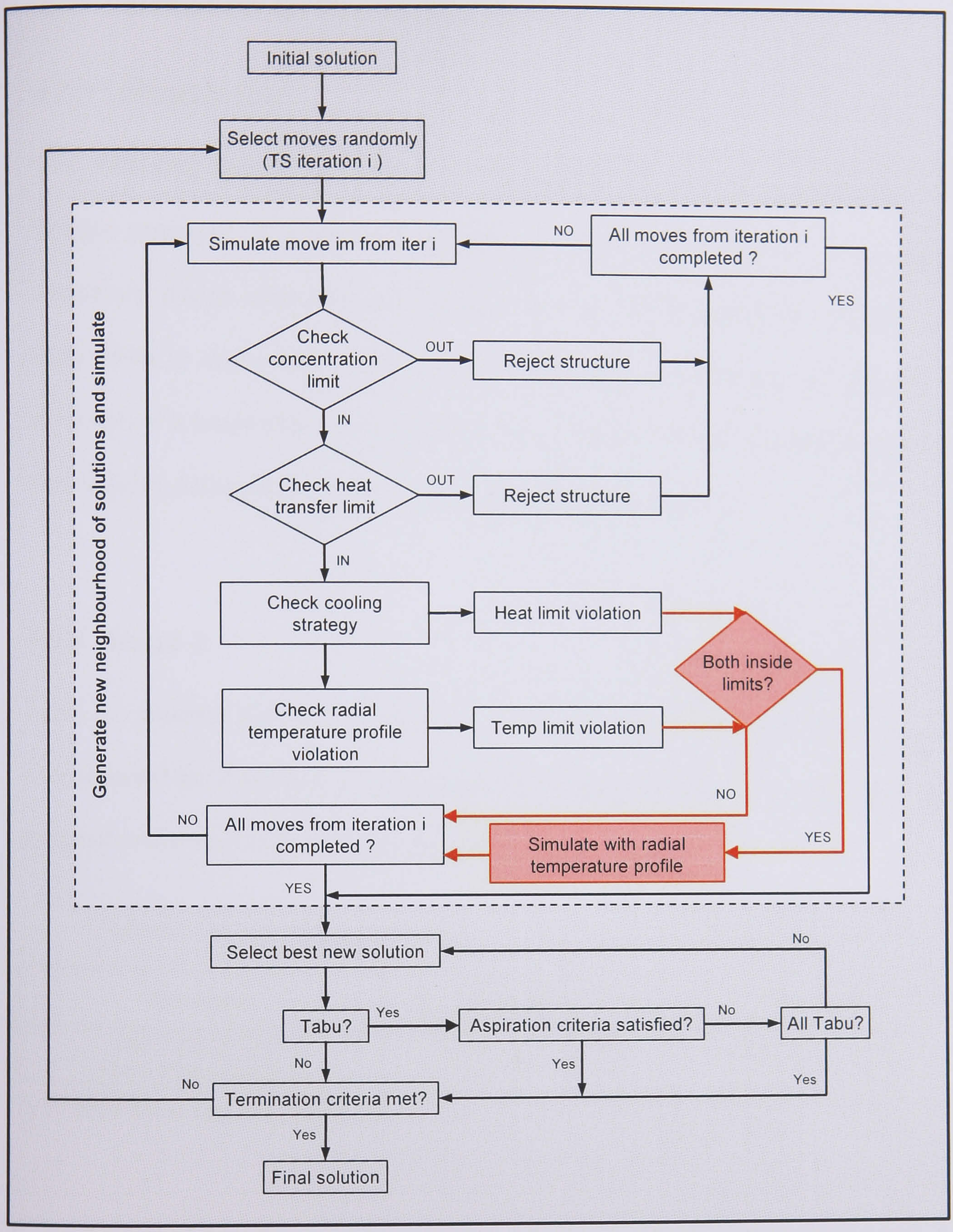

Figure 6.7: Tabu Search algorithm for Stage 4 involving PFRs structures.

6.5 Illustration Of The Methodology

6.5.1 Introduction

The following section presents the evolution of the optimal conceptual process designs proposed as a result of the multi-level approach (Stage 1). The optimal conceptual design identified in Chapter 5 for the styrene production process is the three PFRs in series with ethylbenzene side feeding. For comparison reasons, the evolution of a single PFR is also presented. For all cases, the results correspond to the best solution obtained out of ten converged optimisation runs.

6.5.2 Stage 2

Table 6.1 presents the OFV for Stages 1 and 2. A reduction of the OFV in Stage 2 was expected since the search space is smaller in this stage due to the new constraints imposed to the longitudinal temperature profile of the reactors.

Table 6.1: OFV and CPU times in Stages 1 and 2 for the styrene production process.

Structures	OFV (M$/yr)		CPU (hr)[1]	
	Stage 1	Stage 2	Stage 1	Stage 2
One PFR (MTR)	10.73	9.41	0.93	1.30
Three PFRs (MTRs)	11.37	10.85	12.47	16.05

[1] CPU times are average values of all runs.

For both structures the SOR (steam over reactant) is close to its lower limit in all the reactors (Table 6.2).

Table 6.2: Selectivities, ethylbenzene conversion and SOR for structures optimised in Stages 1 and 2 for the styrene production process.

Structure	Stage	Styrene selectivity (%)	Benzene selectivity (%)	Toluene selectivity (%)	Ethylbenzene conversion (%)	SOR inlet reactors (%)	SOR outlet reactors (%)
One PFR (MTR)	**1**	92.56	2.77	4.35	98.97	7.0	11.0
	2	92.47	3.55	3.99	98.86	7.0	10.6
Three PFRs (MTRs)	**1**	90.28	3.10	6.30	99.17	7.0, 7.1 and 7.0	8.9, 8.3 and 8.8
	2	89.04	4.08	6.54	99.18	7.1, 7.0 and 8.1	9.8, 9.6 and 8.5

Product profits (Table 6.3) evolve according to the amount of ethylbenzene that is converted to each product. In Stage 2, the ethylbenzene conversion is lower for the single PFR structure (Table 6.2) and therefore more flow is externally recycled. As a consequence, the external compressor is more expensive to buy and operate (Tables 6.3, 6.4). Due to the existence of more external recycle, more steam must be fed to the reactive section while keeping the SOR at its lowest constraint in the inlet of the reactor. Therefore, the feed compressor becomes also more expensive. The ethylbenzene conversion for the three PFRs structure is practically the same in both stages and as a result the external recycle is kept almost constant. As a consequence, no changes in the external compressor cost are expected. An improved steam feed distribution along the catalyst load is identified and as a result seven mols/s less are fed to the system (126 mols/s for Stage 1 and 119 mols/s for Stage 2). This reduction allows saving on raw material costs and requires a cheaper feed compressor to purchase and operate.

Table 6.3: Product value, operational costs and heat absorbed in the reactors for the structures optimised in Stages 1 and 2 for the styrene production process.

Structure	Stage	Product profit (M$/yr)	Raw material (M$/yr)	External compression (M$/yr)	Feed compression (M$/yr)
One PFR (MTR)	**1**	29.17	16.11	0.11	0.47
	2	29.08	16.25	0.12	0.50
Three PFRs (MTRs)	**1**	28.77	15.42	0.08	0.32
	2	28.51	15.35	0.08	0.30
Structure	**Stage**	**Hot utility (M$/yr)**	**Cold utility (M$/yr)**	**Reactor heating utility (M$/yr)**	**Heat absorbed per reactors (W)**
One PFR (MTR)	**1**	0.00	0.01	0.52	2.99E+06
	2	0.00	0.01	0.26	1.52E+06
Three PFRs (MTRs)	**1**	0.00	0.01	0.47	2.72E+06
	2	0.04	0.01	0.28	1.59E+06

The additional limitations imposed on the heat transfer between reactors and utilities for the transition from Stage 1 to Stage 2, result in less catalyst load being employed in both cases (Figure 6.8). Consequently, cheaper reactors are needed (*i.e.* smaller and with less heat exchange area), and less heat is absorbed from the reactors heating utility (Table 6.3).

Table 6.4: Fixed costs in Stages 1 and 2 for the styrene production process.

Structure	Stage	External compressor	Feed compressor	Reactors	Heat exchange network
One PFR (MTR) (M$)	**1**	0.30	1.04	0.22	1.75
	2	0.33	1.10	0.17	5.28
Three PFRs (MTRs) (M$)	**1**	0.25	0.75	0.32	1.65
	2	0.25	0.72	0.25	3.12

The extra constraints on the temperature profiles make the heat exchanger network (HXN) up to three times more expensive than in Stage 1 (Table 6.4). The inlet temperature of the reactors is 99 degrees higher for the single PFR structure and 100 for the three PFRs in series, whereas the outlet temperatures tend to be similar (Figure 6.8). These changes in temperatures along with the change in the amount of recycle and steam to be heated result in more expensive HXNs.

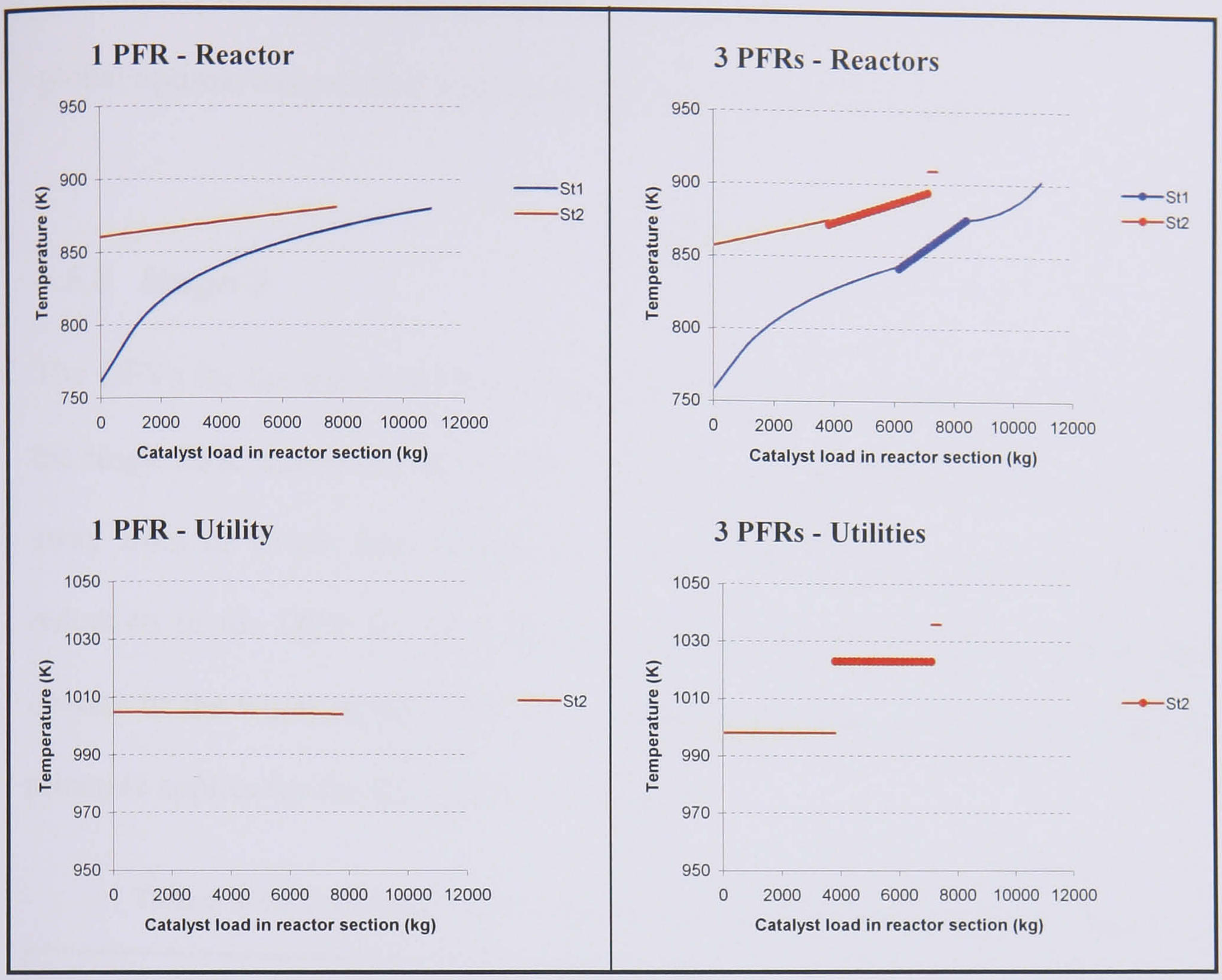

Figure 6.8: Temperature profiles for one and three PFRs in Stage 1 and 2 for the styrene production process: a) reactors, b) utilities.

The approach presented in Stage 2 proves that heat issues are particularly important for heterogeneously catalysed gas-phase reaction systems when considering reactors that exchange heat with a utility media. This suggests that, when screening process designs, previous developments in process synthesis that took into account reactor heat transfer issues should be upgraded with new approaches that are able to include the interactions with the utility media. The results confirm that the interactions between the reactive section and other sub-systems of the process flowsheet must be taken into account. Modifications in the temperatures of the reactors can have significant effects on the cost of other sub-systems (*e.g.* HXN), which can have a large impact on the overall process performance. If these interactions are not

considered, the search can be driven towards misleading optimal designs, as non-global optimal temperature regions for the reactors may be suggested.

6.5.3 Stage 3

The OFVs for the transition from Stage 2 to Stage 3 are presented in Table 6.5. For the single PFR, due to the fact that the temperature of the catalyst bed in Stage 2 is far away from its lower limit (temperature range: 861-881 K; lower limit: 400 K), a reduction in the OFV is not expected since each sub-CSTR of the reactor should operate in the worst of the cases at the same temperature in both stages. The same principle applies for the three PFRs in series.

Table 6.5: OFV and CPU times in Stages 2 and 3 for the styrene production process.

Structures	OFV (M$/yr)		CPU (hr)[1]	
	Stage 2	Stage 3	Stage 2	Stage 3
One PFR (MTR)	9.41	9.94	1.30	1.11
Three PFRs (MTRs)	10.85	10.93	16.05	19.47

[1] CPU times are average values of all runs.

However, since the diameter of the catalyst particle and the diameter and number of reactor tubes, are degrees of freedom for the optimisation in Stage 3, an improvement of the OFVs could be expected. These design variables for Stages 1, 2 and 3 are presented in Table 6.6.

Table 6.6: Diameter of the catalyst particle and diameter and number of reactor tubes for Stages 1, 2 and 3 for the styrene production process.

Structures	Stage	Diameter catalyst particle (mm)	Diameter of tubes (mm) / Nominal diameter of tubes (DN)	Number of tubes that form the reactors
One PFR (MTR)	1 and 2 3	4.7 2.2	25 mm DN=25	30000 11000
Three PFRs (MTRs)	1 and 2 3	4.7 4.2	25 mm DN=25	30000 10000

Two opposite effects on the reaction rates have been observed when the size of the catalyst particle is reduced. On one hand, the reduction increases the reaction rates enhancing raw material conversions, as better heat transfer is attained. On the other hand, it increases pressure losses along the reactor, which means that components partial pressures are lower and thus reaction rates decrease. In this case study, computational experimental observations indicate that the first effect has more impact on the process performance and optimisations always give preference to heat transfer issues over pressure losses. When reducing in Stage 3 the number of reactor tubes for the single PFR structure in order to decrease the reactor cost, heat transfer limitations appear and the catalyst size is reduced to improve heat transfer properties. That is not the case for the three PFRs structure as almost no heat limitations appear when decreasing the number of reactor tubes, and the size of the catalyst particle does not need to be modified much. Due to the changes in the catalyst particle and reactor tubes, the temperature profiles of the reactors and those of the utility media differ for the two stages and for both cases (Figure 6.9).

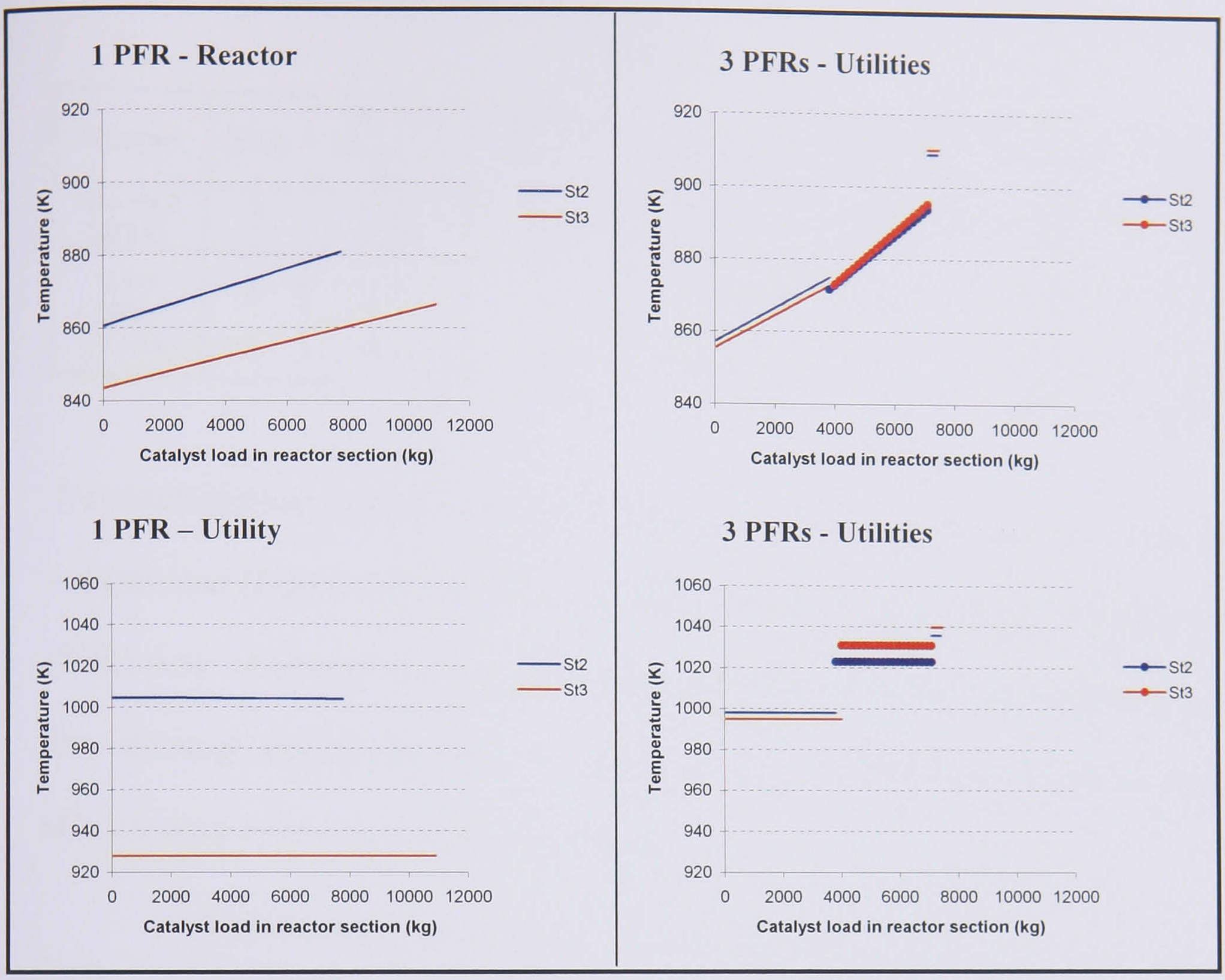

Figure 6.9: Temperature profiles for one and three PFRs in Stage 2 and 3 for the styrene production process: a) reactors, b) utilities.

The ethylbenzene process conversion for the single PFR structure increases if compared with Stage 2 (Table 6.7), which means that less ethylbenzene is externally recycled. Consequently, the operational and fixed costs for the external compressor decrease (Tables 6.8, 6.9). As another consequence, less steam must be fed to the reactive section to keep the SOR at its lowest constraint in the inlet of the reactor (Table 6.7). For that reason, the feed compressor and raw material costs are also minor. For the three PFRs structure, the results are practically the same for Stages 2 and 3 except for the reactors fixed cost (Table 6.8).

Table 6.7: Selectivities, ethylbenzene conversion and SOR in Stages 2 and 3 for the styrene production process.

Structure	Stage	Styrene selectivity (%)	Benzene selectivity (%)	Toluene selectivity (%)	Ethylbenzene conversion (%)	SOR inlet reactors (%)	SOR outlet reactors (%)
One PFR (MTR)	**2**	92.47	3.55	3.99	98.86	7.0	10.6
	3	93.06	2.74	4.20	98.94	7.0	11.0
Three PFRs (MTRs)	**2**	89.04	4.08	6.54	99.18	7.1, 7.0 and 8.1	9.8, 9.6 and 8.5
	3	89.16	4.09	6.41	99.18	7.1, 7.0 and 8.1	9.8, 9.5 and 8.5

The reactors fixed costs are lower in both cases, despite containing more or the same catalyst load (Figure 6.9), due to the different diameter and number of reactor tubes (Table 6.6). Although reactors have substantially been modified in structural terms, they exchange similar heats with the utility media as in Stage 2 and therefore, similar utility reactor costs are required (Table 6.9).

Table 6.8: Fixed costs in Stages 2 and 3 for the styrene production process.

Structure	Stage	External compressor	Feed compressor	Reactors	Heat exchange network
One PFR (MTR) (M$)	**2**	0.33	1.10	0.17	5.28
	3	0.31	1.06	0.11	4.71
Three PFRs (MTRs) (M$)	**2**	0.25	0.72	0.25	3.12
	3	0.25	0.72	0.12	3.10

The HXN becomes cheaper for the single PFR structure because of a combination of different factors:

i) There are lesser amounts of recycle and steam to be heated.

ii) The reactor inlet and outlet temperatures are reduced 17 and 14 degrees respectively.

Regarding the three PFRs structure, the recycled amount and the reactors inlet and outlet temperatures are very similar if compared to the previous stage. As a result, a similar HXN cost is obtained.

Table 6.9: Product value, operational costs and heat absorbed in the reactors in Stages 2 and 3 for the styrene production process.

Structure	Stage	Product profit (M$/yr)	Raw material (M$/yr)	External compression (M$/yr)	Feed compression (M$/yr)
One PFR (MTR)	**2**	29.08	16.25	0.12	0.50
	3	29.23	16.15	0.11	0.48
Three PFRs (MTRs)	**2**	28.51	15.35	0.08	0.30
	3	28.53	15.35	0.08	0.30
Structure	**Stage**	**Hot utility** (M$/yr)	**Cold utility** (M$/yr)	**Reactors heating utility** (M$/yr)	**Heat absorbed per reactors** (W)
One PFR (MTR)	**2**	0.00	0.01	0.26	1.52E+06
	3	0.00	0.01	0.27	1.55E+06
Three PFRs (MTRs)	**2**	0.04	0.01	0.28	1.59E+06
	3	0.04	0.01	0.28	1.59E+06

The approach developed in Stage 3 aims to account for the radial heat transfer effects of catalytic fixed bed reactors. It proves to be computationally efficient as similar CPU efforts are required for Stage 2 and 3 (Table 6.5) and to search the space robustly as no convergence problems are reported. With this tool, structural changes of the reactors can be screened and substantially different reactors can be identified. According to the author's experience, such screening is very difficult if not impossible to do with accurate models involving differential equations. The approach is expected to reveal much more significant differences in terms of reactor operational temperatures, if the reactors from design candidates identified in Stage 2 operate at or very close to their temperature limits.

6.5.4 Stage 4

The OFVs for the evolution of designs for Stages 3 and 4 are presented in Table 6.10. The change in the process models employed in Stage 4 does not necessarily imply improving or worsening the OFVs with respect to Stage 3. Consequently, the performances cannot be predicted beforehand.

Table 6.10: OFV and CPU times in Stages 3 and 4 for the styrene production process.

Structures	OFV (M$/yr)		CPU (hr)[1]	
	Stage 3	Stage 4	Stage 3	Stage 4
One PFR (MTR)	9.94	10.55	1.11	35.47
Three PFRs (MTRs)	10.93	10.70	19.47	39.69

[1] CPU times are average values of all runs.

For both structures, in Stage 4, the initial simulations of the optimal designs identified in Stage 3, result in having a HLV. To improve heat transfer properties and remove the HLV, the search progresses towards the reduction of the nominal diameter (DN) of the reactors tubes (Table 6.11).

Table 6.11: Diameter of the catalyst particle and diameter and number of reactor tubes for Stages 3 and 4 for the styrene production process.

Structures	Stage	Diameter catalyst particle (mm)	Nominal diameter of tubes (DN)	Number of tubes that form the reactors
One PFR (MTR)	3	2.2	DN=25	11000
	4	2.7	DN=20	11000
Three PFRs (MTRs)	3	4.2	DN=25	10000
	4	2.2	DN=20	12000

For the single PFR, once the DN of the reactor tubes is reduced, the diameter of the particle is increased with regard to Stage 3. The fact that no HLV appears after decreasing the DN indicates that heat transfer issues are not so limiting, and pressure losses can be reduced by increasing the catalyst particle size. Regarding the three PFRs structure, heat transfer issues are still limiting the performance after reducing the DN of the reactor tubes. Therefore, the size of the catalyst particle must be kept lower to improve heat transfer, despite producing more pressure losses. Due to the changes in the catalyst particle and reactor tubes, the reactors temperature profiles and those of the utility media vary as shown in Figure 6.10.

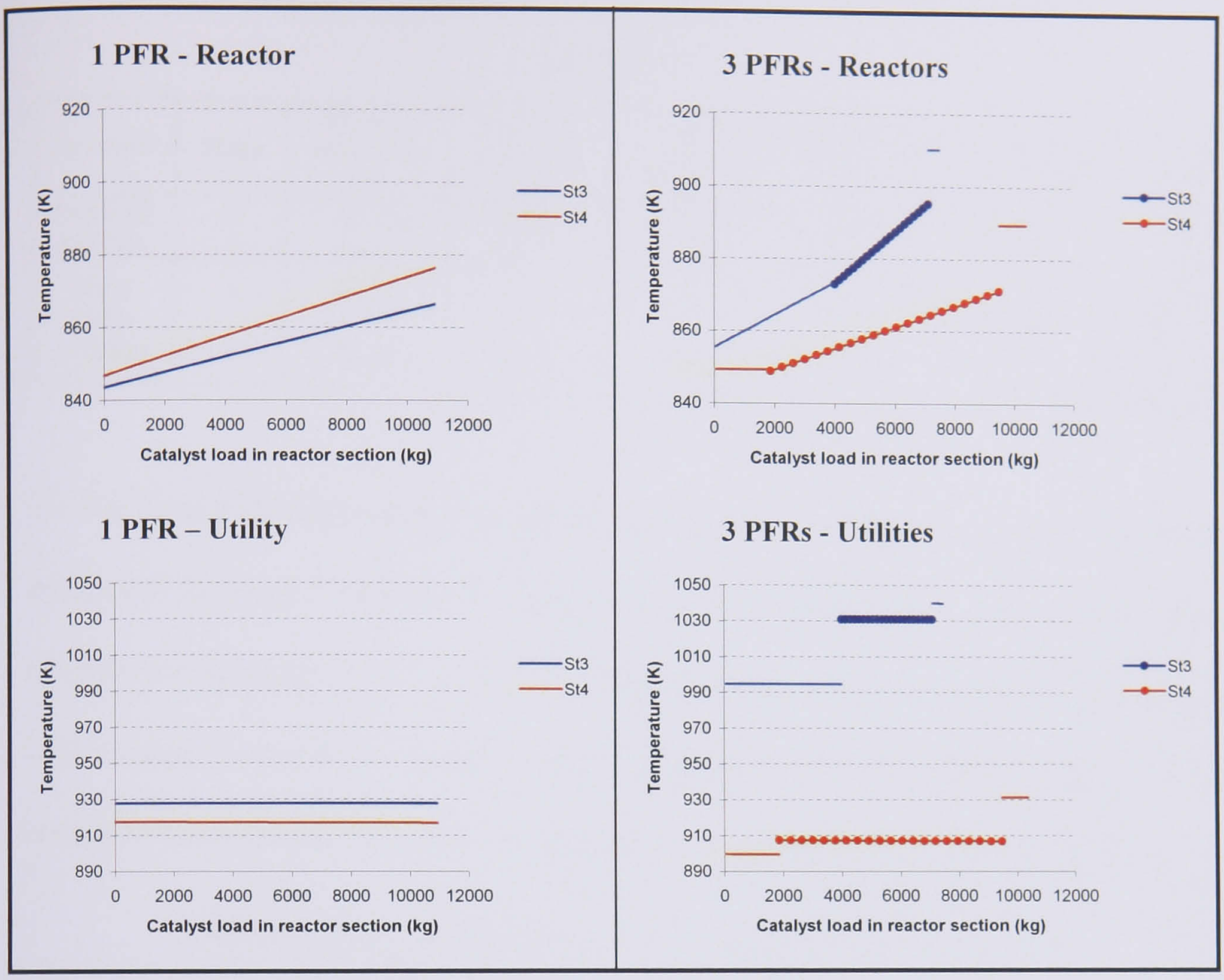

Figure 6.10: Temperature profiles for one and three PFRs in Stage 3 and 4 for the styrene production process: a) reactors, b) utilities.

For the single PFR structure in Stage 4, the ethylbenzene process conversion increases if compared to Stage 3 (Table 6.12). Therefore, less external recycle is compressed and the operational and fixed costs of the external compressor are lower (Table 6.13, 6.14). The SOR at the inlet of the reactor is not exactly at its lowest constraint, but the smaller recycle results in less steam fed to the reactive section and therefore in less raw material costs. Consequently, the feed compressor is also cheaper to buy and operate.

Table 6.12: Selectivities, ethylbenzene conversion and SOR in Stages 3 and 4 for the styrene production process.

Structure	Stage	Styrene selectivity (%)	Benzene selectivity (%)	Toluene selectivity (%)	Ethylbenzene conversion (%)	SOR inlet reactors (%)	SOR outlet reactors (%)
One PFR (MTR)	**3**	93.06	2.74	4.20	98.94	7.0	11.0
	4	91.75	3.26	3.86	99.15	7.2	12.2
Three PFRs (MTRs)	**3**	89.16	4.09	6.41	99.18	7.1, 7.0 and 8.1	9.8, 9.5 and 8.5
	4	90.92	3.43	5.34	99.14	7.2, 7.2 and 8.8	8.1, 11.2 and 9.5

For the three PFRs structure, the ethylbenzene process conversion slightly decreases if compared to Stage 3, and more external recycle is compressed. Hence, the external compressor becomes more costly. The SORs at the inlet of each reactor are slightly higher than in previous stages, which combined with the bigger external recycle results in more steam fed to the system and in a more expensive feed compressor.

Table 6.13: Fixed costs in Stages 3 and 4 for the styrene production process.

Structure	Stage	External compressor	Feed compressor	Reactors	Heat exchange network
One PFR (MTR) (M$)	**3**	0.31	1.06	0.11	4.71
	4	0.26	0.98	0.11	3.85
Three PFRs (MTRs) (M$)	**3**	0.25	0.72	0.12	3.10
	4	0.26	0.81	0.17	3.92

The different amounts of ethylbenzene recycled and steam fed, together with the changes in the temperature profiles (Figure 6.10), result in different HXN costs (Table 6.13).

For the three PFRs structure, the reactors are more expensive because they contain more catalyst load (Figure 6.10) despite being structurally very similar to the ones identified in the previous stage (Table 6.11). For the single PFR, the catalyst load and the reactor cost are the same as in Stage 3.

Table 6.14: Product value, operational costs and heat absorbed in the reactors in Stages 3 and 4 for the styrene production process.

Structure	Stage	Product profit (M$/yr)	Raw material (M$/yr)	External compression (M$/yr)	Feed compression (M$/yr)
One PFR (MTR)	**3**	29.23	16.15	0.11	0.48
	4	29.22	15.95	0.09	0.44
Three PFRs (MTRs)	**3**	28.53	15.35	0.08	0.30
	4	28.89	15.55	0.09	0.35
Structure	**Stage**	**Hot utility** (M$/yr)	**Cold utility** (M$/yr)	**Reactors heating utility** (M$/yr)	**Heat absorbed per reactors** (W)
One PFR (MTR)	**3**	0.00	0.01	0.27	1.55E+06
	4	0.00	0.01	0.28	1.59E+06
Three PFRs (MTRs)	**3**	0.04	0.01	0.28	1.59E+06
	4	0.05	0.01	0.25	1.44E+06

The change in the OFVs of Stage 4 cannot be predicted because the increase of modelling detail does not imply obtaining better or worst results. An interesting observation is that the DNs of the reactor tubes are reduced from 25 in Stage 3 to 20 in Stage 4. This can be explained because the models employed in Stage 4 result in different heat transfer limitations than those employed in Stage 3. This also results in different reactor temperature profiles (Figure 6.10). The approach presented in Stage 4 proves to be very computationally demanding (Table 6.10).

6.6 Conclusions

The multi-level approach (Stage 1) presented in Chapter 5 proved to handle the complex kinetics involved in the heterogeneously catalysed gas-phase reaction systems fast and reliably for process design screening purposes. Stage 1 provides good insights in terms of process design trade-offs (feeding, bypassing, mixing patterns, etc.) and enables the reliable identification of potential process performance

improvements along with the process complexities associated. However, in terms of the temperature management, it was clear that the longitudinal temperature profiles proposed for the PFRs could only be reached if one had every single volume, in which the PFRs are discretised, under control. But having the temperature profiles fully controlled is not implemented in practice. The idea of having multiple heat exchangers within a single reactor seems rather unpractical and uneconomical. In order to assess the practical heating / cooling for such reactors, temperature and heat management issues needed to be addressed. For such purpose, the multi-stage evolution of designs has been presented in this chapter.

The multi-stage evolution of designs occurs in several stages. Stage 2 has proved that heat issues are critical for heterogeneously catalysed gas-phase reaction systems. During the screening of non-isothermal reactor designs, the interactions with the utility media must be taken into account as the full control of each individual volume is neither practical nor economical. For the illustration example presented, the realistic heating schemes proposed have remarkably impacted the performances. The approach developed in Stage 3 searches the space robustly while including radial heat transfer effects in catalytic fixed beds. For the case study presented, structural changes in the reactors that deliver favourable heat transfer policies with the utility media have been efficiently identified. However, the additional changes included in the rigour of modelling do not have much impact on the performance. This conclusion is also applicable for the transition between Stage 3 and 4. Although the approach developed in Stage 4 allows performing the superstructure optimisation of highly complex process design schemes with time consuming reactor models, the real impact on process performance with respect to Stage 3 is minor. Consequently, it can

be concluded that once the practical heating / cooling strategy is realised, the OFV does not change much regardless the addition of detail in the models employed. However, for the case studied, Stage 3 is indispensable because it allows identifying key structural modifications in the reactors that make possible realistic heat transfer policies with the utility media. Besides, for those hypothetic cases that were constrained in Stage 2 by the temperatures in the catalytic fixed beds (*i.e.* $T_{isc} \approx T_{upper\ limit}$ or $T_{isc} \approx T_{lower\ limit}$), Stage 3 would have a real impact on the performance by reducing / increasing the operating temperatures inside the units. The reduction / increase of temperatures would result in a decrease of reaction rates and thus product formation.

At any stage of the evolution of designs, information on the optimal operating conditions is created. This information can be communicated to the kinetic development team to guide new experiments and validate the experimental models in the optimal regions in which the catalyst is to be used. Stages 2 and 3 have proved to be computationally proficient and robust. Therefore, they could be ready for the integration of the experimental kinetic development and the process design activities. The time consuming approach developed in Stage 4, could be used to test kinetic models at advanced stages of the experimental development.

Finally, regarding the styrene production process, the evolution of the optimal conceptual design identified in Stage 1, the three PFRs structure, reveals after Stage 4 an OFV enhancement of 11 % if compared to the adiabatic reactor typically found in industry.

CHAPTER 7.

A Case Study In Acetic Acid Production

7.1 Introduction

The Decision Support Framework presented in Chapters 5 and 6 is employed here for the study of an acetic acid production process. The objective of the application is to identify trends and key features of the system that enhance the overall process performance in terms of Economic Potential (EP). Appendix 3 presents the data for the process, the kinetic model, the relevant process design features of the system and the capital and operational cost expressions along with the cost of the raw materials and products.

Acetic acid can be produced by methanol carbonylation, acetaldehyde oxidation, methyl formate isomerisation, methane carbonylation, ethylene oxidation and fermentation. More than 60 % of the world production is through the methanol carbonylation (initially proposed by BASF in the mid 50s and later improved by Monsanto in 1970 and BP Chemicals in 1996). The study presented here accounts for the gas-phase heterogeneously catalysed selective oxidation of ethane over a Mo1V0.25Nb0.12Pd0.0005Ox catalyst (Linke *et al.*, 2002a, b). The feed in gaseous state (ethane and oxygen) is fed to the reaction units (Figure 7.1) to produce acetic

acid. Water, carbon dioxide and ethylene are the by-products formed. The reactive units are followed by a flash expansion to separate water and acetic acid from non-condensable components. The water / acetic acid stream is separated in a distillation column. Non-condensable components are treated in an absorber where the oxygen and the carbon dioxide are removed. The hydrocarbons are recycled to the reactive units.

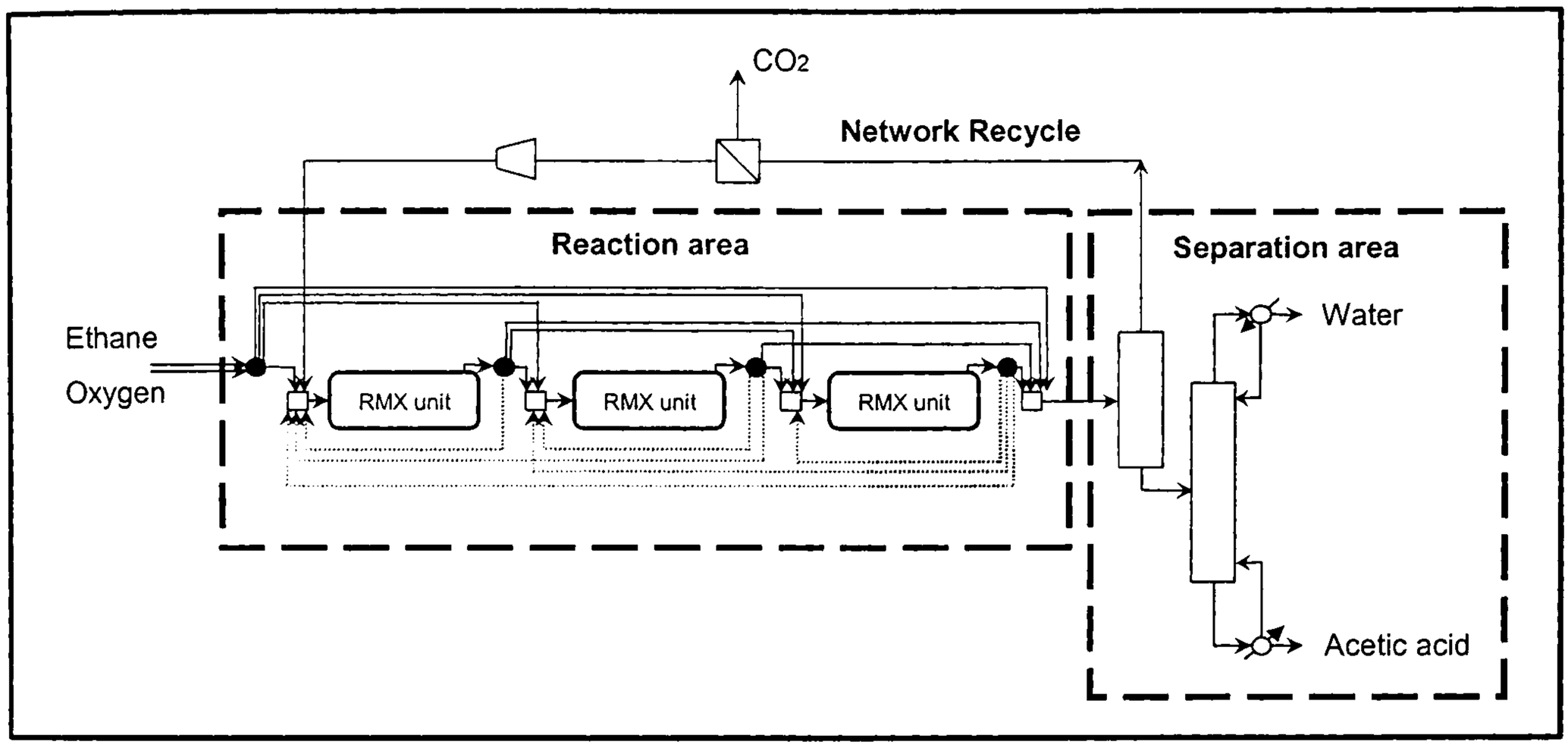

Figure 7.1: Superstructure representation for the acetic acid production process.

In the following section, the multi-stage evolution of designs for the acetic acid production process is detailed. After that, the computational efforts involved in each stage are discussed and finally, the conclusions are presented.

7.2 Multi-Stage Evolution Of Designs

7.2.1 STAGE 1: Multi-Level Approach Development And Results

7.2.1.1 Introduction

For this case study, the steps involved in Stage 1, which are the basis of the multi-level approach (see Figure 5.8), are summarised in:

- **Step A) Base case structure:** Establishment of two initial base cases.
- **Step B) Performance targeting:** Establishment of a third base case in order to identify the maximum possible objective function value (OFV) that can be achieved.
- **Step C) Increase search space - 1:** Setting of targeted structures based on the analysis of results from Steps A and B.
- **Step D) Increase search space - 2:** Setting of more targeted structures based on the analysis of results from Step C.

The solutions presented are the best results out of ten converged optimisation runs (except where stated).

Step A) Base case structure

The two initial base cases, which employ conventional reactor schemes, are a single CSTR and a single PFR.

The single CSTR is operated at 542 K and its OFV is -7.5 M$/yr. In this case, the

process selectivity is 61.0 %, the ethane conversion 10.2 % and the oxygen conversion 30.3 %.

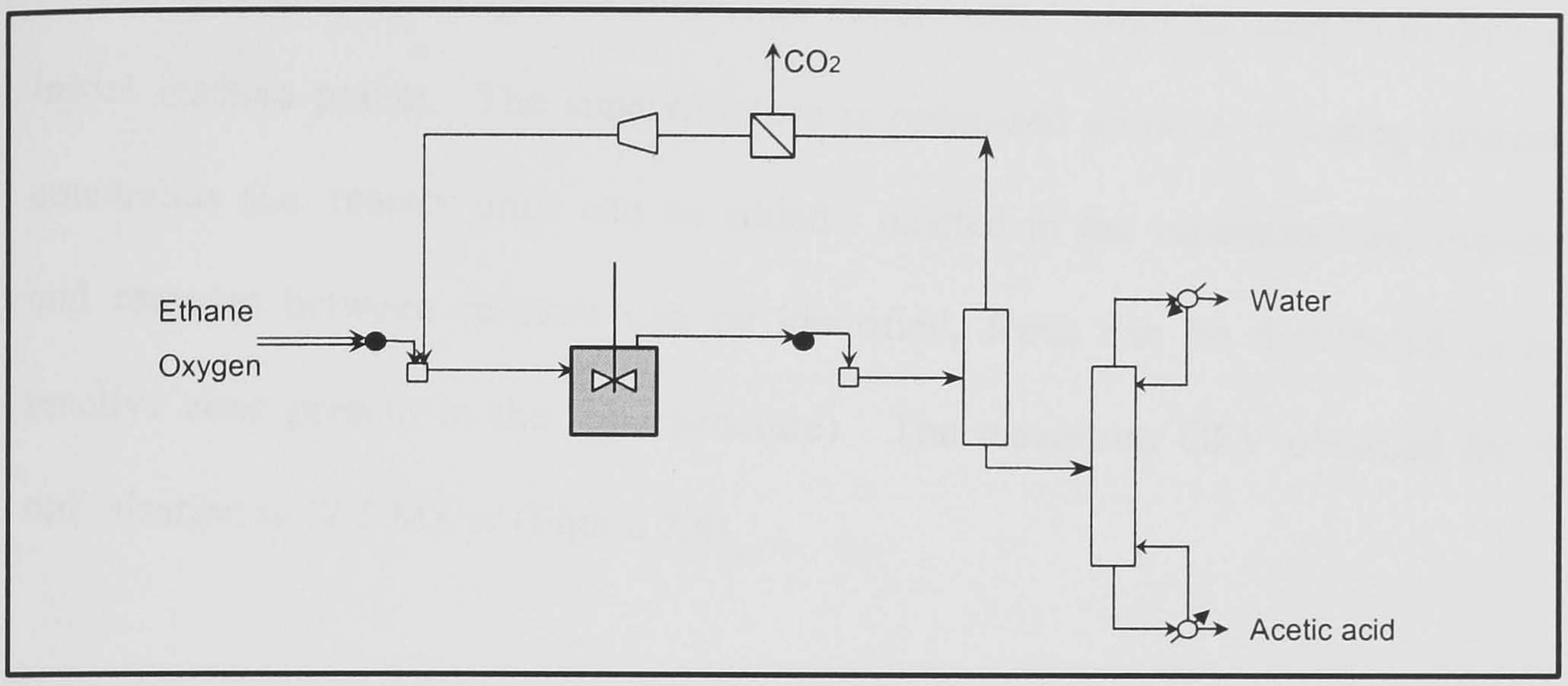

Figure 7.2: Superstructure representation for the CSTR base case structure for the acetic acid production process.

The EP for a single PFR is 8.5 M$/yr and its temperature follows a logarithmic profile with an initial value of 545 K and a final value of 570 K. The process selectivity is 57.8 %, the ethane conversion 54.1 % and the oxygen conversion 82.0 %.

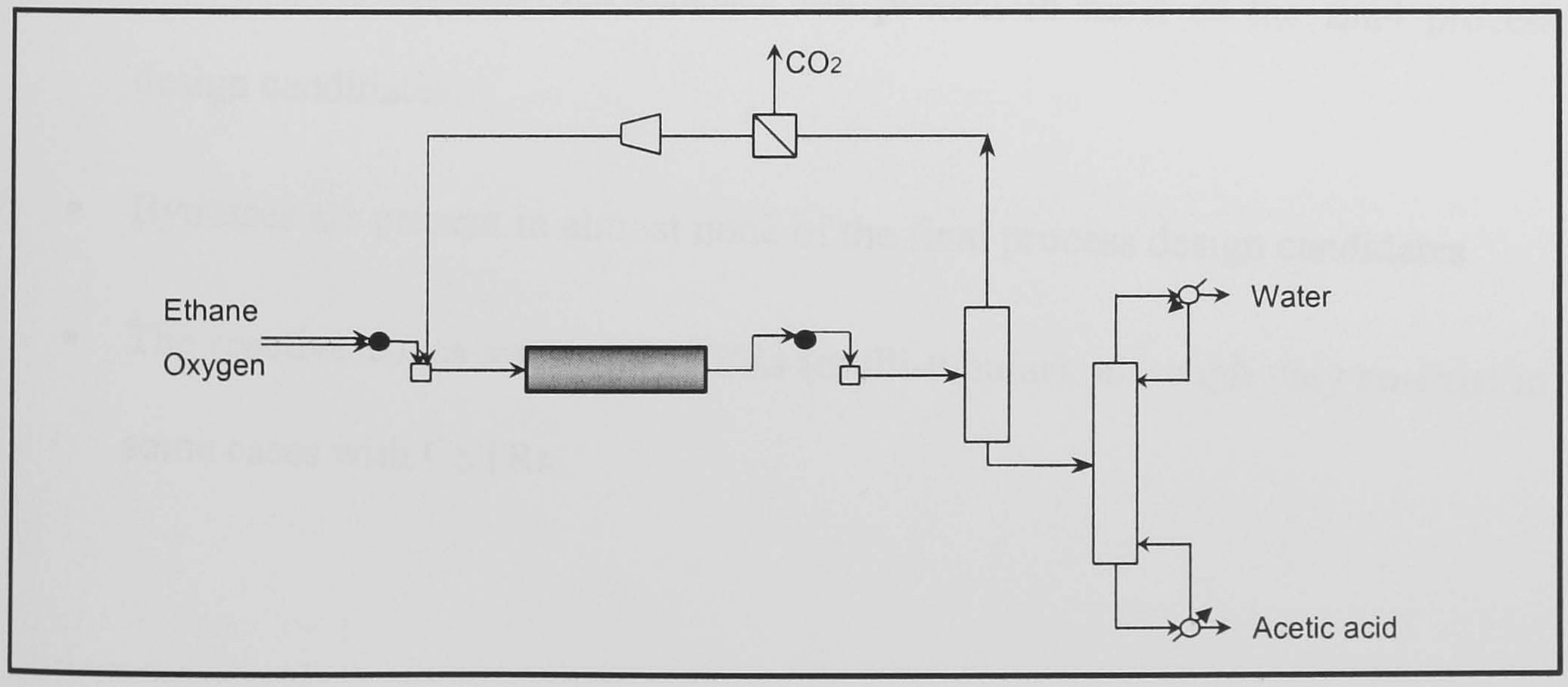

Figure 7.3: Superstructure representation for the PFR base case structure for the acetic acid production process.

Step B) Performance targeting

A third base case is established to identify the maximum achievable OFV. The base case is the result of the optimisation of 25 experiments, which all start from different initial feasible points. The superstructure is optimised without imposing structural constraints (*i.e.* reactor units can be added / deleted in the superstructure, bypasses and recycles between reactors can be identified, feeds can be distributed to any reactive zone present in the superstructure). The maximum OFV obtained for the optimisation is 22.5 M$/yr (Figure 7.4).

The analysis of the experiments shows that:

- Oxygen side stream feeding is present in many of the final process design candidates.
- Ethane side stream feeding is present in less than half of the final process design candidates.
- Internal recycles between reactors are present in most of the final process design candidates.
- Bypasses are present in almost none of the final process design candidates.
- The reactive zones are mainly PFRs (multi-tubular), although they co-exist in some cases with CSTRs.

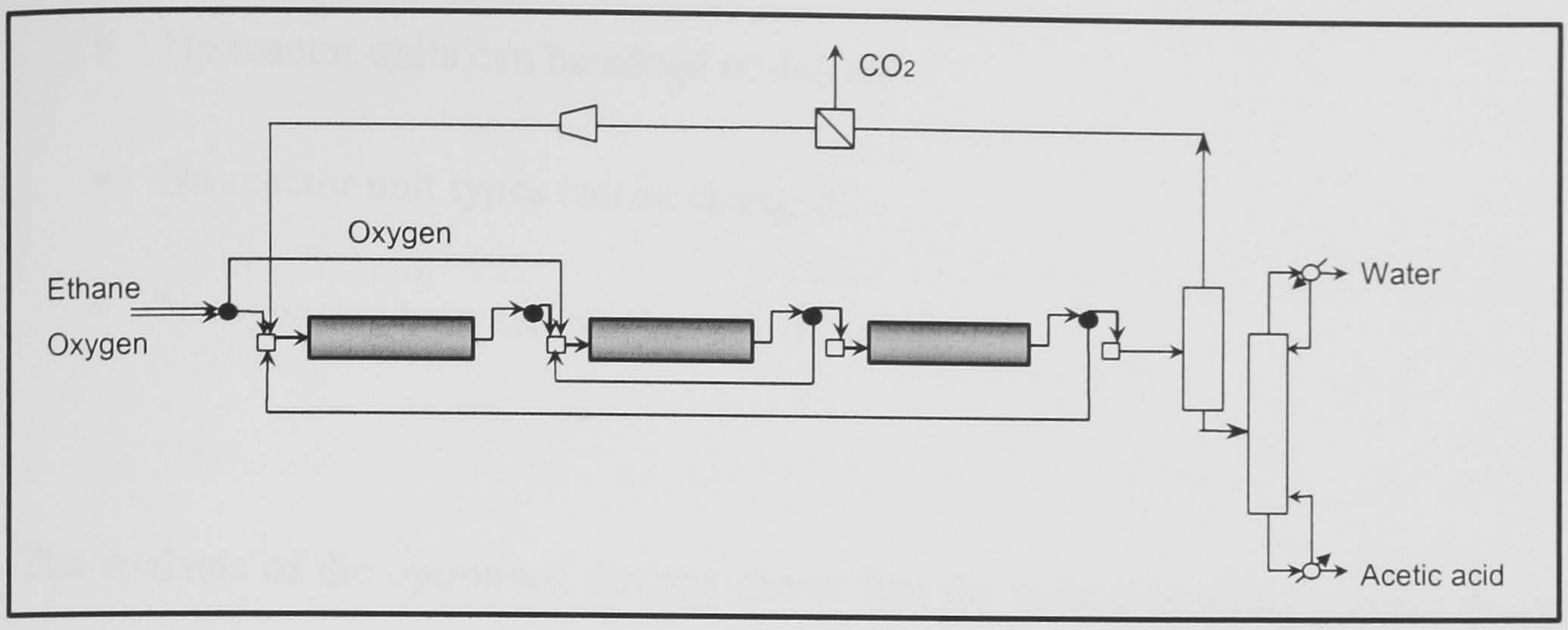

Figure 7.4: Resulting superstructure representation for the performance targeting step in the acetic acid production process.

Step C) Increase search space - 1

Targeted structures based on the analysis of results from the previous steps are investigated. The case studies explored are as follows (all the PFRs are multi-tubular reactors):

- Structures with internal recycle:
  - PFR.
  - PFR + PFR.
  - CSTR + PFR.
  - PFR + CSTR.
- Structures without internal recycle
  - CSTR + CSTR.
  - PFR + PFR.
  - CSTR + PFR.
  - PFR + CSTR.

Three structural limitations are imposed to all experiments:

- No reactor units can be added or deleted.
- No reactor unit types can be changed.
- No bypasses between reactors are allowed.

The analysis of the optimised designs shows that the most promising process design candidates are the ones in which:

- side streams of oxygen feed are identified, and;
- recycles between reactors are allowed.

Step D) Increase search space - 2

Based on the analysis of results from the previous steps, new targeted structures are explored to study the following effects:

- Effect of oxygen side feeding: In order to identify whether any relationship between oxygen feed distribution along the reactor and the OFV exists, three PFRs in series are optimised.
- Effect of internal recycle: Due to the fact that high internal recycle flows are observed in Step C, new targeted studies are set to investigate the effect of lower internal recycle flows. The cases are:
  - PFR
  - CSTR + PFR
  - PFR + CSTR

- PFR + PFR
- PFR + PFR + PFR

- Effect of diluting the feed: Two new studies are performed in order to assess the impact of different means of feed dilution on the OFV. The objective is to check whether the dilution effect of the recycle can be substituted by any other form of dilution. The new dilutions are achieved adding an extra feed stream to the reaction section (a single PFR). The extra feed, which is a new degree of freedom for the optimisation, consists of a pure component involved in the system (water or carbon dioxide).

7.2.1.2 Analysis Of Results From The Targeted Structures (Steps C And D)

Structures formed only by combinations of CSTRs and PFRs

The comparison between structures formed only by PFRs and structures formed by CSTRs and PFRs (CSTR + PFR and PFR + CSTR), proves that the addition of back-mixing does not improve the OFV.

Structures formed by one PFR, two PFRs and three PFRs in series

In this section, the results obtained with the structures involving PFRs are discussed. Experiments with different internal recycle limits for the three structures have been performed. The OFVs, the ethane conversions, the process selectivity and the acetic acid production are shown in Figures 7.5, 7.6, 7.7 and 7.8. For recycle limits above 750 mols/s there is no improvement observed for the single PFR. This case, which is not shown in the figures below, results in an OFV of 20.5 M$/yr, an ethane conversion of 74.8 % and a process selectivity of 67.3 %. For the two PFRs in series,

internal recycles are identified from the second reactor to the first and / or second reactor. Oxygen side streams are identified for all the cases. Ethane side streams are not identified for any case. For the three PFRs in series, the search identifies oxygen side feeding for all the cases. These side streams are present for all cases in the second reactor and in five out of six of the cases in the third reactor. Ethane side feeding is not identified for any case. For recycle limits above 500 mols/s, there is no improvement observed for the two and three PFRs cases.

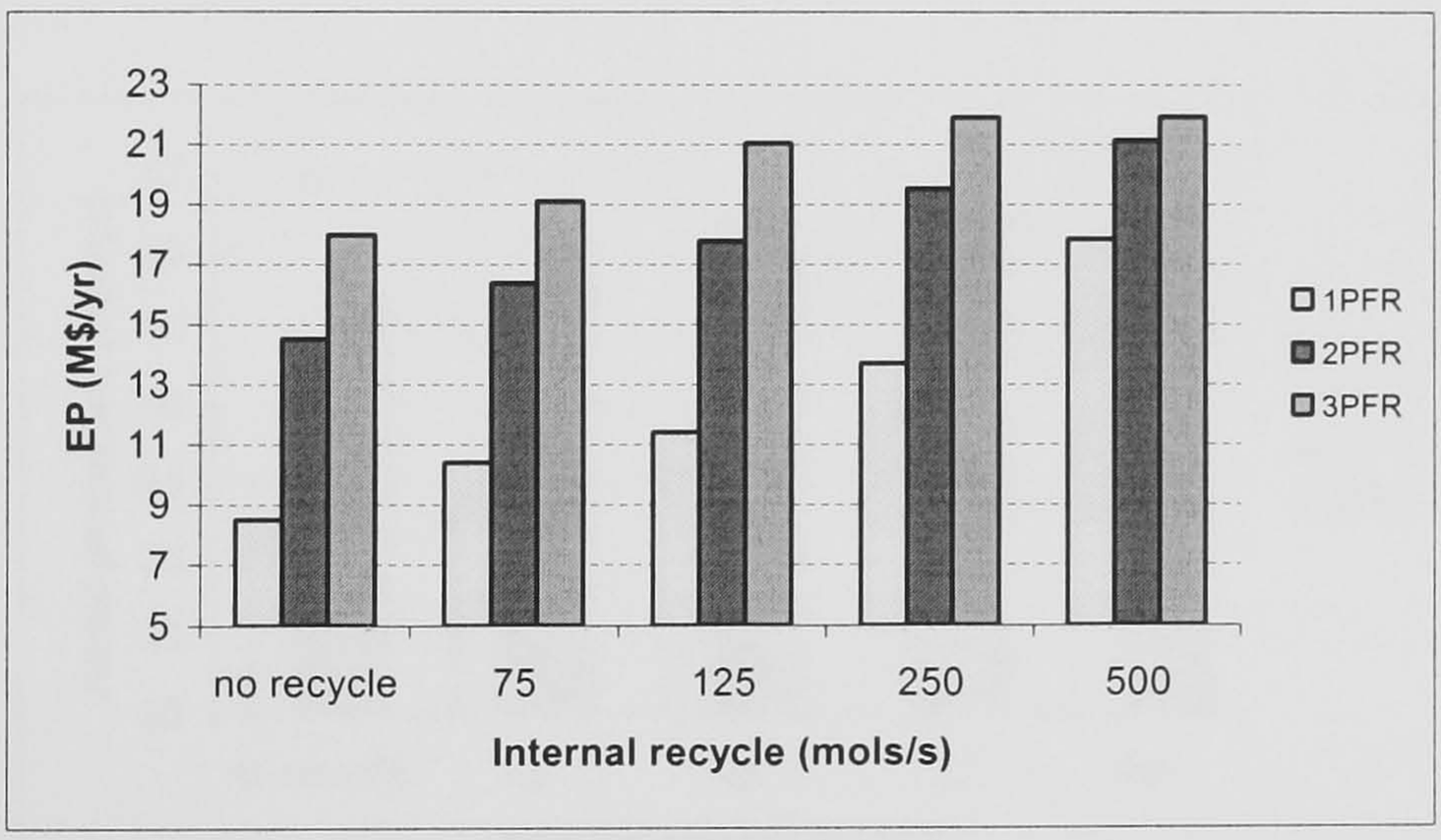

Figure 7.5: EP (M$/yr) for the one, two and three PFRs structures for the acetic acid production process.

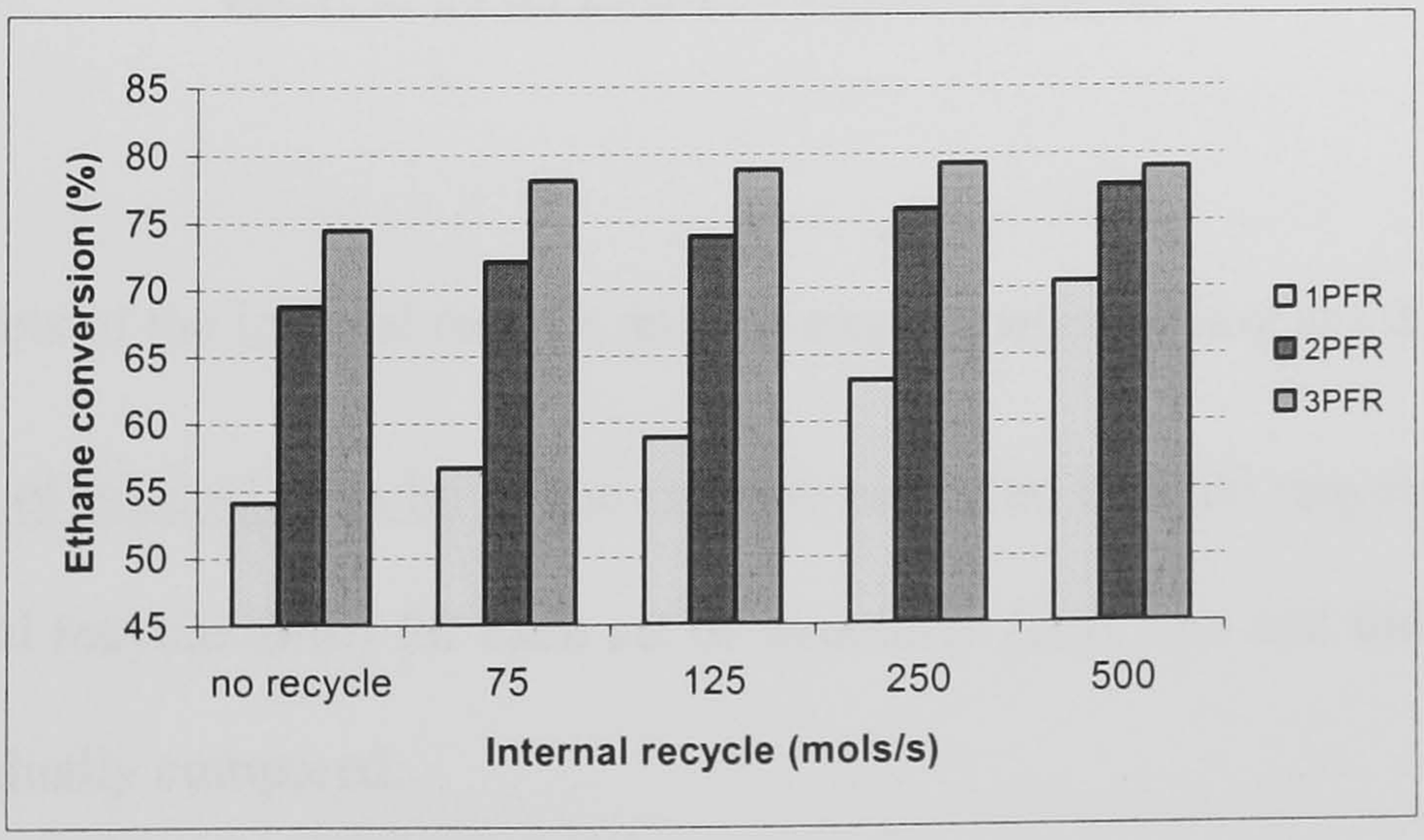

Figure 7.6: Ethane conversion for the one, two and three PFRs structures for the acetic acid production process.

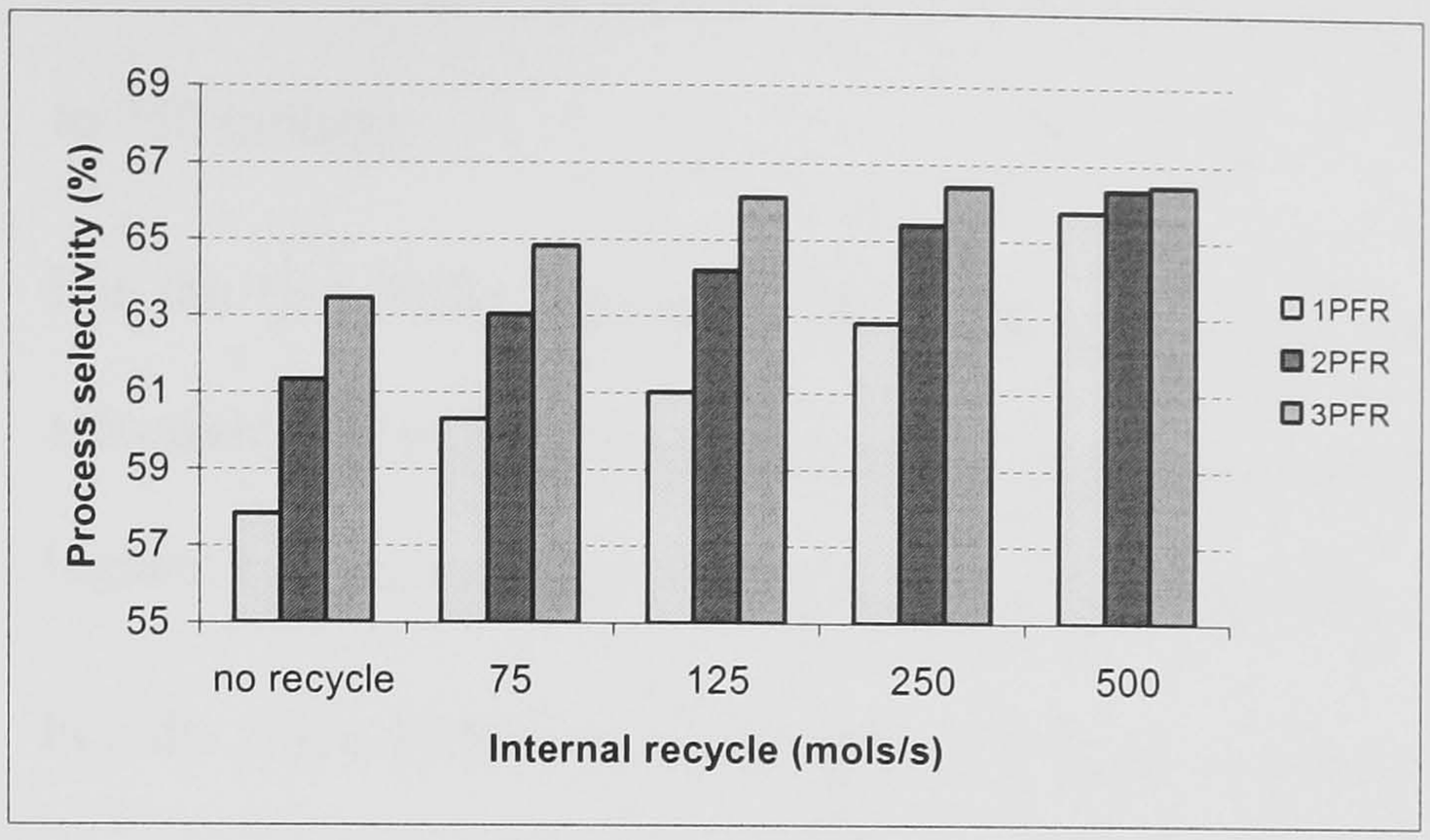

Figure 7.7: Process selectivity for the one, two and three PFRs structures for the acetic acid production process.

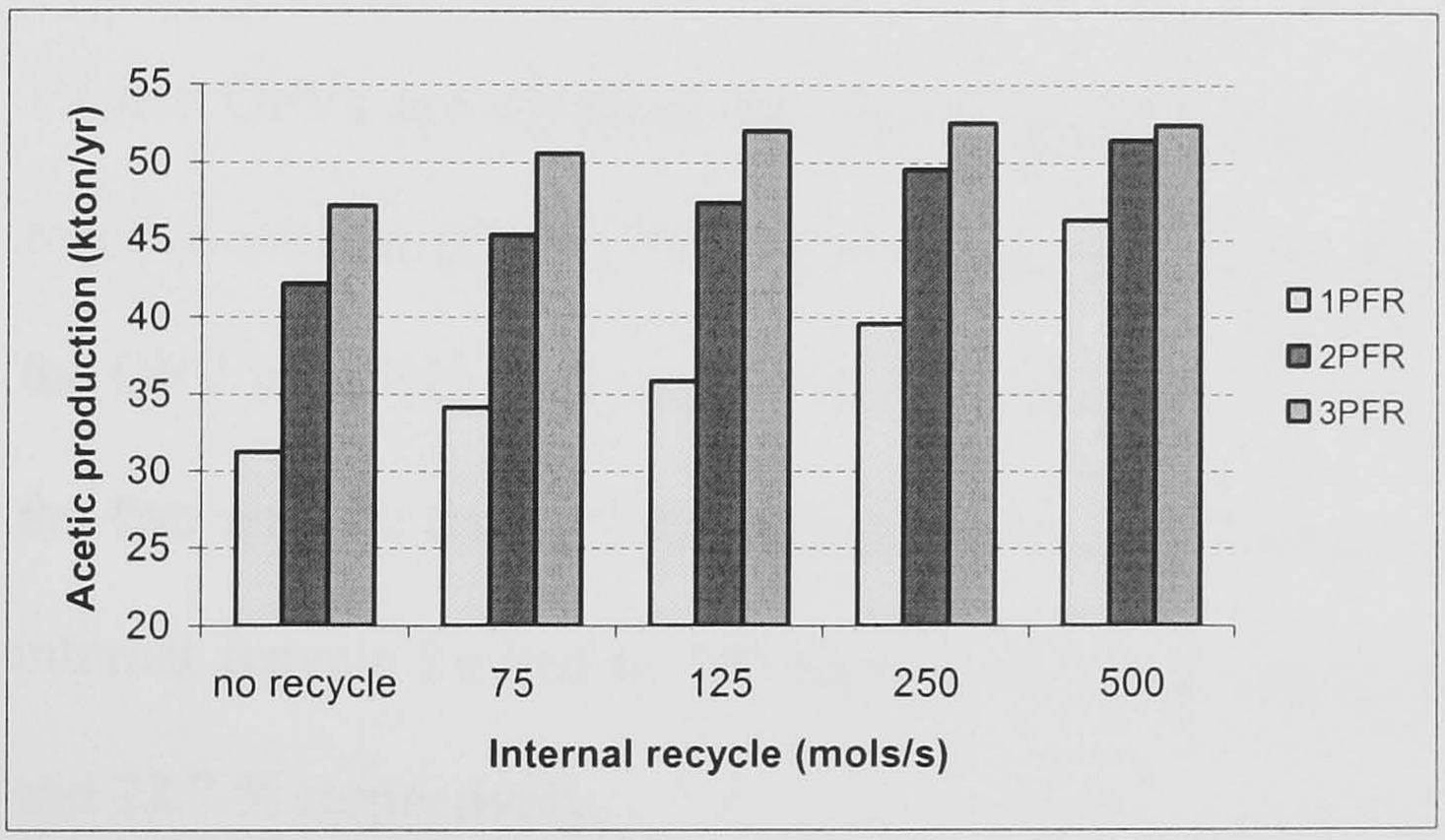

Figure 7.8: Acetic acid production for the one, two and three PFRs structures for the acetic acid production process.

Next, the effects of the internal recycle and the oxygen side feeding are discussed:

- Effect of internal recycle: If the extreme cases (no internal recycle and highest internal recycle limit) for each set of structures (one, two and three PFRs) are individually compared:
    - For the one PFR structures, the presence of internal recycle rises the OFV up to 141 %, the process selectivity up to 16.3 % and the ethane

conversion up to 38.0 % (the highest internal recycle limit refers here to 750 mols/s).

- For the two PFRs structures, the OFV rises up to 45.6 %, process selectivity up to 8.2 % and the ethane conversion up to 13.0 % (the highest internal recycle limit for this case is 500 mols/s).

- For the three PFRs structures, the OFV rises up to 21.9 %, process selectivity up to 4.7 % and the ethane conversion up to 6.1 % (the highest internal recycle limit now is 500 mols/s).

- Effect of oxygen feed distribution:

  - Higher OFVs are obtained for higher oxygen distribution along the reactive section (Figure 7.5). For the cases without internal recycle, the OFV improves with respect to the single PFR, 71 % and 112 % for the two and the three PFRs cases respectively. For the cases with an internal recycle limited to 500 mols/s, the OFV improves by 18.4 % and 22.7 % respectively.

  - Higher ethane conversions are obtained for higher oxygen distribution (Figure 7.6). For the cases without internal recycle, the ethane conversion increases with regard to the single PFR, 27.1 % and 37.6 % for the two and the three PFRs cases respectively. For the cases with an internal recycle limited to 500 mols/s, ethane conversions increase by 10.2 % and 12.1 % respectively.

  - Regarding process selectivity, at low internal recycle limits the highest selectivities are obtained for higher oxygen distribution (Figure 7.7). This trade-off progressively changes as more internal recycle is

allowed. For an internal recycle limited to 750 mol/s, the single PFR reaches a value of 67.3 % (not shown in Figure 7.7), which is the highest value obtained so far.

- Oxygen conversions are kept in the range of 79-82 % for one PFR structures, between 80-86 % for the two PFRs structures and between 83-85 % for the three PFRs structures.

Next, the costs for the three sets of structures are discussed. For the single PFR case, the results for a structure with unlimited internal recycle are also included. This structure is employed later on, in the study of the different means of feed dilution and in the evolution of stages. For this case the internal recycle identified is 827 mols/s. The resulting OFV is the same as the case in which the recycle is limited to 750 mol/s (20.5M$/yr). The ethane conversion is 74.8 %, the process selectivity is 67.2 % and the oxygen conversion is 78.6 %.

The capital costs for the three sets of structures are presented in Figures 7.9, 7.10 and 7.11. For each individual set of structures, the heat exchanger network (HXN) capital cost is progressively reduced at higher internal recycles because the required heat exchange area is reduced and the number of heat exchange units is kept constant. When no internal recycle is allowed, the area is higher than the case with the smallest internal recycle limit (75 mols/s). However, the number of heat exchanger units is smaller. The combined effect on the capital cost equation (Equation A2.3) generates a lower capital cost. The reactor fixed cost is constant as it depends on the volume, which is the maximum allowable in all the cases, and on the maximum pressure inside

the reactor, which is the same for all the cases (Equations A2.6, A2.7 and A2.8).

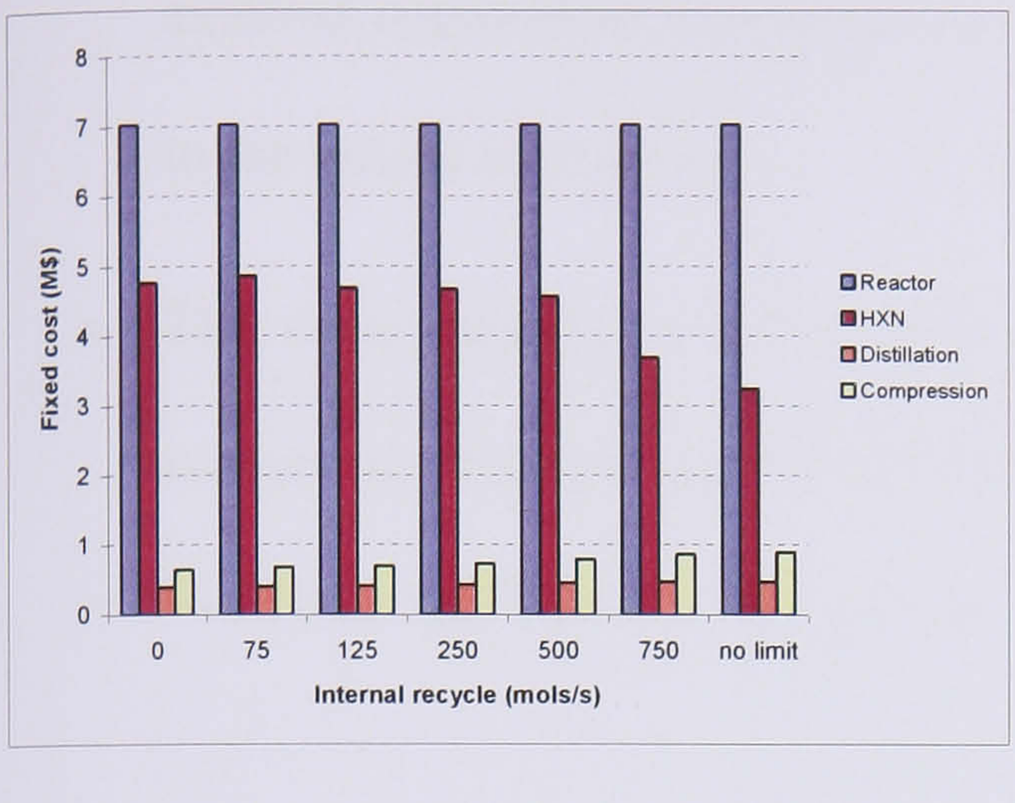

Figure 7.9: Fixed costs for one PFR with different internal recycle limits for the acetic acid production process.

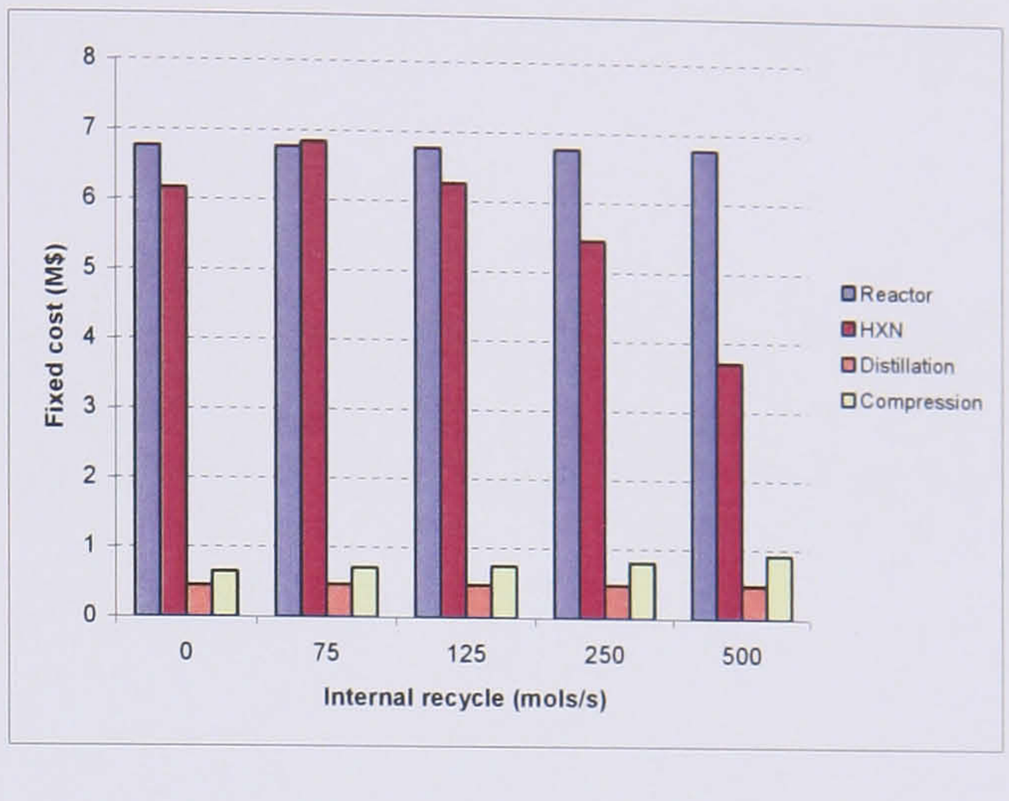

Figure 7.10: Fixed costs for the two PFRs with different internal recycle limits for the acetic acid production process.

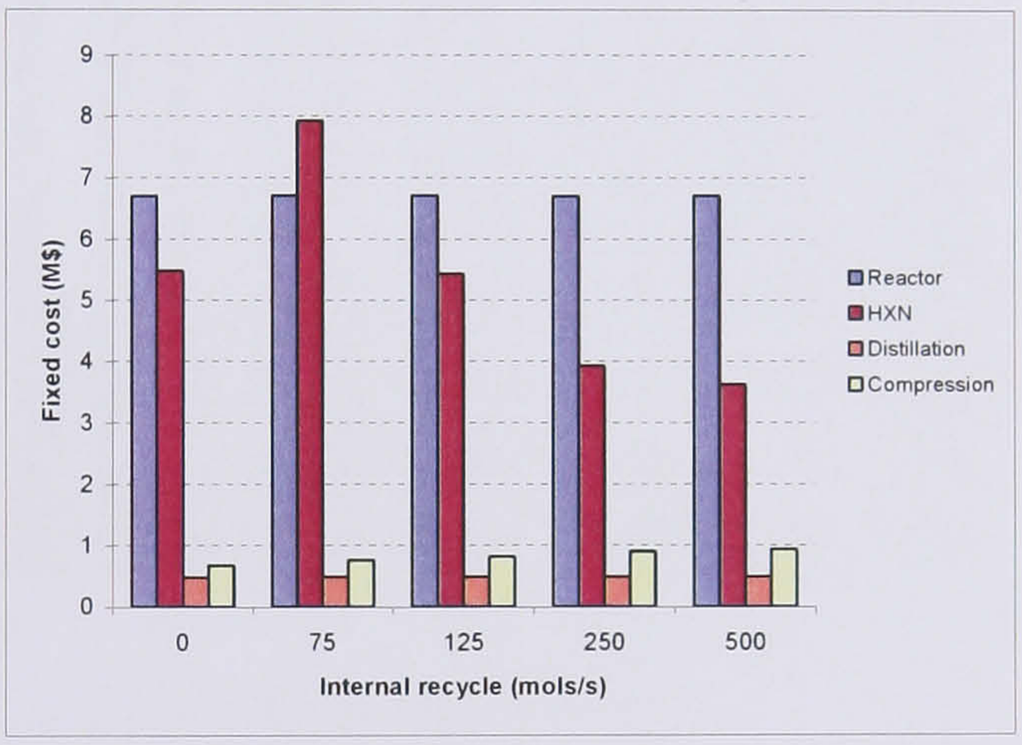

Figure 7.11: Fixed costs for the three PFRs with different internal recycle limits for the acetic acid production process.

For the single PFR structures, Figure 7.12 details the capital costs for the distillation and the compression. The higher the internal recycle limit is:

- The more acetic acid and water are produced and as a result, the bigger (*i.e.* more expensive) the condensers and reboilers are.
- The bigger the internal compressor is.

- The fewer amount is externally recycled and consequently, the cheaper the external compressor becomes. The external recycle is inversely proportional to the ethane conversion.
- The more oxygen is fed to the system and therefore, the bigger the feed compressor becomes, as for all cases the oxygen feed is at its upper bound (13 % of the total feed into the reactor -see Appendix 3-).

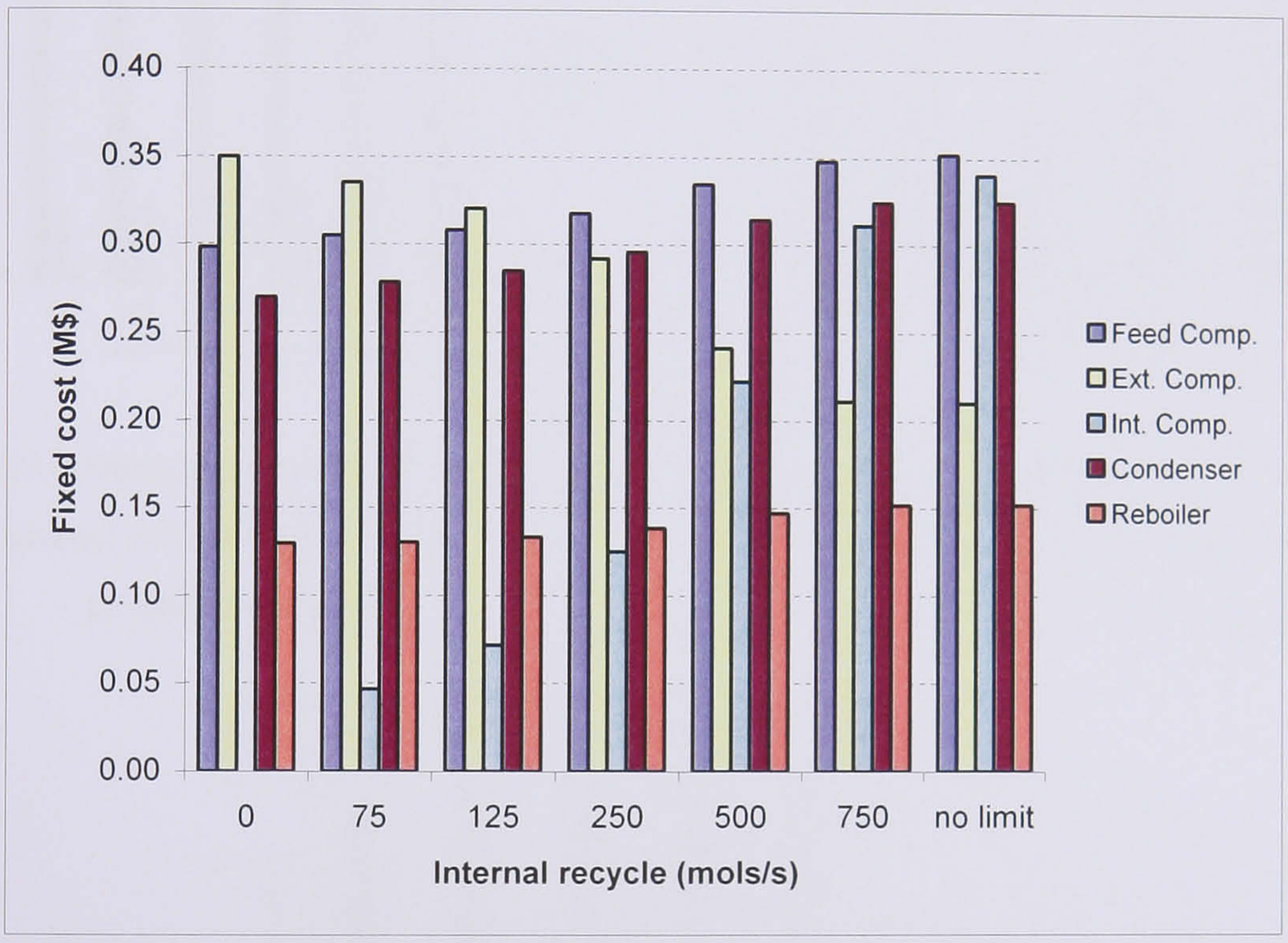

Figure 7.12: Compression and distillation fixed costs for one PFR with different internal recycle limits for the acetic acid production process.

Similar behaviours are observed for the structures involving two and three PFRs.

The operational costs for the three sets of structures are presented in Figures 7.13, 7.14 and 7.15. Raw material costs refer to the oxygen and ethane costs. Utility costs group the hot and cold utility for the heat integration, the cooling water for the condenser and the steam for the reboiler of the distillation column. Compression costs gather the external and internal recycle and the feed compression. At higher

internal recycles:

- More oxygen can be fed to the system and therefore higher raw material costs are obtained.
- More utility and compression costs are required.

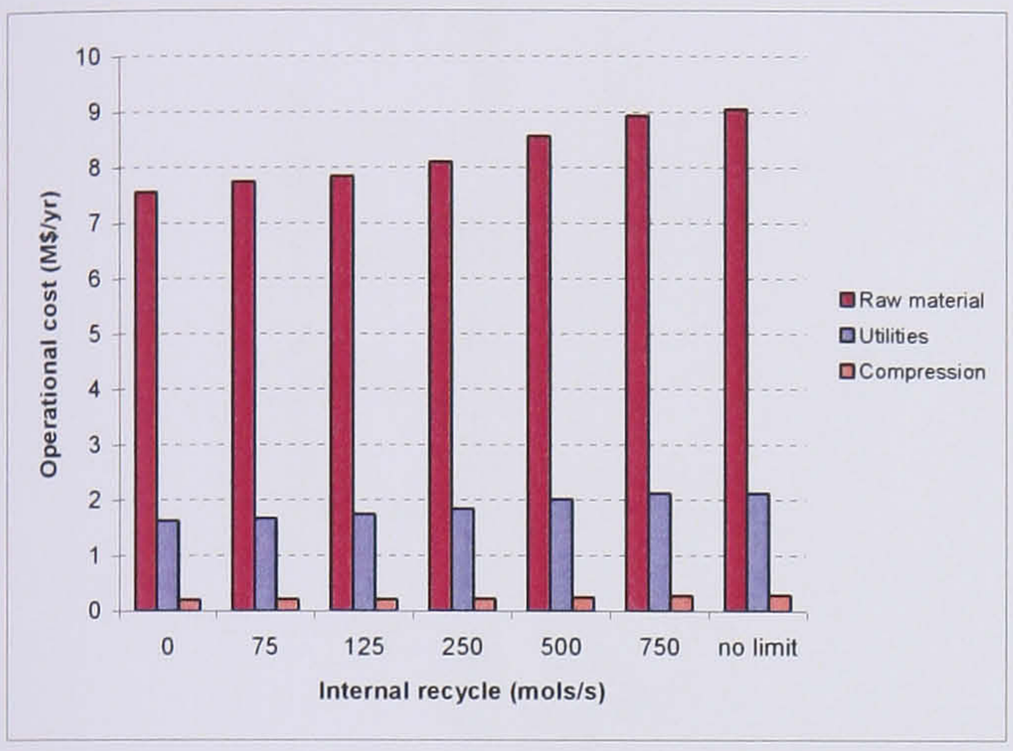

Figure 7.13: Operational costs for one PFR with different internal recycle limits for the acetic acid production process.

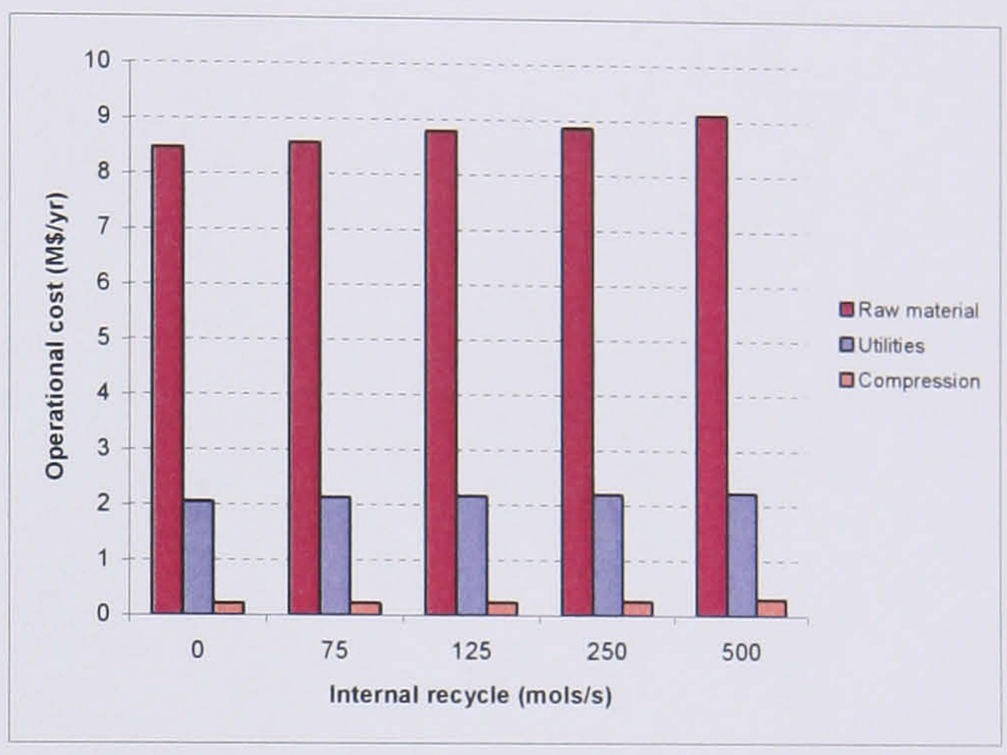

Figure 7.14: Operational costs for the two PFRs with different internal recycle limits for the acetic acid production process.

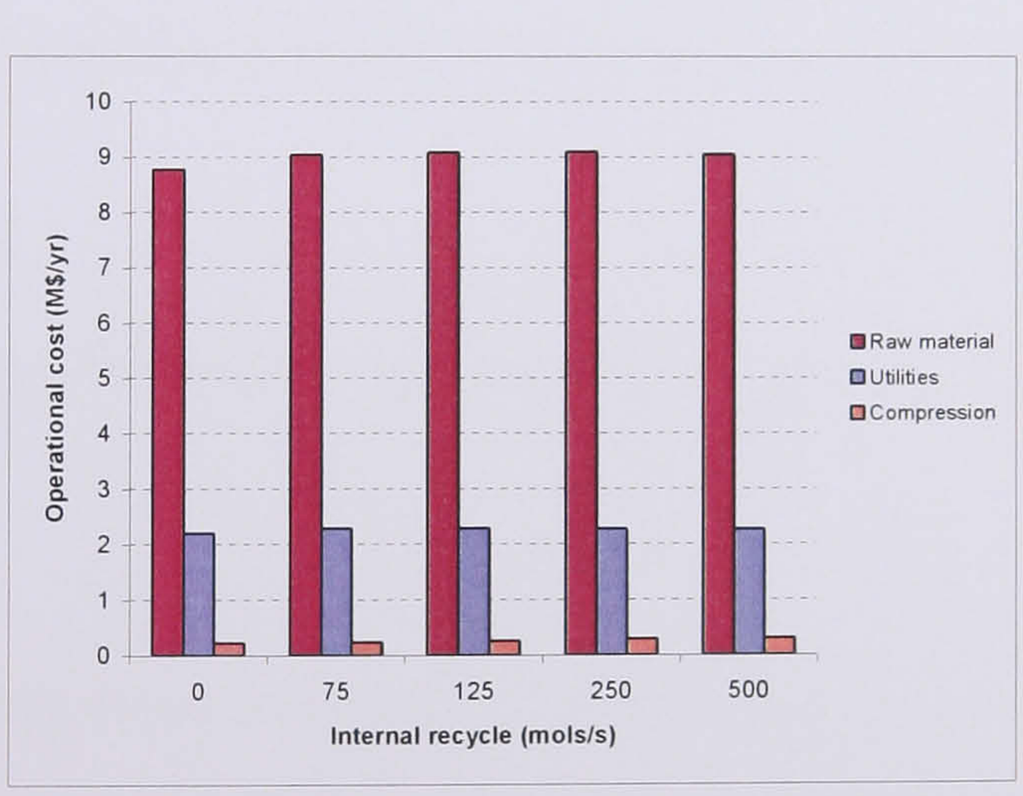

Figure 7.15: Operational costs for the three PFRs with different internal recycle limits for the acetic acid production process.

For the single PFR structures, utilities and compression costs are detailed in Figure 7.16. The bigger the compressors, the reboiler and the condenser of the distillation column are, the more expensive is to operate them. No hot utility is required for any

of the cases. All operational costs increase when increasing the internal recycle limit, except for the external compression cost. This cost decreases when the internal recycle limit grows because less flow is externally recycled.

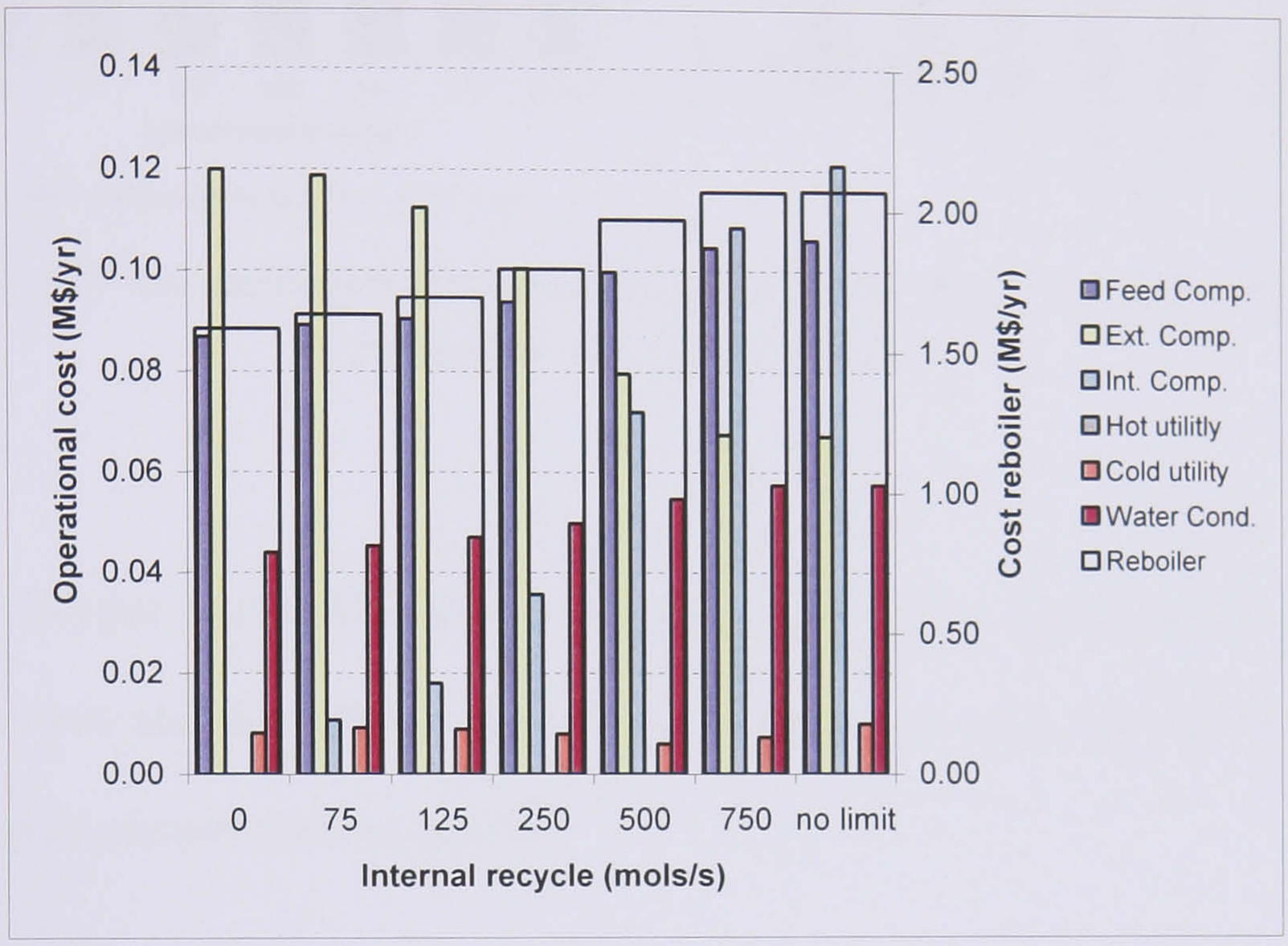

Figure 7.16: Compression and utilities operational costs for one PFR with different internal recycle limits for the acetic acid production process.

Similar behaviours are observed for the structures involving two and three PFRs.

Un-reacted oxygen has been assumed during the whole study to be separated in the absorber. In the case where the oxygen was not separated but completely recycled, the raw material costs would impact the OFV with similar trade-offs for all the cases. For a single PFR, Figure 7.17 shows the OFV and the benefit obtained by recycling the oxygen for different internal recycle limits.

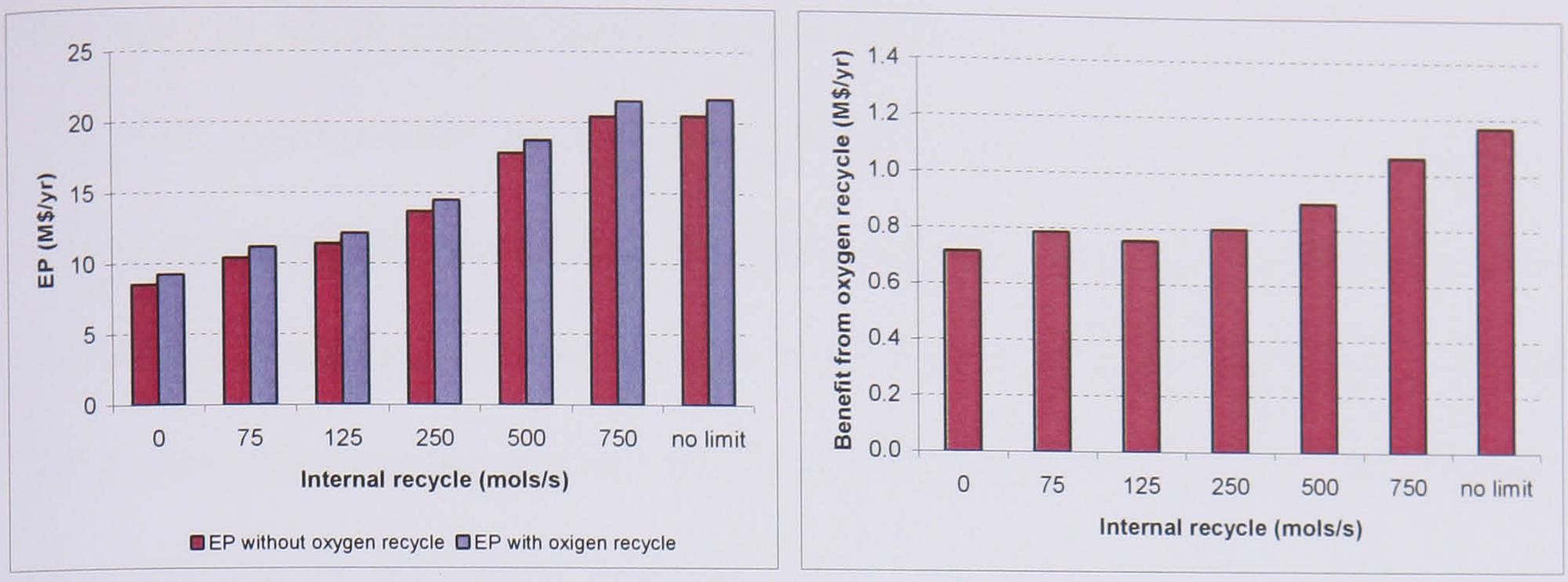

Figure 7.17: OFV and benefit from oxygen recycling for one PFR with different internal recycle limits for the acetic acid production process.

Since the oxygen conversion follows the same trends and is higher for the structures formed by two and three PFRs in series, the influence of such a recycle in the OFV happens to be comparable but smaller.

Structures with different feed dilution

A comparison of the performances of three structures consisting of one PFR in which the feed is diluted by different means is presented. The three diluting agents considered are:

- The internal recycle. The PFR with unlimited internal recycle is selected over the case with a limitation of 750 mols/s, as there is no interest in limiting the dilution.
- Water that is fed to the reactor.
- Carbon dioxide that is fed to the reactor.

The case in which carbon dioxide is selected as the diluting agent results exactly in the same performance as the single PFR without internal recycle. During the optimisation search, the amount of carbon dioxide is progressively reduced from the initial value to zero. Carbon dioxide has no effects on the kinetics of the system, other than reducing the partial pressures of the other components inside the reactor, thus reducing the production of acetic acid.

Figure 7.18 shows the OFV, the process selectivity and the ethane and oxygen conversions for the structures where:

- No diluting agent is present (one PFR without internal recycle).
- Internal recycle (unlimited case) is the diluting agent.
- Water is the diluting agent.

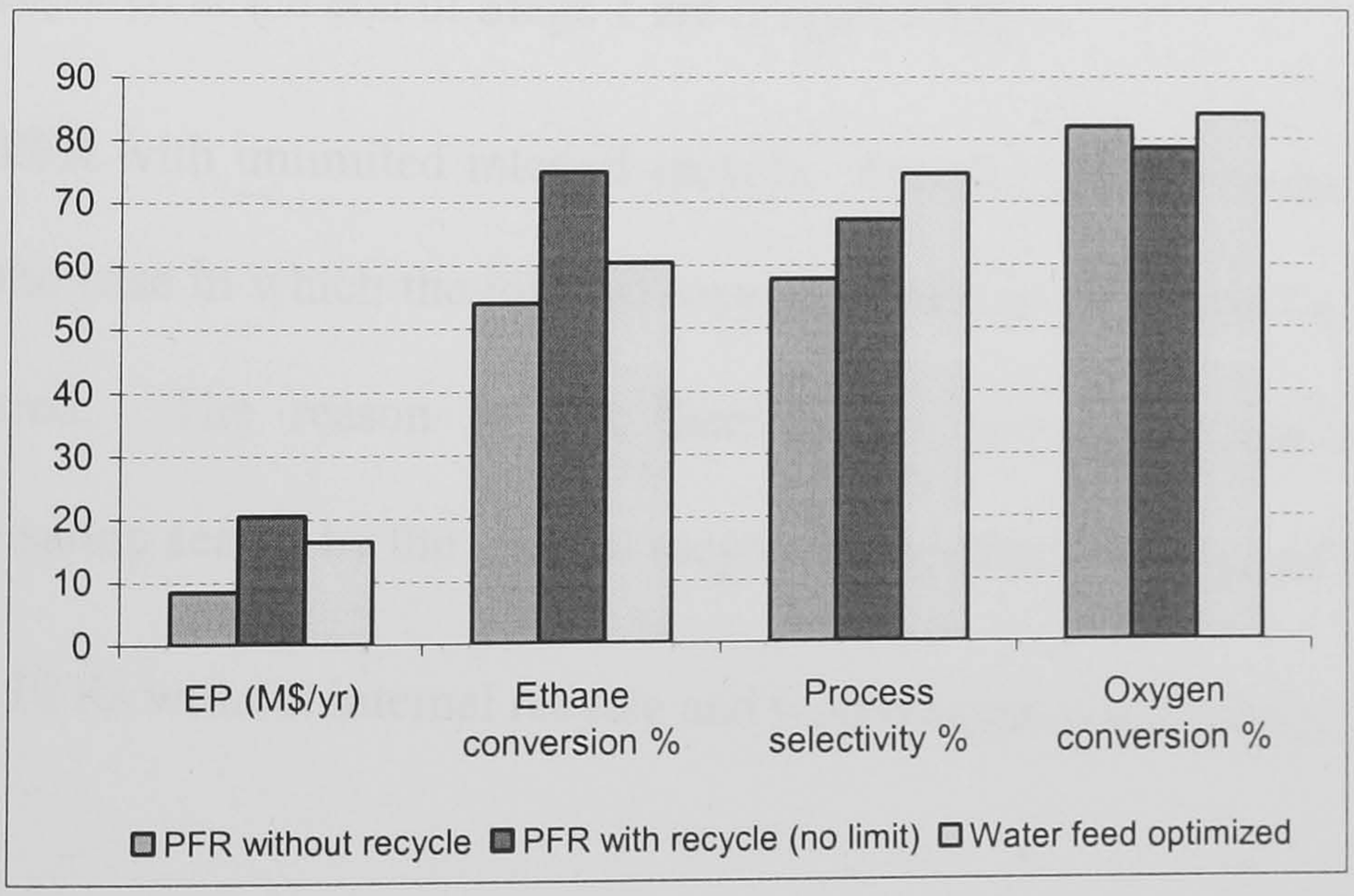

Figure 7.18: Results for structures with different dilutions for the acetic acid production process.

The OFV is increased by 93 % (16.4 M$/yr) with respect to the single PFR without internal recycle (8.5 M$/yr) when the feed is diluted with water. However, this case

does not outperform the OFV of the single PFR with unlimited internal recycle (20.5 M$/yr). The presence of water strongly accelerates the rate of the ethylene oxidation to acetic acid (Linke *et al.*, 2002a) and produces the highest process selectivity observed so far (Figure 7.18). For this design option, the use of internal compressors is avoided and therefore, both capital and operational costs decrease. However, a bigger external compressor is needed as the ethane conversion becomes lower. In addition, as more water must be separated from the acetic acid in the distillation column, higher operational and capital costs for both condenser and reboiler are required. The overall impact of these costs on the performance indicates that this design option is not as appealing as the single PFR with unlimited internal recycle.

7.2.1.3 Optimal Conceptual Process Designs Identified In Stage 1

After the conclusions obtained in the previous analysis of results, the design candidates proposed at the end of Stage 1 are (Figure 7.19):

- One PFR with unlimited internal recycle. Despite producing the same OFV than the case in which the internal recycle is limited to 750 mol/s, this case is preferred. The reason is that there is no interest in constraining the optimisation search by the internal recycle in the later evolution of stages.

- Three PFRs without internal recycle and with oxygen side feeding.

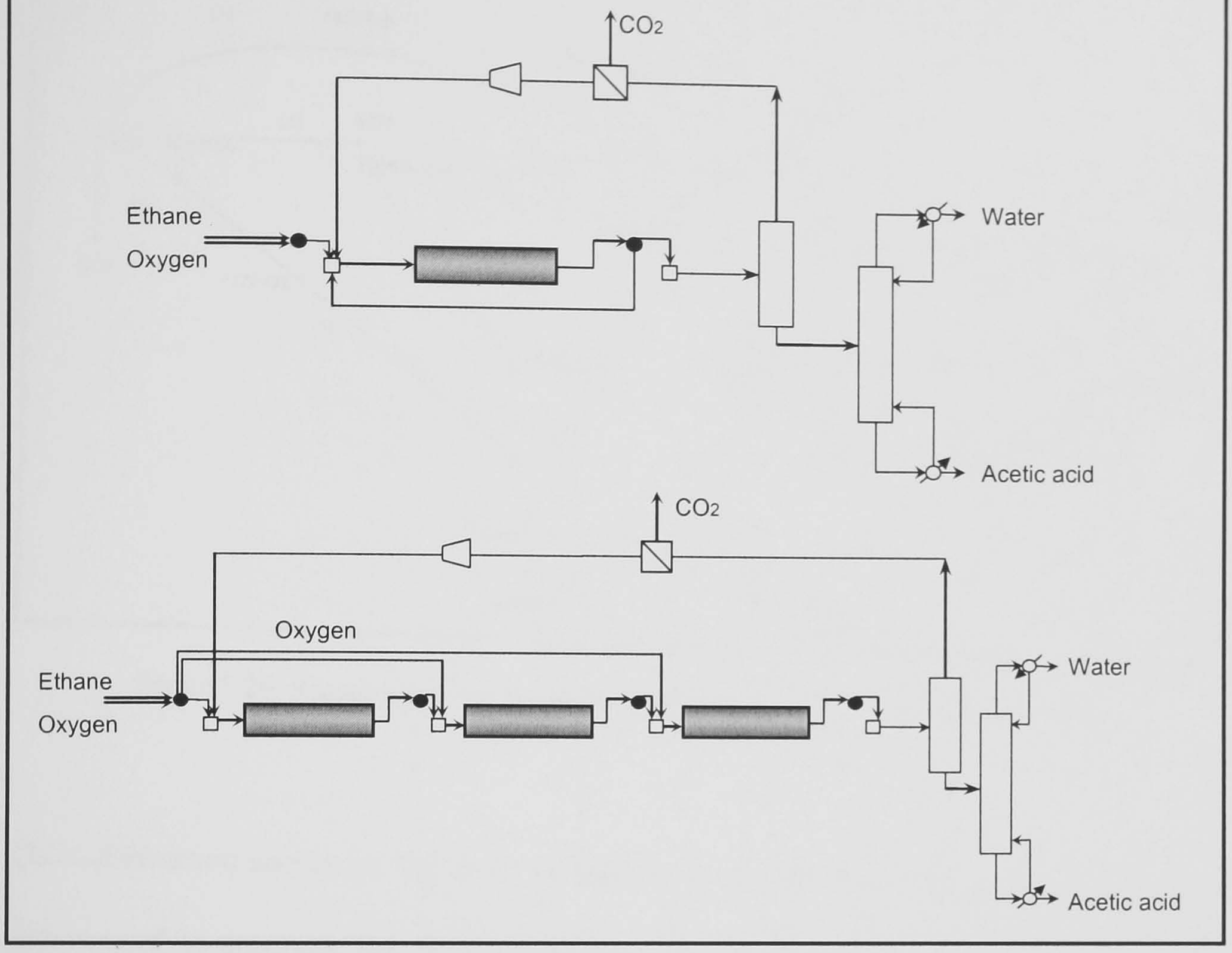

Figure 7.19: Superstructure representation for the optimal conceptual designs proposed at the end of Stage 1 for the acetic acid production process.

7.2.1.4 Observations And Insights

In this section a comparison between the two optimal conceptual design structures suggested in Stage 1 is presented. A single PFR without internal recycle is also included in the discussion for comparison reasons.

Figure 7.20 shows the reaction path for the oxidation of ethane to acetic acid.

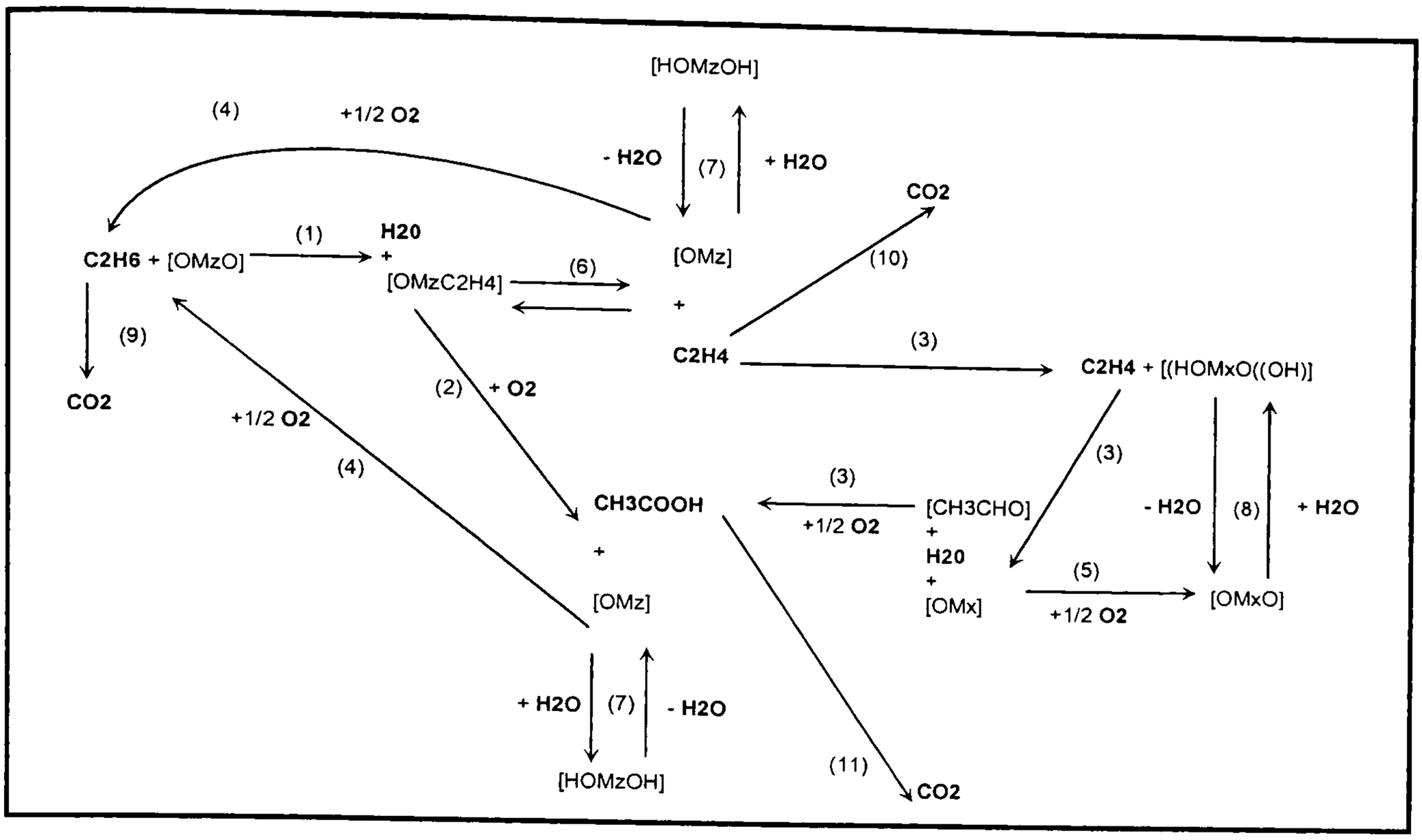

Figure 7.20: Reaction path for the partial oxidation of ethane (Linke *et al.*, 2002a).

The information shown in Table 7.1 relates to the single PFR without internal recycle and is used to compare the different cases. The concentration values (C_i) presented correspond to the concentrations at the beginning and at the end of the reactor. Reaction rates (r_i) and θs are average values for the whole reactive zone. θ is the normalized surface coverage.

Table 7.1: Concentrations and reaction rates for one PFR without internal recycle for the acetic acid production process.

Variable	Value	Variable	Value
C_{C2H6} (mol/m^3)	298 → 262*	$\theta_{[OMz]}$	$1.23*10^{-1}$
C_{O2} (mol/m^3)	45.0 → 8.0	r_1 (mol/s/kg_cat)	$5.31*10^{-4}$
C_{C2H4} (mol/m^3)	Constant ≈ 8.4	r_2 (mol/s/kg_cat)	$2.72*10^{-4}$
$C_{CH3COOH}$ (mol/m^3)	0 → 9.0	r_3 (mol/s/kg_cat)	$1.34*10^{-4}$
C_{CO2} (mol/m^3)	0 → 12.0	r_4 (mol/s/kg_cat)	$7.29*10^{-4}$
C_{H2O} (mol/m^3)	0 → 28.0	r_5 (mol/s/kg_cat)	$1.18*10^{-4}$
$\theta_{[(HOMxO)\ (OH)]}$	$4.85*10^{-5}$	r_6 (mol/s/kg_cat)	$2.48*10^{-4}$
$\theta_{[OMxO]}$	$8.63*10^{-1}$	r_8 (mol/s/kg_cat)	$1.18*10^{-4}$
$\theta_{[Omx]}$	$1.37*10^{-1}$	r_9 (mol/s/kg_cat)	$1.44*10^{-4}$
$\theta_{[OMzO]}$	$8.98*10^{-2}$	r_{10} (mol/s/kg_cat)	$1.10*10^{-4}$
$\theta_{[OMzC2H4]}$	$7.87*10^{-1}$	r_{11} (mol/s/kg_cat)	$1.97*10^{-5}$
$\theta_{[HOMzOH]}$	$7.35*10^{-5}$		

*298 → 262 indicates that at the beginning of the reactor, the concentration is 298 mol/m^3 whereas at the end it is 262 mol/m^3

Table 7.2 shows the deviations observed between one PFR without internal recycle and: i) one PFR with internal recycle; ii) three PFRs without internal recycle.

Table 7.2: Deviations observed between one PFR without internal recycle and: one PFR with internal recycle; three PFRs without internal recycle for the acetic acid production process.

	One PFR with recycle	**Three PFRs (side feeding of oxygen)**
Objective (M$/yr)	20.5 (*Increase 141 %)	18.0 (Increase 112 %)
Process selectivity	Increase 16.3 %	Increase 9.74 %
Ethane conversion	Increase 38.3 %	Increase 37.6 %
C_{C2H6} (mol/m^3)	Decrease 19 %	Decrease 11 %
C_{O2} (mol/m^3)	Same inlet value. Decrease of 30 % in conversion, which means that there is more oxygen along the reactor.	Same inlet value. Instead of decreasing constantly, the concentration recovers the inlet value at fractions 0.30 and 0.46 of the reactor zone, due to the oxygen side feed streaming.
C_{C2H4} (mol/m^3)	Concentration ≈ 0.05	Concentration ≈ 4.32
$C_{CH3COOH}$ (mol/m^3)	15.0 → 21.0	0 → 18.6
C_{CO2} (mol/m^3)	14.5 → 20.8	0 → 21.1
C_{H2O} (mol/m^3)	36.6 → 52.5	0 → 50.5
$\theta_{[(HOMxO)(OH)]}$	Increase of 3 orders of magnitude	Increase of 1 order of magnitude
$\theta_{[OMxO]}$	Decrease 10 %	Same values
$\theta_{[OMx]}$	Increase 46 %	Increase 1 %
$\theta_{[OMzO]}$	Increase 59 %	Increase 34 %
$\theta_{[OMzC2H4]}$	Decrease 3 %	Decrease 1 %
$\theta_{[HOMzOH]}$	Increase 81 %	Increase 10 %
$\theta_{[OMz]}$	Decrease 22 %	Decrease 18 %
r_1 (mol/s/kg_cat)	Increase 40 %	Increase 13 %
r_2 (mol/s/kg_cat)	Increase 37 %	Increase 26 %
r_3 (mol/s/kg_cat)	Strong increase: Despite $[C_2H_4] \rightarrow 0$, it is 1-2 orders of magnitude higher at the beginning of the reactor unit and increases 100% at the end, due to a $[H_2O]$ increase.	Increase 35 %
r_4 (mol/s/kg_cat)	Increase 20 %	Increase 7 %
r_5 (mol/s/kg_cat)	Strong increase: 1-2 orders of magnitude higher at the beginning of reactor unit. Increase 100% at the end	Decrease 34 %
r_6 (mol/s/kg_cat)	Increase 27 %	Same values
r_8 (mol/s/kg_cat)	Strong increase: 1-2 orders of magnitude higher at the beginning of reactor unit. Increase 100 % at the end	Decrease 34 %
r_9 (mol/s/kg_cat)	Increase 38 %	Increase 17 %
r_{10} (mol/s/kg_cat)	Decrease 99 %	Increase 20 %
r_{11} (mol/s/kg_cat)	Increase 1 order of magnitude	Decrease 36 %

SUMMARY	There is a general increase in all reaction rates but r_{10}. Regarding the reactions that produce directly acetic acid: r_2: has increased; there is more concentration of oxygen along the reactor zone and values of $\theta_{[OMzC2H4]}$ are practically identical. r_3: has substantially increased; although the value of C_2H_4 is maintained close to 0, the value of $\theta_{[(HOMxO)\ (OH)]}$ is increased 3 orders of magnitude. The formation of by-product CO_2 increases. However, inside the reactive zone, the increase in the concentration is smaller. That is an increase of 6 mol/m^3 instead of the 12 mol/m^3 for the single PFR without internal recycle. The formation of by-product H_2O increases although the increase in the concentration inside the reactive zone is smaller. That is an increase of 16 mol/m^3 instead of the 28 mol/m^3 for the single PFR without internal recycle.	There is a relevant increase in the reaction rates directly involved in the production of acetic acid (r_2, r_3). r_1, which takes place before r_2, also increases, whereas r_6 that is the previous reaction to r_3 keeps the same values. r_2: there is much more concentration of oxygen along the reactor zone and values of $\theta_{[OMzC2H4]}$ are practically identical. r_3: although the value of C_2H_4 is reduced by 48 %, the value of $\theta_{[(HOMxO)\ (OH)]}$ is increased 1 order of magnitude. Competitive reactions to r_3 (r_5 and r_8) suffer an important decrease. Consumption of acetic acid to produce ethane (r_4), slightly increases The formation of by-product CO_2 increases. Here, the increase in the concentration inside the reactive zone is bigger. That is an increase of 21 mol/m^3 instead of the 12 mol/m^3 for the single PFR without internal recycle. The production of CO_2 from ethane and ethylene (r_9 and r_{10}) increase, whereas its formation from acetic acid (r_{11}) decreases. The formation of by-product H_2O increases. Here again, inside the reactive zone, the increase in the concentration is also bigger. That is an increase of 51 mol/m^3 instead of the 28 mol/m^3 for the single PFR without internal recycle.

* Increase / Decrease with respect to the PFR without internal recycle refer to the average values along the reactive zones

Common features are observed for both cases with respect to the PFR without internal recycle:

- The concentration of ethylene along the reactor zone is reduced.
- Both reaction rates producing acetic acid are increased (r_2 and r_3).
- Ethane is kept along the reactor zone more diluted and its conversion is for both cases nearly 75 % (74.8 % for the option with internal recycle and 74.5 %

for the three PFRs structure). Therefore, it cannot be concluded that the option with internal recycle generates more profits because less ethane is purged in the absorber and transformed to acetic acid.

The main difference between the single PFR with internal recycle and the three PFRs without internal recycle is that the reaction rates r_3, r_5, r_8 and r_{11} are much higher for the first case. Although ethane and ethylene must be kept at lower concentrations by diluting the system in order to enhance the OFV, the concentration of ethylene is much lower for the first case. The concentration profiles for the acetic acid, carbon dioxide, water and oxygen follow different trends (Table 7.2). Figure 7.21 illustrates the rate improvements for the single PFR with internal recycle over the single PFR without internal recycle.

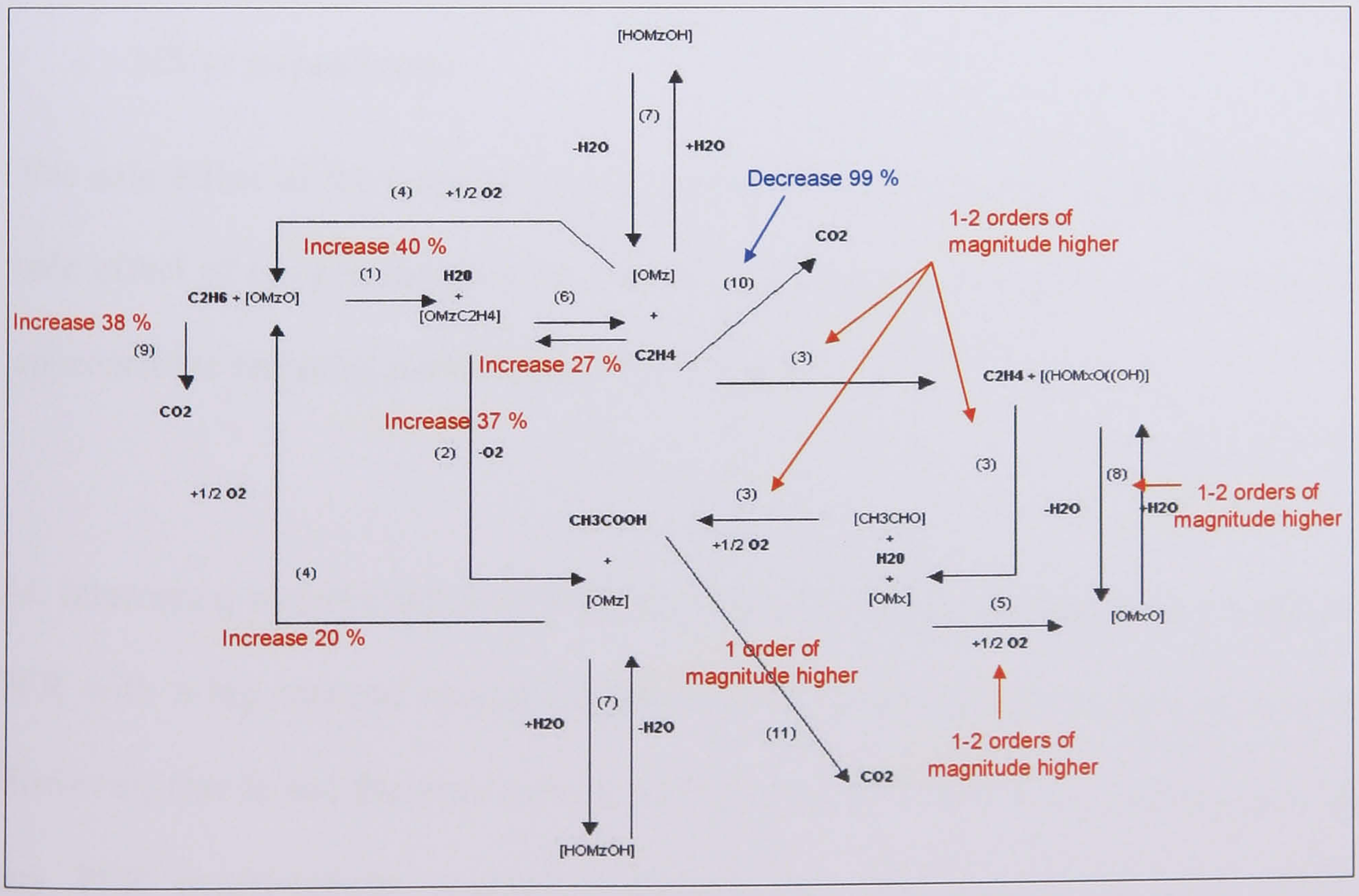

Figure 7.21: Rate improvements for the single PFR with internal recycle over the single PFR without internal recycle.

7.2.1.5 Conclusions

Back-mixing in the form of CSTRs is not a potential flow pattern for this case:

- The OFV for a single CSTR is negative (-7.5 M$/yr).
- For structures combining CSTRs and PFRs, the performances are not improved with respect to structures involving only PFRs.

Regarding structures with only PFRs, two features enhance the performance:

- The presence of internal recycle enhances the OFV of a single PFR up to 141 % (from 8.5 to 20.5 M$/yr). The maximum OFV for any structure is approached asymptotically as the internal recycle limit is increased.
- The presence of oxygen side feeding when more than one PFR is involved, improves the OFV if compared with a single PFR up to 112 % for the three PFRs structure and up to 72 % for the two PFRs structure (18.0 and 14.5 M$/yr respectively).

The sole effect of the internal recycle has more positive impact on the OFV than the sole effect of oxygen distribution. When both features are combined, performances approach the targeting performance (22.5 M$/yr).

An interesting observation is as follows. From the reaction engineering textbook, a PFR with a big internal recycle would result in a similar performance as a CSTR. However, that is not the case here as a CSTR shows much worse performance than any PFR (multi-tubular reactor) with recycle. The reason for such different performances resides in the different operating temperatures attained. The high temperatures needed to carry out the oxidation reactions, which are reached in multi-

tubular reactors (MTRs), cannot be attained in a CSTR. The average operating temperatures in MTRs with recycles are circa 565 K, whereas the temperature reached in a CSTR is 542 K. On one side, the overall heat transfer coefficient is higher for CSTRs than for MTRs; on the other, the heat transfer area for CSTRs is much smaller than for MTRs. The multiplication of both values, at equal catalyst load (50000 kg), results in a much smaller UA value for a CSTR (circa 33 kW/K) than for a MTR (circa 220 kW/K). As a consequence, CSTRs cannot remove as much heat as MTRs, resulting in much lower operating temperatures and thus performances.

The designs proposed at the end of the multi-level approach are the single PFR with unlimited internal recycle and the three PFRs without internal recycle and with oxygen side feeding.

7.2.2 STAGES 2, 3 And 4: Results

7.2.2.1 Introduction

In the next section, the evolution of the optimal conceptual process designs proposed at the end of Stage 1 is presented. For comparison reasons, the evolution of a single PFR without internal recycle is also presented. Afterwards, the results of experiments in which FLBRs have been used, are discussed. The results showed in this section are the best solutions out of ten converged optimisation runs (except where indicated).

7.2.2.2 One PFR Without Recycle

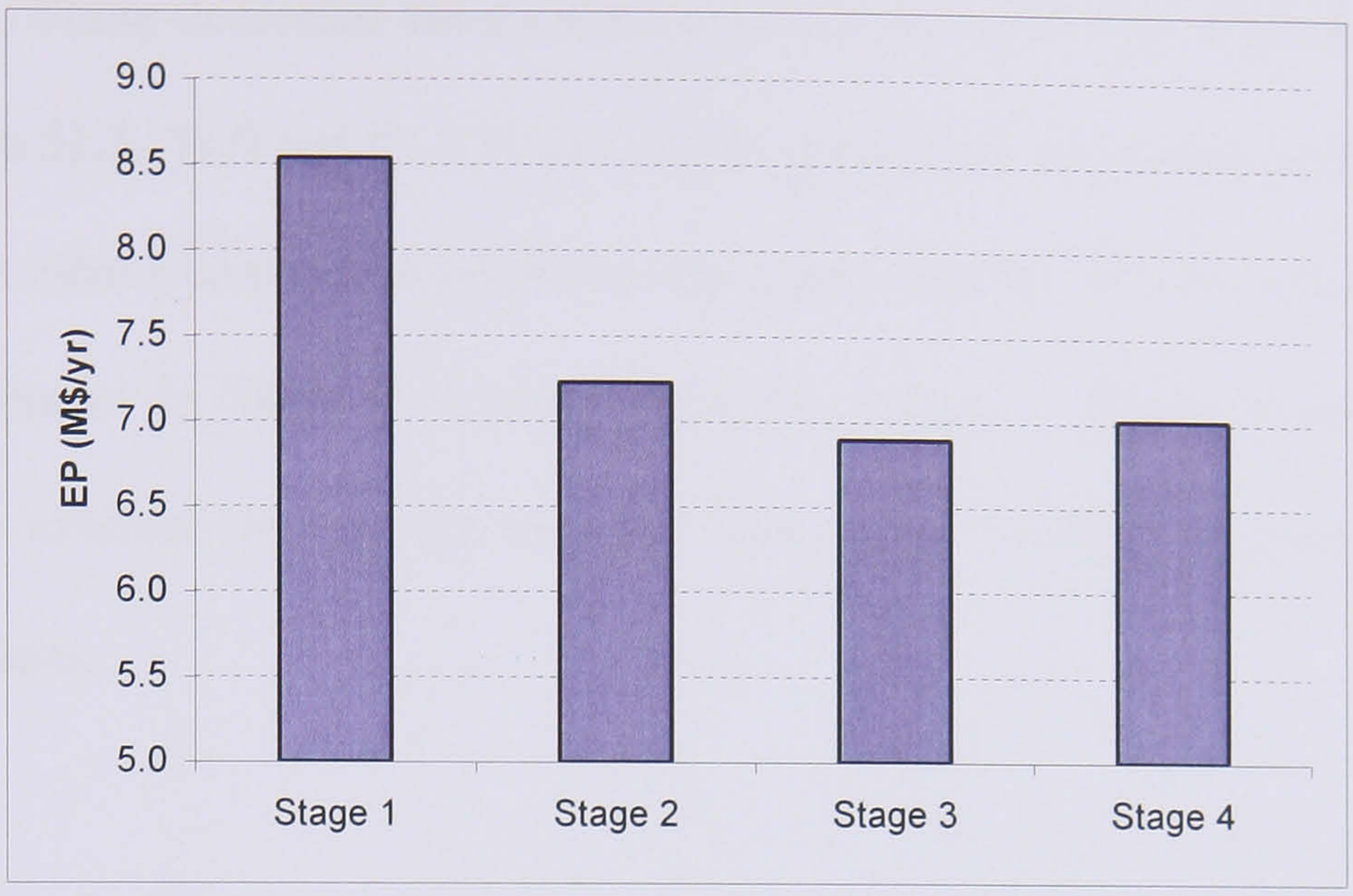

Figure 7.22: EP (M$/yr) for one PFR without internal recycle for the four stages for the acetic acid production process.

The decrease in the OFV from Stage 1 to Stage 3 (Figure 7.22) was expected since the evolution of stages implies the reduction of the search area by new constraints. The reduction of 15.3 % in the OFV from Stage 1 to 2 is mainly due to the increase in the HXN fixed cost (2.71 M$; annualised increased cost = 1.0 M$/yr; Figure 7.23). In Stage 1, the constraints on the longitudinal temperature profile for the reactor are very relaxed. Therefore, the optimisation is able to identify designs that by adjusting such profiles minimise the HXN fixed cost. In Stages 2 and 3, tighter constraints on the longitudinal temperature profile of the reactor are gradually added. As a result, the HXN fixed cost cannot reach such low values without violating the new constraints. When comparing Stages 3 and 4, Stage 4 does not present extra constraints on the longitudinal temperature profile of the reactor. The flow streams remain similar and as a result the HXN fixed cost is the same for both stages. Another relevant change in the fixed costs for the different stages is in the cost of the reactor. The small reduction in its cost in the last two stages is due to the use of fewer tubes (Table 7.3).

A small reduction in the condenser and reboiler fixed costs is also observed for Stages 2, 3, and 4. These decreases are a consequence of the reduction of ethane conversion from 54.1 to 51.5, 51.0 and 51.3 % (*i.e.* lower acetic acid and water production). The reduction in ethane conversion results in that approximately 30 mols/s more of ethane, leave the reactor in Stage 2, 3 and 4 than for Stage 1. Since ethane is recycled through the external recycle, the external compressor is bigger and more expensive for these stages.

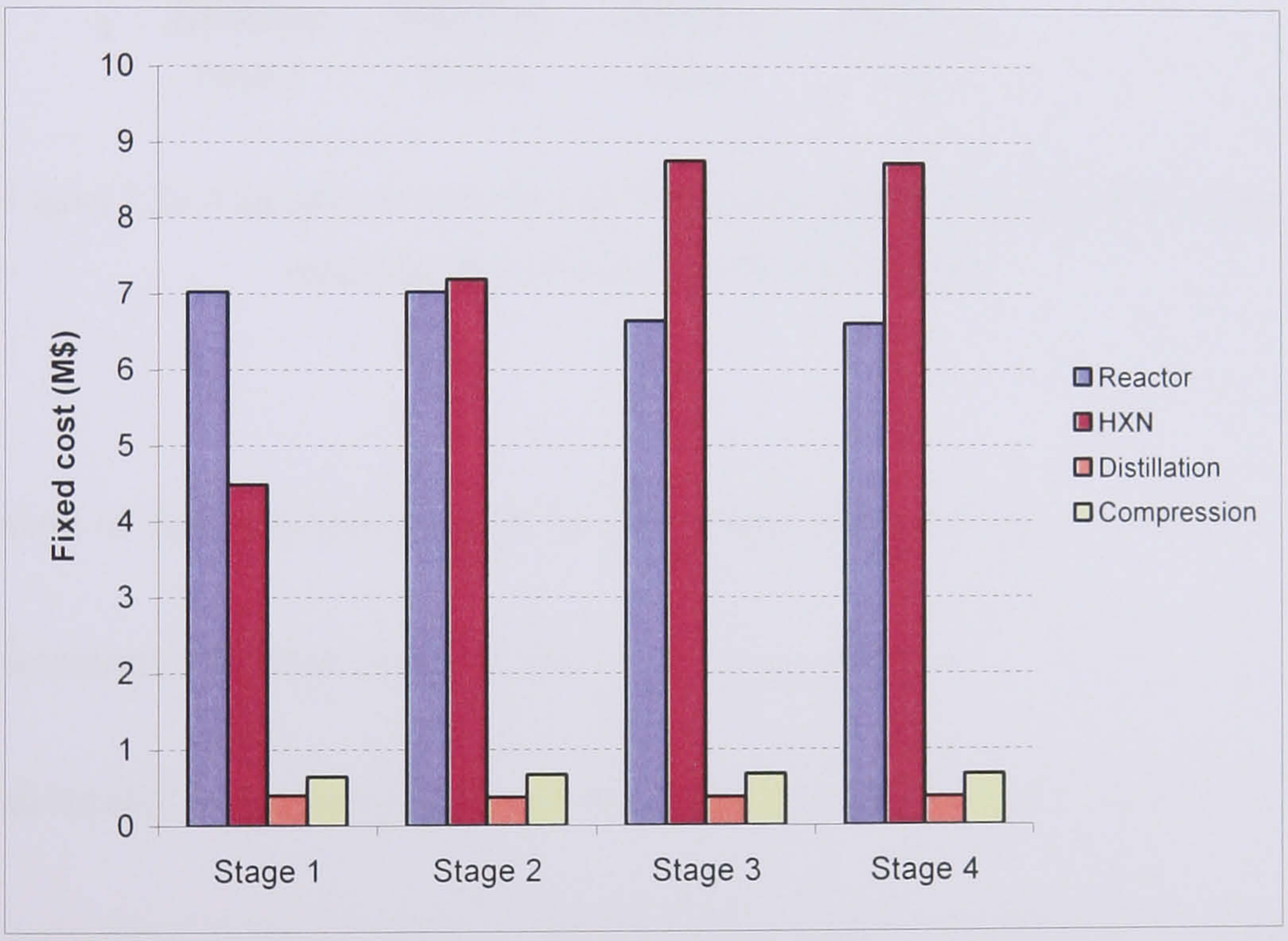

Figure 7.23: Fixed costs for one PFR without internal recycle for the four stages for the acetic acid production process.

Regarding operational costs (Figure 7.24), the increase observed in the raw material cost is related to the increase of the external recycle. At higher recycles, more oxygen is feed as it always remains at its upper bound, which is 13 % of the total inlet molar flow to the reactor. However, the fixed cost of the feed compressor increases inappreciably. Both utilities and compression costs also vary insignificantly.

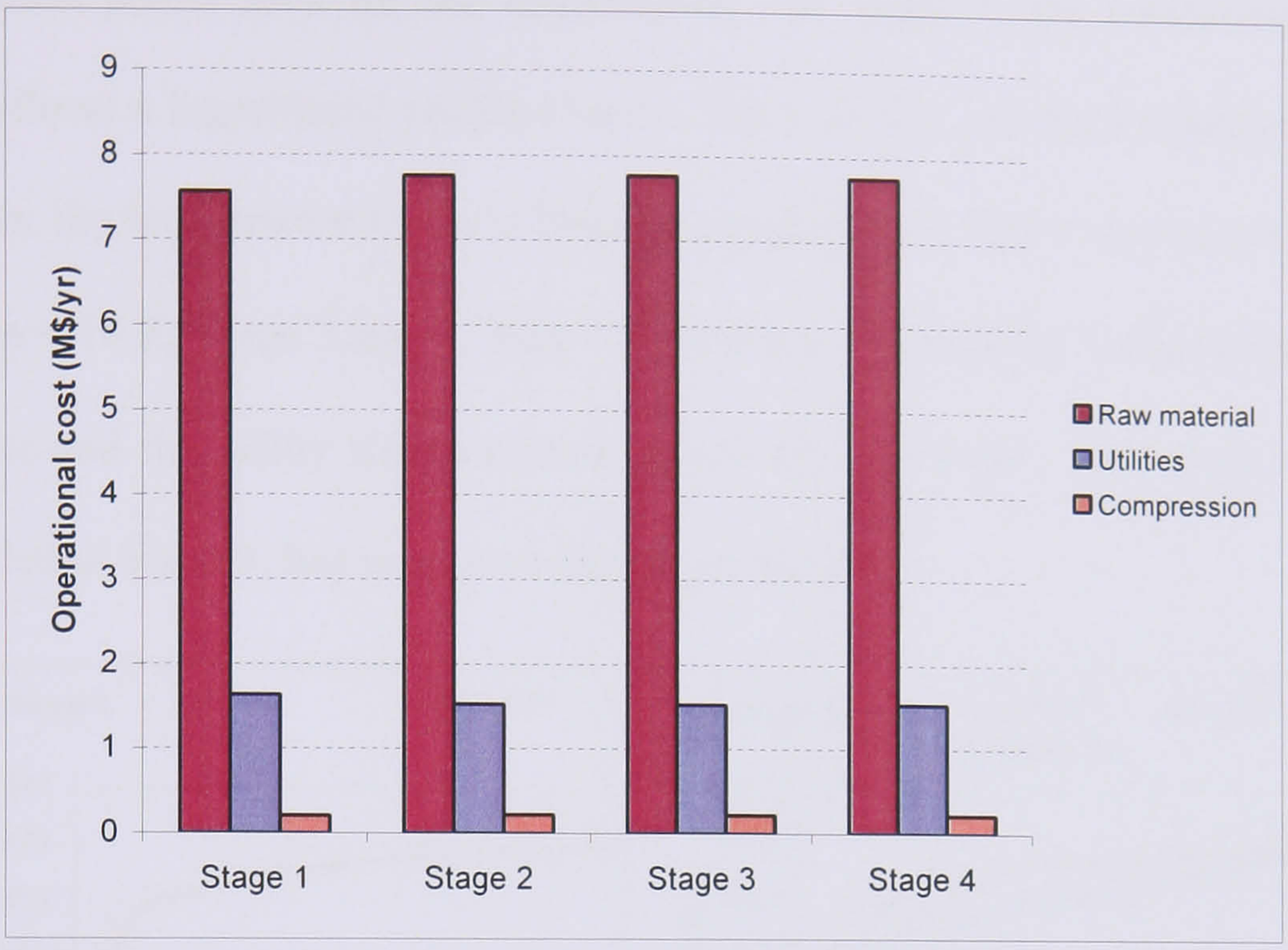

Figure 7.24: Operational costs for one PFR without internal recycle for the four stages for the acetic acid production process.

The evolution of designs identifies in Stage 3 and 4 (Table 7.3):

- A nominal diameter (DN) of 20 for the reactor tubes.
- A diameter of the catalyst particle smaller than for Stage 1 and 2 (4.5 mm).
- A reduction in the number of reactor tubes with respect to Stage 1 and 2.

Table 7.3: Reactor design parameters for one PFR without internal recycle for the four stages for the acetic acid production process.

Average values:	**Stage 1 and 2**	**Stage 3**	**Stage 4**
Diameter of the tube	25mm	ND=20	ND=20
Diameter of catalyst particle	5mm	4.5mm	4.5mm
Number of tubes	30000	29000	27000

Figure 7.25 shows the evolution of the longitudinal temperature profiles of the reactor and the cooling media. STi refers to the temperature inside the reactor for Stage i, and

HXSTi refers to that of the utility media for the same stage. The X axis represents the discretisation points used for the calculations. In Stage 1, the temperature of the reactor follows a logarithmic profile (Tout - Tin = 25 K). As the evolution of stages progresses, the temperature tends to become progressively flatter and lower (Stage 2: Tout - Tin = 18 K; Stage 3 and 4: Tout - Tin ≅ 6 K). After Stage 3, the temperature of the reactor and the utility media remain practically the same. The extra modelling detail added in Stage 4, has nearly no impact on the OFV.

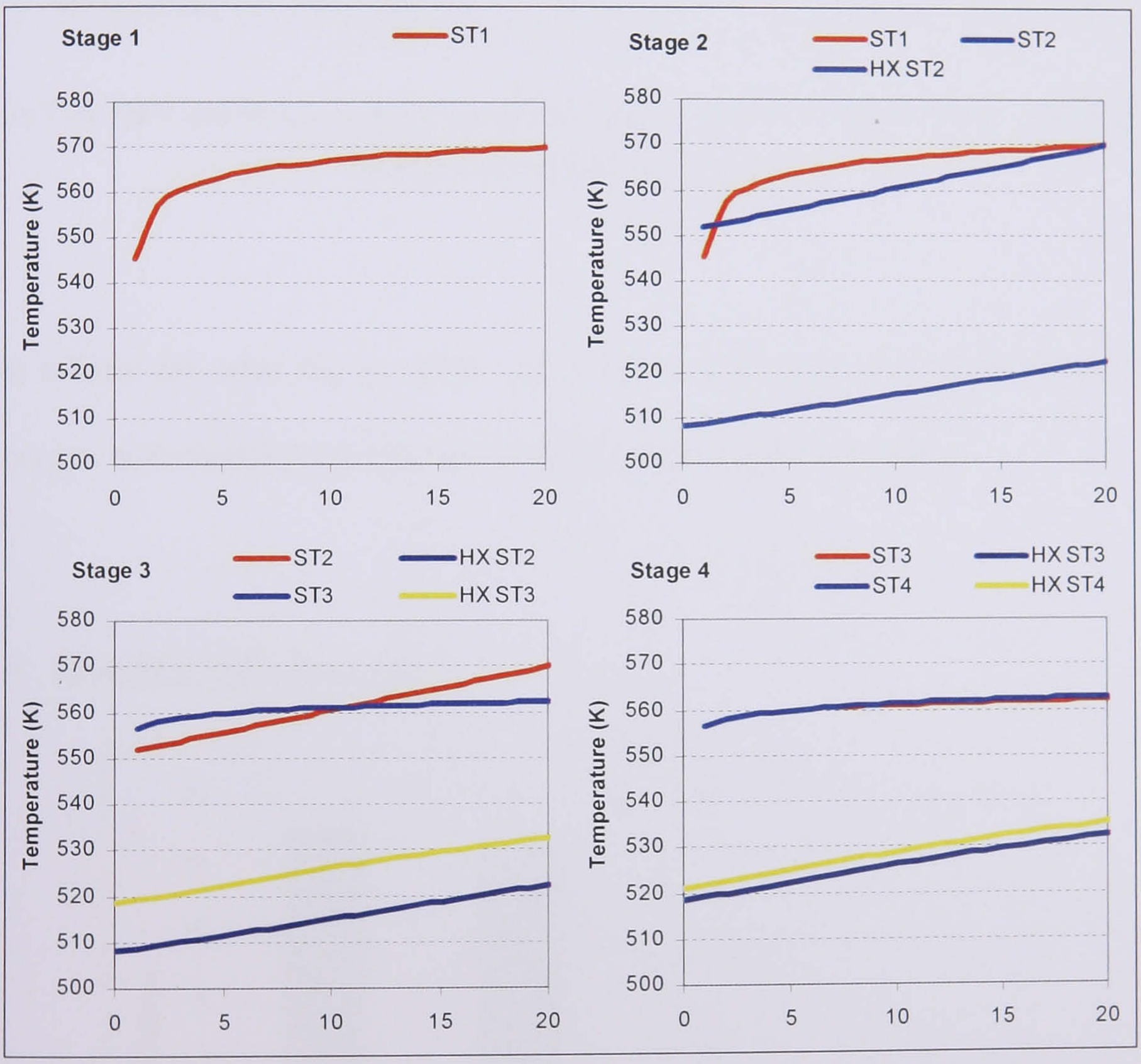

Figure 7.25: Reactor and utility temperature profile evolution for one PFR without internal recycle for the four stages for the acetic acid production process.

In the case where the oxygen was not separated but completely recycled, the benefit in the raw material costs would follow similar trends and influence in a equivalent

manner the OFV for each one of the cases (Figure 7.26). The OFV for Stage 4 would reach 8.17 M$/yr.

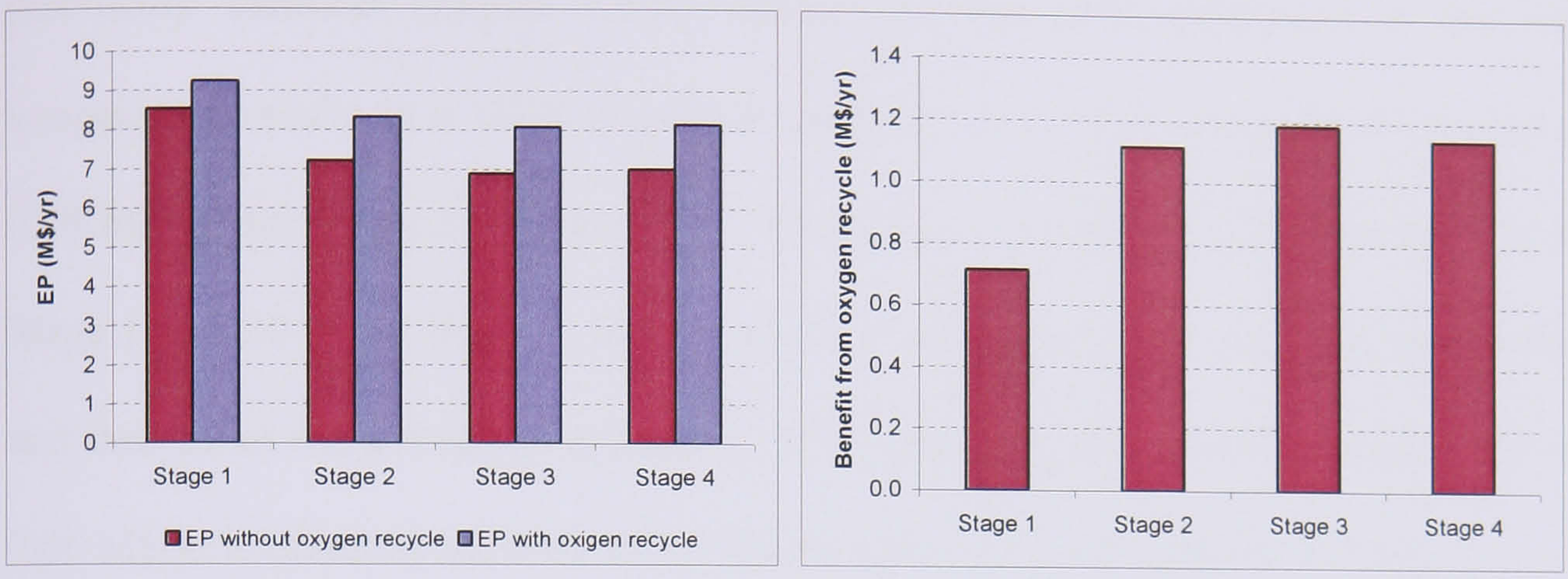

Figure 7.26: OFV and benefit from the oxygen recycling for one PFR without internal recycle for the acetic acid production process.

Similar effects are seen for the PFR with unlimited recycle and for the three PFRs with oxygen side distribution (therefore no figures are presented later).

7.2.2.3 One PFR With Recycle

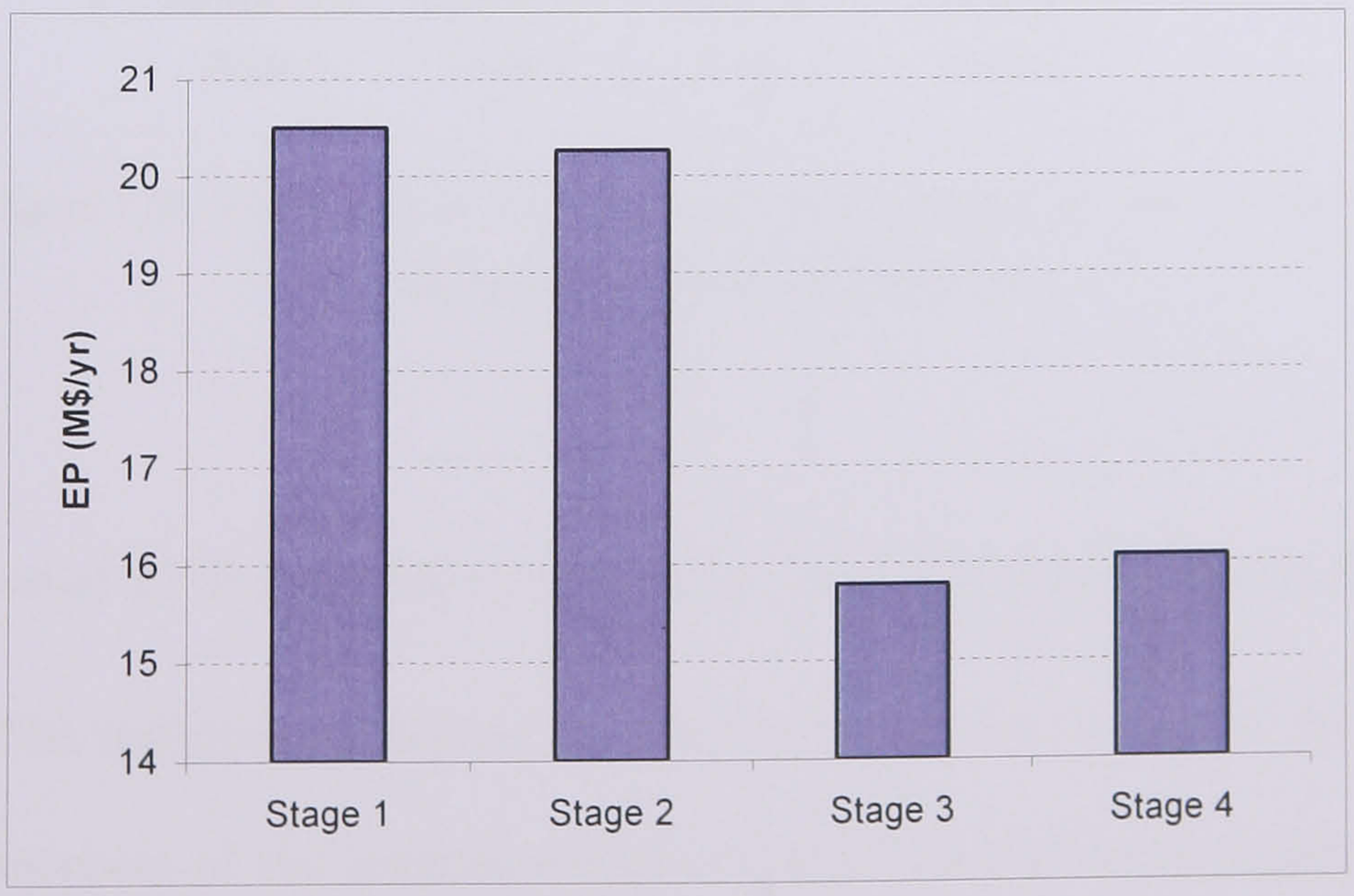

Figure 7.27: EP (M$/yr) for one PFR with internal recycle for the four stages for the acetic acid production process.

The transition from Stage 1 to 2 (Figure 7.27) results in almost no impact on the OFV (decrease of 0.24 M$/yr). The temperature profile of the reactor in both cases is practically identical (Figure 7.30). However, only 8°C difference in the inlet temperature results in a HXN fixed cost increase of 1.3 M$ (annualised increase of 0.48 M$/yr) for Stage 2 (Figure 7.28). The ethane conversion rises from 74.8 % for Stage 1 to 76.0 % for Stage 2, which results in an increase of acetic acid production, and thus in an extra 0.18M$/yr benefit. The remaining difference between OFVs of 0.06 M$/yr is offset by the rest of the changes in the fix and operational costs.

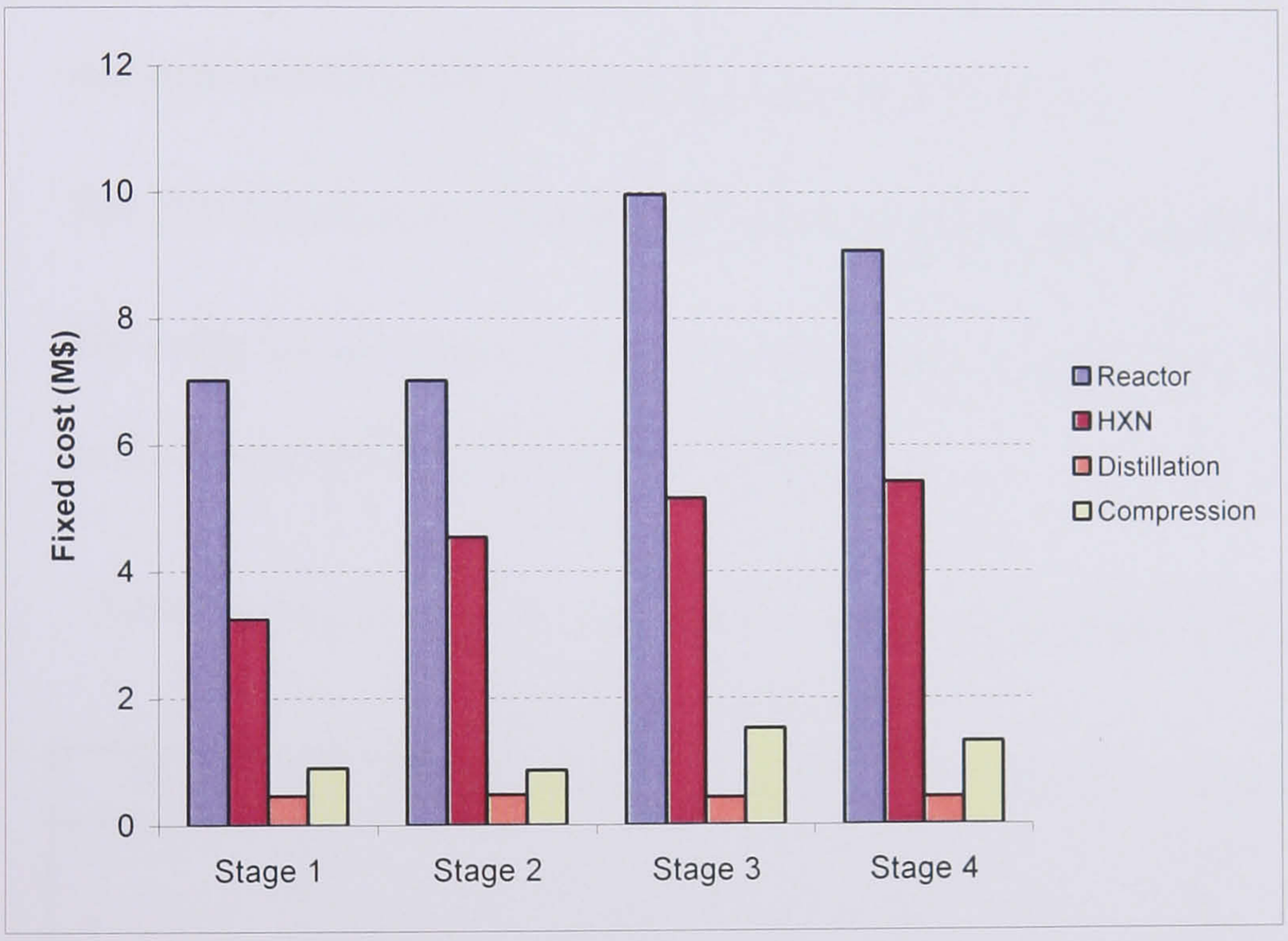

Figure 7.28: Fixed costs for one PFR with internal recycle for the four stages for the acetic acid production process.

The reduction of 22 % in the OFV from Stage 2 to 3 is due to several factors:

1. The reduction of ethane conversion (from 76.0 % to 69.0 %) results in an increase of the internal recycle (Table 7.4) and consequently, in an extra cost of external compressor of 0.57 M$ (annualised cost of 0.21 M$/yr).

2. The increase of the internal recycle and the decrease of the diameter of the reactor tubes (Table 7.5), make the number of reactor tubes increasing considerably to keep low pressure losses. The compression costs only increase 0.3 M$/yr with respect to Stage 2 (Figure 7.29). The increase in the number of tubes results in an increase in the reactor fixed cost of 2.94 M$, which represents an annualised increase of 1.1 M$/yr (Figure 7.28).

3. The increase of the overall recycle makes the amount of oxygen fed to the system greater (it remains at its upper bound: 13 % of the total inlet flow to the reactor). This fact involves an extra cost of 1.0 M$/yr in raw material and 0.03 M$ in the feed compressor fixed cost.

4. The HXN fixed cost increases 0.6 M$ (annualised increase of 0.2 M$/yr).

5. The reduction of ethane conversion also results in a decrease of acetic acid production and thus of profits by 1.8 M$/yr.

Table 7.4: Recycle flows for one PFR with internal recycle for the four stages for the acetic acid production process.

Stage	Internal recycle (mols/s)	External recycle (mols/s)
1	827	279
2	754	266
3	2695	344
4	2001	344

Table 7.5: Reactor design parameters for one PFR with internal recycle for the four stages for the acetic acid production process.

Average values:	Stage 1 and 2	Stage 3	Stage 4
Diameter of the tube	25mm	ND=20	ND=20
Diameter of catalyst particle	5mm	4.5mm	4.5mm
Number of tubes	30000	45000	41000

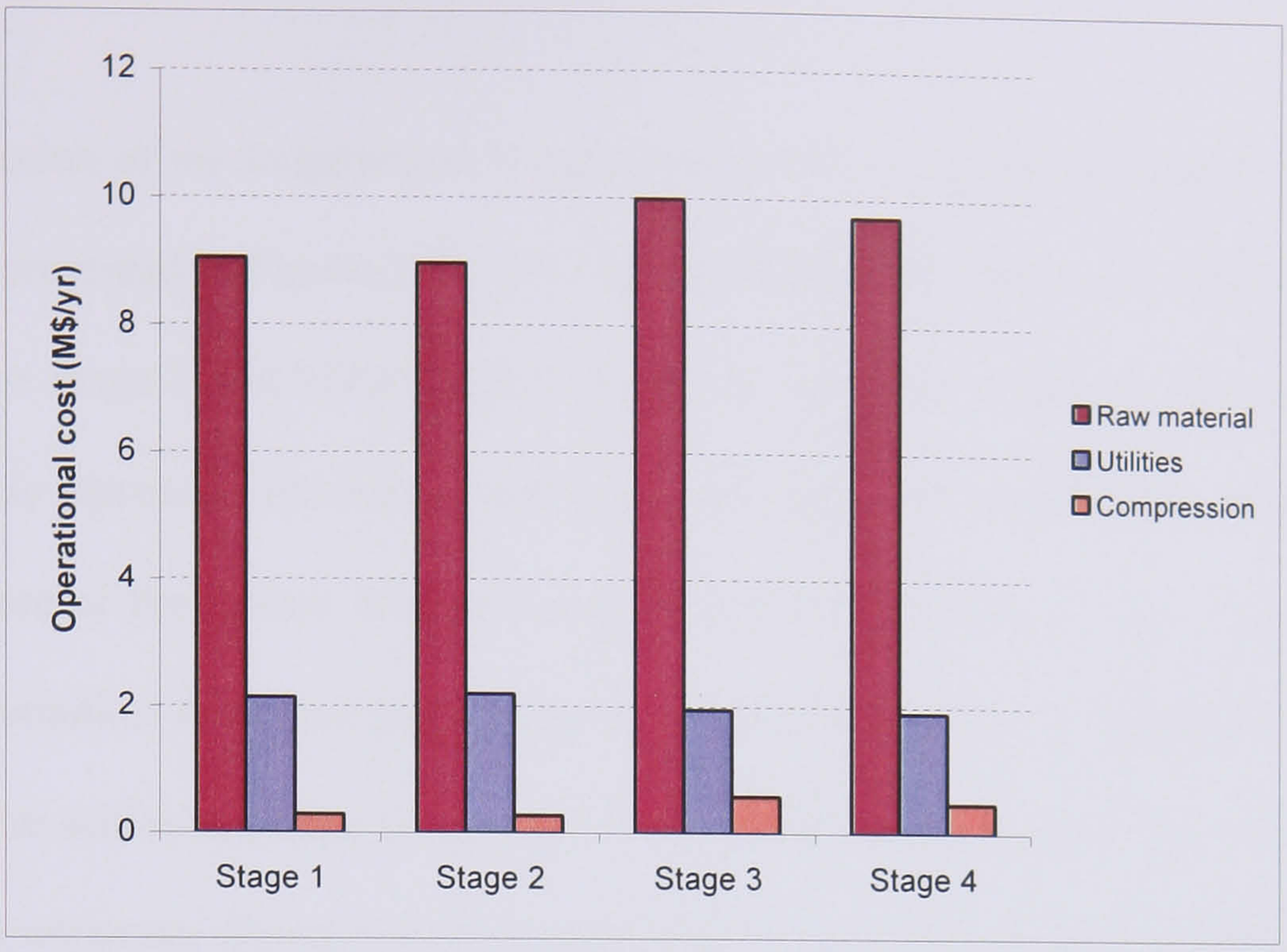

Figure 7.29: Operational costs for one PFR with internal recycle for the four stages for the acetic acid production process.

As the evolution of stages progresses (Stage 1 to Stage 2 and 3), tighter constraints on the longitudinal temperature profile of the reactor are added, resulting in higher HXN fixed costs. The HXN fixed costs for Stages 3 and 4 should be very similar as no extra constraints on the longitudinal temperature profile of the reactor are added in Stage 4. However, the recycle flows (Table 7.4) have influence on the HXN fixed cost, which result in an overall increasing effect for the new stage (Figure 7.28). Besides, as less internal recycle flow needs to be compressed in Stage 4 (Table 7.4), a smaller (*i.e.* cheaper) internal compressor is needed. Since the total flow recycled is also smaller, the reactor cost is also reduced as fewer tubes are needed to keep high pressures inside the reactor (Table 7.5). For the same reason, less oxygen is fed and a cheaper feed compressor is required. The changes in the fix and operational costs related to the condenser and reboiler are unnoticeable for the transition from Stage 3 to Stage 4.

The evolution of the longitudinal temperature profile of the reactor and of the utility media is presented in Figure 7.30. Here again, STi refers to the temperature inside the reactor for Stage i, and HXSTi refers to that of the utility media for the same stage. The X axis represents the discretisation points used for the calculations. Initially, the temperature of the reactor follows a logarithmic profile (Stage 1: T_{out} - T_{in} = 15 K). As the evolution of stages progresses, the temperature tends to decrease and flatter profiles are achieved (Stage 2: T_{out} - T_{in} = 7 K; Stage 3 and 4: T_{out} - T_{in} = 3 K). Once again, no important changes in the temperature of the reactor and of the utility media are observed in Stage 4. The extra modelling detail added in Stage 4 has also practically no impact on the OFV.

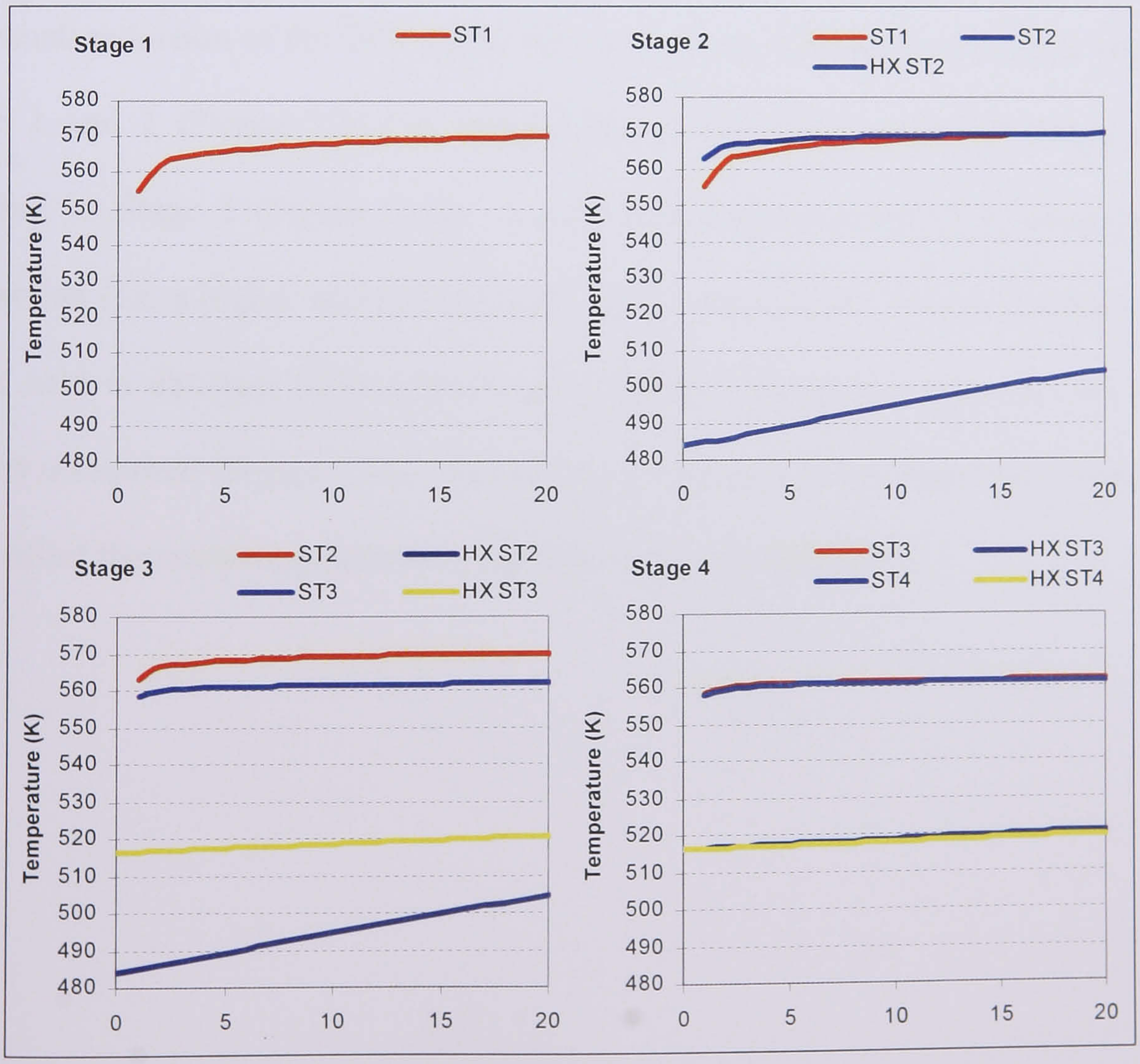

Figure 7.30: Reactor and utility temperature profile evolution for one PFR with internal recycle for the four stages for the acetic acid production process.

7.2.2.4 Three PFRs Structure Without Internal Recycle

In Stage 3, two different DNs for the reactor tubes are identified (Table 7.6). For the following discussion, Stage 3a and 4a make reference to DN=20, while Stage 3b and 4b refer to DN=15. The results showed are the best solutions out of 14 converged optimisation runs for Stage 1 and 2, out of ten for Stages 3a and 4a, and out of four for Stages 3b and 4b.

Table 7.6: Reactor design parameters for the three PFRs structure without internal recycle for the four stages for the acetic acid production process.

Average values:	**Stage 1 and 2**	**Stage 3a**	**Stage 3b**	**Stage 4a**	**Stage 4b**
Diameter of the tube	25mm	ND=20	ND=15	ND=20	ND=15
Diameter of catalyst particle	5mm	4.5mm	3.0mm	4.5mm	3.0mm
Number of tubes	30000	25000	34000	27000	35000

The small reduction of the OFV (0.66 M$/yr) that results from the transition between Stage 1 and 2 (Figure 7.31), is mainly due to the lower operating temperatures required in Stage 2 (Figure 7.34). Lower temperatures result in a lower ethane conversion (*i.e.* a higher external recycle). As a consequence, a lower production of acetic acid is obtained (0.56 M$/yr) and a higher oxygen raw material cost (0.23 M$/yr) is required (Figure 7.33). The rest of the changes in the fixed and operational costs offset the remaining difference between OFVs of 0.13 M$/yr.

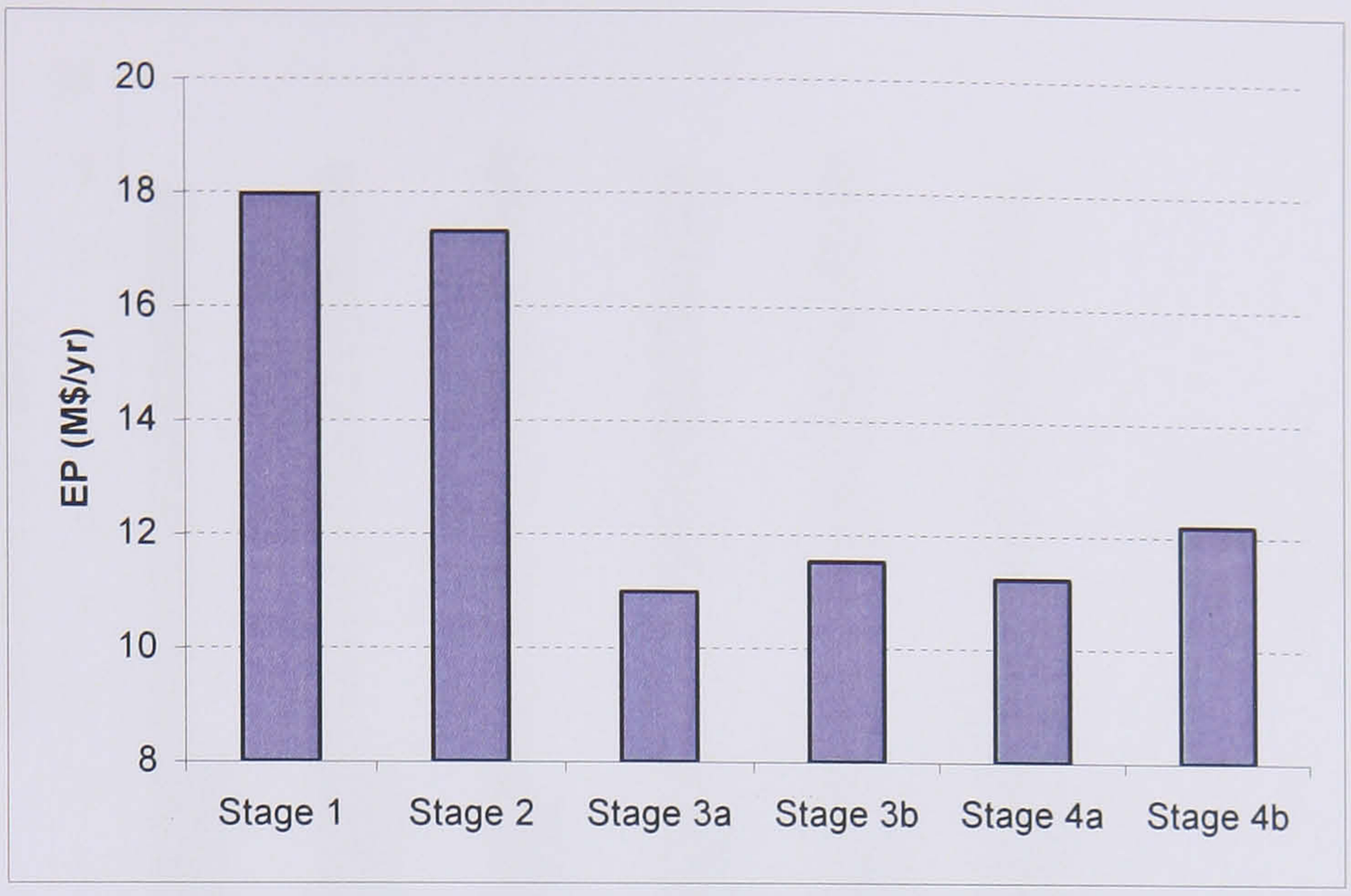

Figure 7.31: EP (M$/yr) for the three PFRs structure without internal recycle for the four stages for the acetic acid production process.

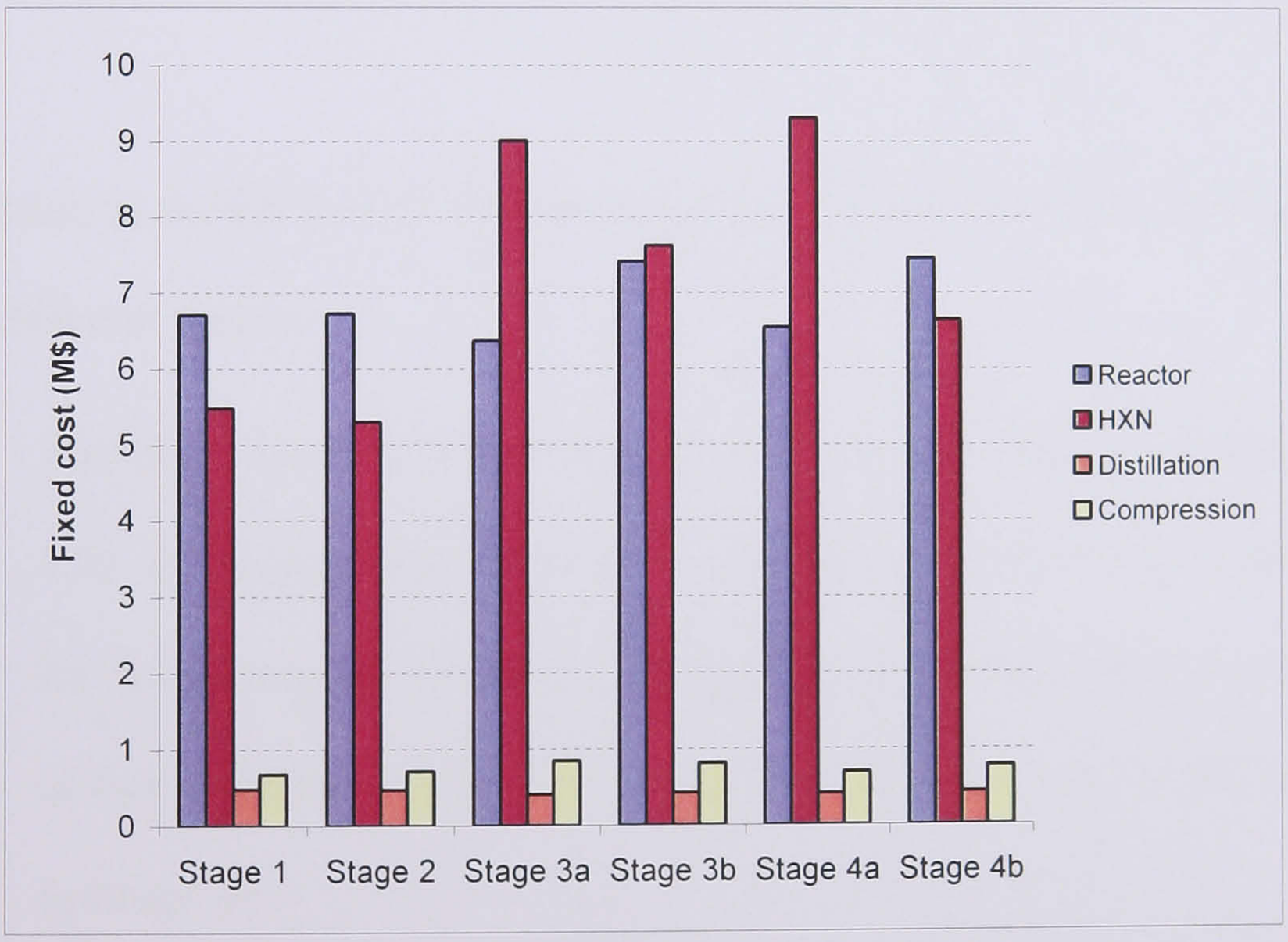

Figure 7.32: Fixed costs for the three PFRs structure without internal recycle for the four stages for the acetic acid production process.

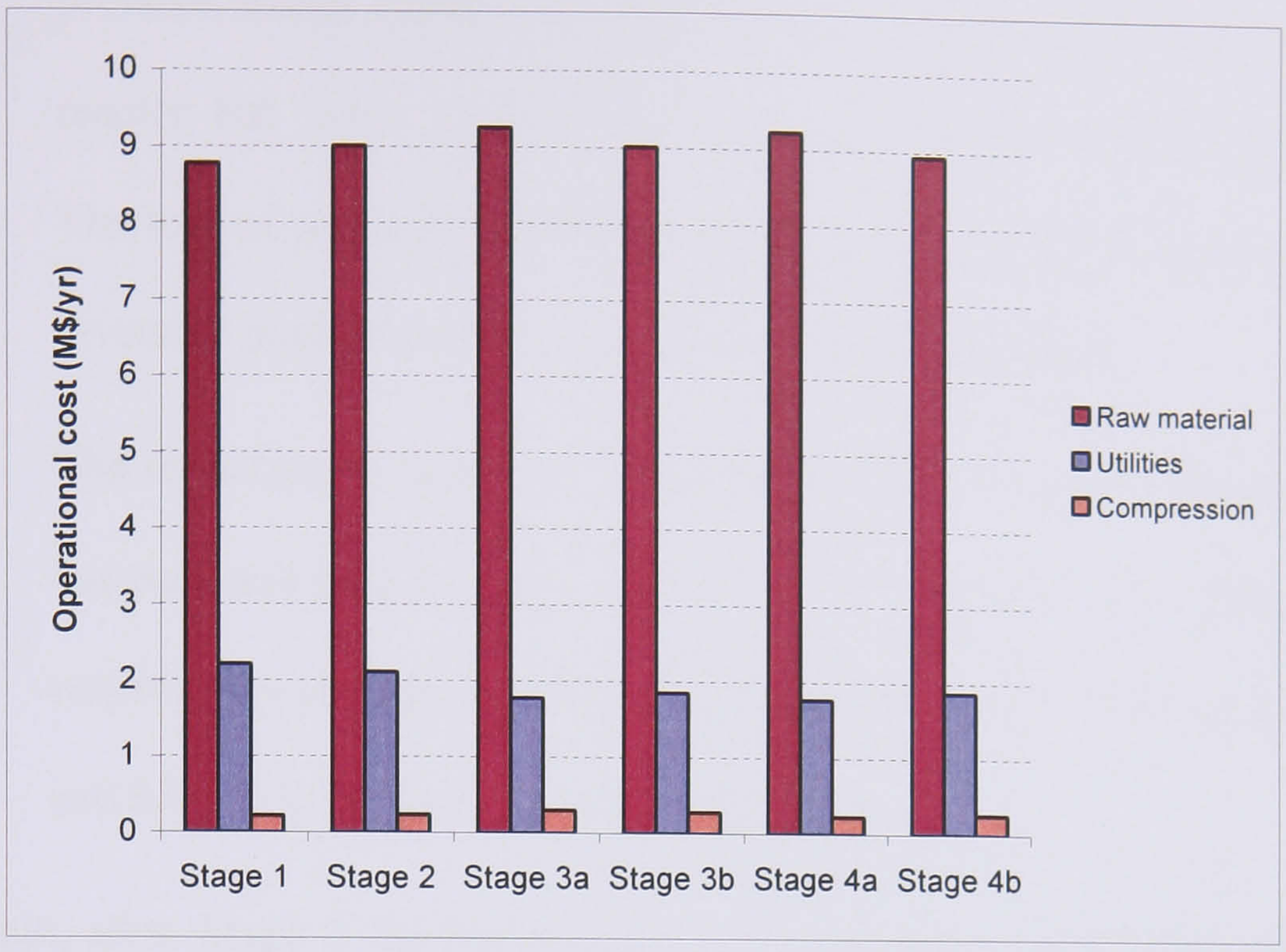

Figure 7.33: Operational costs for the three PFRs structure without recycle for the four stages for the acetic acid production process.

The reduction in the OFV of 37 % from Stage 2 to 3a and of 33 % from Stage 2 to 3b is due to different factors:

1. The HXN fixed cost increases by 3.71 and 2.33 M$, as shown in Figure 7.32, (annualised increased cost = 1.4 and 0.9 M$/yr) due to the increase, for both cases, of the number of heat exchange units (from 11 to 14), and of heat exchange area (from 5300 m^2 to 10600 in Stage 3a and to 8200 m^2 in Stage 3b).

2. The decrease of the number of reactor tubes (Table 7.6) in Stage 3a results in a 0.36 M$ cheaper reactor (annualised decreased cost of 0.1 M$/yr). Its increase in Stage 3b makes the reactor 0.69 M$ more expensive (annualised increased cost of 0.3 M$/yr). At the beginning of the search in Stage 3, the DNs of the reactor tubes are reduced to improve heat transfer properties. Then, the number of reactor tubes is balanced against the

pressure losses inside the reactors (more tubes mean a more expensive reactor but lower pressure losses, which implies smaller compressors). The loss of pressure is affected proportionally to the external recycle and inversely proportionally to the DNs of the reactor tubes.

3. The reduction in acetic acid production due to the lower reactor operating temperatures (Figure 7.34), results in a loss of profit of 5.1 and 4.9 M$/yr respectively (ethane conversion descends from 72.3 % in Stage 2 to 60.5 and 63.4 % in Stage 3a and 3b respectively).

Once again, after Stage 3 the temperature of the reactors and of the utility media remain very similar (Figure 7.34). The extra modelling detail added in Stage 4, has almost no effect on the OFV. The small increase of the OFV in Stage 4b is mainly due to the reduction in the HXN cost as can be seen in Figure 7.32 (0.98 M$; annualised decrease of 0.36 M$/yr).

Raw material and compression costs are proportional to the recycles present in each stage (Table 7.7). Utility costs are proportional to the amount of water and acetic acid produced in the reactive section.

Table 7.7: External recycles for the three PFR structure without internal recycle for the four stages for the acetic acid production process.

Stage	**External recycle (mols/s)**
1	287
2	312
3a	445
3b	425
4a	443
4b	418

The evolution of the longitudinal temperature profile of the reactors and of the utility

media is presented in Figure 7.34. Once again, STi refers to the temperature inside the reactor for Stage i, and HXSTi refers to that of the utility media for the same stage. The X axis represents the total catalyst load.

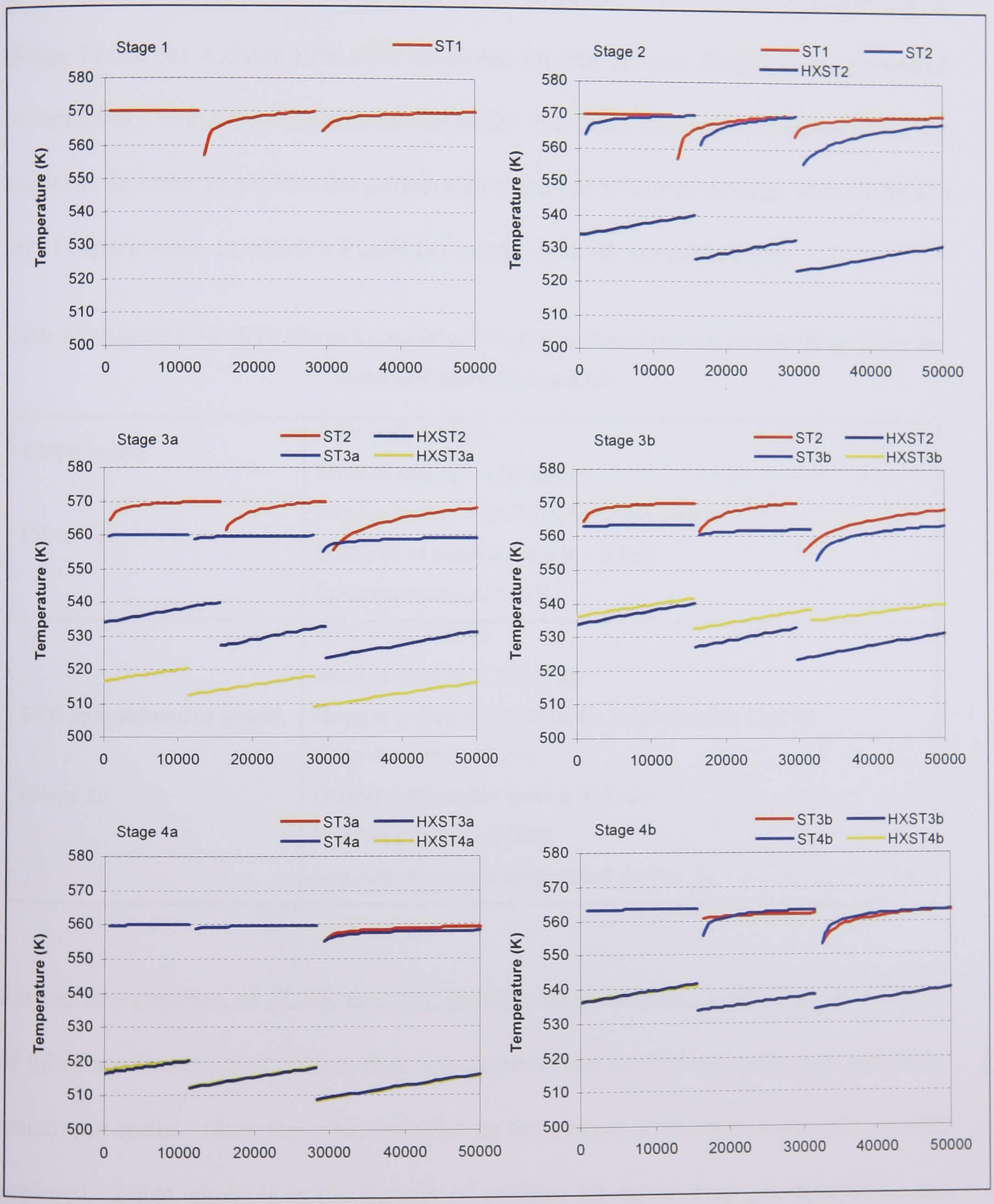

Figure 7.34: Evolution of the reactor temperature profiles for the three PFRs structure without internal recycle for the four stages for the acetic acid production process.

7.2.2.5 Experiments with Fluidised Bed Reactors (FLBR)

At a first glance, the well-mixing behaviour presented by a CSTR or a PFR with high internal recycle ratio, could be assimilated to the well-mixing presented by FLBRs. The results obtained in earlier stages of the synthesis exercise for a single CSTR (Stage 1) and for a single PFR with unlimited internal recycle (Stage 2) are presented in Table 7.8. The different performance of the two cases has been explained in earlier sections. In order to explore the performance and behaviour of designs with FLBRs, a set of experiments, in which a FLBR cell model is used, are carried out.

Table 7.8: Results for a CSTR (Stage 1) and for a PFR with unlimited internal recycle (Stage 2) for the acetic acid production process.

CSTR model **(Stage 1)**	OFV = -7. 5 M$/yr Mass of catalyst = 50000 kg Oxygen in feed = 38.70 mol/s (equivalent to 3.7 %) Diameter of catalyst particle = 5 mm Isotherm reactor at 542 K
PFR approximation model **(Stage 2)**	OFV = 20.3 M$/yr Mass of catalyst = 50000 kg Oxygen in feed = 117.82 mol/s (equivalent to 13.0 %) Tube diameter = 25 mm Diameter of catalyst particle = 5 mm Number of tubes = 30000 Logarithmic reactor temperature profile: T_{in} = 563 K, T_{out} = 570 K

For the investigation of FLBR designs, initially single FLBRs with different number of tubes are investigated. After that, experiments are carried out with two and three reactors in series. Next, the effect of diluting the system with internal recycles is also explored. Later, changes in the density of orifices for the reactor gas distributor are also considered. Finally, a sensitivity study for the reactor cost function is presented.

In general, the literature has a lack of cost models for operational units. Particularly, reliable cost models for FLBRs are very difficult to obtain. For the set of experiments presented here, in order to eliminate from the OFV the influence of the FLBR fixed cost, the total reactive section fixed cost is assumed to be, except in the sensitivity study, the cost of a CSTR, which is five times that of a single FBR with the same catalyst load (see Appendix 2). This assumption is valid for every case regardless the number of reactors in the reactive section and the number of tubes in them.

Single FLBRs formed by different number of tubes

In this section the results obtained with single FLBRs with different number of reactor tubes are discussed. Figure 7.35 shows the performances obtained for a range of reactor tubes from 1 to 20. The OFV approaches asymptotically a value of -0.22 M$/yr as the number of tubes increases, which indicates that these designs significantly underperform those involving PFRs.

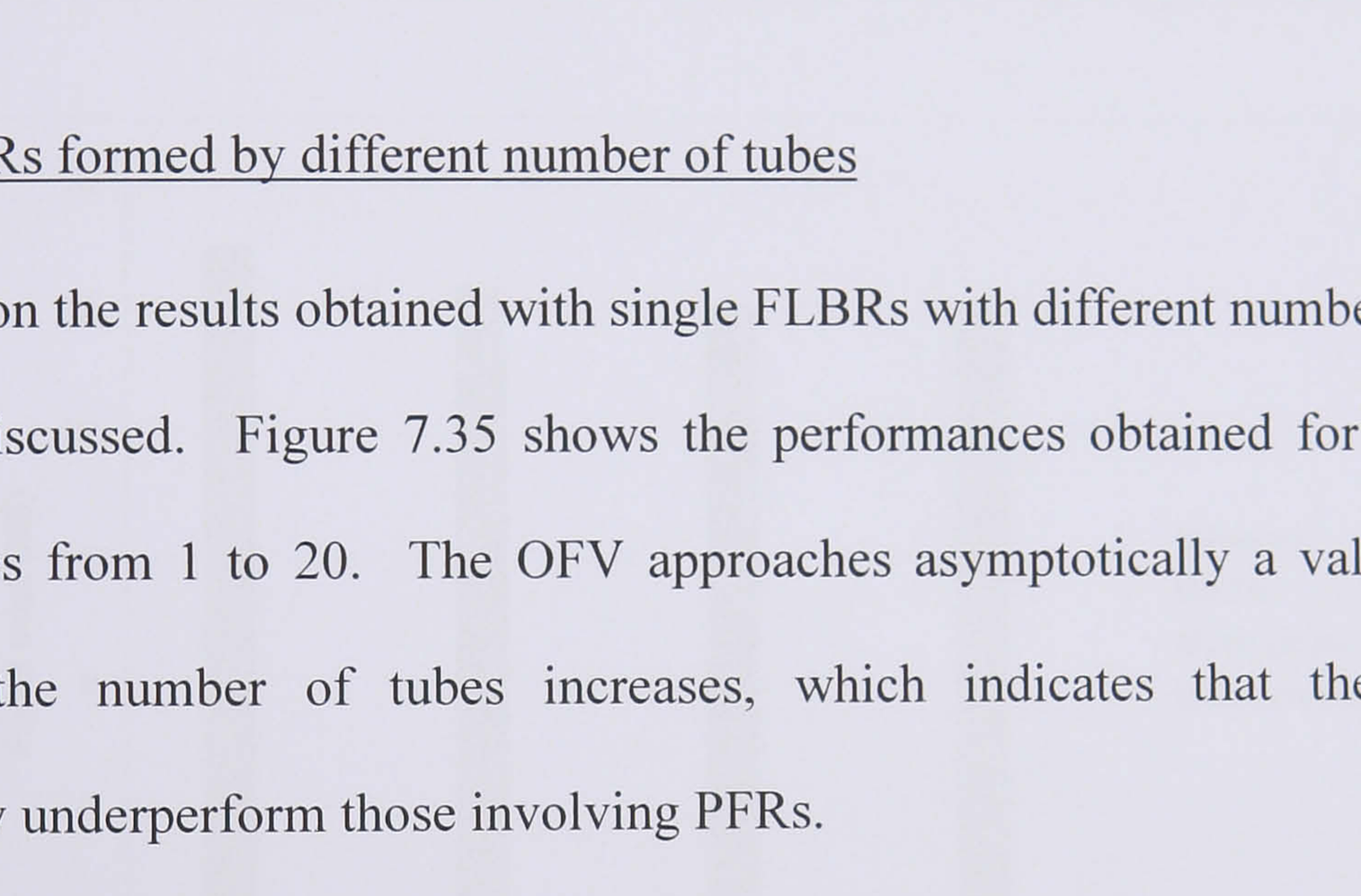

Figure 7.35: OFV for single FLBRs with different amount of tubes for the acetic acid production process.

The HXN fixed cost (Figure 7.36) decreases at higher number of tubes as the HXN area is progressively reduced and the number of heat exchanger units is kept constant. The area is reduced because there is more driving force at higher number of tubes as higher reactor temperatures can be attained. Higher operating temperatures can be reached because the presence of more tubes increase the heat exchange surface of the reactor and more heat can be released (Table 7.9). The fact that the utility temperature is at its lower limit for all the cases (400 K), indicates that the systems are constrained by heat transfer issues. The rest of the costs vary inappreciably.

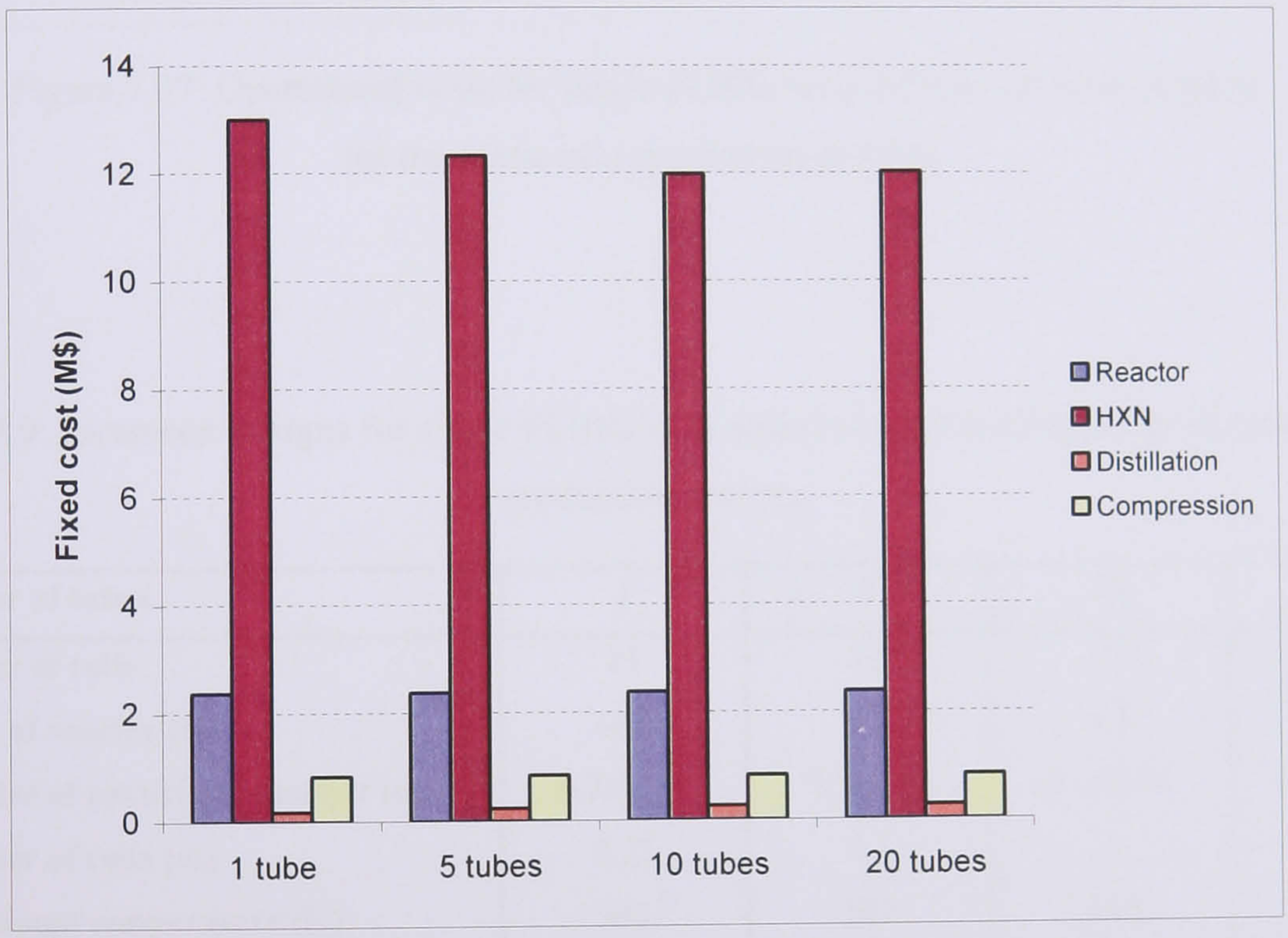

Figure 7.36: Fixed costs for single FLBRs with different number of tubes for the acetic acid production process.

The oxygen feed increases when increasing the number of reactor tubes. Since the presence of oxygen favours the exothermic reactions, more oxygen can be fed to reactors with more tubes. Consequently, the raw material cost raises (Figure 7.37). Utilities increase as more acetic acid and water are produced. Compression costs vary unnoticeably.

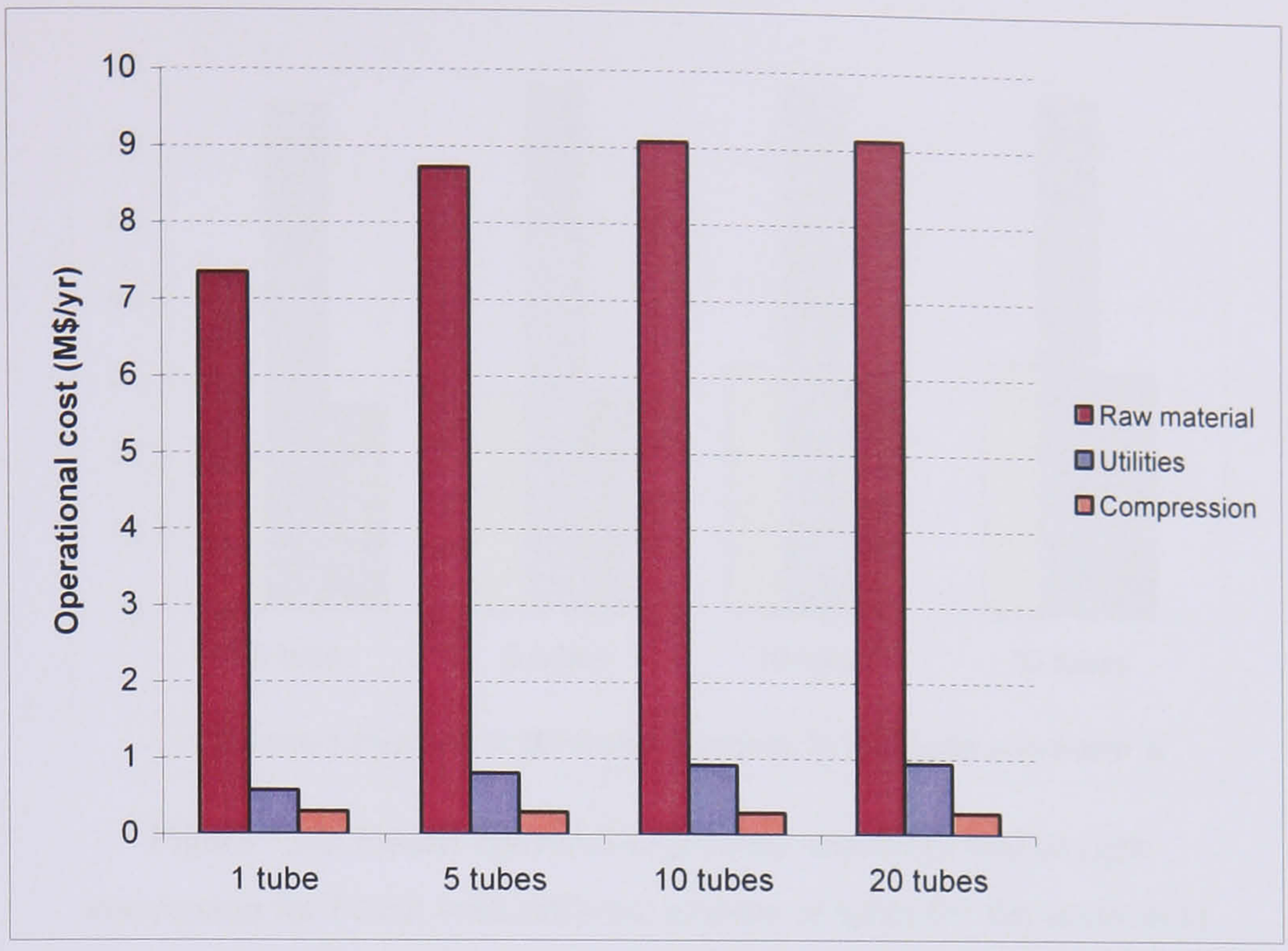

Figure 7.37: Operational costs for single FLBRs with different number of tubes for the acetic acid production process.

Table 7.9: Parameter designs for single FLBRs with different number of tubes for the acetic acid production process.

Number of tubes	1	5	10	20
Number of cells	21	21	20	19
Height of reactor (m)	10.9	4.8	4.3	2.1
Diameter of particle of catalyst (m)	6.26E-04	3.51E-04	4.15E-04	2.20E-04
Diameter of tube (m)	2.25	1.5	1	1
Operational temperature (K)	542	544	545	549
Void fraction	0.6	0.6	0.5	0.5
Oxygen in feed (%)	7.9	11.5	12.8	13
Heat released per reactor (kW)	8.68E+03	1.27E+04	1.48E+04	1.53E+04

The process selectivity ranges between 65-68 %, the ethane conversion approaches asymptotically a value of 33 % and of 32 % for the oxygen conversion (Figure 7.38).

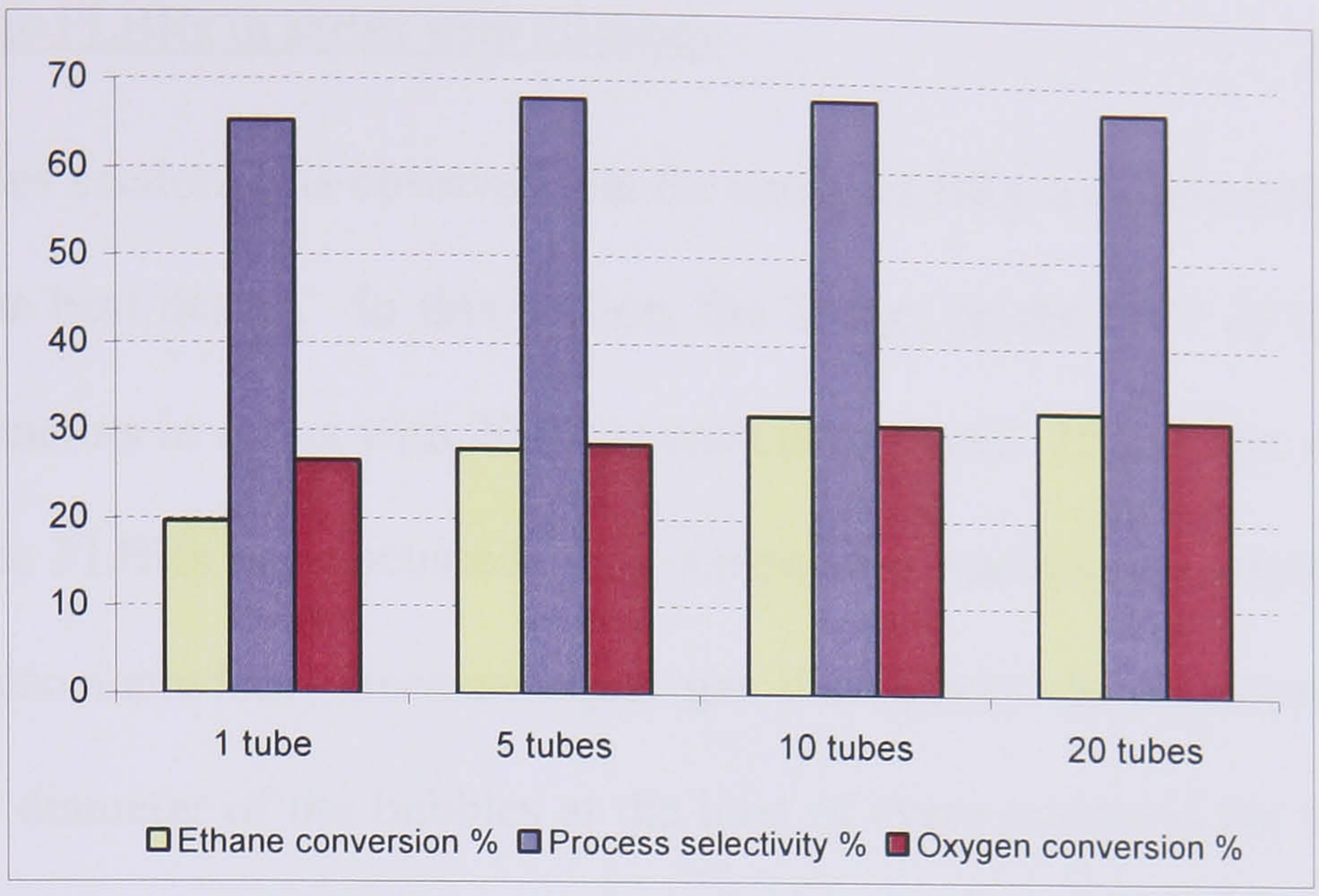

Figure 7.38: Ethane conversion, process selectivity and oxygen conversion for FLBR with different amount of tubes for the acetic acid production process.

In the case where the oxygen was not separated but completely recycled, the benefit in the raw material costs would follow similar trade-offs and influence in a similar mode the OFV for each one of the cases (Figure 7.39). The benefit achieved for FLBRs with 10 and 20 tubes, is the biggest one observed so far due to the low oxygen conversions in FLBRs (Figure 7.38). Regardless these improvements, the design candidates still cannot compete against the ones involving structures with PFRs.

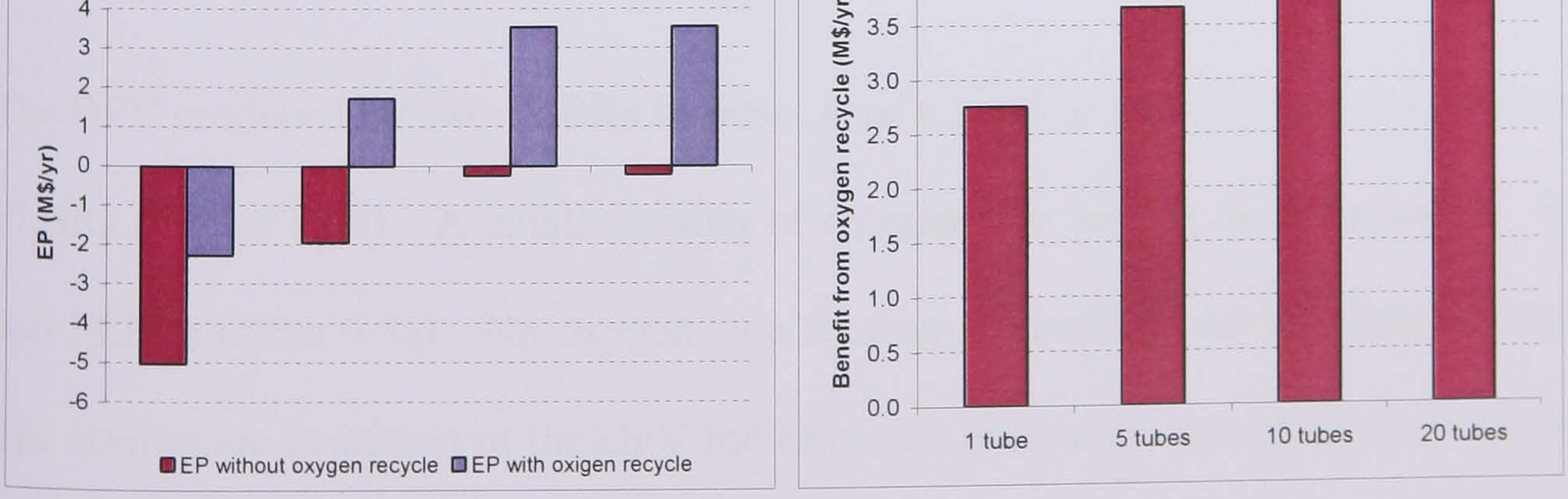

Figure 7.39: OFV and benefit from the oxygen recycling for single FLBRs with different amounts of tubes for the acetic acid production process.

Two and three FLBRs in series with 20 tubes

In the previous section, it is observed that for single FLBRs, a reactor with 20 tubes in parallel is the best design. In this section, the impact on the OFV of increasing the number of reactors in series with 20 tubes each is assessed. The results obtained with two and three FLBRs are discussed. For comparison reasons, the results of a single FLBR are also included. Because equal gas distributors are employed for all the reactors, the diameter of the bubbles at the inlet of every reactor is the same, despite the reactor being placed in first, second or third position.

Figure 7.40: OFV for one, two and three FLBRs with 20 tubes in parallel for the acetic acid production process.

The OFV produced by two FLBRs in series is of 6.2 M$/yr and of 6.1 M$/yr by three FLBRs (Figure 7.40). A small fraction of oxygen side feeding is identified for the two FLBRs (circa 9 %). No oxygen side feeding is identified for the three FLBRs. The asymptotic evolution of the OFV indicates that more units would not improve the performance. The improvement of the OFV for both cases with respect to the single FLBR is explained by the higher ethane conversions reached (Figure 7.41). Bigger heat exchange surfaces of reactor allow reaching higher operating temperatures in

both cases (Table 7.10) and thus higher ethane conversions (the surface for one FLBR is 264 m^2, for two FLBRs is 454 m^2 and for three FLBRs is 405 m^2).

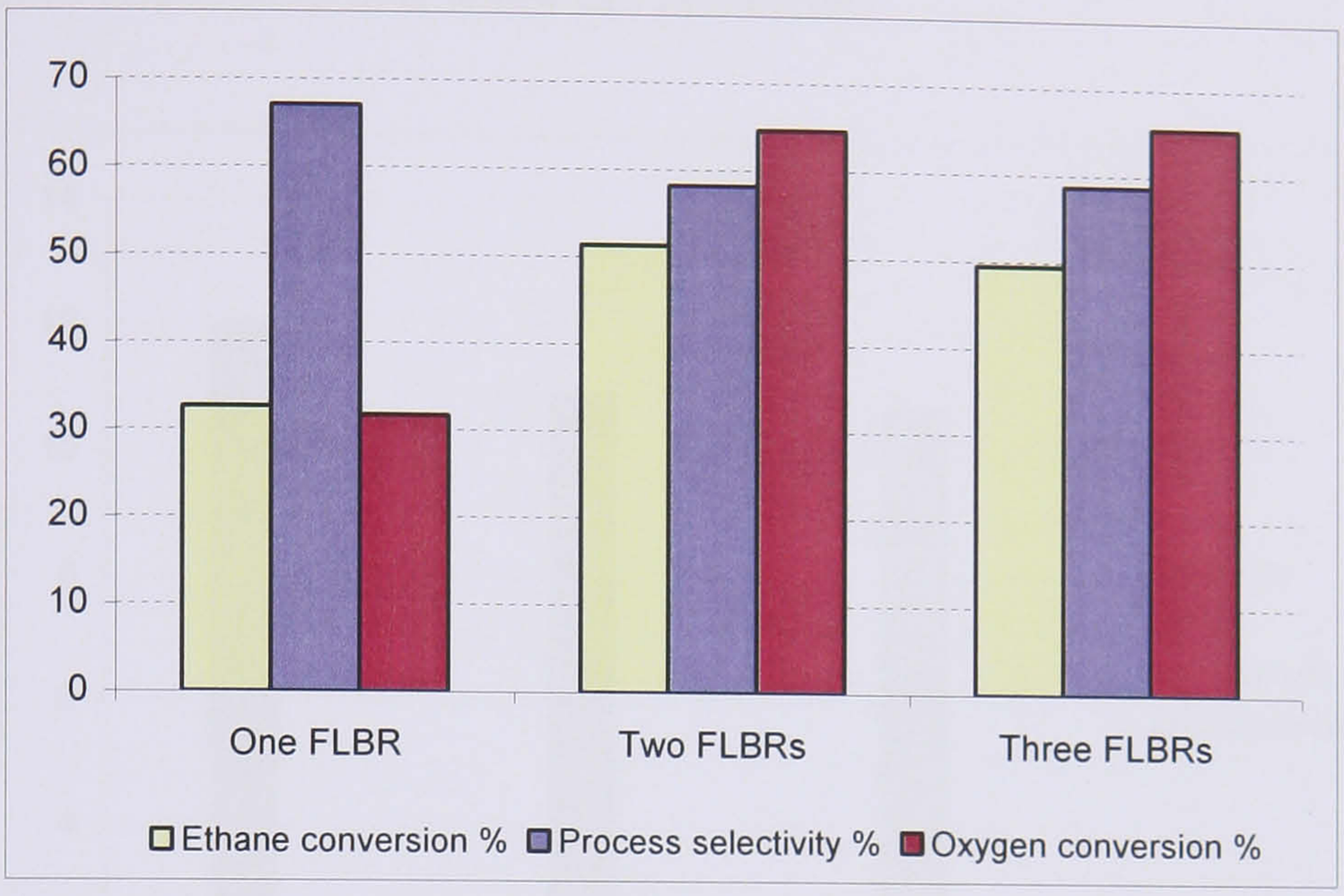

Figure 7.41: Ethane conversion, process selectivity and oxygen conversion for one, two and three FLBRs with 20 tubes for the acetic acid production process.

Table 7.10: Parameter designs for one, two and three FLBRs in series with 20 tubes in parallel (1) for the acetic acid production process.

FLBR in series	**Diameter of tube (m)**	**Operational temperatures (K) (% catalyst load - 50000 kg))**	**Oxygen in feed (%)**	**Heat released per reactor (kW)**
One	1.00	549 (100 %)	13.0	1.53E+04
Two	0.75	562 (54 %) 570 (46 %)	12.7 9.1	1.45E+04 1.17E+04
Three	0.75	559 (60 %) 564 (27 %) 570 (13 %)	12.7 8.0 5.7	1.44E+04 6.75E+03 3.42E+03

The HXN fixed cost (Figure 7.42) is reduced as the number of FLBRs increases in the structure. For two FLBRs, the HXN area is reduced by 18 % and the number of heat exchangers is increased by one. For three FLBRs, the HXN area is reduced by 16 % but the number of heat exchangers is maintained. The combination of both changes results in lower HXN fixed costs. The area reductions are consequence of the higher

temperatures at which the hot streams leave the reactors (*i.e.* there is more driving force). Compression costs do not change appreciably. Distillation costs slightly increase as more acetic acid and water are produced.

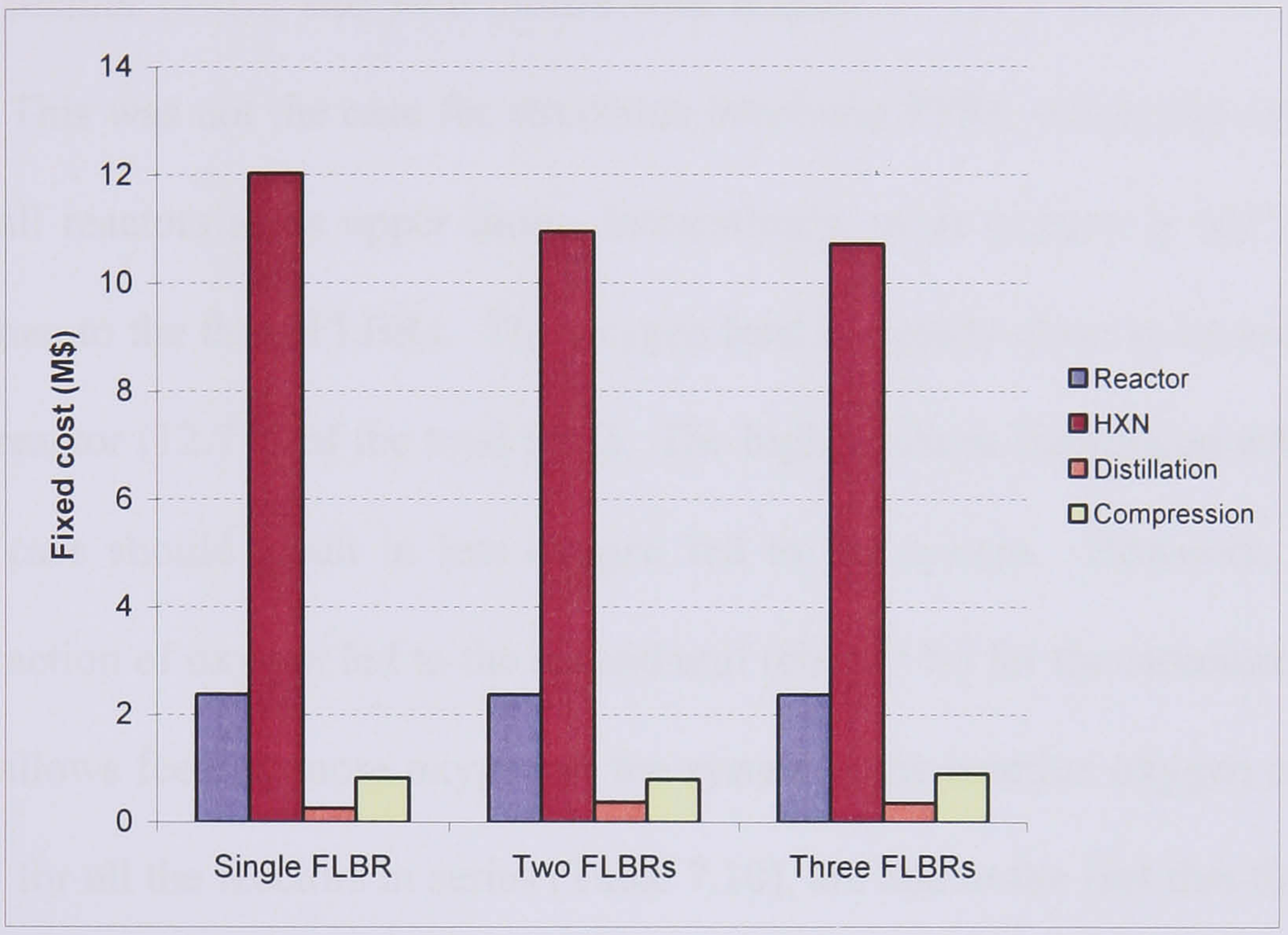

Figure 7.42: Fixed costs for one, two and three FLBRs with 20 tubes in parallel for the acetic acid production process.

Regarding operational costs, utilities increase as more acetic acid and water are produced (Figure 7.43). Compression costs change inappreciably. For two and three FLBRs, the amount of oxygen fed to the system decreases. This explains the decrease of the raw material cost (Figure 7.43). This behaviour is opposite to the one observed for structures formed by PFRs in series, where as the number of reactors increased also did the oxygen raw material cost. Such different behaviours are explained as follows: firstly, the ethane conversion increases here from 33 % for one FLBR, to 51 % for two FLBRs and to 50 % for three FLBRs (Figure 7.41). Consequently, there is less accumulation of ethane in the system for the last two cases resulting in reduced external recycle flows. This same behaviour was observed for the structures

involving PFRs. Secondly, due to the fact that the oxygen feed approaches, for all the cases, its maximum percentage limit in the first reactor but not in the rest of reactors (Table 7.10), the total amount of oxygen entering the reactive system for the last two cases is smaller (101.2 and 94.0 mols/s with respect to 121.1 mols/s for the single FLBR). This was not the case for structures involving PFRs, where the oxygen feed was for all reactors at its upper limit. Interestingly, more oxygen is fed to the two FLBRs than to the three FLBRs. The oxygen feed is equally close to its constraint in the first reactor (12.7 % of the total feed). The higher ethane conversion achieved for the first case should result in less oxygen fed to the system. However, the small bypass fraction of oxygen fed to the second unit (circa 9 %) for the structure with two FLBRs, allows feeding more oxygen to the system. The inactive oxygen constraints observed for all the reactors in series (Table 7.10), are due to the fact that the systems are constrained by heat release issues. For this case study, the presence of oxygen favours the exothermic reactions taking place. Having the cooling utility temperature at its lower limit, constraints the amount of oxygen that can be fed to the units.

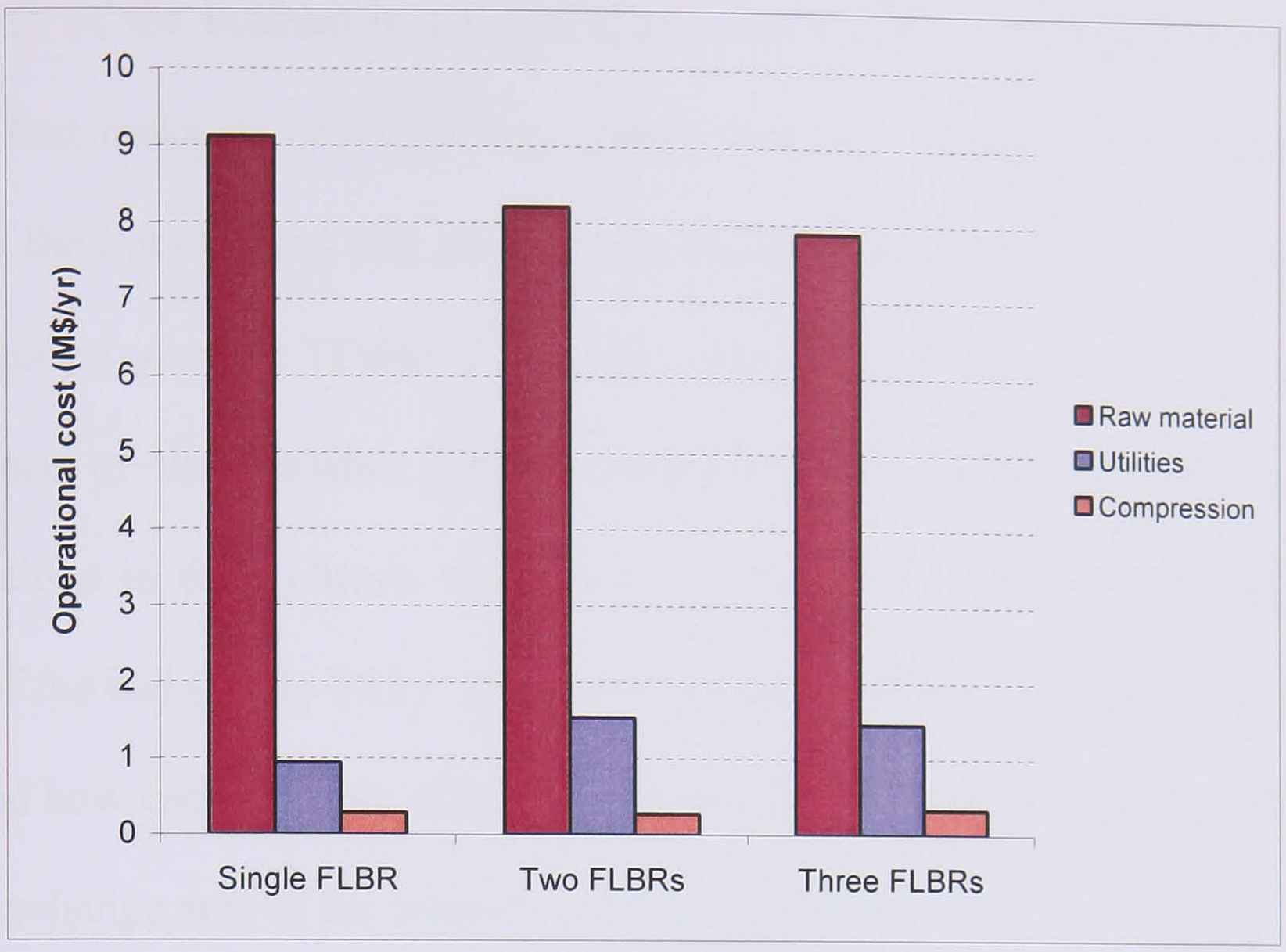

Figure 7.43: Operational costs for one, two and three FLBRs with 20 tubes in parallel for the acetic acid production process.

The heat exchange area of the reactors is the design factor that most impacts the OFVs. Operating oxygen concentrations and temperatures are effects of the exchange area. As already mentioned, the areas for one, two and three FLBRs are 264, 454 and 405 m^2 respectively. The higher area of two FLBRs allows releasing more heat in the reactive section (Table 7.10), which in parallel increases the acetic acid production, thus achieving higher performances. The difference in the area with respect to the three FLBRs is due to the longer overall height of the reactors (4.8 m for the two FLBRs compared to 4.3 m for the three FLBRs -Table 7.11-), despite resulting in less cells in total (36 for the two FLBRs compared to 51 for the three FLBRs). Such differences are consequence of the growth of the bubbles through the reactors (Section 6.4.2.3). The size of the bubbles must always be lower than the size of the tube. This constraint defines the resulting number of cells from the model, which at the same time defines the height of the reactor (*i.e.* the reactor heat exchange area).

The growth of the bubbles is a function of a multitude of non-linear functions and variables that make its understanding rather complex. The variables that affect the growth of the bubbles and that are different for these two structures are the diameter of the catalyst particle (Table 7.11), the viscosity and density of the gas (as a consequence of the pressure and temperature of the system and the component concentrations in each phase), the amount of flow fed to the system and the void fraction of the bed (Table 7.11). A much more exhaustive study would be required to understand how each variable affects the growth of the bubbles before conclusions on the heat exchange area of the reactors could be discussed.

Table 7.11: Parameter designs for one, two and three FLBRs in series with 20 tubes in parallel (2) for the acetic acid production process.

FLBR in series	Number of tubes	Number of cells	Height of reactor (m)	Void fraction	Diameter of particle of catalyst (m)
One	20	19	2.1	0.50	2.20E-04
Two	20	19 17	2.6 2.2	0.60	3.21E-04
Three	20	20 18 13	2.5 1.2 0.6	0.55	3.26E-04

Once again, in the case that the oxygen was not separated but completely recycled, the benefit in the raw material costs would follow similar trade-offs in all cases (Figure 7.44). For the two and three FLBR in series, the OFVs would reach values of 7.9 and 7.6 M$/yr respectively. These OFVs are close to the one obtained for a single PFR in Stage 4 (8.2 M$/yr) under the same conditions. However, the performances are still very far from the results obtained in Stage 4 for the single PFR with internal recycle and the three PFRs with oxygen feed distribution; even when the oxygen remaining at the outlet of the reactive units is not recycled but purged in the absorber (OFV = 16.1

and 12.2 M$/yr respectively).

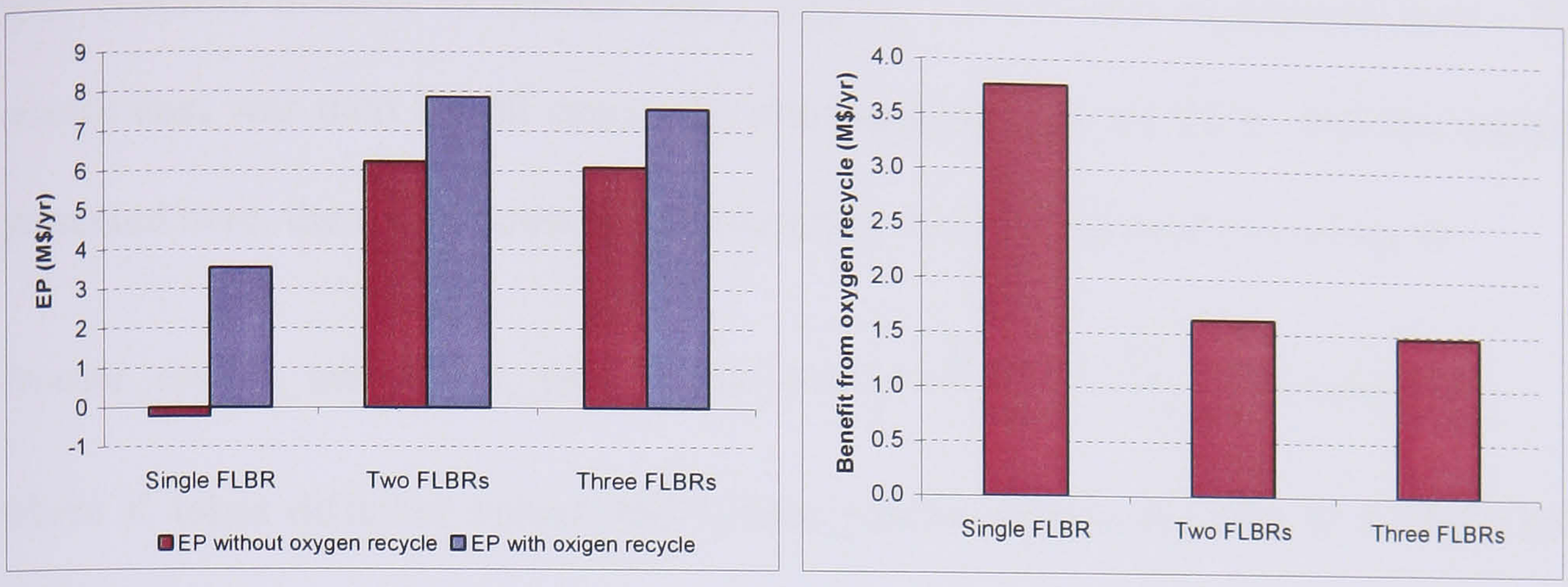

Figure 7.44: OFV and benefit from the oxygen recycling for one, two and three FLBRs with 20 tubes in parallel for the acetic acid production process.

Analysis of the effect of internal recycles

The dilution of the system with internal recycles does not improve the OFV for any of the structures considered (one, two and three FLBRs).

Analysis of the effect of the change of the gas distributor

Experiments with different orifice densities for the gas distributor (range studied 600-1000 orifices/m^2) show that this design parameter has no influence on the performance of the designs over a threshold of 800 orifices/m^2 (*i.e.* above 800 the performances remain unchanged.). Below 800 orifices/m^2 lower performances are obtained.

Sensitivity analysis of the reactor cost function

A sensitivity study on the reactor cost function is carried out to illustrate the high dependence of results and conclusions on the cost functions employed when searching

for new process design options. The same set of experiments carried out for a FLBR with different number of reactor tubes (Figure 7.35) is also considered here. The reactor cost was then for all cases, the same and equal to a CSTR. For the analysis presented here, the reactor cost is substituted by a cost calculated according to:

$$Reactor\_cost(N\_tubes, K) = 1\_tube\_reactor\_cost \cdot \left(1 + \frac{N\_tubes \cdot K}{100}\right) \qquad \text{(Equation 7.1)}$$

where K takes different values and 1_tube_reactor_cost is the cost of a single tube FLBR (equal to a CSTR).

Figure 7.45 shows the performances obtained with different values of K for single FLBRs for a range of tubes between 1 and 20. The figure also shows the OFV for cases where the FLBRs are priced as MTRs formed by 30000 tubes (as for PFRs in Stage 1 and 2).

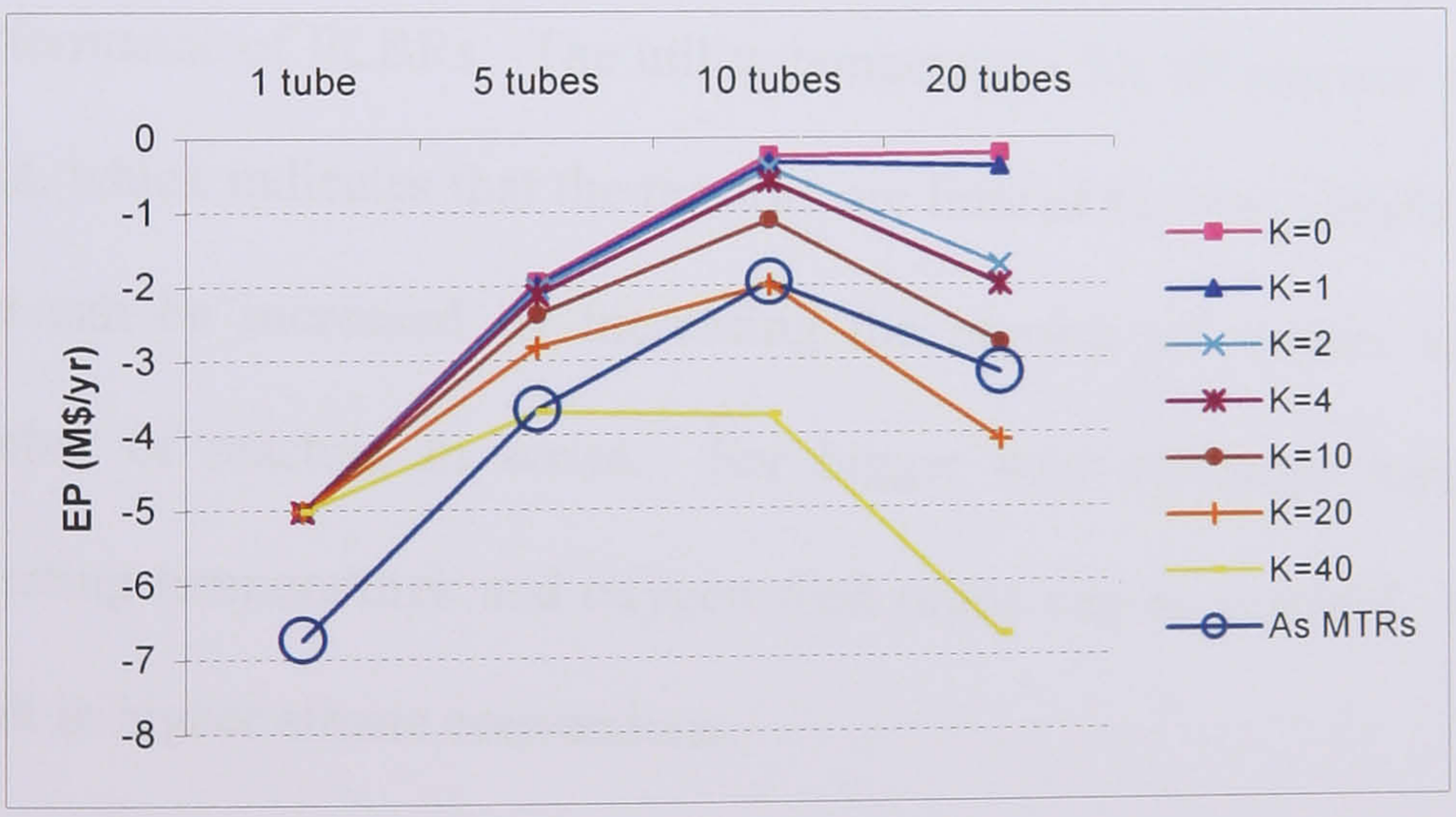

Figure 7.45: OFV for a single FLBR with different amount of tubes for the acetic acid production process.

As previously shown in Figure 7.35, the OFV approaches asymptotically a value of -0.22 M$/yr when all reactors have the same cost and equal to a single tube FLBR (K = 0). For all other values of K lower than 40, maximum performances are obtained

when the FLBR consists of ten tubes in parallel. The same occurs when the reactors are priced as MTRs. For K = 40, the maximum occurs for a FLBR formed by five tubes in parallel. It is obvious from observation, the strong impact that the reactor cost function has on the OFVs, which proves that crude cost functions can compromise results and conclusions at early stages of process design. Even for the hypothetic case in which the reactor fixed cost was zero, the 20 tube FLBR would still not outperform the structures formed by PFRs, as it would reach an OFV of 0.84M$/yr.

Conclusions regarding design candidates involving FLBRs

From the analysis of results, the main conclusions obtained after comparing different design candidates with FLBRs are:

- The heat exchange area of the reactor is the design factor that most impacts the performance of FLBRs. The utility temperature for all reactors is at its lower limit, which indicates that the reactors are limited by heat transfer issues. The area can be increased by increasing the number of reactor tubes and the number of reactors in series. For bigger heat exchange surfaces, higher operating temperatures and oxygen feed ratios can be reached. Both factors result in higher ethane conversions.

- Despite that for more tubes per reactor the height of the reactor is reduced as the catalyst amount is equally divided per tube, the number of cells per reactor is practically constant. This indicates that bubbles grow at different rates for different number of reactor tubes.

- The use of the same gas distributor in every reactor enables the bubbles to go back to their initial size when entering new units. This permits the bubbles flowing longer distances as their size is periodically reduced and kept longer below the diameter of the tube.

- The increase in the density of perforations of the gas distributor (range = 800 ± 200 perforations/m^2) has no impact on the performance over a threshold (800 perforations/m^2). Under the threshold values, lower performances are obtained.

- FLBRs with internal recycles do not improve the OFV of any equivalent structure without recycle.

- Regarding the catalyst particle diameter, it has been observed from computational experimentation that smaller particles improve heat transfer. However, below a certain value, the diameter has practically no impact on the process performance as it cannot improve anymore the heat transfer. No clear identification of the optimum diameter of the catalyst particle is obtained. For the best designs, it ranges between 0.22 and 0.33 mm. These sizes are one order of magnitude higher than the ones presented by Linke *et al.* (2002b), despite imposing similar sizes to the ones they suggest for the initial solutions from which the optimisations start. The reason is that a lower density of catalyst is employed here (600 kg/m^3 with respect to the 3100 kg/m^3). Both works (Linke *et al.* (2002b) and the current research) suggest designs falling in the region A of the Geldart classification and very close to the limit with region B.

- Regarding the void fraction of the bed, higher values improve heat transfer properties as they result in longer reactor tubes (*i.e.* higher heat exchange areas). All final designs are at or very close to the maximum fraction allowed inside the FLBR.

- There is a need for accurate cost functions when searching for new process design candidates, as they significantly impact OFVs.

The conclusions obtained after comparing designs involving FLBRs with designs involving other types of reactor are:

- For this case study, the well-mixing behaviour of CSTRs and the back-mixing degree of PFRs with high internal recycles are not equivalent to the degree of well-mixing present in the FLBRs.

- Design candidates involving FLBRs present poorer performances than structures involving PFRs mainly because they are much more limited by heat transfer issues.

7.3 Computational Experience

The use of network recycles, introduced in Section 3.3.2, requires a two-step approach to solve effectively the system of equations derived from the superstructure representation (this approach applies for all stages except for Stage 4). In the first step ("without external recycle"), the system of equations is formed by those equations that define the reactor network and the separation section without including

the network recycle. The solution of this sub-system is the initial solution required by the non-linear solver algorithm to solve the full system of equations including the network recycle ("with external recycle").

The tables found below for Stages 1, 2 and 3 show average values for:

- 1. CPU times.
- 2. Number of function evaluations.
- 3A. Percentage of convergence of the step without external recycle.
- 3B. Total percentage of convergence of steps without and with external recycle.
- 4. Percentage of the function evaluations that having converged in both steps are inside the internal recycle limit.
- 5. Percentage of the function evaluations that having converged in both steps are inside the internal recycle limit and within the oxygen limit.
- 6. Percentage of the function evaluations that having converged in both steps are inside the internal recycle limit, within the oxygen limit and within temperature limits (see Section 5.2.2.5).
- 7. For Stages 2 and 3, percentage of the function evaluations that having converged in both steps are inside the internal recycle limit, within the oxygen limit, within temperature limits and in which the temperature minimisation problem has been successful (see Section 6.2.2), which does not mean that is within the limits.

- Percentage of cases assessed by the search algorithm (equal to the overall percentage of convergence of both steps, times the percentage of the function evaluations that having converged in both steps are inside all limits and where applies, in which the temperature minimisation problem has been successful).

For Stage 4, the tables show the same information but with two modifications:

- 3. The percentages regarding to 3A and 3B are substituted by one single percentage of convergence as the multipliers method approaches the system of equations in a single step (see Section 6.4.1).
- 7. The function evaluations that having converged are inside the internal recycle limit, within the oxygen limit, within temperature limits and in which the temperature minimisation problem has been successful, only applies for PFRs structures.

All sets of experiments include ten runs except for the three PFRs structure without internal recycle that includes: 14 runs for Stage 1 and 2; ten runs for Stage 3a and 4a; four runs for Stage 3b and 4b. All simulations except where indicated were conducted using an Intel XEON 2.0 GHz processor.

Table 7.12: Computational experience for structures with one PFR for Stage 1 for the acetic acid production process.

Structures with one PFR	Recycle limit (mols/s)									
Average values	**0**	**75**	**125**	**250**	**500**	**750**	**no limit**	**0 - CO_2 dilution**	**0 - H_2O dilution**	**Average**
1. CPU time (h)	2.3	1.8	2.0	2.0	1.8	1.9	3.0	2.7	3.2	**2.3**
2. Function evaluations	27300	23198	30678	26282	29748	30539	30800	34021	30992	**29284.2**
3A. Converged without external recycle (%)	97.72	99.27	99.96	99.89	99.80	99.83	99.78	99.98	99.96	**99.58**
3B. Converged with external recycle (%)	96.97	98.31	99.61	99.77	99.33	98.76	98.43	99.97	99.93	**99.01**
4. Cases converged within internal recycle limits (%)	-	80.22	68.44	78.48	74.90	76.48	-	-	-	**75.70**
5. Cases converged within O_2 limit (%)	77.68	73.71	66.87	70.61	69.04	70.59	79.14	77.52	78.22	**73.71**
6. Cases converged within temperature limit (%)	73.27	71.90	66.01	69.80	68.74	70.25	74.56	74.59	75.47	**71.62**
Solutions assessed by search algorithm (%)	71.05	70.68	65.75	69.64	68.28	69.38	73.39	74.57	75.42	**70.91**

Table 7.13: Computational experience for structures with two PFRs for Stage 1 for the acetic acid production process.

Structures with two PFRs	Recycle limit (mols/s)						
Average values	**0**	**75**	**125**	**250**	**500**	**750**	**Average**
1. CPU time (h)	7.0	7.6	8.0	7.9	6.4	7.9	**7.46**
2. Function evaluations	28291	33943	31776	30543	28675	28106	**30222.3**
3A. Converged without external recycle (%)	95.94	95.99	95.87	95.54	95.26	94.40	**95.50**
3B. Converged with external recycle (%)	95.55	95.01	94.75	94.14	93.13	92.23	**94.14**
4. Cases converged within internal recycle limits (%)	-	84.73	83.15	86.35	87.65	90.86	**86.55**
5. Cases converged within O_2 limit (%)	73.77	70.93	71.52	73.96	78.74	78.33	**74.54**
6. Cases converged within temperature limit (%)	60.43	65.13	66.00	69.02	76.62	74.87	**68.68**
Solutions assessed by search algorithm (%)	57.74	61.88	62.54	64.98	71.36	69.05	**64.65**

Table 7.14: Computational experience for structures with three PFRs for Stage 1 for the acetic acid production process.

Structures with three PFRs	**Recycle limit (mols/s)**					
Average values	**0**	**75**	**125**	**250**	**500**	**Average**
1. CPU time (h)	30.1	25.9	24.7	37.7	35.2	**30.7**
2. Function evaluations	52411	44541	41579	54245	51112	**48777.6**
3A. Converged without external recycle (%)	93.99	92.68	93.02	92.28	90.85	**92.6**
3B. Converged with external recycle (%)	91.88	89.22	88.89	88.40	86.95	**89.1**
4. Cases converged within internal recycle limits (%)		82.10	79.67	77.93	84.82	**81.1**
5. Cases converged within O_2 limit (%)	76.86	76.42	77.54	75.39	77.24	**76.7**
6. Cases converged within temperature limit (%)	68.87	73.56	75.28	73.61	71.18	**72.5**
Solutions assessed by search algorithm (%)	63.28	65.63	66.92	65.07	61.89	**64.57**

For Stage 1, the increase in CPU efforts responds to the increase of the combinatorial size of the problem. Due to the complexities of the highly non-linear kinetic models involved, the bigger the search space is:

- The more frequently the non-linear solver fails to converge (see rows 3B in the tables shown above).
- The less percentage of solutions can be assessed by the search algorithm; the change from two PFRs to three PFRs structures is insignificant (see last rows in the tables presented above).

Table 7.15, 7.16, 7.17 and 7.18 show the computational experience for the three structures involved in the evolution of stages.

Table 7.15: Computational experience for Stage 1 - three final design candidates for the acetic acid production process.

Average values	1PFR	1PFR with recycle without limit	3PFR
1. CPU time (h)	2.3	3.0	30.12
2. Function evaluations	27316	30750	52411
3A. Converged without external recycle (%)	97.72	99.78	94.00
3B. Converged with external recycle (%)	96.97	98.43	91.88
4. Cases converged within internal recycle limits (%)	-	100.00	-
5. Cases converged within O_2 limit (%)	77.68	79.14	76.86
6. Cases converged within temperature limit (%)	73.27	74.56	68.87
Solutions assessed by search algorithm (%)	71.05	73.39	63.28

Table 7.16: Computational experience for Stage 2 for the acetic acid production process.

Average values	1PFR	1PFR with recycle without limit	3PFR
1. CPU time (h)	2.2	2.9	32.2
2. Function evaluations	22517	25553	54710
3A. Converged without external recycle (%)	99.86	99.98	96.27
3B. Converged with external recycle (%)	99.84	99.00	94.88
4. Cases converged within internal recycle limits (%)	-	100.00	-
5. Cases converged within O_2 limit (%)	72.42	79.50	81.39
6. Cases converged within temperature limit (%)	70.79	77.52	72.99
7. Cases converged with successful temperature profile optimisation problem	70.79	77.52	72.99
Solutions assessed by search algorithm	70.68	76.74	69.25

CPU times and percentage of convergence are very similar for Stage 1 and 2 (rows 1 and 3B). The temperature profile optimisation problem in Stage 2 succeeds to converge for all the cases (same values for rows 6 and 7). The percentage of solutions that can be assessed by the search algorithm is similar in both stages (last rows).

Table 7.17: Computational experience for Stage 3 for the acetic acid production process.

Average values	1PFR	1PFR with recycle without limit	3PFR (DN=20)	3PFR (DN=15)
1. CPU time (h)	1.1	2.4	19.5	21.9
2. Function evaluations	11414	21796	34295	34576
3A. Converged without external recycle (%)	99.73	99.28	95.33	96.86
3B. Converged with external recycle (%)	99.33	98.05	93.64	95.30
4. Cases converged within internal recycle limits (%)	-	100.00	-	-
5. Cases converged within O_2 limit (%)	74.53	67.63	80.40	83.34
6. Cases converged within temperature limit (%)	70.33	62.56	59.34	59.87
7. Cases converged with successful temperature profile optimisation problem	70.33	62.56	59.34	59.87
Solutions assessed by search algorithm	69.86	61.34	55.57	57.06

As in Stage 3 the search area is considerably reduced, the CPU times are lower with respect to the previous stages. The percentage of convergence is very similar to the previous two stages. The temperature profile optimisation problem succeeds to converge in all the cases. The percentage of solutions that can be assessed by the search algorithm is reduced with respect to previous stages for the PFR with internal recycle and for the two cases of the three PFRs structure. For these cases, the search tries to push the structure above the oxygen and temperature limits:

- For the PFR with internal recycle, the "Cases converged within O2 limit (%)" (row 5) decreases from 79.50 to 67.63 and the "Cases converged within temperature limit (%)" (row 6) from 77.52 to 62.56.

- For the three PFRs structure the "Cases converged within temperature limit (%)" (row 6) decreases from 72.99 to 59.34 and 59.87.

Table 7.18: Computational experience for Stage 4 - PFRs structures for the acetic acid production process.

Average values	1PFR	1PFR with recycle without limit	3PFR (DN=20)	3PFR (DN=15)
1. CPU time (h)	42.51	35.98	91.14	56.50
2. Function evaluations	1537	1661	1542	2227
3. Converged (%)	45.90	56.68	53.97	35.06
4. Cases converged within internal recycle limits (%)	-	100.00	-	-
5. Cases converged within O_2 limit (%)	66.47	66.72	88.38	90.04
6. Cases converged within temperature limit (%)	66.47	62.16	76.30	71.61
7. Cases converged with successful temperature profile optimisation problem	66.27	62.02	76.19	71.61
Solutions assessed by search algorithm	30.42	35.15	41.12	25.11

In Stage 4, the use of the multipliers approach implies the use of an iterative method to solve the system of differential equations for structures involving PFRs, which is highly-time consuming if compared with previous stages. The temperature profile optimisation problem does not succeed to converge in all the cases although it does for most of them. The percentage of solutions that can be assessed by the search algorithm is considerably reduced mainly because the percentage of convergence is much lower for all the cases with respect to previous stages (rows 3 for Stage 4 and 3B for previous stages). For each case, the number of function evaluations that have been assessed by the algorithm is between 4675 (1537 x 10 runs x 0.3042 –from Table 7.18-) and 6340 (1542 x 10 runs x 0.4112), except for the 3PFR DN=15 that is 2236 (2227 x 4 runs x 0.2511). Such a high number of function evaluations in such a small search space permits thinking that the global optimum has been found.

Table 7.19: Computational experience for Stage 4 - single FLBR structures for the acetic acid production process.

Average values	1 tube	5 tubes	10 tubes	20 tubes
1. CPU time (h)	55.83	60.60	69.96	66.17
2. Function evaluations	23025	12234	14797	8076
3. Converged (%)	86.38	67.48	64.56	56.28
4. Cases converged within internal recycle limits (%)	-	-	-	-
5. Cases converged within O_2 limit (%)	99.80	96.80	93.11	93.35
6. Cases converged within temperature limit (%)	99.80	96.79	93.10	93.35
Solutions assessed by search algorithm	86.21	65.31	62.38	52.54

The percentage of solutions that can be assessed by the search algorithm when using the FLBR model for single units is reduced from 86 % to 53 % as more tubes in parallel are employed. This percentage mainly depends on the convergence ratio and in less extent on the closeness of the solutions to the oxygen limit. Table 7.9 gives an idea on how far from the oxygen limit the search has been performed, showing the percentage of oxygen in the feed for the final structures. Due to the iterative nature of the multipliers approach, CPU times are also very high for cases in which FLBRs are involved.

Table 7.20: Computational experience for Stage 4 - one, two and three FLBRs in series with 20 tubes in parallel for the acetic acid production process.

Average values	1 reactor	2 reactors	3 reactors
1. CPU time (h)	66.17	49.95	48.35
2. Function evaluations	8076	13204	17044
3. Converged (%)	56.28	70.12	69.53
4. Cases converged within internal recycle limits (%)	-	-	-
5. Cases converged within O_2 limit (%)	93.35	90.90	85.84
6. Cases converged within temperature limit (%)	93.35	90.90	85.84
Solutions assessed by search algorithm	52.54	63.74	59.69

If FLBRs in series are employed, the amount of converged solutions increases by 14 % in both cases. The complexity of the system and the number of function

evaluations (row 2) increase with respect to a single FLBR. Computational times cannot be compared because a different computer (Pentium D920 2.80GHz) was employed to run these sets of optimisation runs.

7.4 Conclusions

The partial oxidation of ethane to acetic acid has been studied from the process synthesis point of view.

Results from the multi-level approach (Stage 1), show that back-mixing in the form of CSTRs is not an interesting flow pattern for this case. On one side, the OFV for a single CSTR is negative (-7.5 M$/yr); on the other, for combinations of CSTRs and PFRs, the structures do not improve the performances of those with just PFRs. Regarding structures with only PFRs, two features have proved to have a positive impact on the performance:

- The presence of internal recycle enhances the OFV of a single PFR (8.5 M$/yr) up to 141 % (20.5 M$/yr). The maximum OFV for any given structure is approached asymptotically as the internal recycle limit is increased.
- The presence of oxygen side feeding when more than one PFR is involved, improves the OFV of a single PFR up to 112 % (18.0 M$/yr) for the three PFRs structure and 72 % (14.5 M$/yr) for the two PFRs structure.

The single effect of the internal recycle has more positive influence on the OFV than the single presence of oxygen distribution. If both features are combined, the

performance enhancement is even higher and OFVs approach closely the targeting performance (22.5 M$/yr).

The evolution of stages proves that the assessment of heat and temperature issues in the field of superstructure-based optimisation reactor networks requires an improved approach from those employed in the past. In Stage 2, the practical heating / cooling for PFRs is assessed without compromising the computational effort. The approach proposed in Stage 3, allows including radial heat transfer phenomena in the PFR models. Although they can determine whether designs are realistic or not, radial effects are normally ignored in reactor networks approaches because they need of highly time consuming two-dimensional models. Results in this stage prove that the simple approach used, is an excellent approximation of the system modelled by differential equations. Besides, the method is highly computationally efficient. The approach described in Stage 4 allows solving PFR models based on differential equations (and FLBR models based on cell units) within superstructure-based optimisation approaches. Although the approach has been able to solve very complex systems from the mathematical point of view, the elevated computational efforts required indicate that efforts in the future must be done to speed up the time of computation and increase convergence ratios. Besides, the extra detail added to the process models in the transition from Stage 3 to Stage 4 results in minor impacts on the OFVs.

At the end of Stage 4, the single PFR with internal recycle outperforms the single PFR without internal recycle by 129.1 %. The three PFRs without internal recycle and

with oxygen feed distribution outperform the single PFR without internal recycle by 60.3 % for Stage 4a and by 73.8 % for Stage 4b. Besides, the OFVs have decreased with respect to Stage 1 as follows:

- For the single PFR without internal recycle: 17.8 %.
- For the single PFR with internal recycle: 21.6 %.
- For the three PFRs without internal recycle and with oxygen feed distribution: 37.4 % for Stage 4a and 32.1 % for Stage 4b.

The active constraints in all the solutions involving PFRs are:

- The maximum mass of catalyst allowed per superstructure.
- The maximum temperature allowed inside the reactor.
- The purity and recovery of acetic acid.
- The maximum concentration of oxygen allowed at the inlet of the reactor.
- The maximum internal recycle amount allowed.

The designs including single FLBRs have proved to have much less potential than designs including only MTRs. All the FLBR designs considered in this work are limited by heat transfer issues. The fact that the temperature of the utility is at its lower limit for all cases confirms it. As a consequence, the reactor heat exchange area is the design factor that most impacts the performance of FLBRs. The area can be increased by increasing the number of reactor tubes and the number of reactors in

series. Higher heat exchange surfaces allow reaching higher ethane conversions by increasing operating temperatures and oxygen feed flows.

All designs including FLBRs have as active constraints:

- The maximum mass of catalyst allowed per superstructure.
- The minimum temperature of the cooling utility.
- The purity and recovery of acetic acid.
- Few designs also have as constraint the maximum concentration of oxygen at the inlet of the reactor.

CHAPTER 8.

Conclusions

8.1 Introduction

This thesis has proposed a process synthesis strategy based on a transition of design stages. Different stages represent different layers of abstraction in the complexity of the models that characterise reaction-separation and reactive / separation systems. The process design exercise starts at a highly conceptual level where the screening and selection of synthesis options are performed. The approach is followed by a multi-level design method, where the synthesis option selected is explored, trade-offs are identified and optimal conceptual process designs suggested. Finally, the proposed optimal designs are iteratively evolved into more accurate designs by using more detailed models.

The major contributions of this work are:

1. A conceptual screening tool for the reactive liquid-liquid extraction as a process design option, which is based on mapping the information regarding the solvent phase onto the superstructure of a single-phase reactor network.

2. A decision support framework that addresses the incapacities of existing process synthesis approaches to effectively manage the numerical and combinatorial complexities that arise from combining experimental kinetic models and reactor-separator-recycle systems, for heterogeneously catalysed gas-phase reaction processes. The aim of the framework is to establish the reliable and robust systematic process design identification followed by the evolution of designs. The ultimate aim is to make possible the integration of experimental modelling and process design activities.

8.2 Discussion Of The Proposed Developments

8.2.1 Screening Of Reactive Liquid-Liquid Extraction Processes

The rapid screening of a synthesis option to compare its potential with that of other options is the first stage of the synthesis exercise. The identification of trade-offs for potential synthesis options can help speeding up the synthesis exercise, by aiding the initialisation of later time consuming optimisations with rigorous models. Such reduction of time and efforts can result in more profitable projects. To illustrate this fact, this thesis presents an approach to screen fast and reliably reactive liquid-liquid extraction as a process design option. The approach is based on mapping the information regarding the mass separating agent (solvent) phase onto the superstructure model of a single-phase reactor network, with the help of a novel transfer rate expression for liquid-liquid extraction processes. The method has been applied to two biochemical examples of very different complexity. The approach has

proved to be highly computationally efficient as compared with classic reactive separation superstructure-based optimisation approaches that involve liquid-liquid equilibrium and mass transfer models that are usually very complex and detailed. The precision of the approach appears to be satisfactory for high-level decision-making at initial stages of process synthesis.

8.2.2 Decision Support Framework

The decision support framework developed in this work aims to be a helpful tool in the near future to allow the computationally effective high-level coordination of process design and kinetic investigation activities. Initially, the framework relies on a multi-level approach that identifies the maximum performance of a system regardless its complexity, allows the engineer to understand what design trends improve process performances, and permits the engineer matching the increase of complexity of the designs with the enhancement of the objective function values. The approach eases the understanding of the bottlenecks of the system and suggests different optimal conceptual designs for the engineer to judge. The treatment of heat and temperature management issues in the multi-level approach appears to be very ideal. Accordingly, efforts have been focussed on the development of alternative and more accurate ways to manage heat transfer complexities without compromising computational times. These developments are the basis of the multi-stage approach, in which during successive stages the level of detail of the reactor models is increased. The increase in the level of detail aims to capture progressively non-ideal behaviours to evolve the initial process designs into designs that can be reached in practice. In Stage 2, temperature profiles for the reactors that can be attained with common co-current cooling / heating strategies found in industry are suggested. Therefore, practical

solutions to the heat exchange between the reactors and their utility media are proposed. Such developments overcome previous drawbacks in non-isothermal reactor network applications where unreachable and / or unrealistic profiles were proposed. In Stage 3, the radial heat propagation effects for catalytic fixed bed reactors are included in a highly effective computational approach. Stage 4 deals with highly accurate and time-consuming reactor models. Cell models and differential equation based models are employed to effectively optimise complex layouts. Although, four stages illustrate the methodology proposed, more successive stages could enrich further the process designs. However, it has been observed that after Stage 3, there is not much justification in increasing the level of modelling detail, as further stages result in very similar performances and require much more computational efforts.

The first three stages have proved to be highly computationally efficient and robust, and therefore could be employed in the integration of kinetic development and process design activities. The computational efforts of Stage 4 are prohibitive. Its use in the integration of design activities appears not to be appropriate if the screening of design candidates is the purpose. However, the new approach developed in this stage, allows successfully performing superstructure optimisation with highly complex process design schemes and reactor models. It could be used to test kinetic models at advanced phases of their development in order to increase confidence in the results.

All stages rely on superstructure process representations that have been developed for

heterogeneously catalysed gas-phase reaction systems and include practical constraints found in practical applications. The reactor representations incorporate combinations of ideal and non-ideal reactor models. The constraints included in the formulation relate on one hand, to the limitation of the amount of components that can create fouling, dangerous operating scenarios, induce to unwanted side reactions, etc. On the other hand, they relate to temperature and heat management issues in the reactive section. Separation options are represented in aggregated form to decouple the synthesis problem and keep it at solvable complexity. Energy integration between process streams allows the effective screening of many heat exchange network design options. The presence in the process representation of reaction options, separation options, energy integration and network recycles, allows approaching the synthesis problem from a broad perspective. As a consequence, the synergies between sub-systems of the process are captured, and the optimal solutions are identified in the context of the overall design goal.

At any stage of the multi-stage design procedure, information on the optimal operating conditions is generated and could be communicated to the kinetic development team. Such information could be used to guide new experiments in order to validate the models in the optimal regions in which the catalyst is to be used. The integration of experimental modelling and process synthesis activities could become available in the near future.

CHAPTER 9.

Future Work

9.1 Introduction

This thesis has presented the development of methods that allow the systematic exploration of the chemical and process development cycle and methods for the quick and reliable screening of process design options. Both developments identify innovative process design schemes with significant improvement in the performances if compared with conventional process designs. However, like in any work at a research stage a number of limitations exist. The limitations identified and the areas of future research suggested are detailed in the following sections.

9.2 Reactive-Separation Approaches

As illustrated in the approach to reactive liquid-liquid extraction, many other reactive-separation options could be tackled mapping the separating agent phase onto the superstructure model of a single phase reaction network. Such developments can achieve a significant reduction of computational efforts and deliver more profitable projects for cases in which time consuming simulations involve:

i) Complex detailed mass transfer and phase-equilibrium models.

ii) Elevated combinatorial complexity of the options available.

Following the presented rationale, similar approaches should be developed for synthesis options such as reactive-distillation, reactive-membrane separation, reactive-absorption, etc. For the specific approach presented in this work, many other components and groups of components could be used for the regression of the Param expression, in order to capture the chemical-physical phenomena involved in reactive liquid-liquid extraction for a wider range of mixtures.

9.3 Separation Representations

The separation representations presented in this work are an area of improvement. Separation representations should be developed further and tested. Specifically the energy integration would be an issue as separation operations usually require most of the energy employed in a process. The energy used cannot be integrated with the rest of the process easily if the decoupling of these systems takes place and they are approached in separate efforts. Every sequence forming the separation representation should come with information on the energy used and at least an estimate of the potential for integration of these units with the rest of the process. Besides, the cost function of the separation representation could be approached in a similar manner as the synthesis strategy presented in this work. It could be conceptual at the beginning of the synthesis exercise and include more information and detail towards the end of it.

9.4 Ideal Fluidised Reactor Model

The development of an ideal and conceptual reactor model that truly captures the complexities of interfacial transfer, phase equilibrium and multi-phase flow present in fluidised bed reactors is a major problem identified in this research. On one side, the simplest two-phase fluidised bed models are far too complex to effectively screen different options at early stages of process design. Their application to superstructure-based optimisation approaches involves prohibitively high computational efforts. On the other hand, ideal reactor models such as the CSTR or the PFR are inadequate for reliably predicting fluidised bed reactor behaviours. Consequently, a conceptual fluidised bed reactor model able to capture reliably trade-offs of the chemical-physical phenomena occurring inside the reactor would be of enormous benefit to the process design community. On top of that, the fluidised bed reactor can be considered as the simplest multi-phase reactor and the idea of considering other more complex multi-phase reactors for the reliable and quick screening of process design options appears nowadays to be impossible. Kelkar & Ng (1998, 2000) have developed a systematic approach for screening multi-phase reactors at early stages of process design. However, in their own words the approach is still not able to capture the complexities of hydrodynamics in fluidised bed reactors.

9.5 Cost Models

The degree in which the optimisation results reproduce reality relies extremely on the ability of the cost models, used for developing the objective function, to reproduce it. Cost functions are more inclusive than typical reactor design objectives such as

conversions, selectivities or yields, since they take into account cost effects of reactors and cover a wider range of equipments. There are methods that correlate the cost of equipments to past acquisitions (*e.g.* Guthrie, 1974) but their use is not straightforward and they are unsuitable for screening purposes. Similarly, there are computer programs to estimate costs that are not adequate for screening intentions. The appropriate cost data for screening design candidates is in the form of cost functions that are not easily available in the literature for all equipments. Besides, the confidence on their validity is usually low since the spread of data for same types of equipment is wide. As a result, the process economics can be misrepresented by using inaccurate cost functions and the quality of the optimisation solutions compromised. The availability to the process design community of reliable cost functions for a wider range of equipments is of crucial importance if novel designs that yield better performances are to be considered industrially.

9.6 Simulation Solvers

Alternative numerical solvers for flowsheet simulation could be tested for the later stages of the synthesis process where differential and algebraic equations are involved. The multipliers approach presented provides a flexible approach to solve complex systems where differential equations and cell reactor models with multiple connections between reactors are present. However, it fails in approximately 15 to 45 % of the cases assessed and therefore, there is some potential for improvement. Numerical solvers able to treat differential equations at the same time as algebraic equations should be employed as they could result in more robust results in terms of

numerical solutions. Their implementation can be very challenging for the mathematical complexities involved.

9.7 Computational Efforts

Although the computational efforts required to solve the complex mass transfer and phase-equilibrium models have been partially tackled in this work, there is still immense room for improvement. It is obvious that, future developments in computer performance will speed up the complex optimisation processes. However, current developing tools allow bypassing computational burdens with innovative ideas. Distributed computing applications are with no doubt one of the key routes for that purpose. Recently, Yang *et al.* (2005) presented a novel optimisation scheme for large-scale size distributed computing environments that will facilitate data analysis and knowledge extraction in the course of optimisation. Their developments include concepts from Simulated Annealing. The novel optimisation scheme consists of several solution groups associated with a system temperature, which is employed to assess the solution quality of each group. The solutions in the groups are created by performing alterations in the form of temperature Markov processes on existing solutions that are already placed in them. Because the Markov processes are independent from each other, they can be executed in large-scale distributed computing environments, continuously generating solutions that are stored in a database. As the optimisation goes on, the solutions are reassigned to the groups. The resulting group accumulates the set of optimal solutions. Since the solutions are stored in a database, knowledge regarding key individual features that enhance

performances is accessible to be extracted. With that purpose, Labrador-Darder *et al.* (2007) have developed a novel approach for the extraction, interpretation and exploitation of design knowledge in process synthesis. They combine knowledge models in the form of ontologies and clustering tools to analyse the solutions of superstructure optimisation. The developments are based on the dynamic evolution of the knowledge models. The superstructure is optimised and updated employing the knowledge models at different stages. The transition between stages represents the transition between layers of abstraction. The initial stages contain the most abstract knowledge models and the superstructure representation embeds all possible connections between units. As the optimisation evolves, the superstructures are customised and result in simpler layouts, whereas the knowledge models are constantly enriched. Therefore, detailed models can be employed in later stages of the optimisation. The analysis of solutions is addressed with the development of a multi-dimensional vector that includes information on the different features of the superstructure representation and that can be processed with a customised clustering method.

CHAPTER 10.

References

Papers And Books

Abdalla, B. K., Elnashaie, S., S., E., H., Alkhowaiter, S., Elshishini, E., 1994, "Intrinsic kinetics and industrial reactors modeling for the dehydrogenation of ethylbenzene to styrene on promoted iron oxide catalysts", *Applied Catalysis A: General*, 113, 89-102.

Achenie, L. K. E., Biegler, L. T., 1986, "Algorithmic Synthesis of Chemical Reactor Networks using Mathematical programming", *Industrial Engineering Chemical Fundamentals*, 25, 621-627.

Achenie, L. K. E., Biegler, L. T., 1988, "Developing targets for the performance index of a chemical reactor network", *Industrial & Engineering Chemistry Research*, 27, 1811.

Achenie, L. K. E., Biegler, L. T., 1990, "A superstructure based approach to chemical reactor network synthesis", *Computers & Chemical Engineering*, 14(1), 23-40.

Adjiman, C. S., Dallwig, S., Floudas C. A., Neumaier A., 1998a, "A global optimization method, αBB, for general twice-differentiable constrained NLPs - I. Theoretical advances", *Computers & Chemical Engineering*, 22(9), 1137-1158.

Adjiman, C. S., Androulakis, I. P., Floudas, C. A., 1998b, "A global optimization method, αBB, for general twice-differentiable constrained NLPs - II. Implementation and computational results", *Computers & Chemical Engineering*, 22(9) 1159-1179.

Adler, R., 2000a, "Stand der Simulation von heterogen-gaskatalystischen Reaktionsablaufen in Festbettrohrreaktoren – Teil 1", *Chemie Ingenieur Technik*, 72, 555-564.

Adler, R., 2000b, "Stand der Simulation von heterogen-gaskatalystischen Reaktionsablaufen in Festbettrohrreaktoren – Teil 2", *Chemie Ingenieur Technik*, 72, 688-699.

Ahmad, S., Linnhoff, B., Smith, R., 1990, "Cost optimum heat exchanger networks – 2. Targets and design for detailed capital cost models", *Computers & Chemical Engineering*, 14(7), 751-767.

Ashley, V. M, 2004, "On the development of knowledge driven optimisation methods – Application to complex reactor network synthesis", Ph.D Thesis, School of Engineering, PRISE, University of Surrey.

Ashley, V. M., Linke, P., 2004, "A novel approach to reactor network synthesis using knowledge discovery and optimisation techniques", *Chemical Engineering Research & Design*, 82(8), 952-960.

Ashley, V. M., Linke, P., 2005, "On the development and implementation of knowledge-driven optimisation schemes: an application in non-isothermal reactor network synthesis" *Computer-Aided Chemical Engineering,* Elsevier, Volume 20, Part 1, 175-180.

Balakrishna, S., L. T. Biegler, 1992a, "Constructive targeting approaches for the syntheis of chemical reactor networks", *Industrial & Engineering Chemistry Research*, 31(1), 300-312.

Balakrishna, S., Biegler, L. T., 1992b, "Targeting strategies for the synthesis and energy integration of nonisothermal reactor networks", *Industrial & Engineering Chemistry Research*, 31(9), 2152-2164.

Balakrishna, S., Biegler, L. T., 1993, "A unified approach for the simultaneous synthesis of reaction, energy, and separation systems". *Industrial & Engineering Chemistry Research*, 32(7), 1372-1382.

Barbosa, D., Doherty, M. F., 1988, "The Simple Distillation of Homogeneous Reactive Mixtures", *Chemical Engineering Science*, 43(3), 541-550.

Bauer, R., Schlünder, E. U., 1978a, "Effective radial thermal conductivity of packings in gas flow. Part I. Convective transport coefficient", *International Chemical Engineering*, 18, 181-189.

Bauer, R., Schlünder, E. U., 1978b, "Effective radial thermal conductivity of packings in gas flow. Part II. Thermal conductivity of the packing fraction without gas flow'", *International Chemical Engineering*, 18, 189-204.

Berry, D. A., Ng, K. M., 1997, "Synthesis of reactive crystallization processes", *AIChE* Journal, 43(7), 1737-1750.

Biegler, L. T., Grossmann, I. E., Westerberg, A. W., 1997, "Systematic methods of chemical process design", Prentice-Hall, Englewood Cliffs, NJ.

Bollen, A. M., 1999, "Collected tales on mass transfer in liquids", Ph.D Thesis, Department of Mathematics and Natural Sciences, University of Groningen.

Cardoso, M. F., Salcedo, R. L., Feyo de Azevedo, S., Barbosa, D., 2000, "Optimization of reactive distillation processes with simulated annealing", *Chemical Engineering Science*, 55(21), 5059-5078.

Cavin, L., Fischer, U., Glover, F., Hungerbuhler, K., 2004, "Multi-objective process design in multi-purpose batch plants using a Tabu Search optimisation algorithm", *Computers & Chemical Engineering*, 28(4), 459-478.

Chen, H., S., Stadtherr, M., A., 1981, "A modification of Powell's Dogleg method for solving systems of non-linear equations", *Computers & Chemical Engineering*, 5(3), 143-150.

Ciric, A. R., Gu, D., 1994, "Synthesis of non-equilibrium reactive distillation processes by MINLP optimization", *AIChE Journal*, 40(9), 1479-1487.

Dixon, A. G., 1996, "An improved equation for the overall heat transfer coefficient in packed beds", *Chemical Engineering and Processing*, 35(5), 323-331.

Dixon, A. G., Cresswell, D. L., 1979, "Theoretical prediction of effective heat transfer parameters in packed beds", *AIChE Journal*, 25(4), 663-676.

Dubois, J. L., 2006, "Catalytic nano-oxides research and development in Europe: present and future", Arkema, Seville, Spain.

Echt, W., 2002, "Hybrid systems: combining technologies leads to more efficient gas conditioning", Laurance Reid Gas Conditioning Conference 2002, University of Oklahoma.

Eduljee, H. E., 1975, "Equations replace Gilliland's plot", *Hydrocarbon Process*, 54(9), 120-122.

Elnashaie, S. S. E. H., Abdallah, B. K., Elshishini, S. S., Alkhowaiter, S., Noureldeen, M. B., Alsoudani, T., 2001, "On the link between intrinsic catalytic reactions kinetics and the development of catalytic process. Catalytic dehydrogenation of ethylbenzene to styrene", *Catalysis Today*, 64(3-4), 151-162.

Elnashaie, S. S. E. H., Elshishini, S. S., 1994, "Modelling, simulation and optimization of industrial fixed bed catalytic reactors", London: Gordon and Breach Science Publisher.

Esposito, W. R., Floudas, C. A., 2002, "Deterministic global optimization in isothermal reactor network synthesis", *Journal of Global Optimization*, 22(1-4), 59-95.

Ergun, S., 1952, "Fluid flow through packed columns", *Chemical Engineering Progress*, 48(2), 89-94.

Feinberg, M., 2002, "Toward a theory of process synthesis", *Industrial & Engineering Chemistry Research*, 41(16), 3751-3761.

Feinberg, M., Hildebrandt, D., 1997, "Optimal reactor design from a geometric viewpoint - I. Universal properties of the attainable region", *Chemical Engineering Science*, 52(10), 1637-1665.

Fenske, M. R., 1932, "Fractionation of Straight-Run Pennsylvania Gasoline" *Industrial & Engineering Chemistry*, 24, 482-485.

Fournier, R. L., 1986, "Mathematical model of extractive fermentation: application to the production of ethanol", *Biotechnology & Bioengineering*, 28, 1206-1212.

Fraga, E. S., 1996, "The automated synthesis of complex reaction – separation processes using dynamic programming", *Chemical Engineering Research & Design*, 74(A), 249-260.

Glasser, D., Hildebrandt, D., Crowe, C., 1987, "A geometric approach to steady flow reactors: The attainable region and optimization in concentration space", *Industrial & Engineering Chemistry Research*, 26(9), 1803-1810.

Glasser, D., Hildebrandt, D., 1997, "Reactor and process synthesis", *Computers & Chemical Engineering*, 21(Supplement 1), S775-S783.

Glover, F., 1986, "Future paths for integer programming and links to artificial intelligence", *Computers and Operations Research*, 13(5), 533-549.

Guthrie, K. M., 1974, "Process plant estimating, evaluation and control", Solana Beach, California, Craftsman Book Co.

Hauan, S., Westerberg, A. W., Lien, K. M., 2000a, "Phenomena-based analysis of fixed points in reactive separation systems", *Chemical Engineering Science*, 55(6), 1053-1075.

Hauan, S., Ciric, A. R., Westerberg, A. W., Lien, K. M., 2000b, "Difference points in extractive and reactive cascades. I – Basic properties and analysis", *Chemical Engineering Science*, 55(16), 3145-3159.

Hildebrandt, D., Glasser, D., 1990, "The attainable region and optimal reactor structures", *Chemical Engineering Science*, 45(8), 2161-2168.

Hildebrandt, D., Glasser, D., Crowe, C. M., 1990, "Geometry of the attainable region generated by reaction and mixing: with and without constraints", *Industrial & Engineering Chemistry Research*, 29(1), 49-58.

Hirschfelder, J. O., Curtiss, C. F., Bird, R. B., 1954 "Molecular theory of gases" John Wiley & Sons, New York.

Hohman, E. C., 1971, "Optimum Networks of Heat Exchange", Ph.D Thesis, University of Southern California.

Hopley, F., Glasser, D., Hildebrandt, D., 1996, "Optimal reactor structures for exothermic reversible reactions with complex kinetics", *Chemical Engineering Science*, 51(10), 2399-2407.

Horn, F., 1964, "Attainable and non-attainable regions in chemical reaction technique", *Proceedings of the Third European Symposium on Chemical Reaction Engineering*, 293-303.

Ismail, S. R., Pistikopoulos, E. N., Papalexandri, K. P., 1999, "Synthesis of combined reactive and reactor / separation systems utilizing a mass / heat exchange transfer module", *Chemical Engineering Science*, 54, 2721-2729.

Ismail, S. R., Proios, P., Pistikopoulos, E. N., 2001, "Modular synthesis framework for combined separation/reaction systems", *AIChE Journal*, 47(3), 629-649.

Jackson, R., 1968, "Optimisation of chemical reactors with respect to flow configuration", *Journal of Optimisation Theory and Applications*, 2, 240.

Kato, K., Wen, C. Y., 1969, "Bubble assemblage model for fluidized-bed catalytic reactors", *Chemical Engineering Science*, 24(8), 1351-1369.

Kelkar, V. V., Ng, K. M., 1998, "Screening procedure for synthesizing isothermal multi-phase reactors", *AIChE Journal*, 44(7), 1563-1578.

Kelkar, V. V., Ng, K. M., 2000, "Screening multi-phase reactors for non-isothermal multiple reactions", *AIChE Journal*, 46(2), 389-406.

Kokossis, A. C., Floudas, C. A., 1990, "Optimisation of complex reactor networks – I. Isothermal operation", *Chemical Engineering Science*, 45(3), 595-614.

Kokossis, A. C., Floudas, C. A., 1991, "Synthesis of isothermal reactor-separator-recycle systems", *Chemical Engineering Science*, 46(5-6), 1361-1383.

Kokossis, A. C., Floudas, C. A., 1994, "Optimisation of complex reactor networks – II. Non-isothermal operation", *Chemical Engineering Science*, 49(7), 1037-1051.

Koning, B., 2002, "Heat and mass transport in tubular packed bed reactors at reacting and non-reacting conditions". Ph.D. Thesis, University of Twente.

Labrador-Darder, C., Kokossis, A. C., Linke, P., 2007, "On the systematic extraction of knowledge in process synthesis and chemical process design", Accepted in the *Proceedings of ESCAPE17*, Bucharest, Rumania.

Lakshmanan, L., Biegler, L. T., 1996a, "Synthesis of optimal chemical reactor networks", *Industrial & Engineering Chemistry Research*, 35(5), 1344-1353.

Lakshmanan, L., Biegler, L. T., 1996b, "Synthesis of optimal chemical reactor networks with simultaneous mass integration", *Industrial & Engineering Chemistry Research*, 35(12), 4523-4536.

Lakshmanan, L., Biegler, L. T., 1997, "A case study for reactor network synthesis: the vinyl chloride process", *Computers & Chemical Engineering*, 21(Supplement 1), S785-S790.

Lei, F., Rotboll, M., Jorgensen, S. B., 2001, "A biochemically structured model for Saccharomyces cerevisiae", *Jounal of Biotechnology,* 88(3), 205-221.

Lei, F., Jorgensen, S. B., 2001, "Estimation of kinetic parameters in a structured yeast model using regularisation", *Jounal of Biotechnology,* 88(3), 223-237.

Levenspiel, O., 1998, "Chemical Reaction Engineering", 3rd edition, Wiley-VCH, ISBN: 047125424X, Chapter 20, Page 451.

Lin, B., Miller, D. C., 2004a, "Tabu search algorithm for chemical process optimization", *Computers & Chemical Engineering*, 28(11), 2287-2306.

Lin B., Miller, D. C., 2004b, "Solving heat exchanger network synthesis problems with Tabu Search" *Computers & Chemical Engineering*, 28(8), 1451-1464.

Linke, D., Wolf, D., Zeiss, S., Dingerdissen, U., Baerns, M., 2002a, "Catalytic partial oxidation of ethane to acetic acid over $Mo_1V_{0.25}Nb_{0.12}Pd_{0.0005}O_x$. II. Kinetic Modelling", *Journal of Catalysis*, 205(1), 32-43.

Linke, D., Wolf, D., Zeiss, S., Dingerdissen, U., Mleczko, L., Baerns, M., 2002b, "Catalytic partial oxidation of ethane to acetic acid over $Mo_1V_{0.25}Nb_{0.12}Pd_{0.0005}O_x$: reactor operation", *Chemical Engineering Science*, 57(1), 39-51.

Linke, P., 2001, "Reaction and separation process integration", Ph.D Thesis, Department of Process Integration, UMIST, University of Manchester.

Linke, P., Kokossis, A. C., 2003a, "On the robust application of stochastic optimisation technology for the synthesis of reaction/separation systems", *Computers & Chemical Engineering* 27(5), 733-758.

Linke, P., Kokossis, A. C., 2003b, "Attainable designs for reaction and separation processes from a superstructure-based approach", *AIChE Journal* 49(6), 1451-1470.

Linke, P., Kokossis, A. C., 2007, "A multi-level methodology for conceptual reaction-separation process design", *Chemical Product and Process Modelling* 2(3), Article 2.

Linke, P., Kokossis, A. C., van den Berg, H., 2003, *Chapter 13: Process Synthesis/Integration*. In Stankievicz, A., and J. Mouljen (eds.): Re-engineering the process plant: Process intensification, pp. 409-446. Amsterdam: Marcel Dekker. ISBN 0-8247-4302-4.

Linnhoff, B., Flower, J. R., 1978, "Synthesis of heat exchanger networks: I. Systematic generation of energy optimal networks", *AIChE Journal*, 24(4), 633-642.

Linnhoff, B., Mason, D. R., Wardle, I., 1979, "Understanding heat exchanger networks", *Computes & Chemical Engineering*, 3(1-4), 295-302.

Logtenberg, S. A., Dixon, A. G., 1998, "Computational fluid dynamics studies of fixed bed heat transfer", *Chemical Engineering and Processing*, 37(1), 7-21.

Luyben, W. L., 2001, "Design of cooled tubular reactor systems", *Industrial Engineering and Chemistry Research*, 40(24), 5775-5783.

Marcoulaki, E. C., Kokossis, A. C., 1996, "Stochastic optimisation of complex reaction systems", *Computers & Chemical Engineering*, 20(Supplement 1), S231-S236.

Marcoulaki, E. C., Kokossis, A. C., 1999, "Scoping and screening complex reaction networks using stochastic optimisation", *AIChE Journal*, 45(9), 1977-1991.

Martin, H., 1978, "Low Peclet number particle to fluid heat and mass transfer in packed beds", *Chemical Engineering Science*, 33(7), 913-919.

Mehta, V. L., Kokossis, A. C., 1997, "Development of novel multi-phase reactors using a systematic design framework", *Computers & Chemical Engineering*, 21(Supplement), S325-S330.

Mehta, V. L., Kokossis, A. C., 1998, "New generation tools for multi-phase reaction systems: A validated, systematic methodology for novelty and design automation", *Computers & Chemical Engineering*, 22(Supplement), S119-S126.

Mehta, V. L., Kokossis, A. C., 2000, "Nonisothermal synthesis of homogeneous and multi-phase reactor networks", *AIChE Journal*, 46(11), 2256-2273.

Meima, G. R., Menon, P. G., 2001, "Catalyst deactivation phenomena in styrene production", *Applied Catalysis A: General*, 212(1-2), 239–245.

Montolio-Rodriguez, D., Linke, D., Linke, P., 2007, "Systematic identification of optimal process designs for the production of acetic acid via ethane oxidation", *Chemical Engineering Science*, 62(18-20), 5602-5608.

Murray, J. D., 1965, "On the mathematics of fluidization. I. Fundamental equations and wave propagation", *Journal of Fluid Mechanics*, 21, 465-493.

Nagel, G. Adler, R., 1971, "Anwendung der Kollokationsmethode auf die Berechnung Polytroper Rohrreaktoren", *Chemische Technik*, 23(6), 335-341.

Nicol, W., Hildebrandt, D., Glasser, D., 1997, "Process synthesis for reaction systems with cooling via finding the Attainable Region", *Computers & Chemical Engineering*, 21(Supplement 1), S35-S40.

Nisoli, A., Malone, M. F., Doherty, M. F., 1997, "Attainable Regions for Reaction with Separation", *AIChE Journal*, 43(2), 374-387.

Okasinski, M., Doherty, M. F., 1998, "Design methods for kinetically controlled, staged reactive distillation columns", *Industrial & Engineering Chemistry Research*, 37(7), 2821-2834.

Olbert, G., Corr, F., 2007, "Reactor having a heat exchange medium circulation", United States Patent 7273593.

Papalexandri K. P., Pistikopoulos, E. N., 1996 , "Generalized modular representation framework for process synthesis", *AIChE Journal*, 42(4), 1010-1032.

Petterson, F., 2005, "Synthesis of large-scale heat exchanger networks using a sequential match reduction approach", *Computers & Chemical Engineering*, 29(5), 993-1007.

Pretel, E. J., Lopez, P. A., Bottini, S. B., Brignole, E. A., 1994, "Computer-aided molecular design of solvents for separation processes", *AIChE Journal*, 40(8), 1349-1360.

Rigopoulos, S., Linke, P., 2002, Systematic development of optimal activated sludge process designs. *Computers & Chemical Engineering* 26(4-5), 585-597.

Rooney, W., Biegler, L. T., 2000, "Multi-period reactor network synthesis", *Computers & Chemical Engineering* 24(9-10), 2005-2068.

Rooney, W., Hausberger, B. P., Biegler, L. T., Glasser, D., 2000 "Convex attainable region projections for reactor network synthesis", *Computers & Chemical Engineering*, 24(2-7), 225-229.

Samant, K. D., Ng, K. M., 1998, "Synthesis of extractive reaction processes", *AIChE Journal*, 44(6), 1363-1381.

Schweiger, C., Floudas, C. A ., 1999, "Optimization framework of the synthesis of chemical reactor networks", *Industrial & Engineering Chemistry Research*, 38(3), 744-766.

Seider, W. D., Seader, J.D., Lewin, D. R., 1999, "Process design principles: synthesis, analysis and evaluation", John Wiley & Sons, New York.

Sheel, J. G. P., Crowe, C. M., 1969, "Simulation and optimization of an existing ethyl benzene dehydrogenation reactor", *Canadian Journal of Chemical Engineering*, 47, 183-187.

Silvaco International, 1994, "ATHENA 2D Process Simulation Framework User's Manual", Santa Clara, California.

Sit, S. P., Grace, J. R., 1981 "Effect of bubble interaction on interphase masss transfer in gas fluidised beds", *Chemical Engineering Science*, 36, 327.

Smejkal, Q., Linke, D., Baerns, M., 2005, "Energetic and economic evaluation of the production of acetic acid via ethane oxidation", *Chemical Engineering and Processing*, 44(4), 421-428.

Smirnov, E. I., Kuzmin, V. A., Zolotarskii, I. A., 2004, "Radial thermal conductivity in cylindrical beds packed by shaped particles", *Chemical Engineering Research and Design*, 82(A2), 293 296.

Smith, R., 2005, "Chemical process design and integration", Wiley, ISBN: 0-471-48681-7.

Smith, E. M. B., Pantelides, C. C., 1995, "Design of reaction/separation networks using detailed models", *Computers & Chemical Engineering*, 19(Supplement 1), S83-S88.

Stein, E., Kienle, A., Esparta, A. R. J., Mohl, K. D., Gilles, E. D., 1999, "Optimization of a reactor network for ethylene glycol synthesis – an algorithmic approach", *Computers & Chemical Engineering*, 23, S903-S906.

Tantimuratha, L., Kokossis, A. C., Muller, F. U., 2000, "The heat exchanger network design as a paradigm of technology integration", *Applied Thermal Engineering*, 20(15-16), 1589-1605.

Tarafder, A., Rangaiah, G. P., Ray, A. K., 2005, "Multi-objective optimization of an industrial styrene monomer manufacturing process", *Chemical Engineering Science*, 60(2), 347-363

Townsend, D. W., Linhoff, B., 1984, "Surface area targets for heat exchanger networks", IChemE 11th Annual Research Meeting on Heat Transfer, Bath.

Treybal, R. E., 1963, "Liquid Extraction", McGraw-Hill, New York.

Tsoka, C., Johns, W. R., Linke, P., Kokossis, A. C., 2004, "Towards sustainability and green chemical engineering: tools and technology requirements", *Green Chemistry*, 8, 401-406.

Turton, R., 2005. Personal communication.

Underwood, A. J. V., 1932, "The theory and practice of testing stills", *Transactions of Institution of Chemical Engineers*, 10, 102.

Underwood, A. J. V., 1948, "Fractional distillation of multi-component mixtures", *Chemical Engineering Progress*, 44(8), 603-614.

Veawab, A., Aroonwilas, A., Chakma, A., Tontiwachwuthikul, P., 2001, "Solvent formulation for CO_2 separation from flue gas streams", First National Conference on Carbon Sequestration, The National Energy Technology Laboratory, US.

Wankat, P. C., 1988, "Equilibrium stage separation", Elsevier, New York.

Wen, C. Y., Yu, Y. H., 1966, "A generalized method for predicting the minimum fluidization velocity", *AIChE Journal*, 12(3), 610-612.

Werther, J., 1992, "Scale-up modelling for fluidized bed reactors", *Chemical Engineering Science*, 47(9-11), 2457-2462.

Westerberg, A. W., 2004, "A retrospective on design and process synthesis", *Computers & Chemical Engineering*, 28(4), 447-458.

Winterberg, M., Tsotsas, E., 2000a, "Correlations for effective heat transport coefficients in beds packed with cylindrical particles", *Chemical Engineering Science*, 55(23), 5937-5943.

Winterberg, M., Tsotsas, E., 2000b, "Impact of tube-to-particle-diameter ratio on pressure drop in packed beds", *AIChE Journal*, 46(5), 1084-1088.

Winterberg, M., Tsotsas, E., Krischke, A., Vortmeyer, D., 2000, "A simple and coherent set of coefficients for modelling of heat and mass transport with and without chemical reaction in tubes filled with spheres", *Chemical Engineering Science*, 55(5), 967-979.

Wolf, J., 2004, "Pressure drop in an interconnected pressurised fluidised bed reactor for chemical looping combustion", Research Report, ISSN: 1104–3466., Royal Institute of Technology (KTH), Stockholm, Sweden.

Yang, S., Kokossis, A. C., Linke, P., 2006, "Towards a novel optimisation algorithm with simultaneous knowledge acquisition for distributed computing environments", *Computer Aided Chemical Engineering*, Elsevier, Volume 21, Part 1, 327-332.

Yee, A. K. Y., Ray, A. K., Rangaiah, G. P., 2003, "Multi-objective optimizations of an industrial styrene reactor", *Computers & Chemical Engineering*, 27(1), 111-130.

Zheng, Z., Lu, J., Li, D., Ma, G., 1998, "The kinetics study in liquid-liquid systems with constant interfacial area cell with laminar flow", *Chemical Engineering Science*, 53(13), 2327-2333.

Web Pages

http://www.eng-tips.com. ENG TIPS FORUMS. Accessed 14th December 2004.

APPENDIX 1

Multi-Phase Process Representations

The mathematical formulation presented by Linke & Kokossis (2003b) regarding RMX units is as follows.

A1.1 Synthesis Units

The RMX unit mathematical formulation includes the balance equations around the mixers and splitters associated with the sub-units that form the RMX units. Previous to the formulation, some basic index sets for the superstructure elements are presented:

RM	{rm is a reactor / mass exchanger unit}
S	{s is a fluid phase state}
F_s	{f is a raw material source in $s \in S$ }
P_s	{p is a product in $s \in S$ }
SP_s	{sp is a splitter in $s \in S$ }
MI_s	{mi is a mixer in $s \in S$ }
CP_s	{cp is a component in $s \in S$ }
$SK_{s,rm}$	{sk is a well-mixed sub-unit in $s \in S$ of $rm \in RM$ }
RX_s	{rx is a reaction in $s \in S$ }

Partitions of the previous basic index sets include the following subsets:

RM^A $\{rm \mid rm \in RM$ is an active RMX unit$\}$

S^A $\{s \mid s \in S$ is an active fluid state$\}$

F_s^A $\{f \mid f \in F$ is an active raw material source in $s \in S^A\}$

P_s^A $\{p \mid p \in P$ is an active product in $s \in S^A\}$

SP_s^A $\{sp \mid sp \in SP$ is an active splitter in $s \in S^A\}$

MI_s^A $\{mi \mid mi \in MI$ is an active mixer in $s \in S^A\}$

$RX_{s,rm}^A$ $\{rx \mid rx \in RX$ is an active reaction in $s \in S^A$ of $rm \in RM^A\}$

$SP_{s,rm}^{RM}$ $\{sp \mid sp \in SP_s^A$ splits the outlet of $s \in S^A$ in $rm \in RM^A\}$

$SP_{s,rm,sk}^{IRM}$ $\{sp \mid sp \in SP_s^A$ splits the outlet of $s \in S^A$ in $sk \in SK_{s,rm}$ of $rm \in RM^A\}$

$MI_{s,rm,sk}^{RM}$ $\{mi \mid mi \in MI_s^A$ is a mixer in $s \in S^A$ prior to $sk \in SK_{s,rm}$ of $rm \in RM^A\}$

$MI_{s,rm}^{PRM}$ $\{mi \mid mi \in MI_s^A$ is a final product mixer in $s \in S^A$ of $rm \in RM^A\}$

Based on the previous sets, the rest of variables are:

$FF_{s,f,rm,cp}$ {flowrate of component cp in $f \in F_s^A$ through $mi \in MI_{s,rm,sk}^{RM}$}

$OUTR_{s,rm,cp}$ {flowrate of component cp in $s \in S^A$ through $sp \in SP_{s,rm}^{RM}$}

$OUTSK_{s,rm,sk,cp}$ {flowrate of component cp in $s \in S^A$ through $sp \in SP_{s,rm,sk}^{IRM}$}

$INR_{s,rm,sk,cp}$ {flowrate of component cp in $s \in S^A$ through $mi \in MI_{s,rm,sk}^{RM}$}

$FSF_{s,f,rm,sk}$ {fraction of the $FF_{s,f,rm,cp}$ through $mi \in MI_{s,rm,sk}^{RM}$}

$SKP_{s,rm,sk}$ {fraction of $OUTSK_{s,rm,sk,cp}$ entering $mi \in MI_{s,rm}^{PRM}$}

$SRR_{s,rm,rm,sk}$ {fraction of $OUTR_{s,r,cp}$ entering $mi \in MI_{s,rm,sk}^{RM}$}

$RXR_{s,rx,rm,sk}$ {specific reaction rate of $rx \in RX_{s,rm}^A$ in $sk \in SK_{s,rm}$ of $rm \in RM^A$}

$\upsilon_{s,rx,cp}$ {stoichiometric coefficient for $cp \in CP$ in $rx \in RX^{A}_{s,rm}$}

$V_{s,rm}$ {volume of $s \in S^{A}$ in $rm \in RM^{A}$}

$\varepsilon_{s,rm,sk}$ {hold-up of $sk \in SK_{s,rm}$}

Next, the balance equations describing the well-mixed cells sk of the RMX units are presented. Inlet streams to the RMX units are raw material streams and outlet flows from other units present in the superstructure. Initially the balances of each mixer prior to the sub-units are:

$$\sum_{f \in F} FF_{s,f,rm.cp} \cdot FSF_{s,f,rm,sk} + PREV_{sk} + \sum_{s^* \in S_S^T} OUTR_{s,rm,cp} \cdot SRR_{s,rm,rm,sk} - INR_{s,rm,sk,cp} = 0$$

(Equation A1.2)

$$\forall f \in F^{A}, cp \in CP, sk \in SK_{s,rm}, rm \in RM^{A}, s \in S^{A}$$

$$PREV_{sk=1} = 0$$

$$PREV_{sk \in SK_{s,rm} \setminus \{1\}} = OUTSK_{s,rm,sk\ 1,cp} \cdot \left(1 - SKP_{s,rm,sk-1}\right)$$

The balances of the sub-units are:

$$INR_{s,rm,sk,cp} + \sum_{rx \in RX^{A}_{s,rm}} \nu_{s,rx,cp} \cdot RXR_{s,rx,rm,sk} \cdot \frac{\varepsilon_{s,rm,sk} \cdot V_{s,rm}}{\left|SK_{s,rm}\right|} \cdot OUTSK_{s,rm,sk,cp} + \sum_{s^* \in S \setminus \{s\}} MTR_{s^*,s,rm,sk,cp} = 0$$

$$\forall cp \in CP, sk \in SK_{s,rm}, rm \in RM^{A}, rx \in RX^{A}_{s,rm}, s \in S^{A}$$

(Equation A1.3)

The balances of the final product mixer are:

$$\sum_{sk \in SK_{s,rm}} OUTSK_{s,rm,sk,cp} \cdot SKP_{s,rm,sk} - OUTR_{s,rm,cp} = 0$$

$$\forall\, cp \in CP, sk \in SK_{s,rm}, rm \in RM^{A}, s \in S^{A}$$

(Equation A1.4)

Finally, the constraints on the split fractions are:

$$\sum_{s^* \in S_s^T} SRR_{s,rm,rm,sk} - 1 < 0$$

$$\forall\, sk \in SK, rm \in RM^{A}, s \in S^{A}$$

$$\sum_{sk \in SK_{rm}} FSF_{s,f,rm,sk} - 1 = 0$$

$$\forall\, f \in F, sk \in SK, rm \in RM^{A}, s \in S^{A}$$

(Equation A1.5)

A1.2 Superstructure Generation

The synthesis units are connected in every possible physical combination in the reactive phase through mixers and splitters forming the superstructure representation.

More partitions of the previous basic index sets include the next subsets:

$SP_{s,f}^{F}$ $\{sp \mid sp \in SP^{A}$ splits a raw material stream $f \in F_s^{A}\}$

$SP_{s,p}^{P}$ $\{sp \mid sp \in SP^{A}$ splits a product stream $p \in P_s^{A}\}$

$MI_{s,p}^{P}$ $\{mi \mid mi \in MI^{A}$ is a mixer of $p \in P_s^{A}\}$

$CP_{s,p}^{P}$ $\{cp \mid cp \in CP$ is a component in $p \in P_s\}$

$CP_{s,f}^{F}$ $\{cp \mid cp \in CP$ is a component in $sp \in SP_{s,f}^{F}\}$

$CP_{s,rm}^{RM}$ $\{cp \mid cp \in CP$ is a component in the outlet of $sp \in SP_{s,rm}^{RM}\}$

All the variables employed in the superstructure formulation are defined over the previous index sets and subsets. The following set of variables includes the flow rates of each component through splitters and mixers:

$FD_{s,f,cp}$ {component flow rate through $sp \in SP^{F}_{s,f}$ }

$INPR_{s,rm,cp}$ {component flow rate through $mi \in MI^{RM}_{s,rm}$ }

$INP_{s,p,cp}$ {component flow rate through $mi \in MI^{P}_{s,p}$ }

$OUTP_{s,p,cp}$ {component flow rate through $sp \in SP^{P}_{s,p}$ }

The next set of variables includes the set of split fractions of streams connecting splitters to mixers of the superstructure:

$SFR_{s,f,rm,sk}$ {fraction of $FD_{s,f,cp}$ entering $mi \in MI^{RM}_{s,rm,sk}$ }

$SFP_{s,f,p}$ {fraction of $FD_{s,f,cp}$ entering $mi \in MI^{P}_{s,p}$ }

$SRP_{s,r,p}$ {fraction of $OUTR_{s,r,cp}$ entering $mi \in MI^{P}_{s,p}$ }

$SPR_{s,p,rm,sk}$ {fraction of $OUTP_{s,p,cp}$ entering $mi \in MI^{RM}_{s,rm,sk}$ }

Finally for the transfer rate:

$MTR_{s^*,s,rm,sk,cp}$ {rate of mass transfer from phase $s^* \in S$ to phase $s^* \in S \setminus \{s^*\}$ of $cp \in CP$ in $sk \in SK_{s,rm}$ }

Following the shadow compartment concept (Mehta & Kokossis 1997, 2000), mass transfer rates $MTR_{s^*,s,rm,sk,cp}$ are calculated as functions of mixing patterns and flow directions in the compartments of states s and s*. The existence of mass transfer links

between the different compartments of the RMX units is a degree of freedom for the optimisation.

The mathematical formulation for the superstructure is defined as follow. Initially, the balance equations around mixers $mi \in MI^{RM}_{s,rm,sk}$ prior to RMX units are defined as:

$$\sum_{f \in F_s^A} FD_{s,f,cp} \cdot SFR_{s,f,rm,sk} + \sum_{rm \in RM^A} OUTR_{s,rm,cp} \cdot SRR_{s,rm,rm,sk} + PREV_{sk} + \sum_{p \in P_s^A} OUTP_{s,p,cp} \cdot SPR_{s,p,rm,sk} - INR_{s,rm,sk,cp} = 0$$

(Equation A1.6)

$$\forall f \in F^A, cp \in CP, sk \in SK_{s,rm}, rm \in RM^A, p \in P^A, s \in S^A$$

$$PREV_{sk=1} = 0$$

$$PREV_{sk \in SK_{s,rm} \setminus \{1\}} = OUTSK_{s,rm,sk-1,cp} \cdot \left(1 - SKP_{s,rm,sk}\right)$$

For outlet mixers of RMX units $mi \in MI^{PRM}_{s,rm}$:

$$\sum_{sk \in SK_{s,rm}} OUTSK_{s,rm,sk,cp} \cdot SKP_{s,rm,sk} - OUTR_{s,rm,cp} = 0$$

(Equation A1.7)

$$\forall cp \in CP, sk \in SK_{s,rm}, rm \in RM^A, s \in S^A$$

For network product mixers $mi \in MI^{P}_{p}$:

$$\sum_{f \in F_s^A} FD_{s,f,cp} \cdot SFP_{s,f,p} + \sum_{r \in RM^A} OUTR_{s,rm,cp} \cdot SRP_{s,rm,p} - OUTP_{s,p,cp} = 0$$

(Equation A1.8)

$$\forall f \in F^A, cp \in CP, rm \in RM^A, p \in P^A, s \in S^A$$

APPENDIX 2

Problem Data For The Styrene Production Process

A2.1 Relevant Process Design Features

A2.1.1 Feeding

- Two streams form the feed: ethylbenzene with impurities and steam. Both streams can be fed together to the first reactor or separately distributed amongst the different reactor zones. Table A2.1 presents the ethylbenzene feed with impurities employed in this work (Sheel & Crowe, 1969).

Table A2.1: Feed for the styrene production process.

Component	Value (kmol/h)
Ethylbenzene (Eb)	36.87
Styrene (St)	0.67
Benzene (Bz)	0.11
Toluene (Tol)	0.88
Steam	To be optimised

A2.1.2 Connectivity

- Internal recycles are defined as those that are possible between reactor zones before the condensers (see Figure 5.9).

- The external recycle departing from the distillation sequence is fed exclusively to the first reactor.

A2.1.3 Pressure

- The inlet pressure to the first reactor is $P_{in} = 2.4$ bars.
- The feeds are assumed to be compressed from 1 to 2.4 bars.
- The pressure suction for the external recycle compressor is 0.4 bar, which is the pressure at which the distillation sequence operates.

A2.1.4 Catalyst

- There is a maximum limit of catalyst of 10895 kg per structure (Elnashaie *et al.*, 2001).
- The maximum total mass of catalyst in complex superstructures, *i.e.* with more than one reactor present, is the same as the one for a single reactor superstructure.
- Catalyst particles are assumed to be cylinders with the same height and length (4.7 mm).

A2.1.5 Reactors

- The overall reaction is:

$$C_2H_5CH_2CH_3 \longleftrightarrow C_6H_5CHCH_2 + side\_products \qquad \text{(Equation A2.1)}$$

- The wall thickness for all reactors is $2 \cdot 10^{-3}$ m (Chapter 5). Where the nominal diameter of the tubes is optimized (Chapter 6), the wall thickness varies.
- The wall conductivity for all reactors is 15 W/m/K (stainless steel).

- The temperature within the reactor is maintained between 400 and 1000 K.

A2.1.6 Utilities for Reactors

- $U_{utility\_media}$ is 1325 Btu/ft^2/h/K (7523 W/m^2/K) for molten salt as cooling medium which corresponds to the 25 % lowest value of the range for the HITEC® molten salt.

- $U_{utility\_media}$ is assumed to be 3500 Btu/ft^2/h/K (19873 W/m^2/K) for molten salt as heating medium. The maximum value for the HITEC® molten salt is 2900 Btu/ft^2/h/K for the range of temperatures 575 to 790 K. A higher value for the heat transfer coefficient has been selected here due to the higher temperature values at which the heating media operates (850-1200 K approximately).

- The upper limit for the utility temperature is 1200 K, whereas the lower limit is 422 K.

A2.1.7 Optimization

- Classic approaches for designing chemical processes assume a fixed production rate of desired product (here styrene). However, in this work the process is optimised given a fixed feed rate of ethylbenzene with impurities of 32 kilotons/yr (Sheel & Crowe, 1969). The amount of the second feed (steam) will be determined by the optimisation.

- The objective function to be maximised is the Economic Potential (EP).

- The interest rate is set to 5 % and the payback period to 3 years.

- The ΔT_{min} for the linear minimisation problem of Stage 2 (Chapter 6) is 15 K.

- %HV maximum limit is 5.

A2.1.8 Separation

- The condensed fractions in the condenser are assumed to be 100 % for the styrene, 99.5% for the ethylbenzene, 99% for the toluene and 98 % for the benzene. This assumption proves to be very accurate if the partial condenser is modelled as in Tarafder *et al.* (2005). The exit temperature of the condenser is set at 333 K at a pressure of 1.9 bar. The solubility of non-condensable gases in the organic phase is negligible, and the organic compounds (ethylbenzene, styrene, benzene and toluene) are totally immiscible in water.

- Short-cut distillation methods are employed to model the distillation columns. It is assumed that this case study is a retrofit scenario in terms of reactors, in which the separation section is already in place when the synthesis exercise begins. The equations employed are the Fenske equation to calculate N_{min} (Fenske, 1932), the Underwood algorithm (Underwood 1932-1948) to calculate R_{min} and the Gilliland correlation in the Eduljee form (Eduljee, 1975) to calculate the reflux.

- In the first distillation column after the condenser, the recovery fractions for the light key component (toluene) and for the heavy key component (ethylbenzene) are assumed to be 99.9 %.

- In the benzene / toluene distillation column, no other component is fed. The recovery fraction for the toluene is assumed 99.9 % and its purity in industry normally is 99.7 %.

- In the ethylbenzene / styrene distillation column, no other component is fed. The recovery fraction for the styrene is assumed 99.7 % and its purity in industry normally is 99.7 %. The amount of ethylbenzene recovered in the column and recycled to the first reactor will be obtained by a short-cut design method. However a fraction recovered by the column must be in advanced specified to close the recycle. The percentage of recovery for the ethylbenzene fed to the column is assumed to be 99.9 %. The calculated and estimated values are compared to test whether errors are within a specified tolerance. If the error is not within the tolerance, the structure is rejected and not considered in the optimisation process. The scaled error is defined as:

$$-0.001 \leq \frac{\text{fraction\_calculated} - 0.999}{0.999} \leq 0.001 \qquad \text{(Equation A2.2)}$$

- It is assumed that the reflux is in all the distillation columns 1.1 times the minimum reflux.

- All the streams leaving and arriving to the columns are considered for the heat integration.

A2.1.9 Steam To Oil Ratio

- The molar ratio of the steam to ethylbenzene, SOR (steam over reactant), is set above seven (Yee *et al.*, 2003) to prevent coke formation on the catalyst surface and to eliminate coke deposits from the catalyst surface. With the coke deposits removal, the catalyst is regenerated. SOR is usually restricted in industrial practice below 20 (Yee *et al.*, 2003) because higher values affect the economics of the process. Extra energy is required to produce the excess steam and to condense it after the reactor.

A2.2 Kinetic Model

The kinetics for the catalytic dehydrogenation of ethylbenzene to produce styrene (Table A2.2, Figure A2.1) are taken from the ATHENA Process Simulation Framework case study (Silvaco International, 1994): "Catalytic production of styrene". The kinetic constants follow the Arrhenius expression.

Table A2.2: Kinetics for the catalytic dehydrogenation of ethylbenzene.

Rate equation	A_i	E_i / R (K)
[1] $r_1 = k_1\left(p_{ethylbenzene} - p_{styrene}p_{hydrogen}/K_{eb}\right)$	1.51286	10925
$r_2 = k_2 p_{ethylbenzene}$	$5.6197 \times 10^{+5}$	25000
$r_3 = k_3 p_{ethylbenzene} p_{hydrogen}$	1.3446	11000
$r_4 = k_4 p_{steam} p_{ethylene}$	9.3016×10^{-1}	12500
$r_5 = k_5 p_{steam} p_{methane}$	5.3163×10^{-2}	7900
$r_6 = k_6 p_{steam} p_{carbon\_monoxide}\left(P/T^3\right)$	1.6769×10^{9}	8850

[1] Where the equilibrium constant Keb for reaction 1 takes the form: $K_{eb}=\exp[-(122725-126.3*T-0.002194*T^2)/8.314*T]$.

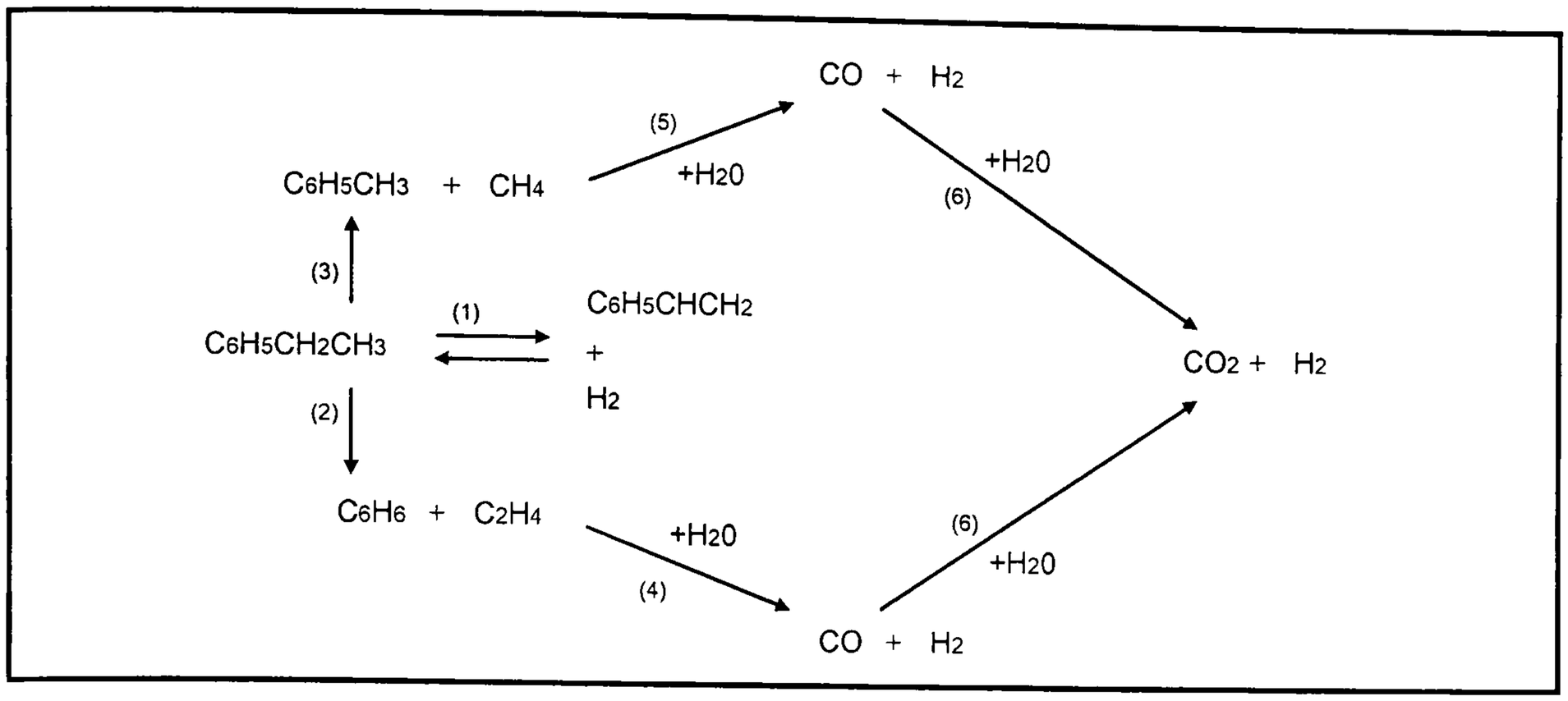

Figure A2.1: Kinetic path for the styrene production process.

For the same kinetic parameters as the ones employed here, Abdalla *et al.* (1994), Elnashaie and Elshishini (1994), and Yee *et al.* (2003) have compared the performances obtained with two different reactor models: 1) a pseudo-homogeneous one dimensional PFR model without radial temperature profile approximation; 2) a more detailed heterogeneous model that takes into account the diffusion in the catalyst pellet. All studies concluded that both models showed very similar performances due to the fact that mass transfer does not limit the reactions in the system. These conclusions were reached for catalyst particles with equal or bigger diameter, than the ones employed here. Therefore, models based on a pseudo-homogeneous PFR model that does not take into account diffusion in the catalyst pellet, can be employed here without experiencing inaccuracies.

A2.3 Capital And Operational Costs

A2.3.1 Heat Exchanger Network

The capital cost for the heat exchanger network can be estimated from Luyben (2001) and the assumption that all heat exchangers have the same area (Ahmad *et al.*, 1990):

$$HX_{COST} = HX_{UNITS} \cdot 0.0073 \cdot \left(\frac{A_{HX_{NETWORK}}}{HX_{UNITS}} \right)^{0.65} \qquad \text{(Equation A2.3)}$$

The cold utility is taken by cooling water that is fed to the system at 300 K and leaves at 319 K (Biegler *et al.*, 1997). The specific heat (C_{PW}) is $7.53 \cdot 10^{-2}$ kJ/gmol K and the cost is $2.47 \cdot 10^{-7}$ \$/gmol (Biegler *et al.*, 1997). The flow is calculated from the heat balance:

$$\dot{F}_{COOLING\_WATER} = \frac{COLD\_UTILITY}{CP_W \cdot (T_{OUT} - T_{IN})} \qquad \text{(Equation A2.4)}$$

The hot utility is given either by oil or by a furnace. The price of the oil is \$60/kW yr (Pettersson, 2005). The price of the fuel for the furnace is 174 \$/kW yr (Tantimuratha *et al.*, 2000) and the fixed cost of the furnace (Tantimuratha *et al.*, 2000):

$$FURNACE_{COST} = 3.211 \cdot 10^{-4} \cdot HOT\_UTILITY^{0.7} \qquad \text{(Equation A2.5)}$$

A2.3.2 Reactors Cooling/Heating Media

Reactors are not heat integrated with the rest of the process because of practical controllability issues. The heat exchange media employed is molten salt. If the reactor requires heating, the cost of the molten salt is taken as the cost of the hot

utility employed (174 $/kW yr). If the reactor requires cooling, the cost of the molten salt is taken as zero because it would recover high grade heat that could be used in the generation of steam. The generated steam could be sold and therefore be a benefit. Results in Chapter 5 and 6 show that only heating utility is required.

A2.3.3 Catalyst Cost

It has been observed that all the optimal design candidates contain at least 70% of the maximum catalyst load allowed. With a catalyst estimate price of 7 $/kg for oxidation reactions (Dubois, 2006), the maximum difference in catalyst load between design candidates (30%), would result in a maximum difference catalyst cost of 0.02 M$ every time the catalyst is replaced. According to Meima & Menon (2001), it is typically replaced every 1-2 years, which results in a difference cost of 0.02-0.01 M$/yr. Due to these small maximum differences in annual costs and for simplicity reasons, the catalyst cost is not included in the development of the objective function value.

A2.3.4 FBRs

The cost of the FBR is calculated as the cost of a pressure vessel (Turton, 2005):

$$FBR_{COST} = F_P \cdot \left(10^{K1+K2\cdot\log(VOLUME_{REACTOR})} + K3\cdot\log\left(VOLUME_{REACTOR}{}^{2}\right)\right) \qquad \text{(Equation A2.6)}$$

where:

$$F_p = \frac{\left(P_{max}+1.0\right)\cdot D_v}{\left[\left[2.0\cdot\left(850-0.6\cdot\left(P_{max}+1\right)\right)\right]+0.00315\right]\cdot 0.0063} \qquad \text{(Equation A2.7)}$$

where D_v is the diameter of the vessel and P_{max} the maximum pressure in the vessel.

The parameters take the following values:

$K1 = 3.49$
$K2 = 0.38$
$K3 = 0.09$

(Equations A2.8)

A2.3.5 CSTRs And MTRs

CSTR and MTRs are priced multiplying a factor (5 and 30 respectively) by the price of a FBR with the same catalyst load. To calculate these two factors, initially a correlation (cost vs. volume) is obtained for CSTRs with ASPEN Icarus (considering a stirred vessel), whereas for MTRs it is assumed that the cost is twice that of a tubular heat exchanger with the same heat transfer area (Luyben, 2001). Then, the ratios $\frac{\text{cost CSTR}}{\text{cost FBR}}$ and $\frac{\text{cost MTR}}{\text{cost FBR}}$ are calculated assuming for all reactors the same catalyst load (Table A2.3).

Table A2.3: Ratios for the cost of CSTRs and MTRs.

Catalyst load (kg)	$\frac{\text{cost CSTR}}{\text{cost FBR}}$	$\frac{\text{cost MTR}}{\text{cost FBR}}$
9000	5.9	34.8
10000	5.7	33.9
20000	4.5	27.5

Finally, factors of 5 and 30 are chosen as representative values. The multiplying factor of 30 is assuming MTRs of 30000 tubes. When MTRs with different number of tubes are used, the cost is obtained as:

- If number of tubes $>$ 30000:

$$\text{Reactor\_cost} = \text{Reactor\_cost}(30000\ \text{tubes}) \cdot \frac{\text{number\_of\_tubes}}{30000} \quad \text{(Equation A2.9)}$$

- If 30000 > number of tubes > 20000:

$$\text{Reactor\_cost} = \text{Reactor\_cost}(30000\ \text{tubes}) \qquad \text{(Equation A2.10)}$$

- If number of tubes < 20000:

$$\text{Reactor\_cost} = \text{Reactor\_cost}(30000\ \text{tubes}) \cdot \frac{\text{number\_of\_tubes}}{20000} \qquad \text{(Equation A2.11)}$$

A2.3.6 Compressors

The compression is assumed to be an adiabatic compression of an ideal gas with 75% efficiency. The formula for the capital cost of a compressor (Luyben, 2001) is:

$$\text{COMPRESSOR}_{\text{COST}} = 0.00433 \cdot \text{W}_{\text{COMPRESSOR}}^{\ 0.82} \qquad \text{(Equation A2.12)}$$

where:

$$\text{W}_{\text{COMPRESOR}} = \frac{\text{F}_{\text{R}} \cdot \gamma \cdot \text{R} \cdot \text{T}_{\text{SUCTION}}}{0.75 \cdot (\gamma - 1)} \cdot \left[\left(\frac{\text{P}_{\text{DISCHARGE}}}{\text{P}_{\text{SUCTION}}} \right)^{(\gamma-1)/\gamma} - 1 \right] \qquad \text{(Equation A2.13)}$$

where γ is the ratio of heat capacities, R is the constant of ideal gases and F_r is the flow to be compressed (gmol/s). For the compression cost, the price of electricity is \$0.07 kWh (Luyben, 2001) and it is calculated (Luyben, 2001) as:

$$\text{COMPRESSION}_{\text{UTILITY}} = 0.613 \cdot 10^{-3} \cdot \text{W}_{\text{COMPRESSOR}} \qquad \text{(Equation A2.14)}$$

The compressor work takes the same formula as before.

A2.3.7 Distillation Columns

The vessels of the distillation columns are assumed not to differ from one process

design candidate to another and therefore are not priced. The condensers and reboilers are heat integrated.

A2.3.8 Raw Material And Product Values

The prices for the raw components (ethylbenzene and superheated steam) and for the products are taken from Yee *et al.* (2003).

Table A2.4: Raw material and product values.

Component	Value ($/ton)
Ethylbenzene	429.51
Styrene	988.94
Benzene	394.30
Toluene	367.91
Ethylene	0.0
Methane	0.0
Superheated steam	19.98
Carbon monoxide	0.0
Carbon dioxide	0.0
Hydrogen	0.0

A2.4 Selectivity And Conversion Definitions

According to Yee *et al.* (2003), the molar selectivities and the ethylbenzene molar conversion are defined as:

$$\text{Styrene selectivity} = \frac{ST_{outlet} - ST_{inlet}}{EB_{inlet} - EB_{outlet}} \cdot 100 \qquad \text{(Equation A2.15)}$$

$$\text{Benzene selectivity} = \frac{BZ_{outlet} - BZ_{inlet}}{EB_{inlet} - EB_{outlet}} \cdot 100 \qquad \text{(Equation A2.16)}$$

$$\text{Toluene selectivity} = \frac{TOL_{outlet} - TOL_{inlet}}{EB_{inlet} - EB_{outlet}} \cdot 100 \qquad \text{(Equation A2.17)}$$

$$\text{Ethylbenzene conversion} = \frac{EB_{inlet} - EB_{outlet}}{EB_{inlet}} \cdot 100 \qquad \text{(Equation A2.18)}$$

APPENDIX 3

Problem Data For The Acetic Acid Production Process

A3.1 Relevant Process Design Features

A3.1.1 Feeding

- Two streams form the feed: ethane and oxygen. Both streams can be fed together to the first reactor or separately distributed amongst the different reactor zones.

A3.1.2 Connectivity

- Internal recycles are defined as those that are possible between reactor zones before the flash separation (Figure 7.1).

- The external recycle departing from the flash separation is fed exclusively to the first reactor.

A3.1.3 Pressure

- The inlet pressure to the first reactor is P_{in} = 16 bars.

- The feeds are assumed to be compressed from 12 to 16 bars.

- The pressure suction for the external recycle compressor is calculated assuming a loss of pressure ΔP_{OR} = 1 bar from the last active reactor. That is for the materials flowing through heat exchangers and the flash operation. Therefore the suction pressure for the outlet compressor is calculated as:

$$P_{OC} = P_{in} - \sum_{R=1}^{no\_reactors} \Delta P_R - \Delta P_{OR} \qquad \text{(Equation A3.1)}$$

A3.1.4 Catalyst

- There is a maximum limit of catalyst of 50000 kg per structure.
- The maximum total mass of catalyst in complex superstructures, *i.e.* with more than one reactor present, is the same as the one in a single reactor superstructure.
- Catalyst particles are assumed to be cylinders with the same height and lenght (5 mm).

A3.1.5 Reactors

- The overall reaction is:

$$C_2H_6 + O_2 \longleftrightarrow CH_3COOH + side\_products \qquad \text{(Equation A3.2)}$$

- The wall thickness for most reactors is $2 \cdot 10^{-3}$ m. For the stages where the nominal diameter of the tubes is optimised, the wall thickness varies.
- The wall conductivity for all reactors is 15 W/m/K (stainless steel).
- The cooling / heating stream of the reactor is not integrated in the Problem Table algorithm.

- The number of orifices per square meter of the distributor of the fluidised bed reactors (FLBRs) is 800.

A3.1.6 Utilities

- Utility_media is 400 W/m²/K (for oil as cooling or heating media as in Linke *et al.*, 2002b).

- The upper limit for the heating utility temperature is 700 K, whereas for the cooling utility the lower limit is 400 K. The temperature within the reactor is maintained between 450 and 570 K. The upper limit is set after Linke *et al.* 2002b.

A3.1.7 Optimisation

- The process is optimised given a fixed feed rate of ethane (50 ktons/yr). The amount of the second component fed (oxygen) is determined by optimisation.

- The objective function to be maximised is the Economic Potential (EP).

- The interest rate is set to 5 % and the payback period to 3 years.

- The ΔT_{min} for the linear minimisation problem of Stage 2 (Chapter 6) is 15 K.

- %HV maximum limit is set to 5.

A3.1.8 Separation

- There is an assumed loss of 5 % of the hydrocarbons present in the stream treated in the absorber.

- The acetic acid purity in the bottom product of the distillation column is set to 99.9 % and its recovery to 99 %.

- It is assumed that the number of theoretical plates in the distillation column is 40 (Smejkal *et al.*, 2005).

- Separation systems are represented in aggregated form to keep the superstructure model at solvable complexity. This is achieved through cost expressions developed using separation systems approaches. This expressions capture the cost separations for given stream compositions and flow rates. For this case the separation system is a single distillation column in which acetic and water are separated. It is assumed that this case study is a retrofit scenario in terms of reactors, in which the separation section is already in place when the synthesis exercise begins. To develop the cost expressions, shortcut methods are employed. The equations used in the shortcut calculations are the Fenske equation to calculate N_{min} (Fenske, 1932), the Underwood algorithm (Underwood 1932-1948) to calculate R_{min} and the Gilliland correlation in the Eduljee form (Eduljee, 1975) to calculate the reflux. The vessel of the distillation column has not been valued since it is assumed not to vary significantly from one process design candidate to another. Therefore, only the condenser and the reboiler have been valued to develop the cost expressions. Initially, the separation synthesis problem is repeatedly solved for several cases. Since the components passed from the reaction section to the separation section are known, their flows and compositions can be estimated to narrow the ranges to be used in developing the cost functions. The range of flows in which the cost functions have been developed is: a) acetic throughput: 11-31 mols/s; b) water throughput 24-124 mols/s. The

solutions of the separation synthesis problem provide the flows and temperatures at the top and bottom of the column. Next, heat balances are performed. Then, heat flows and temperatures are used to calculate the capital and operational costs of the condenser and the reboiler for each case. Finally, with the capital and operational costs for the condenser and reboiler for each case, regressions can be done to obtain equations in the form of:

$$\text{DISTILLATION}_{\text{CAPITAL COST}} = A \cdot \prod_{IC=1}^{NO\_COMPONENTS} \left(\text{Throughput}_{IC}(\text{mol/s})\right)^{B_{IC}}$$

$$\text{DISTILLATION}_{\text{OPERATIONAL COST}} = B \cdot \prod_{IC=1}^{NO\_COMPONENTS} \left(\text{Throughput}_{IC}(\text{mol/s})\right)^{B_{IC}}$$

(Equations A3.3)

For this case study, the fixed cost function developed is:

$$\text{DISTILLATION}_{\text{FIX\_COST}}(10^6\$) = 30.84 \cdot 10^{-3} \cdot \text{Acetic\_throughput}^{41.85 \cdot 10^{-3}} \cdot \text{Water\_throughput}^{606.9 \cdot 10^{-3}}$$

(Equation A3.4)

The average and maximum deviation for the 58 points employed to develop the function are 0.14 and 0.69 % respectively. The operational cost function is:

$$\text{DISTILLATION}_{\text{OPERATIONAL\_COST}}(10^6\$) = 30.35 \cdot 10^{-3} \cdot \text{Acetic\_throughput}^{73.98 \cdot 10^{-3}} \cdot \text{Water\_throughput}^{934.4 \cdot 10^{-3}}$$

(Equation A3.5)

In this case, the average and maximum deviation are 0.51 and 1.89 % respectively.

- The heats from the reboiler and the condenser are not taken into account for the Problem Table Algorithm because of practical controllability issues.

A3.2 Explosion Limits

The gaseous phase reactions take place at high temperatures (450 – 570 K) where high concentrations of oxygen are likely to cause explosions. To avoid them, the amount of oxygen at the inlet of every reactor zone has been limited to 13% (Smejkal *et al.*, 2005). Since oxygen is only consumed and not produced when reaction takes place, its concentration cannot increase inside the reactor zones; thus, it is sufficient to limit the amount of oxygen at the inlet of the reactors.

A3.3 Kinetic Model

The kinetics for the partial oxidation of ethane to produce acetic acid (Table A3.1 A3.2) are taken from Linke *et al.* (2002a). The kinetic constants follow the Arrhenius expression.

Table A3.1: Kinetics for the partial oxidation of ethane (1).

Rate equation	**Kinetic constant at 539 K**	**E_a or ΔH_{ads}**
$r_1 = k_1 p_{C_2H_6} \theta_{[OM_zO]}$	$k_1 = 1.665 \cdot 10^{-9}$ mol (s kg Pa)$^{-1}$	99.7 KJ · mol^{-1}
$r_2 = k_2 p_{O_2} \theta_{[OM_zC_2H_4]}$	$k_2 = 1.251 \cdot 10^{-9}$ mol (s kg Pa)$^{-1}$	92.6 KJ · mol^{-1}
$r_3 = k_3 p_{C_2H_4} \theta_{[(HOM_xO)(OH)]}$	$k_3 = 1.254 \cdot 10^{-5}$ mol (s kg Pa)$^{-1}$	144 KJ · mol^{-1}
$r_4 = k_4 p_{O_2} \theta_{[OM_z]}$	$k_4 = 1.713 \cdot 10^{-8}$ mol (s kg Pa)$^{-1}$	123 KJ · mol^{-1}
$r_5 = k_5 p_{O_2} \theta_{[OM_x]}$	$k_5 = 4.453 \cdot 10^{-9}$ mol (s kg Pa)$^{-1}$	85.2 KJ · mol^{-1}
$r_6 = k_6 p_{C_2H_4} \theta_{[OM_z]} - k_6/K_6 \, \theta_{[OM_zC_2H_4]}$	$k_6 = 6.633 \cdot 10^{-8}$ mol (s kg Pa)$^{-1}$ $K_6 = 2.484 \cdot 10^{-4}$ Pa^{-1}	-137 KJ · mol^{-1} -176 kg · mol^{-1}
$r_7 = k_7 p_{H_2O} \theta_{[OM_z]} - k_7/K_7 \, \theta_{[HOM_zOH]}$	k_7 = - $K_7 = 1.359 \cdot 10^{-7}$ Pa^{-1}	- -220 kg · mol^{-1}
$r_8 = k_8 p_{H_2O} \theta_{[OM_xO]} - k_8/K_8 \, \theta_{[(HOM_xO)(OH)]}$	$k_8 = 2.634 \cdot 10^{-9}$ mol (s kg Pa)$^{-1}$ $K_8 = 5.396 \cdot 10^{-6}$ Pa^{-1}	25.7 KJ · mol^{-1} -38.8 kg · mol^{-1}
$r_9 = k_9 p_{C_2H_6} \theta_{[OM_zO]}$	$k_9 = 3.363 \cdot 10^{-10}$ mol (s kg Pa)$^{-1}$	123 KJ · mol^{-1}
$r_{10} = k_{10} p_{C_2H_4} \theta_{[OM_zO]}$	$k_{10} = 2.019 \cdot 10$-8 mol (s kg Pa)-1	43.3 KJ · mol^{-1}
$r_{11} = k_{11} p_{HOac} \theta_{[OM_zO]}$	$k_{11} = 2.892 \cdot 10^{-9}$ mol (s kg Pa)$^{-1}$	105 KJ · mol^{-1}

Table A3.2: Kinetics for the partial oxidation of ethane (2).

Kinetic parameters
$\theta_{[(HOM_xO)(OH)]} = k_8 p_{O_2} p_{H_2O} / (k_3 p_{O_2} p_{C_2H_4} + k_8 p_{O_2} p_{H_2O} + k_3 k_8 / k_5 p_{C_2H_4} p_{H_2O} + k_8 / K_8 p_{O_2})$ $\theta_{[OM_xO]} = (k_3 p_{C_2H_4} + k_8 / K_8) p_{O2} / (k_3 p_{O_2} p_{C_2H_4} + k_8 p_{O_2} p_{H_2O} + k_3 k_8 / k_5 p_{C_2H_4} p_{H_2O} + k_8 / K_8 p_{O_2}$ $\theta_{[OM_x]} = 1 - \theta_{[(HOM_xO)(OH)]} - \theta_{[OM_xO]}$ $\theta_{[OM_zO]} = k_4 p_{O_2} (k_2 K_6 p_{O_2} + k_6) / [(k_2 K_6 p_{O_2} + k_6) \cdot (k_1 p_{C_2H_6} + k_9 p_{C_2H_6} + k_{10} p_{C_2H_4} + k_{11} p_{HOac}) +$ $K_7 p_{H_2O} (k_2 K_6 k_1 p_{C_2H_6} p_{O_2} + k_2 K_6 k_9 p_{C_2H_6} p_{O_2} + k_2 K_6 k_{10} p_{O_2} p_{C_2H_4} + k_2 K_6 k_{11} p_{O_2} p_{HOac} + k_6 k_1 p_{C_2H_6} +$ $k_6 k_9 p_{C_2H_6} + k_6 k_{10} p_{C_2H_4} + k_6 K_{11} p_{HOac}) + K_6 (k_4 k_1 p_{C_2H_6} p_{O_2} + k_6 k_1 p_{C_2H_6} p_{C_2H_4} + k_6 k_9 p_{C_2H_6} p_{C_2H_4} +$ $k_6 k_{10} (p_{C_2H_4})^2 + k_6 k_{11} p_{C_2H_4} p_{HOac}) + k_4 p_{O2} (k_2 k_6 p_{O_2} + k_6)]$ $\theta_{[OM_zC_2H_4]} = K_6 (k_4 k_1 p_{C_2H_6} p_{O_2} + k_6 k_1 p_{C_2H_6} p_{C_2H_4} + k_6 k_9 p_{C_2H6} p_{C_2H_4} + k_6 k_{10} (p_{C_2H_4})^2 +$ $k_6 k_{11} p_{C_2H_4} p_{HOac}) / [(k_2 K_6 p_{O_2} + k_6) \cdot k_1 p_{C_2H_6} + k_9 p_{C_2H_6} + k_{10} p_{C_2H_4} + k_{11} p_{HOac}) + K_7 p_{H_2O} \cdot$ $(k_2 K_6 k_1 p_{C_2H_6} p_{O_2} + k_2 K_6 k_9 p_{C_2H_6} p_{O_2} + k_2 K_6 k_{10} p_{C_2H_4} p_{O_2} + k_2 K_6 k_{11} p_{O_2} p_{HOac} + k_6 k_1 p_{C_2H_6} +$ $k_6 k_9 p_{C_2H6} + k_6 k_{10} p_{C_2H_4} + k_6 k_{11} p_{HOac}) + K_6 (k_4 k_1 p_{C_2H_6} p_{O_2} + k_6 k_1 p_{C_2H_6} p_{C_2H_4} + k_6 k_9 p_{C_2H_6} p_{C_2H_4} +$ $k_6 k_{10} (p_{C_2H_4})^2 + k_6 k_{11} p_{C_2H_4} p_{HOac}) + k_4 p_{O_2} (k_2 K_6 p_{O_2} + k_6)]$ $\theta_{[HOM_zOH]} = K_7 p_{H_2O} (k_2 k_6 k_1 p_{C_2H_6} p_{O_2} + k_2 K_6 k_9 p_{C_2H_6} p_{O_2} + k_2 K_6 k_{10} p_{O_2} p_{C_2H_4} + k_2 K_6 k_{11} p_{O_2} p_{HOac} +$ $k_6 k_1 p_{C_2H_6} + k_6 k_9 p_{C_2H_6} + k_6 k_{10} p_{C_2H_4} + k_6 k_{11} p_{HOac}) / [(k_2 K_6 p_{O_2} + k_6) \cdot (k_1 p_{C_2H_6} + k_9 p_{C_2H_6} +$ $k_{10} p_{C_2H_4} + k_{11} p_{HOac}) + K_7 p_{H_2O} (k_2 K_6 k_1 p_{C_2H_6} p_{O_2} + k_2 K_6 k_9 p_{C_2H_6} p_{O_2} + k_2 K_6 k_{10} p_{C_2H_4} p_{O_2} +$ $k_2 K_6 k_{11} p_{HOac} p_{O_2} + k_6 k_1 p_{C_2H_6} + k_6 k_9 p_{C_2H_6} + k_6 k_{10} p_{C_2H_4} + k_6 k_{11} p_{HOac}) + K_6 (k_4 k_1 p_{C_2H_6} p_{O_2} +$ $k_6 k_1 p_{C_2H_6} p_{C_2H_4} + k_6 k_9 p_{C_2H_6} p_{C_2H_4} + k_6 k_{10} (p_{C_2H_4})^2 + k_6 k_{11} p_{C_2H_6} p_{HOac}) + k_4 p_{O_2} (k_2 K_6 p_{O_2} + k_6)]$ $\theta_{[OM_z]} = 1 - \theta_{[OM_zO]} - \theta_{[OM_zC_2H_4]} - \theta_{[HOM_zOH]}$

For this specific application Linke *et al.* (2002a) showed that internal diffusion processes can be neglected for particle diameters lower than 1 mm at T < 580 K. Therefore, they assumed for this system a shell catalyst with an external catalyst layer of less than 500 μm thickness. This corresponded to a loading of catalyst support with active component of about 20-50 wt% for the assumed range of catalyst particle diameters of 3-5 mm. As a result of this assumption, internal diffusion was not taken into account in the reactor models. Their mass of catalyst per reactor volume was 600 kg/m^3 for the assumed 50 wt% catalyst on inert support material. All these assumptions are considered here.

A3.4 Capital And Operational Costs

The cost expressions are the same as the ones for the styrene production process except for the following cases.

A3.4.1 Reactors Heating/Cooling Media

Reactors are not heat integrated with the rest of the process because of practical controllability issues. The heat exchange media employed is oil. If the reactor requires cooling, the cost of the oil is taken as zero because it would recover high grade heat that could be used in the generation of steam. The generated steam could be sold and therefore be a benefit. If the reactor requires heating, the cost of the hot oil is taken as the cost of the hot utility (60 $/kW). Results in Chapter 7 show that only cooling utility is required.

A3.4.2 Catalyst Cost

It has been seen that all the reactor networks approach the maximum catalyst load allowed. Therefore, the catalyst price is not included in the study as it would have the same influence in all the process design candidates.

A3.4.3 CSTRs And MTRs

The multiplying factors are 5 for CSTRs and 25 for MTRs according to the ratios $\frac{\text{cost CSTR}}{\text{cost FBR}}$ and $\frac{\text{cost MTR}}{\text{cost FBR}}$ (Table A3.3), which are obtained as for the styrene production process but for a wider range of catalyst load

Table A3.3: Ratios for the cost of CSTR and MTR.

Catalyst load (kg)	$\frac{\text{cost CSTR}}{\text{cost FBR}}$	$\frac{\text{cost MTR}}{\text{cost FBR}}$
9000	5.9	34.8
10000	5.7	33.9
20000	4.5	27.5
30000	4.1	23.9
40000	3.8	21.4
50000	3.6	19.6

A3.4.4 Distillation Column

The cost expressions developed to represent separation systems in aggregated form only consider the condenser and the reboiler. The vessel of the distillation column is assumed not to differ from one process design candidate to another. To develop the cost expressions the following expressions for capital and operational costs have been employed. The capital cost for the condenser follows the same expression as for heat exchangers:

$$CONDENSER_{COST} = 0.0073 \cdot A_{CONDENSER}^{0.65} \qquad \text{(Equation A3.6)}$$

The assumptions to calculate the area of the condenser are found in Biegler *et al.* (1997). The following heat balance can specify the area:

$$A_{CONDENSER} = \frac{q_{CONDENSER}}{U \cdot \Delta T_{LM}} \qquad \text{(Equation A3.7)}$$

The heat exchanged in the condenser is taken by cooling water which has the same specification as the cold utility for the styrene production process. The flow is calculated from the heat balance:

$$\dot{F}_{COOLING\_WATER} = \frac{q_{CONDENSER}}{CP_W \cdot \left(T_{OUT\_COOLING\_WATER} - T_{IN\_COOLING\_WATER}\right)} \qquad \text{(Equation A3.8)}$$

The capital cost for the reboiler also follows the same expression as for the heat exchangers:

$$REBOILER_{COST} = 0.0073 \cdot A_{REBOILER}^{0.65} \qquad \text{(Equation A3.9)}$$

The assumptions to calculate the area of the reboiler are found in Biegler *et al.* (1997).

The area can be specified as:

$$A_{REBOILER} = \frac{q_{REBOILER}}{U \cdot \left(T_{STEAM} - T_{REBOILER}\right)} \qquad \text{(Equation A3.10)}$$

The cost of the steam at 11.5 bar is 11.17 $/ton (Biegler *et al.*, 1997) and the enthalpy of vaporisation (ΔHvap) is 35870 J/gmol. The flow needed is calculated from the following heat balance:

$$\dot{F}_{STEAM} = \frac{q_{REBOILER}}{\Delta H_{VAP}} \qquad \text{(Equation A3.11)}$$

A3.4.5 Raw Material And Product Values

The prices for the raw components and for the product (Table A3.4) are taken from Smejkal *et al.* (2005) and Biegler *et al.* (1997).

Table A3.4: Raw material and product values.

Component	Value ($/ton)
Ethane	72.0
Oxygen	50.0
Steam	11.17
Carbon dioxide as product	0.0
Acetic acid	730

A3.5 Selectivity And Conversion Definitions

The ethane and oxygen conversions and the process selectivity are defined as:

$$\text{Oxygen conversion} = \frac{O2_{\text{in process}} - O2_{\text{out process}}}{O2_{\text{in process}}} \cdot 100 \qquad \text{(Equation A3.12)}$$

$$\text{Ethane conversion} = \frac{C2H6_{\text{in process}} - C2H6_{\text{out process}}}{C2H6_{\text{in process}}} \cdot 100 \qquad \text{(Equation A3.13)}$$

$$\text{Re actor selectivity} = \frac{CH3COOH_{\text{out reactor}}}{C2H6_{\text{in reactor}} - C2H6_{\text{out reactor}}} \cdot 100 \qquad \text{(Equation A3.14)}$$

The reactor selectivity refers to the system formed by the reactors and the internal recycles. Out reactor refers to downstream of the internal recycle leaving the last reactor. $C2H6_{\text{in reactor}}$ refers to the ethane fed to the process plus the ethane externally recycled that gets into the first reactor.